# Universidad de Huelva

## Departamento de Geología


**Desarrollo e implementación de sistemas de tratamiento pasivo tipo DAS en drenajes ácidos de mina con elevada concentración metálica (Monte Romero – Mina Esperanza)**

**Memoria para optar al grado de doctor**
**presentada por:**

**Manuel Antonio Caraballo Monge**

Fecha de lectura: 21 de febrero de 2011

Bajo la dirección de los doctores:

José Miguel Nieto Liñán
Carlos Ayora Ibáñez

**Huelva, 2014**

**ISBN: 978-84-16061-01-3**
**D.L.: H 28-2014**

Universidad de Huelva
Facultad de Ciencias Experimentales
Departamento de Geología

# "Desarrollo e implementación de sistemas de tratamiento pasivo en drenajes ácidos de mina con elevada concentración metálica (Monte Romero y Mina Esperanza)"

Manuel Antonio Caraballo Monge

**Tesis presentada para optar al grado de Doctor en Ciencias en la Universidad de Huelva**

**DIRECTORES:**

**Dr. Jose Miguel Nieto Liñán**

Profesor Titular de Universidad del Área de Cristalografía y Mineralogía del Dpto. de Geología de la Universidad de Huelva

**Dr. Carlos Ayora Ibáñez**

Profesor de Investigación del CSIC. Instituto de Diagnostico Ambiental y Estudios del Agua (IDAEA-CSIC)

This thesis has been funded by the Spanish Government with a FPU grant; contract CTM2006-28151-E/TECNO, CTM2007-66724-C02/TECNO, CTM2010-21956-C02. The research of this thesis was developed mainly in the University of Huelva (UHU).

# ABSTRACT

Acid Mine Drainage (AMD) is formed from the weathering of iron sulfides. This pollution has a devastating effect in the water environment due to its metal toxicity and to the low pH. The Iberian Pyrite Belt (IPB) can be considered one of the largest massive sulfide provinces in the world with mine activities dating from 3,000 years B.C. The special geological environment and the intense mining of the region generate a widespread problem of highly metal polluted AMD.

For abandoned mines (orphan sites) passive systems are the only feasible remediation alternative. The more conventional passive treatment systems dealing with AMD pollution are inefficient when submitted to highly metal polluted AMD. This situation

motivated the main topic covered in this thesis: the design and implementation of a passive treatment system to remediate the highly polluted AMD at the IPB.

To achieve the best understanding of the role played by the precipitation of neoformed mineral phases and reagent dissolution in the passive treatment system, it was decided to develop (first part of the present thesis) a coupled sequential extraction and differential X ray diffraction procedure. This technique showed significant results elucidating the presence of poorly crystalline schwertmannite in samples containing more crystalline goethite. Limestone dissolution and precipitates distribution at the different depths of the reactive material was also clarified by the use of this coupled procedure.

The study of the field (pilot plant) passive treatment system in Monte Romero was covered in the second part of this thesis. The system designed and implemented in Monte Romero was based on the use of limestone and MgO as reagents dispersed in pine wood shaving (inert matrix). The experiment with limestone dissolution achieved a complete or almost complete water removal for Al, As, Cu, Cr and Pb, and higher than 70% Fe. An important removal of divalent metals (Zn, Cd, Co and Ni) was also obtained by the use of MgO as reagent; however, the appearance of a preferential water flow along the walls of the reactive tank made impossible to achieved better results.

The encouraging results obtained in the pilot plant from Monte Romero motivated the implementation of a full scale passive treatment system in Mina Esperanza. The third and final part of this thesis is devoted to the monitoring and characterization of this passive treatment during its 20 month of operation. It was observed a significant increment in water metal removal comparing with more than 80 conventional passive treatment systems employed in the world. The detailed mineralogical and hydrochemical processes involved in the performance of the reactive substrate employed were also unraveled. Three different precipitation zones were observed within the reactive material corresponding, from top to bottom, to the precipitation of Fe, Al and Zn.

# RESUMEN

Se conoce como drenaje ácido de mina (AMD) a la contaminación de las aguas por metales producto de la disolución de sulfuros, eminentemente pirita. El impacto para el medio ambiente alcanzado por el AMD es devastador ya que a la toxicidad aportada por las elevadas concentraciones de metales hay que sumarle el importante descenso de pH típicamente observado en estas aguas. La Faja Pirítica Ibérica (IPB) puede ser considerada como una de las provincias metalogenéticas más grandes del mundo, existiendo evidencias de minería en la región desde 3.000 años A.C. Las especiales características geológicas y de explotación minera de esta región hacen que AMD aquí generado muestre una serie de características muy especiales que dificultad enormemente su descontaminación.

Los sistemas de tratamiento pasivo son los únicos económicamente posibles en minas abandonadas. La ineficiencia mostrada en la descontaminación de AMD con alta carga metálica por los sistemas de tratamiento pasivo más tradicionales motivó el desarrollo de la presente tesis, en la cual se afronta el diseño e implementación de un sistema de tratamiento pasivo capaz de descontaminar el AMD generado en la IPB.

Con el fin de disponer de las herramientas necesarias para la óptima comprensión de los procesos mineralógicos implicados en el funcionamiento del sistema de tratamiento calizo empleado, se desarrolló (en la primera parte de esta tesis) un proceso conjunto de extracciones secuenciales y difracción de rayos X diferencial para la caracterización de fases pobremente cristalinas. Este proceso mostró una gran eficiencia a la hora de discernir la presencia de schwertmannita en muestras que además contenían goethita.

También permitió alcanzar un mejor conocimiento de la disolución de caliza así como de la distribución de los distintos precipitados a lo largo del perfil del material reactivo.

El funcionamiento de un sistema de tratamiento a escala de campo fue cubierto en la segunda parte de esta tesis. Para ello se diseñó e instaló en Monte Romero un sistema basado en el uso de caliza y MgO como materiales reactivos dispersados en virutas de madera. Este sistema consiguió alcanzar una descontaminación total o próxima a su totalidad para Al, As, Cu, Cr y Pb, así como retiradas superiores al 70% del Fe contenido en el agua. La utilización de MgO permitió alcanzar una importante eliminación de los metales trivalentes (Zn, Cd, Co y Ni) aunque ciertos problemas hidráulicos impidieron un mejor funcionamiento de esta sección del tratamiento.

Los buenos resultados obtenidos en los ensayos de campo promovieron el desarrollo en Mina Esperanza de un sistema de tratamiento pasivo de AMD a escala real. De este modo la tercera parte de esta tesis se encargó del control y caracterización de dicho sistema a lo largo de sus 20 meses de funcionamiento. Para ello se evaluó el rendimiento global del sistema obteniéndose una mejora sustancial en la eficiencia, en cuanto a retirada metálica de las aguas, en comparación con los sistemas de tratamiento pasivo más comúnmente empleados. Igualmente se estudió el detalle de los procesos mineralógicos e hidroquímicos involucrados en la eliminación de metales pesados en el interior del material reactivo, observándose (desde la superficie al fondo) el desarrollo de un frente de precipitación de Fe acompañado por otro de precipitación de Al y finalmente un frente de precipitación de Zn.

**Table of Contents:**

**List of Figures and Tables:**

**Chapter 1:**



**Chapter 2:**

# AGRADECIMIENTOS

La escritura en este volumen del trabajo realizado durante los últimos 5 años me ofrece la oportunidad de dejar por escrito lo que muchas veces he intentado reflejar en persona y no es más que mi inmensa gratitud al elevadísimo número de personas que de una u otra forma han hecho posible la aparición de esta tesis.

Sin lugar a dudas he de empezar agradeciéndole a José Miguel Nieto el haber no sólo apostado por mí como investigador y haberme ofrecido desde el primer momento el apoyo económico indispensable para realizar mi trabajo si no también el haberme animado y alentado cuando en infinidad de ocasiones he acudido a él con mis “cuentos de la lechera” y mis ideas de futuro. Indudablemente me contagió desde el principio su inagotable positivismo haciéndome creer firmemente en mis posibilidades como

investigador. Igualmente ha dejado una gran impronta en mi forma de trabajar todas las valiosas aportaciones de Carlos Ayora, quien gracias a sus comentarios ácidos, su enorme calidad como persona e investigador y su total disponibilidad para corregir mis numerosos errores ha conseguido dotar de gran calidad y riqueza todos los trabajos que hemos realizado en común. Creo firmemente que ambos han formado un tándem perfecto como codirectores de esta tesis.

Varias personas han estado desde mis primeros momentos como investigador enseñándome y apoyándome pero quisiera agradecer particularmente la inestimable ayuda prestada por Awi y Tobias, a los cuales puedo considerar como mis mentores en el fascinante mundo de la geología ambiental. Awi me ayudó y me ayuda cada día a desentrañar los misterios de la hidroquímica de las aguas contaminadas por metales mediante nuestras interminables discusiones (sé que te canso a veces) así como mediante las interesantes ideas que comparte y que me mantienen siempre ilusionado con mi trabajo. A Tobias por su parte he de agradecerle el ofrecerme un punto de vista distinto, más metódico y aplicado. Gracias a él aprendí que el valor de una investigación no sólo está en lo descubierto si no en como poder aplicarlo para el bien de la sociedad.

Otra pieza esencial de esta tesis es Francisco Macías quien, a pesar de haberse incorporado al trabajo a mediados de mi etapa doctoral, se ha convertido indiscutiblemente en un artífice indispensable de esta tesis. No sólo he de agradecerle las innumerables horas de trabajo que ha dedicado tanto a las investigaciones abarcadas en este estudio como a la maquetación de la tesis si no que siempre estaré en deuda por su mayor aportación: el devolverme la ilusión día a día por mi trabajo con su incombustible capacidad de fascinarse por cada pequeño descubrimiento. Igualmente nuestras discusiones culinarias y sobre localismos así como los innumerables momentos de risas han sido siempre una vía de escape al estrés del trabajo.

Muchos han sido los compañeros de trabajo que afortunadamente he podido tener y a riesgo de poder olvidar a alguno me gustaría agradecerle su ayuda y compañía a Josan, Manu, Migue, Rafita, Carlos, Juaki, Cinta, Laura, Yolanda y Rocío, así como a todos los componentes del Grupo Tharsis. De manera especial quiero reservar un agradecimiento para el grupo formado por Lola, Dino, Julio, Marco, Hans, Diana y Alba, con los cuales no sólo he disfrutado de las más interesantes conversaciones científicas si no que en ellos he encontrado a un grupo de amigos fascinante que han logrado que mis horas laborales fueran algo más que trabajo y que mi vida en Huelva este cargada de los más hermosos momentos de risas, complicidad, confidencias y amistad. También me gustaría agradecer a los compañeros de química y bioquímica que

en el último año me han aportado un punto de vista diferente de la ciencia así como más de una tarde de cafés y de risas, en particular a Merchi, Encarni, Marta Sierra, Marta de la Vega, Lourdes, Mari Ángeles e Iván.

También hubiera sido imposible todo este trabajo sin la ayuda de todos los componentes de los Servicios Centrales de Investigación de la Universidad de Huelva y especialmente de Mari Paz, Cristóbal, Rafa, María José, Lola, Cinta y José Antonio.

Me siento muy afortunado por poder haber disfrutado durante las estancias de investigación realizadas de una acogida sin igual. Durante mi tiempo en Denver pude formar parte de la familia de Rich Wanty, Diane y Rachel los cuales me hicieron sentir como en casa a pesar de estar a miles de kilómetros de mi hogar. Igualmente estaré eternamente agradecido a mi amigo Federico quien en varias ocasiones hizo de su casa mi hogar en USA. Dentro del USGS aprecio muchísimo la ayuda que me fue prestada por David Borrok, Phillip Verplank y Mike Pribil. También en USA he tenido la enorme suerte de trabajar con el grupo de nanogeociencias del profesor Mike Hochella. En especial me gustaría destacar todo lo aprendido en este campo gracias a Rebecca French así como la amistad que me ha brindado. En Newcastle tuve la suerte de poder trabajar con Adam Jarvis, Rommy Mathies, Jane Davis, Patrick Olmer y Gerardo González. Allí en Newcastle tuve la oportunidad de convivir con Esther Santofimia quien ha llegado a ser una gran amiga y con quien he discutido apasionadamente sobre la contaminación minera. De mi época en Barcelona guardo con enorme cariño la amistad con Patricia Acero, Mapi Asta y Clara Torrentó y de todo el personal del Jaume Almera quienes siempre estuvieron dispuestos a ayudarme en mis trabajos, así como de mis compañeros de piso Jorge y Sara. Igualmente he de agradecer su colaboración y amistad a María Clara Costa, Mónica Martins y María Alexandrino de la Universidade do Algarve quienes me han ayudado a introducirme un poco en el mundo de la microbiología.

Una tesis no sólo lleva detrás el trabajo investigador si no que depende mucho del ánimo y alegría en tu vida diaria para poder soportar la dureza psicológica que muchas veces implica este trabajo. Así, me parece ineludible valorar y agradecer el papel tan importante que muchas personas han tenido a la hora de apoyarme en mí día a día. En mi vida en Huelva María Cerrejón y Lourdes han sido dos grandes apoyos en los momentos malos y dos geniales aliadas en los buenos momentos. Igualmente son merecedores de mi mayor agradecimiento los muchos compañeros de piso que han logrado que cada año tuviera mi pequeña familia onubense, entre los que quisiera destacar a Juan Jesús (más que amigo familia tras 7 años de convivencia), a Marco, a

Abraham y a Fran. En Almonte no puedo olvidarme de mi amigo Javi y su inagotable energía fiestera, de Esther y su perseverancia por hacer de cada día un día feliz, y de otros tantos como Prieto, Alfredo, Oscar, Tyna, Rafa, Báñez, Irene, Luisa, Lisa y muchos más que supieron sacarme una sonrisa cuando más me hizo falta así como darme otra visión del mundo. No puedo dejar pasar esta ocasión para reconocer el importante papel que Oscar desde la distancia en Barcelona ha tenido a la hora de sacar de mí la mejor de las sonrisas y recordarme que si uno se lo propone puede ser por momentos el quinceañero más feliz. Incluyo aquí también el enorme cariño que Ana siempre me ha brindado y la alegría que me ha aportado mi "sobrinillo" Oscar.

Quisiera tener un agradecimiento especial para María, Francisco, Alfonsi y Curro, los cuales durante un periodo largo e importante de mi vida han sido una parte más de mi pequeña familia de Almonte y a los cuales he de agradecerle el que siempre hayan confiado ciegamente en mis posibilidades y me hayan animado y apoyado para conseguir alcanzar todas mis metas. Siempre tendré una deuda de cariño y gratitud con vosotros.

Para terminar me he reservado este párrafo para las cuatro personas más importantes de mi vida: mi padre, mi madre, mi hermana y mi cuñado. Ellos son el núcleo de mi familia y sin lugar a dudas mis más fervientes defensores. A mi padre le debo el poder sentirme orgulloso de la persona que soy pues su ejemplo ha sido el espejo en el que siempre he intentado verme. Conjuntamente con mi madre siempre me han inculcado el valor para afrontar los retos y la confianza para poder superarlos. Su esfuerzo conjunto y privaciones son las responsables de que siempre haya dispuesto del apoyo necesario para poder obtener todas mis metas. Mi madre y sus continuas riñas seguidas de su amor incondicional han sido el acicate sin el cual quizás me hubiera rendido en más de una ocasión. Me siento afortunado por tener a Estrella como hermana pues siempre ha sido el complemento que he necesitado en mi vida, dándome esa otra visión del mundo más artística, emocional y alejada de la ciencia. Sin lugar a dudas el que ella haya caminado en la vida siempre delante de mí me ha hecho más fácil y bello mí día a día. A Francisco he de agradecerle su apoyo en los malos momentos así como el abrirme los ojos a las otras realidades musicales y culturales de la vida sin las cuales esta tesis jamás se hubiera realizado en plazo pues me hubiera vuelto loco con tanta ciencia. Difícilmente pueda devolverles lo mucho que ya me han dado.

# CHAPTER 1. INTRODUCTION

Acid mine drainage (AMD) is an ancient and widespread environmental problem providing one of the most extreme and unique environments on the Earth. Polluted waters in mining areas typically exhibit low pH and high metal contents as a result of the sulfide dissolution taking place after the exposure of these minerals to the surface oxic conditions (Bigham and Nordstrom, 2000).

About 19,300 km of rivers and streams and more than 72,000 ha of lakes and reservoirs in the continental USA have been damaged by AMD (Kleinmann, 1989). In England and Wales, it is estimated that some 1,800 km of surface streams and rivers are currently impacted by AMD (Jarvis et al., 2006), whereas in SW Spain, from a total of 1149 km of the river network examined at the Odiel basin (Fig. 1.1), 427 km were affected by AMD (Sarmiento et al., 2009). These studies clearly present AMD water pollution as a widespread and intense environmental problem that, taking into account only three countries in the world, implies more than 21,500 km of rivers and streams affected.

The hydrochemistry and mineralogy of waters affected by AMD are mainly controlled by $SO_4$-Fe and $SO_4$-Al systems at pH ranging between 1–5 and 5–6, respectively

(Bigham and Nordstrom, 2000). $Fe^{3+}$ hydrolysis tends to buffer AMD pH to around 3.5 by the precipitation of schwertmannite according to the reaction:

$$8Fe^{3+} + xSO^{=-} + (16-2x)H_2O \leftrightarrows Fe_8O_8(OH)_{8-2x}(SO_4)_x + (24-2x)H^+ \quad (1.1)$$

where $1 \leq x \leq 1.86$, as shown by after Bigham et al. (1996) and Yu et al. (1999). Similarly, Al hydrolysis, with a pK1 = 5 and subsequent precipitation of hydrobasaluminite, $Al_4(SO_4)(OH)_{10} \bullet 15H_2O$, buffers AMD pH around a value of 5 (Bigham and Nordstrom, 2000). This hydrolysis reaction can be written as follows:

$$4Al^{3+}_{(aq)} + SO_4^{=}{}_{(aq)} + 25H_2O_{(l)} \leftrightarrows Al_4(SO_4)(OH)_{10} \cdot 15H_20_{(s)} + 10H^+_{(aq)} \quad (1.2)$$

The first part of this thesis discusses the applicability of a specific Sequential Extraction procedure (SE) and Differential X Ray Diffraction (DXRD) for the mineralogical characterization of AMD precipitates comprised primarily of poorly ordered iron and aluminum oxides and sulfates. This study was performed in the Monte Romero passive treatment system operated from August 2005 to June 2006 (Rötting et al. 2008b). This location was chosen because both schwertmannite and hydrobasaluminite are precipitated, and schwertmannite changes through months to goethite. Within this passive treatment system, it is possible to find all intermediate steps between different hydrochemical conditions during AMD neutralization.

The Iberian Pyrite Belt (IPB) (Fig. 1.1), located in the south-west of the Iberian Peninsula, can be considered one of the biggest massive sulfide provinces in the world with a length of over 200 km, a width of about 40 km and original estimated reserves in the order of 1,700 Mt of sulfide ore (Sáez et al., 1999). The result of the intense mining during almost 5,000 years (Leblanc et al., 2000; Nocete et al., 2005) is a region where abandoned sulfide-rich wastes in spoil heaps and tailings and flooded underground mines and opened pits generates an ubiquitous problem of AMD pollution (Nieto et al., 2007; Sarmiento et al. 2009).

Polluted mine waters can be remediated by two generic approaches, active or passive treatment (Johnson and Hallberg, 2005). While the former implies the use of energy and continuous addition of chemicals, the latter relies on natural water flow and biogeochemical reactions. AMD at abandoned mine districts is typically faced by the implementation of passive treatment technologies (Younger et al., 2002). Remediation techniques like permeable reactive barriers, vertical flow wetlands or aerobic wetlands

have been successfully employed to improve water quality in coal mining areas affected by AMD (Younger et al., 2002).

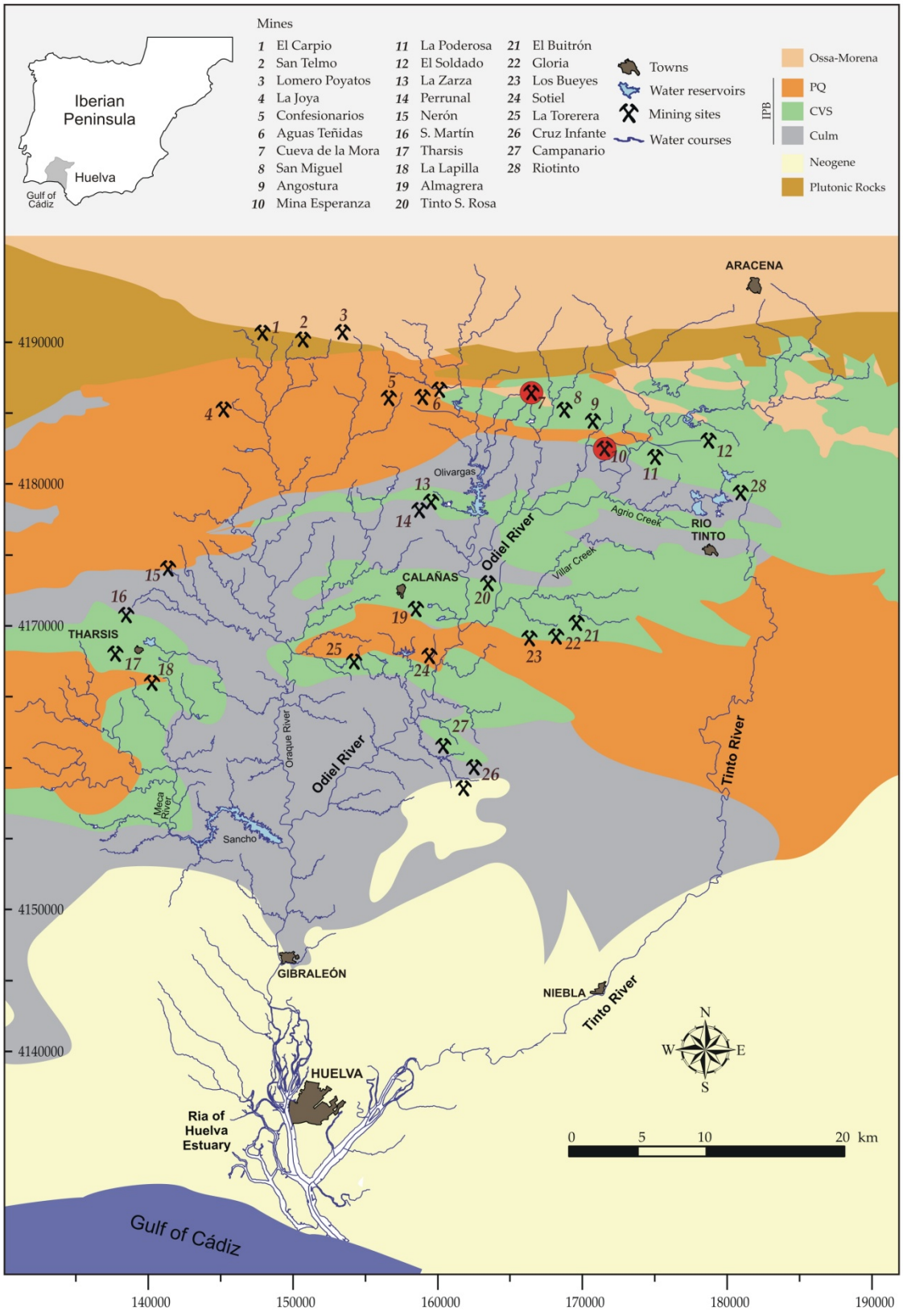


**Figure 1.1. Odiel watershed and main geologic units of the IPB. Modified after Sarmiento et al., 2009 with permission from the author.**

However, the high metal content observed in the AMD from the IPB severely reduces the efficiency of conventional passive treatment systems. To overcome the common clogging problems and losing of reactivity exhibit by traditional reactive substrates submitted to AMD with high metal contents, a novel reactive mixture known as Dispersed Alkaline Substrate (DAS) was developed (Rötting et al., 2008c).

DAS reactive mixture comprises an inert pine wood shavings matrix, to supply a high porosity and to reduce the problems of clogging, and a fine-grained reagent to increase water pH and substrate reactivity. This treatment philosophy lies in the use of two different alkaline reagents, limestone and MgO, to obtain pH values ranging from 6 to 7 and from 8 to 10, respectively. The pH range obtained at the treatment section using limestone induces Fe and Al precipitation and other metal removal by adsorption/coprecipitation processes (i.e. Cu, As, Pb, etc). Complementary, magnesium oxide dissolution buffers solutions between pH of 8.5 and 10.5, which is high enough to precipitate divalent metals such as Zn, Cd, Ni or Co.

Limestone-DAS has been successfully tested in a laboratory column study (Rötting et al., 2008a), where the chemical and hydraulic performance were investigated. A complementary field experiment in the IPB was also performed showing very promising results (Rötting et al., 2008b). During the operation time, this passive treatment system removed 90–100% Al, Cu, Pb and As, about 45% Fe and an average net acidity of 900 mg/L as $CaCO_3$ equivalents. The significant amount of unreacted limestone observed in the reactive tank when it was sampled showed the need for a new study to optimize the limestone-wood shavings ratio of the filling. Moreover, with the exception of Cu, the system did not remove divalent metals (Fe(II), Zn, Cd, Co, Ni, etc.). The work presented in the second part of this thesis is the continuation of these experiments, and the objective is to test the performance of a complete limestone and MgO-DAS remediation pilot plant using natural high metal concentration-AMD.

The third part of the thesis deals with the implementation of a full scale passive treatment system in Mina Esperanza. One of the biggest hurdles that a passive treatment system has to overcome is the long operating time necessary to make the system economically feasible (PIRAMID-Consortium, 2003). Clogging of the porosity and coating of the reactive grains with precipitates (passivation) are the two main operating factors controlling the lifetime of a passive treatment, and both of them depend on the amount of dissolved contaminants in the AMD. Due to the very high metal concentrations of the AMD in Mina Esperanza, this location was selected as representative of the high metal pollution typically observed at the IPB.

The main scope covered in Chapter 4 is to show the encouraging results obtained after 20 months of continuous operation of the full-scale DAS passive treatment system implemented at Mina Esperanza. Water hydrochemistry, precipitate mineralogy and metal removal efficiency of the different sections comprising the treatment were presented to gain a better understanding of the different hydrochemical, mineralogical and operational processes involved in highly polluted AMD remediation.

The last chapter (Chapter 5) of the third part of the thesis is devoted to the detailed study of the different mineralogical and hydrochemical processes controlling the long term performance of the limestone-DAS reactive substrate employed in the reactive tank of the Mina Esperanza passive treatment system. On the basis of the role played by precipitates in limestone consumption/passivation, hydraulic conductivity evolution and removal efficiency, some improvements to the original design are discussed.

## 1.1 THESIS OUTLINE

This thesis is composed of six chapters including the introduction. All the chapters are based on published papers or manuscripts that are under review by international peer-reviewed journals. The thesis has been structured in three parts corresponding to one of the aforementioned objectives.

Chapter 2 deals with the optimization of a Differential X-ray Diffraction and Sequential Extraction coupled technique for the mineralogical characterization of the poorly ordered Fe and Al precipitates commonly observed in AMD environments. The role and distribution of Fe and Al precipitates within the limestone-DAS reagent in the reactive tank at the Monte Romero passive treatment system is discussed.

Chapter 3 addresses the implementation of a complete limestone and MgO-DAS pilot scale passive treatment system in Monte Romero. The hydrochemistry and mineralogy of the different section comprising the passive system in Monte Romero as well as the hydraulic conductivity and metal removal performance and evolution are exposed in this chapter.

Chapter 4 and 5 handle the third objective of this thesis: the design and implementation of a limestone-DAS full scale and long term passive treatment system in Mina Esperanza. The study of the hydrochemistry, mineralogy and metal removal efficiency of the different sections comprising the treatment during its 20 months of operation is covered in Chapter 4. A detailed description of the different sections comprising the system and the remediating philosophy employed in each one is also offered. Chapter 5

is focused on the detailed study of the different mineralogical and hydrochemical processes controlling the long term performance of the limestone-DAS reactive substrate and on the role played by neoformed precipitates in limestone consumption/passivation, hydraulic conductivity evolution and removal efficiency.

Finally, Chapter 6 provides a summary of the main contributions of this thesis.

# PART 1. APPLICABILITY OF A SPECIFIC SEQUENTIAL EXTRACTION PROCEDURE AND DIFFERENTIAL XRD FOR THE MINERALOGICAL CHARACTERIZATION OF AMD PRECIPITATES

# CHAPTER 2. SEQUENTIAL EXTRACTION AND DXRD APPLICABILITY TO POORLY CRYSTALLINE FE AND AL PHASE CHARACTERIZATION FROM AN ACID MINE WATER PASSIVE REMEDIATION SYSTEM

***This chapter is based on the paper:*** **Caraballo, M.A., Rotting, T.S., Nieto, J.M., Ayora, C., 2009. Sequential extraction and DXRD applicability to poorly crystalline Fe- and Al-phase characterization from an acid mine water passive remediation system. American Mineralogist 94, 1029–1038**

## 2.1 ABSTRACT

Fe and Al precipitates play a very important hydrochemical and environmental role in aquatic environments affected by acid mine drainage. Despite their great importance, the reliable characterization of these precipitates usually presents many problems due to the high proportion of amorphous or poorly ordered mineral phases comprising these precipitates and because the coexistence with intermediate to highly crystalline phases. To facilitate and improve the characterization of poorly ordered Fe and Al phases, a coupled differential X-ray diffraction (DXRD) and sequential extraction (SE) study was performed on a set of samples from an acid mine water passive treatment system. By the use of these techniques, the presence of schwertmannite and goethite was shown in

the upper 5 cm of the passive treatment reactive material. Furthermore, a progressive decrease of the $SO_4^{=}$ adsorbed to the schwertmannite surface also was suggested by one of the SE steps. Concerning the Al precipitates, the presence of hydrobasaluminite and amorphous $Al(OH)_3$ was also suggested on the basis of SE and thermodynamic modeling analysis. These techniques also allow a quantitative estimation of the proportion of each mineral. As a result, a complete study of the distribution of each mineral throughout the reactive material profile and the role of each phase in removing metals from the mine water can be obtained. This information is useful not only to improve the reactive material design but also to understand the natural processes taking place in aquatic systems affected by mining.

## 2.2 INTRODUCTION

The hydrochemistry and mineralogy of waters affected by acid mine drainage (AMD) are mainly controlled by $SO_4$-Fe and $SO_4$-Al systems at pH ranges between 1-5 and 5-6, respectively (Bigham and Nordstrom 2000).

Fe(III) hydrolysis tends to buffer AMD pH around 3.5 by the precipitation of schwertmannite according to the reaction:

$$8Fe^{3+} + xSO^{=-} + (16-2x)H_2O \leftrightarrows Fe_8O_8(OH)_{8-2x}(SO_4)_x + (24-2x)H^+ \quad (2.1)$$

where $1 \leq x \leq 1.86$, as shown by after Bigham et al. (1996) and Yu et al. (1999).

In the same way, Al hydrolysis, with a pK1 = 5 and subsequent precipitation of hydrobasaluminite, $Al_4(SO_4)(OH)_{10}\bullet 15H_20$, buffers AMD pH around a value of 5 (Bigham and Nordstrom 2000). This hydrolysis reaction can be written as follows:

$$4Al^{3+}_{(aq)} + SO_4^{=}{}_{(aq)} + 25H_2O_{(l)} \leftrightarrows Al_4(SO_4)(OH)_{10}\cdot 15H_20_{(s)} + 10H^+_{(aq)} \quad (2.2)$$

The mineralogical control that both phases have on AMD hydrochemistry is not only restricted to pH buffering but also to some metal adsorption and coprecipitation processes. Accordingly, schwertmannite has been observed to play an essential role in the adsorption of As (Acero et al. 2006, Fukushi et al. 2004, Regenspurg and Peiffer 2005) and also a main role in the adsorption of Pb and Cu (Lee et al. 2002, Webster et al. 1998). Concerning hydrobasaluminite adsorption processes, an important decrease in

dissolved Cu and Cd have been reported in the presence of this mineral (Sánchez-España et al. 2006).

Many studies have been developed using synthetic schwertmannite (Eskandarpour et al. 2008, Loan et al. 2004) or pure natural schwertmannite especially collected from specific AMD precipitates (Bigham et al. 1996, Kawano and Tomita, 2001, Yu et al., 1999). However, the appearance of isolated schwertmannite in natural precipitates (Regenspurg et al. 2004) or in passive treatment systems (Gagliano et al. 2004, Rötting et al. 2008b) has been reported as quite uncommon.

Being a metastable phase, schwertmannite tends to transform by aging into goethite (Bigham et al. 1996, Burton et al. 2007, Jönsson et al. 2005, Knorr and Blodau 2007), jarosite (Wang et al. 2006) or both minerals (Acero et al. 2006), which implies that all these minerals are commonly found coexisting in mixed precipitates.

The distribution and higher intensity of jarosite and goethite diffractogram peaks compared to those of schwertmannite leads to a serious problem when a mixture of these minerals has to be characterized by X-ray Diffraction (XRD) because schwertmannite peaks are hidden by those of jarosite and goethite. To solve this problem, DRXD can be used (Dold 2003b, Schulze 1981, Singh et al. 1999). Nevertheless, this technique is not completely reliable for examining very poorly crystalline schwertmannite and sometimes needs to be supported by other analytical techniques.

Hydrobasaluminite is also a poorly crystalline phase, whose XRD diffractogram is difficult to relate with the mineral itself (Kim and Kim 2003). Thus, if this mineral belongs to a polymineral precipitate with more crystalline phases it is very difficult to detect even with DXRD.

Recently some studies of poorly and moderately crystallized sulfate and oxide minerals have been developed using new techniques like Visible Near-Infrared Reflectance (VNIR) (Alpers 2008, Bishop 2008), synchrotron XRD and XRF (Root et al. 2007) or X-ray Absorption Near-Edge Structure (XANES) (Alpers et al. 2008, Bishop 2008) and Extended X-ray Absorption Fine Structure (EXAFS) (Alpers et al. 2008, Chen and Jiang 2008). These studies determine not only the mineralogy of the sample but also the site occupied by the different elements in the mineral structure. However, these techniques are not easily available, thus it is desirable to have a previous general study of the samples for an efficient use of the beam time.

Sequential Extraction procedures are accessible and reliable techniques allowing a quantitative and qualitative mineralogical analysis of the sample but also a first insight into the elements distribution in the mineral structure. In this respect, the ability of many different SE procedures to elucidate the availability and general metal distribution on different mineral phases have been reliably demonstrated (Dold 2003b, Fanfani et al. 1997, Pueyo et al. 2008, Rodríguez et al. 2008, Terzano et al. 2007). On the other hand, although some reported works have related the specific Fe-precipitate mineralogy with the different amounts of dissolved iron and sulfur obtained by SE procedures (Dold 2003b, Fanfani et al. 1997, Hall et al. 1996, Li et al. 2007), it still remains necessary to perform new studies focused not only on Fe-oxide and Fe-sulfate minerals but also on Al-sulfate minerals in AMD environments.

Traditionally, studies about the interaction between AMD and passive treatment systems are focused on inflow and outflow water quality, paying no attention to detailed mineralogy developed inside the reactive material (Cocos et al. 2002, Jarvis et al. 2006, Johnson and Younger 2006, Kalin 2004, Kalin and Caetano Chaves 2003, Laus et al. 2007, Sapsford et al. 2007, Shin et al. 2008). The objective of the present work is to test the applicability of a specific SE procedure and DXRD for the mineralogical characterization of AMD precipitates mainly formed by poorly ordered iron and aluminum oxides and sulfates. The Monte Romero passive treatment system (Rötting et al. 2008b) was chosen as the best place to carry out this study because inside its reactive material schwertmannite and hydrobasaluminite precipitate, and the former ages to goethite. Within the passive treatment system, it is possible to find all the intermediate steps between different hydrochemical conditions during AMD neutralization.

## 2.3 MATERIALS AND METHODS

### 2.3.1 Field Site and Sampling Description

All samples used for this study were collected inside the reactive material of the Monte Romero pilot scale passive treatment system in July 2006. At that time the system comprised a cylindrical $3m^3$ reactive tank connected in series with three decantation ponds with an approximate volume of $6m^3$ each. Dispersed Alkaline Substrate (DAS) (Rötting et al. 2008b) was used as the treatment reactive material. This substrate was prepared by mixing 25% (v/v) calcite sand with 75% (v/v) pine wood chips.

The AMD emerging from one shaft of the Monte Romero underground mine was partially collected and channeled to the reactive tank by polyethylene pipes. Prior to the treatment operation, the AMD had a pH near 3.3, a net acidity of 1400–1600 mg/L as $CaCO_3$ equivalents and mean concentrations of 315 mg/L Fe (97% Fe(II)), 310 mg/L Zn, 270 mg/L Ca, 75 mg/L Al, 20 mg/L Mn, 1.5 mg/L Cu and 3200 mg/L sulfate (Rötting et al. 2008b).

During the vertical gravity flow of the AMD across the reactive material some hydrochemical changes occur. Calcite dissolution causes a rise in pH and the subsequent precipitation of schwertmannite (pH between 3 and 4.5) and Al-hydroxysulfates (at pH 5 to 5.5). The precipitation of schwertmannite in the decantation pond consumes the excess of alkalinity, produced by calcite dissolution inside the reactive material, also lowering water pH to values around 3-3.5, according to the reaction (2.1).

For the solid sampling, water flow was stopped and a 90 cm cross section was dug to have a view of the different precipitate layers developed inside the reactive material. From top to bottom, six levels were macroscopically detected by visual changes in color, shape and texture of the precipitates: 1) a friable reddish-dark brown level from 0 to 1 cm, 2) a dark orange level from 1 to 3 cm, 3) a light orange-yellowish zone from 3 to 5 cm, 4) a white-pinkish cemented zone from 5 to 15 cm, 5) a yellowish zone from 15 to 30 cm and finally 6) the apparently unreacted substrate from 30 to 90 cm.

In accordance to that, seven samples were taken to characterize not only the precipitates but also the transition zones between the main precipitate layers. The selected depths were: 0-1, 1-3, 3-5, 5-15, 15-20, 20-30 and 30-40 cm. Samples were oven-dried (40 ºC) until complete dryness (the high porosity of the samples implied that minor pore water was present before the oven-dried process) and were ground in a tungsten carbide mill for 2 min.

### 2.3.2 Analytical Methods

As a first approach to the constituent mineralogy of the samples an XRD study of randomly oriented powder samples was performed using a Bruker D5005 X-ray Diffractometer with Cu Kα radiation and fixed slit-width geometry for radiation incident upon the sample. Diffractometer settings were: 40 kV, 30 mA and a scan range of 3–70º 2θ, 0.05º 2θ step size and 20-s counting time per step.

DXRD is a suitable technique for determining the presence of poorly crystalline minerals in samples that contain a mixture of poorly to highly crystalline minerals. This technique involves the subtraction of a treated sample diffractogram from the diffractogram of the same sample prior to treatment (Schulze 1981). The selective dissolution of minerals changes the relative concentration of the remaining phases in the treated sample; therefore an intensity correction factor (k-factor) is applied to normalize both diffractograms during the subtraction.

The qualitative analysis of the different diffractograms obtained during this study was performed using XPowder (Version 2004.03, Martin 2004), a commercial software package for powder X-ray diffraction analysis.

In addition to the XRD and DXRD study, some gold coated samples and carbon coated polished sections were examined with a JEOL JSM-5410 scanning electron microscope (SEM) to observe the morphology of the constituent minerals. Energy dispersive spectrometry (EDS) was used to obtain a semi-quantitative compositional analysis of single crystals.

The metal concentrations of the different extractants obtained at each step of the SE were determined by Inductively Coupled Plasma Atomic Emission Spectrometry (ICP-AES Yobin-Ybon Ultima2). After every ten samples, standards were used to check the accuracy and possible instrument signal drifting. Due to the mineralogical approach of this study only Fe, Al, S and Ca will be presented, although some other metals were also measured. The detection limit for these four elements was always lower than 0.1 mg/L (0.001 mg/g for the SE in terms of the solid phase concentration).

Saturation indices (SI = logIAP - logK; IAP = ion activity product) of possible minerals with respect to pore water element concentrations (Rötting et al. 2008b) were calculated using PHREEQC (Parkhurst 1995) and the WATEQ4F database (Ball and Nordstrom 1991). Additional thermodynamic data for schwertmannite was taken from Yu et al. (1999).

In order to perform DXRD the SE was performed on multiple replicates (between 2 and 4 as a function of the SE step). These replicates allowed evaluating the procedure reproducibility. Variation coefficients for Al, Fe, Ca and S were always lower than 10%.

### 2.3.3 Sequential Extraction Procedure

The four essential factors defining a SE procedure are: chemicals employed for the extractants, solid-extractant volume ratio, time and nature of the contact between the solid sample and the extractant and environmental conditions during each step of the extraction sequence.

For almost all the minerals concerning this study (gypsum, calcite, schwertmannite and goethite) appropriate selective extractants and careful studies of experiment environmental conditions have been conducted (Dold 2003b, Fanfani et al. 1997, Hall et al. 1996, Sahuquillo et al. 2003, Stumm and Sulzberger 1992). However, to successfully apply these studies to samples with high concentrations of iron oxides and iron oxyhydroxysulfates (e.g. AMD Fe-stromatolites or Fe-precipitates from passive treatment systems) some changes to the sample-extractant volume ratio and the time and nature of contact are needed.

No previous studies of hydrobasaluminite selective extractants have been reported. Therefore, it was decided to subject the samples hosting this mineral to the specific SE steps designed for Fe(III) minerals.

The different SE steps conducted in this study with the type and amount of extractant, the amount of sample and the experiment environmental conditions are summarized in Table 2.1. A more detailed explanation of the selected experimental conditions and a brief description of the expected information offered by each step of the SE are presented here.

*1)* *Water soluble fraction*: Due to the importance of secondary sulfates and other salts in AMD environments, an initial water extraction step is essential for a complete understanding of these environments. This step has a double function, on the one hand the water composition after dissolution of secondary sulfates and other salts reflects the portion of easily available contaminants, and on the other hand these minerals usually appear as well-crystalline phases which is a problem if coexisting poorly crystalline phases are to be detected by XRD (the most intense diffractogram peaks of the former mask the weaker peaks of the latter).

To ensure complete dissolution of all water-soluble minerals present in our samples, a twelve-hour shaking period was selected.

**TABLE 2.1.** Sequential extraction procedure developed for this study.

| Sequential extraction step | Preferentially dissolved minerals | Dissolved phases (in this study) | Elements released to the solution |
|---|---|---|---|
| ***1) Water soluble fraction:*** 200 mg of sample and 20 ml deionizied water, shake for 12 h at room temperature (RT) | Secondary sulfates and other salts | Gypsum | Ca and $SO_4^{2-}$ |
| ***2) Sorbed and exchangeable fraction:*** 20 ml of 1 M $NH_4$-acetate (4.5 pH buffer), shake for 1 h at RT | Calcite and some clay minerals | Calcite | Ca and adsorbed elements |
| ***3) Poorly ordered Fe (III) oxyhydroxides and oxyhydroxysulfates:*** 20 ml of 0.2 M $NH_4$-oxalate (3 pH buffer), 30 minutes shake in darkness and at RT | Mainly Schwertmannite and 2-line ferrihydrite | Schwertmannite, hydrobasaluminite and gibbsite | Fe, Al and $SO_4^{2-}$ |
| ***4) Highly ordered Fe (III) hydroxides and oxides:*** 20 ml of 0.2 M $NH_4$-oxalate (3 pH buffer), 80 ºC water bath for 1h | Goethite, jarosite, 6-line ferrihydrite and hematite | Goethite | Fe |
| ***5) Residue digestion:*** 3 ml of $HNO_3$ + 7.5 ml of HF + 2.5 ml of $HClO_4$ | Silicates | Residue (wood chips) | Organic elements |

*2) Sorbed and exchangeable fraction*: This step has an important role in the study of samples with carbonate minerals because the complete dissolution of calcite and other carbonates takes place during NH4-acetate leach (Fanfani et al. 1997, Hall et al. 1996, Tessier et al. 1979). Due to the high crystallinity of these minerals a complete dissolution of them is necessary if a DXRD for the study of poorly ordered phases is to be conducted.

This step also extracts elements that are adsorbed to mineral surfaces (Dold 2003b, Hall et al. 1996). This knowledge is essential to understand the distribution of some elements (e.g. S as $SO_4^{=}$) in the structure of some minerals (schwertmannite, goethite and hydrobasaluminite in our study), and is important to characterize the availability of some metals.

In this step the 1M NH4-acetate solution was buffered to pH 4.5 by the addition of acetic acid. Five different ratios of solid sample: liquid extractant were selected (in mg/ml): 50:1, 10:1, 5:1, 2.5:1 and 1:1. To have an idea of the effect of reaction time on schwertmannite stability at this pH, two different reaction times were employed during the SE calibration study: two hours for sample 50:1 and one hour for samples 10:1 to

1:1 (Fig. 2.1). As can be observed, the reduction of the reaction time implies a significant decrease on the dissolved iron for this step.

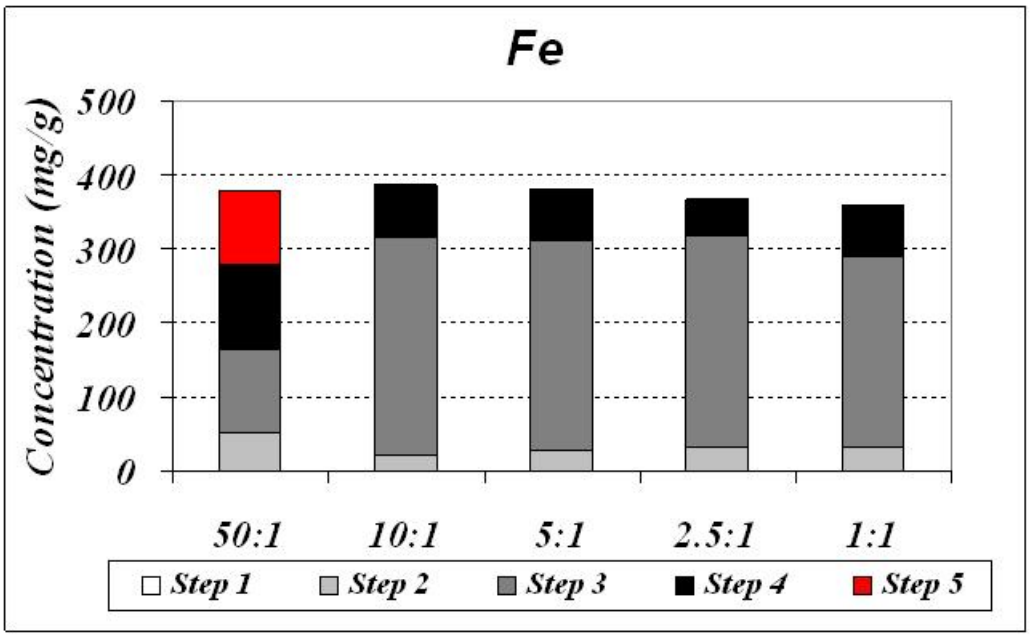


**Figure 2.1. Iron concentration obtained in the different steps of the SE calibration study carried out for the 0-1 cm sample. Different subsamples are labelled by the solid:extractant ratios in mg/ml. Two and one hour reaction times were tested for samples 50:1 and 10:1 to 1:1, respectively.**

*3) Poorly ordered Fe (III) oxyhydroxides and oxyhydroxysulfates*: The specificity and well documented behavior of 0.2M NH4-oxalate for schwertmannite dissolution makes this extractant the best candidate for the study of our samples (Dold 2003a, 2003b, Gagliano et al. 2004, Kumpulainen et al. 2007).

A deep and exhaustive study of the dissolution kinetics of schwertmannite and a proposal for two different SE steps focusing on the specific dissolution of schwertmannite and goethite can be found in Dold (2003a, 2003b). Therefore, it was decided to use the proposed steps for schwertmannite and goethite selective dissolution; however, a preliminary study of the sample-extractant volume ratio was necessary to adjust that procedure to pure schwertmannite or samples with high schwertmannite content.

The results of this calibration study (Fig. 2.1) clearly show that the ratio 50:1 is too high to achieve the complete dissolution of schwertmannite during SE step three, with some schwertmannite remaining after the final digestion step. Although all the other ratios tested lead to the complete dissolution of schwertmannite in the third step of the SE, the total amount of extracted iron decrease observed with the solid:solution ratio. For this

step of the extraction sequence, a ratio of 10:1 was selected to conduct the study of Monte Romero precipitates. Thirty minutes reaction time was selected, based on previous studies (Bigham et al. 1996, Dold 2003b).

*4) Highly ordered Fe (III) hydroxides and oxides*: The study of more crystalline iron precipitates (goethite in this case) was carried out using a SE step presented previously by Dold (2003b). As in step 3 the extractant used was 0.2M $NH_4$-oxalate but in this case the samples were exposed to light and heated to 80ºC in a water bath.

During the different SE experiments carried out for this study, it was observed that the complete dissolution of goethite took place after thirty minutes of digestion. Therefore, the sample-extractant contact time for this step was set to one hour to ensure complete goethite dissolution.

*5) Residue digestion*: After the first four SE steps, the samples used in this study consist almost completely of residual organic material (wood chips) with no expected mineral remaining, with the possible exception of a small residual fraction of detrital and atmospheric particulate (quartz and clays). In accordance to that, the digestion procedure developed for the total digestion of samples with organic and inorganic compounds were selected (Querol et al. 1996). The different acids used at this digestion were HF, to ensure the complete dissolution of the inorganic materials, and $HClO_4$ and $HNO_3$ dissolving the organic material.

## 2.4 RESULTS AND DISCUSSION

### 2.4.1 Mineralogical characterization of the reactive tank

As explained above, six different levels were visually detected during the sampling of Monte Romero DAS-reactive material.

*Layer 1*: *(0-1 cm, friable, reddish-dark brown)* This thin layer is developed at the contact between the supernatant AMD and the DAS-reactive material, where the solution pH is between 3 and 4 (Rötting et al. 2008b). At this pH range and with the metal composition of this water it is reasonable to assume that schwertmannite is the main precipitate mineral. This hypothesis is also suggested by the SI for schwertmannite and goethite (Table 2.2). Another important observation was the complete absence of wood chips in the precipitates that suggests an upward growth of this layer (from the surface of the reactive material to the supernatant water).

**TABLE 2.2.** Saturation index (SI) values for the most probable Al and Fe precipitates in the Monte Romero reactive tank profile

| Depth (cm) | $Al(OH)_3$ | Basal | Gibb | Gt | $Fe(OH)_3$ | Sch | Gyp |
|---|---|---|---|---|---|---|---|
| -5 | -6.1 | -11.8 | -3.4 | 4.0 | -1.9 | 8.9 | -0.4 |
| 5 | -2.6 | -0.1 | 0.1 | 4.7 | -1.2 | 11.6 | -0.2 |
| 10 | -1.8 | 2.3 | 0.9 | 5.4 | -0.5 | 16.5 | -0.1 |
| 15 | -0.1 | 7.5 | 2.6 | 6.4 | 0.5 | 23.2 | -0.1 |
| 20 | 0.6 | 9.5 | 3.3 | 6.2 | 0.3 | 20.5 | 0.0 |
| 35 | 0.7 | 9.9 | 3.4 | 6.2 | 0.3 | 20.2 | 0.0 |
| 50 | 1.0 | 10.3 | 3.6 | 5.4 | -0.5 | 13.8 | 0.0 |
| 80 | 0.7 | 9.4 | 3.4 | 5.2 | -0.7 | 11.7 | 0.0 |
| 90 | 0.9 | 9.9 | 3.6 | 6.3 | 0.4 | 20.2 | 0.0 |
| 100 | 1.0 | 10.0 | 3.7 | 6.7 | 0.8 | 23.0 | 0.0 |

Calculations were performed with PHREEQC 2.7 using hydrochemical data for May 2006 previously presented by Rötting et al., 2008b.
$Al(OH)_3$ = amorphous $Al(OH)_3$, Basal = Basaluminite, Gibb = Gibbsite, Gt = Goethite,
$Fe(OH)_3$ = amorphous $Fe(OH)_3$, Sch = Schwertmannite and Gyp = Gypsum

The first XRD approach to the mineralogical composition of this layer showed a very weak diffractogram with a broad peak centered at 35º 2θ and a clearer 4.18 Å goethite peak (Fig. 2.2, raw sample). To resolve the different peaks belonging to this 35º centered broad peak, the samples were submitted to all the steps of the SE procedure taking away a subsample for XRD analysis at steps 2 and 3. As shown in Fig. 2.2, after NH4-acetate attack (step 2) the diffractogram pattern of the sample remained unaltered. However, when the sample was treated with oxalate (step 3) the diffractogram pattern was substantially altered, and a clear and well-defined goethite diffractogram appears.

To determine which phases were dissolved in the sequential steps, a DXRD study was conducted using diffractograms of the raw sample and that after SE step 3. A K-factor of 0.8 was applied to the step-3 diffractogram to normalize the relative mineral concentration of both samples. The resulting diffractogram is shown in left upper part of Fig. 2.2 where the presence of schwertmannite was revealed by a well-defined 2.54 Å peak.

Although this observation seems to reliably determine the presence of schwertmannite, it is not completely conclusive because 2-line ferrihydrite has its main diffractogram peak at 2.54 Å and is selectively dissolved by NH4-oxalate as well (Dold 2003b). To resolve this issue, a SEM-EDS analysis of the sample was carried out where both

images of the characteristic "pincushion" or "sea-urchin" morphology of schwertmannite and semi-quantitative chemical analysis were obtained (Fig. 2.2).

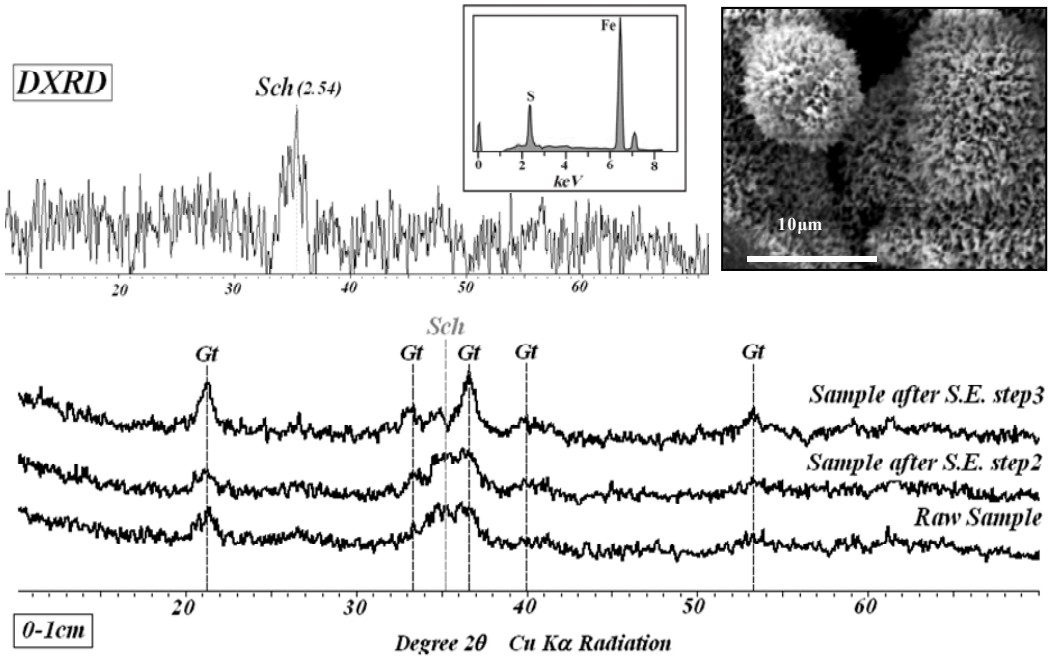


**Figure 2.2. Mineralogical characterization of sample 0-1 cm by XRD, DXRD and SEM-EDS. Gt = Goethite, Sch = Schwertmannite.**

For the SE analysis, a summary of Fe, Al, S and Ca concentrations for each sample, obtained at the different SE steps, is presented in Fig. 2.3. More than a 75% of the total iron was released in step 3. Schwertmannite probably is the mineral phase responsible for most of the iron removed from this layer. Examination of the S released throughout the SE steps revealed that 72% of the schwertmannite S was put into solution in step 2, while the 28% remaining was released during step 3. Taking into account this observation and similarity of the diffractograms of raw and step-2 samples, it can be reliably assumed that no crystalline phase was dissolved during step 2. The amount of S extracted in step 2 suggests that 72% of schwertmannite compositional S is adsorbed to the mineral surface while only 28% is strongly fixed within the crystal structure. This double distribution of S (as $SO_4^{=}$) at the surface and in the inner structure of schwertmannite has been previously reported (Bigham et al. 1990, Jönsson et al. 2005, Webster et al. 1998), however, the amount of adsorbed S reported by them ranged from 30-35% (Bigham et al. 1990, Jönsson et al. 2005) to as high as 60% (Webster et al. 1998), but not as high as the 72% found here. The adsorption of $SO_4^{=}$ also has been

reported to take place at the surface of goethite, but always at nearly insignificant levels when schwertmannite is present (Webster et al. 1998).

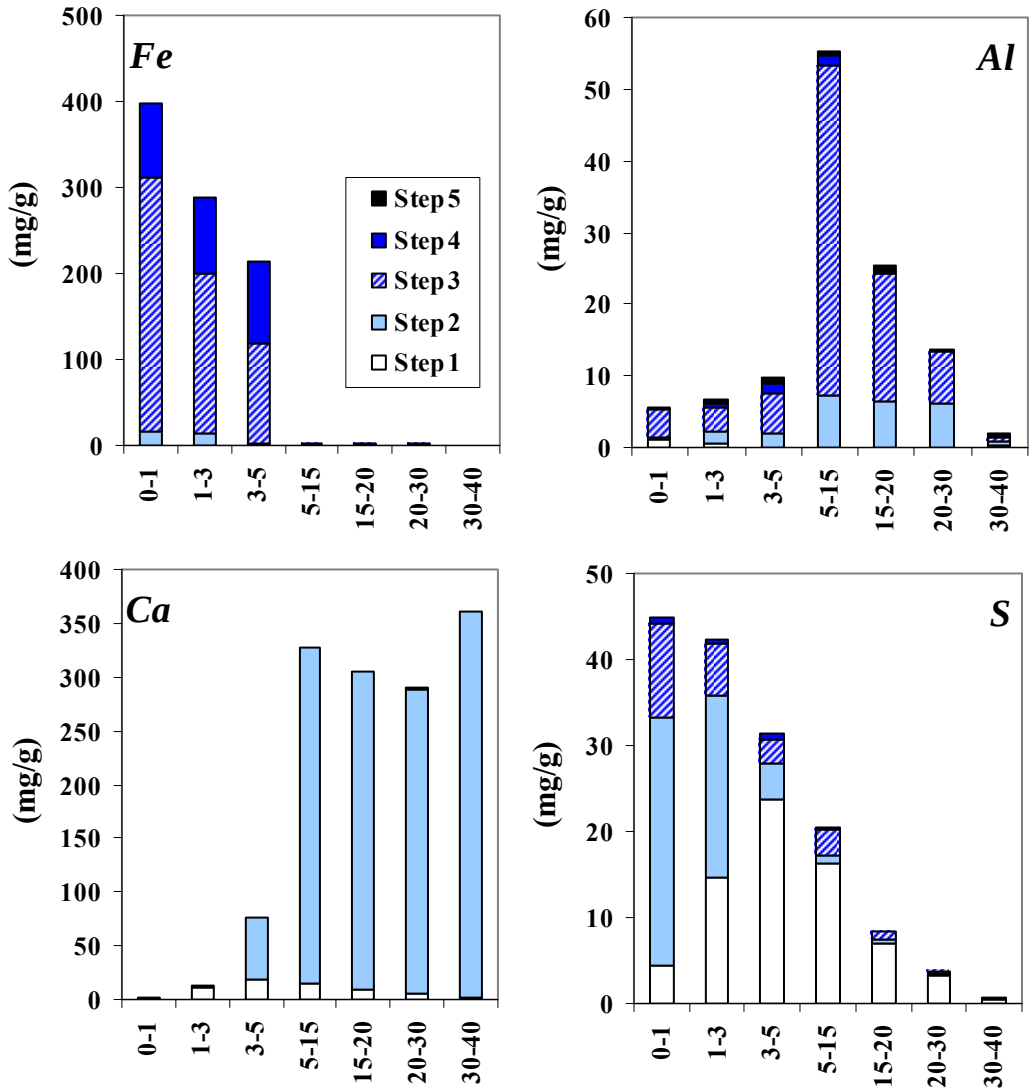


**Figure 2.3. Distribution of Fe, Al, S and Ca concentrations throughout the sample profile on the basis of the SE study.**

The (Fe/S) molar ratio of schwertmannite present in the different representative samples of the iron precipitation zone and the resulting schwertmannite compositional formula for each sample are shown in Table 2.3. The (Fe/S) molar ratio of 4.44 and the schwertmannite stoichiometry, $Fe_8O_8(OH)_{4.4}(SO_4)_{1.8}$, obtained for this sample are identical to the values obtained for the precipitates forming in terraces surrounding the Monte Romero shaft (Acero et al. 2006). Schwertmannite sulfate stoichiometry of this sample is higher than the one proposed by Bigham et al. (1996), but in good agreement with the range of 1.74-1.86 suggested by Yu et al.(1999).

**TABLE 2.3.** Comparison between schwertmannite formula and (Fe/S) molar ratio proposed in the literature and schwertmannite formula and $(Fe/S)_{molar}$ ratio obtained in this study.

| Sample | Fe (mmol/g) steps 2-3 | S (mmol/g) steps 2-3 | X value | Mineral formula | (Fe/S) molar ratio |
|---|---|---|---|---|---|
| Schwertmannite | | | $1^{*} \leq x \leq 1.86^{\#}$ | $Fe_8O_8(OH)_{8-2x}(SO_4)_x$ | 4-8[§] |
| 0-1cm | 5.562 | 1.253 | 1.80 | $Fe_8O_8(OH)_{4.39}(SO_4)_{1.8}$ | 4.44 |
| 1-3cm | 3.576 | 0.861 | 1.93 | $Fe_8O_8(OH)_{4.15}(SO_4)_{1.93}$ | 4.15 |
| 3-5cm | 2.110 | 0.226 | 0.86 | $Fe_8O_8(OH)_{6.28}(SO_4)_{0.86}$ | 9.33 |

X value defines the possible amounts of $(SO_4)$ and (OH) in the schwertmannite compositional formula.
* (Bigham et al., 1996)
# (Yu et al., 1999)
§ (Bigham and Nordstrom, 2000)

*Layer 2: (1-3 cm, dark orange-brown)* This level was the first one developed inside the DAS-reactive material. The XRD analysis for the raw sample (Fig. 2.4) clearly showed the presence of goethite and also suggested the presence of gypsum whereas almost no peaks of schwertmannite were detected. But, subsequently, when the DXRD analysis was performed using sample 1-3 cm after step 2 (to avoid the presence of gypsum) and after step 3, with a K-value of 0.85, the occurrence of schwertmannite was revealed (Fig. 2.4).

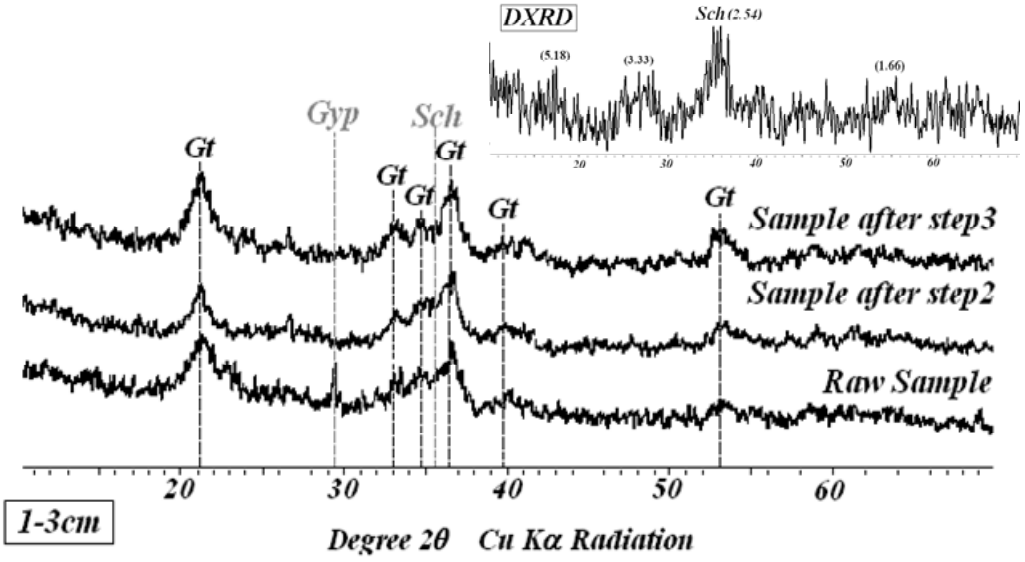


**Figure 2.4. Mineralogical characterization by XRD and DXRD of sample 1-3 cm. Gt = Goethite, Sch = Schwertmannite, Gyp =Gypsum.**

The SE analysis for this sample showed a very similar schwertmannite composition compared to the schwertmannite from layer 0-1 cm (Fig. 2.3), showing 75% adsorbed $SO_4^{=}$ and a (Fe/S)molar ratio of 4.15 (Table 2.3). On the basis of released S and Ca in step 1, the presence of gypsum can be confirmed to appear in this layer. This observation is supported by the previously reported presence of this mineral in the raw

sample diffractogram and by the disappearance of this peak in the 1-3 cm diffractogram following SE step 1.

*Layer 3: (3-5 cm, light orange-yellowish)* This layer corresponds to a hydrochemical transition zone between Fe-rich and Al-rich precipitates, thus any of the mineral phases found in this study could be present in this layer. Initial XRD analyses of the constituent mineral phases of this layer (Fig. 2.5) revealed the unequivocal presence of goethite, gypsum and calcite, although no peaks of schwertmannite or hydrobasaluminite were observed even with DXRD.

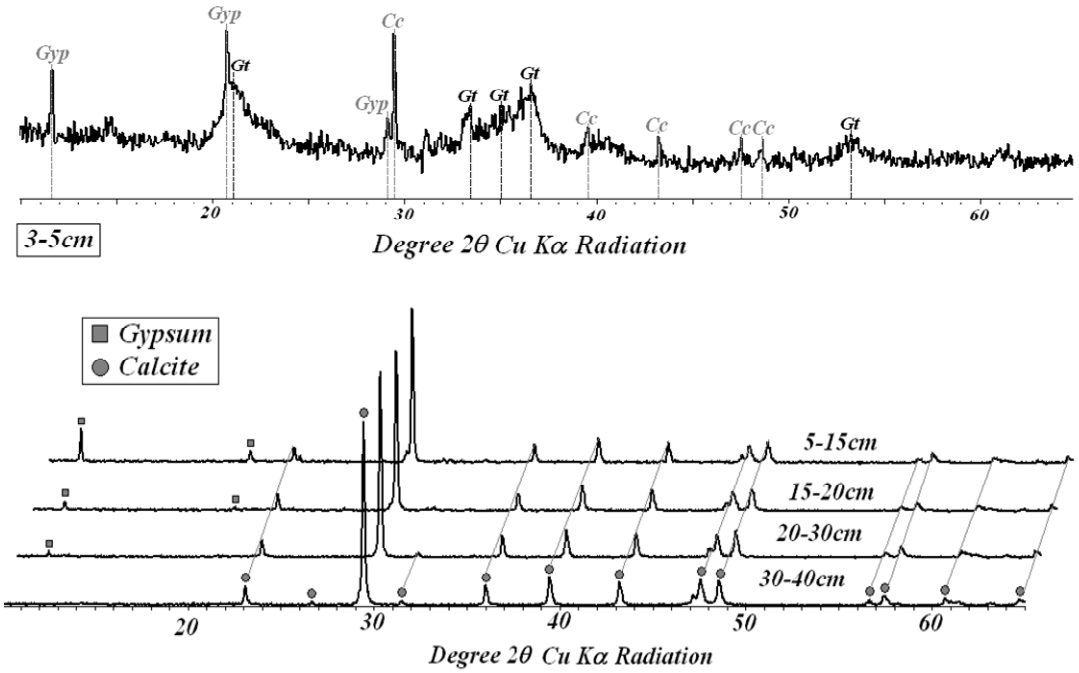


**Figure 2.5. XRD diffractograms for four selected subsamples from 3 to 40 cm. The dominant peaks for the different mineral phases found in each sample have been labelled. Gt = Goethite, Gyp = Gypsum, Cc = Calcite.**

Although the presence of schwertmannite could not be confirmed by the use of X-ray techniques, the amount of iron released in step 3 (Fig. 2.3) suggested the presence of a small amount of this mineral. Examination of released S in step 2 revealed an important decrease of adsorbed $SO_4^{=}$ compared to the concentrations found in the upper levels of the reactor. If schwertmannite occurs in this layer, the (Fe/S) molar ratio (9.33) and the stoichiometry ($Fe_8O_8(OH)_{6.28}(SO_4)_{0.86}$) are different in this level than elsewhere in the reactor. This is the first level in which the presence of calcite has been reported (Fig. 2.5). Taking into account this observation, it is reasonable to assume that due to the presence of this calcite the pH of the AMD at this point is higher compare to layer 2. As

a result of this pH increase, the surface of schwertmannite could be partially occupied by OH- anions, which compete for adsorption sites with $SO_4^=$ (Langmuir 1997).

Examination of the aluminum concentrations obtained in the SE revealed, as expected, a small increase of this element in this layer (Fig. 2.3). Due to the great variety of minerals precipitated in this level and the small amount of Al-precipitates present, a determination of the specific mineral phases responsible for the Al removal was impossible even with SE data. However, on the basis of the hydrochemical data of a previous study (Rötting et al. 2008b) and according to the literature (Bigham and Nordstrom 2000, Nordstrom 1982, Sánchez-España et al. 2006, Sánchez-España and Trevor 2007) hydrobasaluminite is suggested to be the most probable Al-phase precipitated within this layer.

*Layer 4: (5-15 cm, "cemented", white-pinkish)* When this layer was sampled, a significant amount of white-pinkish precipitates filling substrate pores and on surfaces of calcite and wood chips was observed. The presence of these precipitates cemented the reactive material in the DAS layer.

Only gypsum and calcite were detected by XRD (Fig. 2.5) and no evidence of any crystalline or poorly crystalline Al-phase was observed even with DXRD. The fact that a large amount of aluminum was removed from solution in this level suggests that poorly ordered or amorphous Al-phases must be present. This hypothesis is also supported by SEM-EDS observations (Fig. 2.6), where gypsum and an Al-hydroxysulfate were seen to be closely precipitated around calcite grains. In some cases, it appears that excess Ca due to calcite dissolution promotes gypsum precipitation at its surface (Booth et al. 1997, Rötting et al. 2008b) with a later Al-hydroxysulfate precipitation on top (Fig. 2.6 A-B). By contrast, direct precipitation of Al-hydroxysulfate on calcite surfaces (Fig. 2.6 A) has also been observed, suggesting that both Al-hydroxysulfate and gypsum can precipitate directly on the calcite surface. Saturation indexes (Table 2.2) show the pore water saturation with amorphous $Al(OH)_3$, basaluminite and gibbsite.

In the SE of this sample, an important amount of Al was released during step 3. The molar ratio of aluminum to sulfur in this level was as high as 16 while the theoretical Al/S molar ratio for basaluminite or its precursor hydrobasaluminite is 4. All of these results suggest the presence of at least two amorphous or poorly crystalline Al-phases.

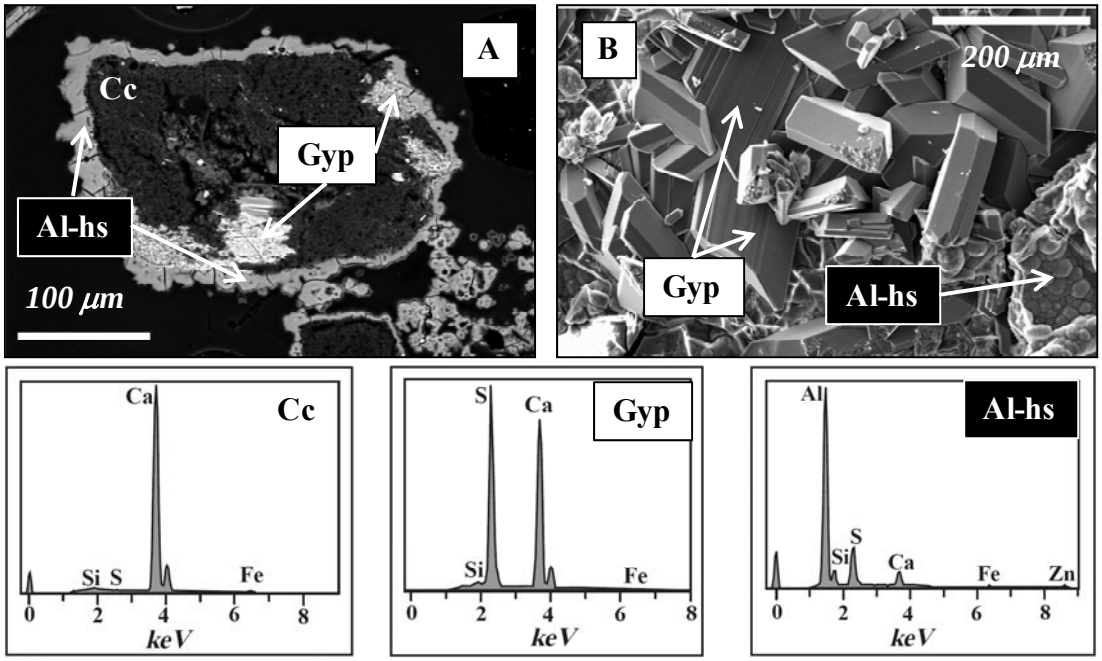


**Figure 2.6. A) SEM image of a calcite grain surrounded by Al-hydroxysulfate (hydrobasaluminite?) (gray) and gypsum (bright white) precipitates. B) Euhedral crystals of gypsum (centre) and amorphous precipitates of Al-hydroxysulfate (lower-right corner of the image). At the bottom of these two images three EDS elemental spectra (calcite = "Cc", gypsum = "Gyp", and Al-hydroxysulfate = "Al-hs") obtained for some of the detected minerals are shown.**

The presence of hydrobasaluminite as the main Al-hydroxysulfate to precipitate in AMD waters at pH 5 has been proposed in some previous studies (Sánchez-España et al. 2006, Kim and Kim 2003, Bigham and Nordstrom 2000) but this mineral is known to dehydrate irreversibly to basaluminite after a few days exposure in the laboratory or even a few hours after X-rayed (Geomare 2004). Taking into account the observed instability of hydrobasaluminite respect to basaluminite, the former would be the Al-hydroxysulfate developed inside the reactive tank while the latter would be the mineral phase actually present in our dried samples. Some studies have reported the coexistence of basaluminite and gibbsite (Nordstrom 1982) and the presence of gibbsite as an aging product of other metastable Al-phases (Berkowitz et al. 2006, Berkowitz et al. 2005, Nordstrom 1982, Sims and Ellis 1983). However the fact that no gibbsite peaks were observed in XRD or DXRD and the moderate to high crystallinity usually shown by this mineral phase, makes unreasonable to assume the presence of this mineral. All the observations exposed (the absence of any Al crystalline phase in XRD, saturation index of amorphous $Al(OH)_3$ close to equilibrium in 15 cm depth pore water and Al/S ratio too high to correspond to any single Al-hydroxysulfate mineral) could be attributed to the presence of amorphous $Al(OH)_3$ together with hydrobasaluminite.

Only a small amount of Al was released during extraction with pH 4.5 NH4-acetate (step 2), showing that this phase is stable at pH below 5, as opposed to the above cited previous studies.

*Layer 5: (15-20 cm and 20-30 cm, yellowish)* This layer was selected based on its color and texture as a different precipitate layer, however XRD and SE analysis revealed that, this layer represents the progressive transition from the upper part of the Al-precipitates level to the unreacted material. As in layer 4, the presence of gypsum and calcite was detected by XRD (Fig. 2.5) and the appearance of hydrobasaluminite and amorphous $Al(OH)_3$ could be suggested, although in this case the amount of Al removed decreases dramatically from the top of this layer towards the unreacted material below (Fig. 2.3).

*Layer 6: (30-40 cm, apparently unreacted substrate)* As expected, this layer corresponds to the unreacted original material where only the presence of calcite was detected by XRD (Fig. 2.5) and SE analysis (Fig. 2.3).

### 2.4.2 General distribution of the precipitates inside the reactive tank

The distribution of precipitates and the role of each mineral in metal removal are synthesized in Fig. 2.7. Inspection of the element removal profiles (Fig. 2.7) clearly shows the presence of two distinct Fe and Al precipitation horizons with a broader gypsum zone.

Detailed inspection of the Fe horizon (0-5 cm) shows that although the mass of goethite in the samples was considerably greater than that of schwertmannite (Table 2.4), the latter was the mineral phase responsible for most of the iron removal (Fig. 2.7B), because each mg of schwertmannite has eight times more iron than a mg of goethite due to each mineral stoichiometry. This mineral proportion also was observed in the XRD analyses for sample 0-1, 1-3 and 3-5 cm (Fig. 2.2, 2.4 and 2.5), where detection of schwertmannite prior to DXRD analysis was impossible due both to the lower crystallinity and concentration of schwertmannite with respect to goethite. The amount of precipitated iron progressively decreased from the top to the bottom of the Fe horizon (Fig. 2.7). Another important result of the SE study of the iron levels was the progressive decrease of $SO_4^{=}$ adsorbed onto schwertmannite with depth (Fig. 2.3). This cannot be displayed in Fig. 2.7B because $SO_4^{=}$ adsorption is overprinted by gypsum precipitation.

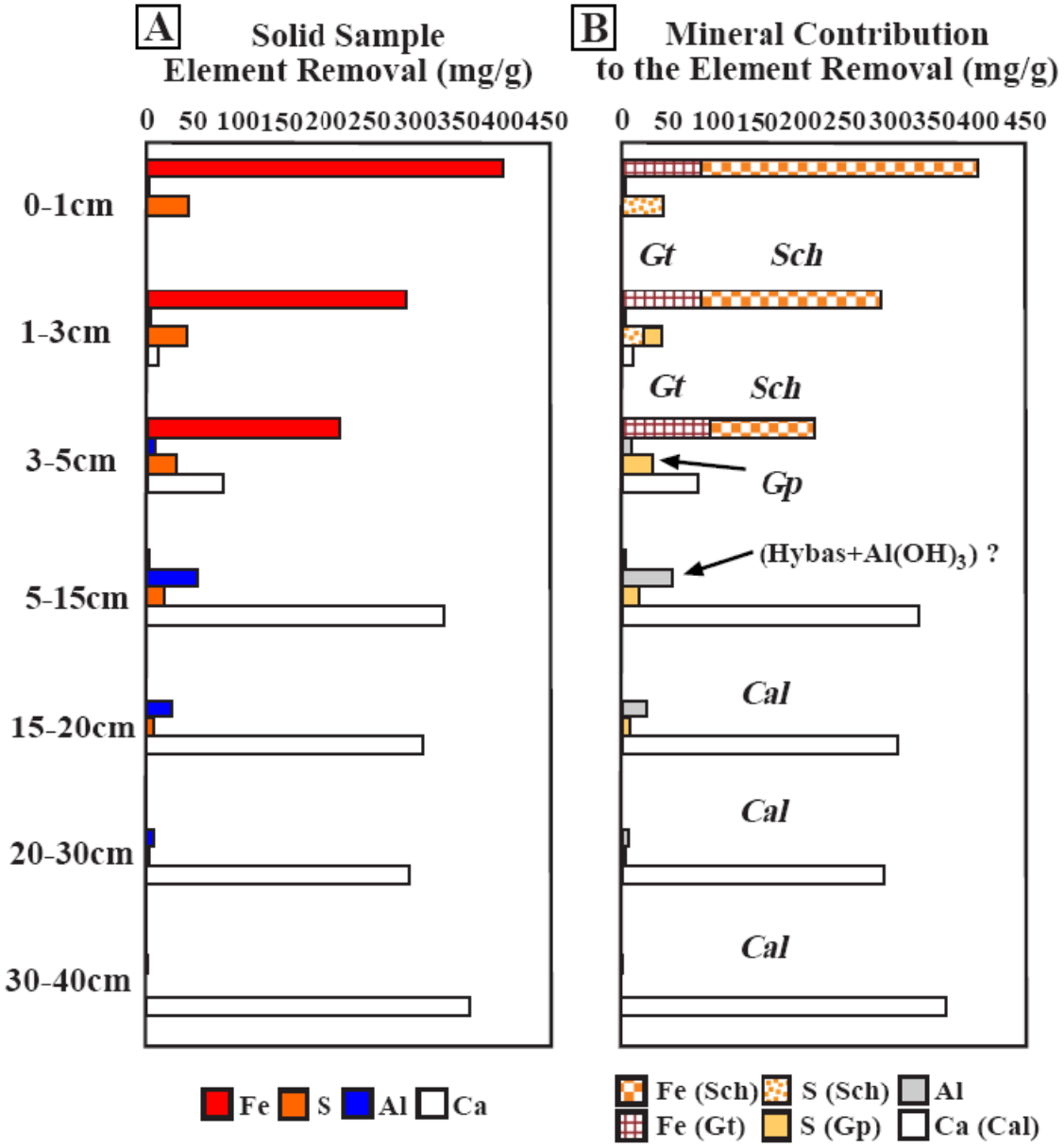


**Figure 2.7. Element removal (left diagram) and mineral contribution to the metal removal (right diagram) across the Monte Romero reactive tank profile. Gt = Goethite, Sch = Schwertmannite, Gyp =Gypsum, Hybas = Hydrobasaluminite, Al(OH)3 = amorphous Al(OH)3, Cc = Calcite. The different areas drawn on the right diagram correspond to the depth evolution of the amount of each element attributed to the different mineral phases.**

Gypsum was found throughout the reactor system, however, a detailed inspection of the analyses showed that this mineral formed almost an independent level superimposed on the Fe and Al levels. From the results of S dissolved in step 1 of the SE (Fig. 2.3), the concentration of gypsum increases throughout the Fe level until reaches its maximum at the boundary between the Fe and Al level, and it decreases downward through the Al level (Fig. 2.7B). This distribution could be the result of gypsum formation by combination of Ca released by calcite dissolution with $SO_4^{=}$ from the acidic mine drainage. The absence of gypsum at the top of the sequence (0-1cm) is consistent with

the direct precipitation of schwertmannite (and its aging product goethite) from the supernatant AMD.

**TABLE 2.4.** Iron layer mineral distribution.

| Sample | Sch (wt%) | Gt (wt%) | Gyp (wt%) | Cc (wt%) |
|---|---|---|---|---|
| 0-1 cm | 30.3 | 68.3 | 1.4 | 0.0 |
| 1-3 cm | 19.2 | 67.5 | 12.5 | 0.8 |
| 3-5 cm | 6.7 | 44.2 | 11.6 | 37.5 |

Mineral weight percentages were calculated using the data obtained for each mineral at the specific steps of the sequential extraction performed. Sch = schwertmannite; Gt = goethite; Gyp = gypsum and Cc = calcite

The distribution of Al precipitates has a number of similarities to the distribution of Fe precipitates. The amount of Al removal progressively decreased from the top to the bottom of the Al-horizon (Fig. 2.7A). Another similarity is that in both cases a single Fe or Al hydroxysulfate phase is not sufficient to explain the removal of these metals. However, while the presence of schwertmannite (Fe-hydroxysulfate) and goethite (Fe-hydroxide) was confirmed, the presence of hydrobasaluminite (Al-hydroxysulfate) and amorphous $Al(OH)_3$ (Al-hydroxide) could only be suggested on the basis of SE analyses and thermodynamic modeling.

Another important observation offered by the SE analysis was the amount of calcite consumed in the different depths of the reactive material. Inspection of the amount of Ca released during the second step of the SE (Fig. 2.3) revealed that almost all the calcite was consumed in the Fe level (0-5 cm) while an important amount of calcite remained undissolved in the Al level. This fact is attributed to calcite passivation process as the precipitation of Al-bearing minerals (and gypsum) shields the calcite surface, rendering it inaccessible to the solution. This passivation hypothesis is also supported by SEM-EDS (Fig. 2.6). However, the advancing Fe precipitation front subsequently redissolves the Al layer and the remaining calcite.

The mineral concentrations interpreted from the SE facilitate an understanding of the general distribution of each mineral phase that forms within the reactive material and also to quantify the importance of each mineral on metal removal. These results also can be used to infer the hydrochemical processes occurring inside the reactive material, which is essential to improve the system efficiency.

# PART 2. DISPERSED ALKALINE SUBSTRATE IMPLEMENTATION AT FIELD SCALE: MONTE ROMERO CASE STUDY

# CHAPTER 3. FIELD MULTI-STEP LIMESTONE AND MgO PASSIVE SYSTEM TO TREAT ACID MINE DRAINAGE WITH HIGH METAL CONCENTRATIONS

***This chapter is based on the paper:*** **Manuel A. Caraballo, Tobias S. Rötting, Francisco Macías, José Miguel Nieto, Carlos Ayora., 2009. Field multi-step limestone and MgO passive system to treat acid mine drainage with high metal concentrations. Applied Geochemistry 24, 2301-2311**

## 3.1 ABSTRACT

Passive treatment systems have become one of the most sustainable and feasible ways of remediating acid mine drainage (AMD). However, conventional treatments present early clogging of the porosity or/and coating of the reactive grains when high acidity and metal concentrations are treated. The performance of fine-grained reagents dispersed in a high porosity matrix of wood shavings was tested as an alternative to overcome these durability problems. The system consisted of two tanks of 3 $m^3$ filled with limestone sand and wood shavings, and one tank of 1 $m^3$ with caustic magnesia powder and wood shavings, separated by several oxidation cascades and decantation ponds. The system treated about 1.5 $m^3$/day of AMD containing an average of 360 mg/L Fe, 120 mg/L Al, 390 mg/L Zn, 10 mg/L Cu, 300 µg/L As and 140 µg/L Pb, a mean pH of 3.08 and a net acidity of 2500 mg/L as $CaCO_3$ equivalents. The water reached pH 5 and 6 in the first and second limestone tanks, respectively (suitable to

remove trivalent metals); and pH 8 to 9 in the MgO tank (suitable to remove divalent metals). After nine months of operation, the system achieved an average removal of 100% Al, Cu, As, Pb, more than 70% Fe, about 25% Zn and 80% acidity. Goethite, schwertmannite, hydrobasaluminite, amorphous $Al(OH)_3$ and gypsum were the main precipitates in the two limestone tanks. Precipitation of divalent metals (Fe (II), Zn, and traces of Cd, Ni and Co) were complete inside the third tank of MgO, but preferential flow along the walls was responsible for its low treatment performance. Goethite, gypsum, Zn-schulenbergite and sauconite are the crystalline solid phases identified in the MgO tank.

## 3.2 INTRODUCTION

Polluted mine waters can be remediated by two generic approaches, active or passive treatment (Johnson and Hallberg, 2005). While the former implies the use of energy and continuous addition of chemicals, the later relies on natural water flow and biogeochemical reactions. The Iberian Pyrite Belt (IPB) in the SW of the Iberian Peninsula (Spain) is the largest massive sulfide district in the world with more than one hundred abandoned sites discharging acid mine drainage (AMD) into the Tinto and Odiel rivers (Sánchez-España et al., 2005). The large number of sources and the lack of any current responsible for the pollution suggest passive treatment systems as the most feasible remediation option for the region.

One of the biggest hurdles that a passive treatment system has to overcome is the long operating time necessary to make the system economically feasible (PIRAMID-Consortium, 2003). Clogging of the porosity and coating of the reactive grains with precipitates (passivation) are the two main operating factors controlling the life time of a passive treatment, and both of them depend on the amount of dissolved contaminants in the AMD. Due to the very high metal concentrations of the AMD from the Iberian Pyrite Belt (IPB) (Cánovas et al., 2007; Nieto et al., 2007), the traditional systems like anoxic limestone drains, ALD (Benner et al., 1999; Cocos et al., 2002; Watten et al., 2005) or reducing and alkalinity producing systems, RAPS (Jage et al., 2001), experience clogging or passivation within a few months of operation. A novel reactive material called dispersed alkaline substrate (DAS) was developed to overcome these problems (Rötting et al., 2008a, b). On the one hand, this reactive mixture contains an inert pine wood shavings matrix, to supply a high porosity and to reduce the problems of clogging, and on the other hand, a fine-grained reagent (e.g. limestone) to increase reactivity and to dissolve the reactive grains completely before passivation occurs.

Limestone-DAS has been successfully tested in a one year laboratory column study (Rotting et al., 2008a), where the chemical and hydraulic performance were investigated. A complementary field experience in the IPB was also performed showing very promising results (Rötting et al., 2008b). During the operation time, this passive treatment system removed 90-100% Al, Cu, Pb and As, about 45% Fe and an average net acidity of 900 mg/L as $CaCO_3$ equivalents. The important amount of unreacted limestone observed in the reactive tank when it was sampled showed the need for a new study to optimize the limestone-wood shavings ratio of the filling. Moreover, with the exception of Cu, the system did not remove divalent metals (Fe(II), Zn, Cd, Co, Ni, etc).

The use of two different alkaline reagents lies in the need to reach pH values between 8 and 9, which is impossible to achieve in AMD by limestone dissolution because, due to the high Ca concentration in these waters, equilibrium with this mineral is reached when the pH is between 6 and 7. Magnesium oxide (MgO) dissolution buffers solutions between pH of 8.5 and 10.5, which is high enough to precipitate divalent metals like Zn, Cd, Ni or Co.

Laboratory experiments to remove divalent metals with MgO (caustic magnesia) have given promising results. Cortina et al., 2003, treated monometallic synthetic solutions (Zn, Cu, Pb, Mn) of pH between 3 and 5.5 with columns filled with caustic magnesia and quartz sand (2-4 mm grain size). Rötting et al., 2006, repeated the same experiment with Cd, Ni and Co. In all cases metal removal finished after 1,000 to 2,000 pore volumes (less than three months), when the columns clogged, and only a minor fraction of the reactive material was consumed. Some experiments performed with multicomponent acid input solutions (Al, Fe and some divalent metals) resulted in a much poorer performance (200 pore volumes) due to fast development of Fe-Al coating of the MgO reagent (Cortina et al., 2003). In order to improve the hydraulic conductivity and the consumption of the reactive substrate, a third laboratory column experiment (Rötting et al., 2008c) was performed using a mixture of pine wood shavings, caustic magnesia sand (MgO-DAS) and a synthetic aqueous solution of pH 5.5 with Zn and Mn. During its one year of operation, the experiment completely removed the metals without any clogging.

The present work is the continuation of these experiments, and the objective is to test the performance of a complete limestone and MgO-DAS remediation pilot plant using natural high metal concentration-AMD. The previous pilot plant experiment (Rötting et al., 2008b) was extended to complete the current treatment (Fig. 3.1), comprising the following elements: one tank of limestone-DAS designed to remove Al, As, and part of

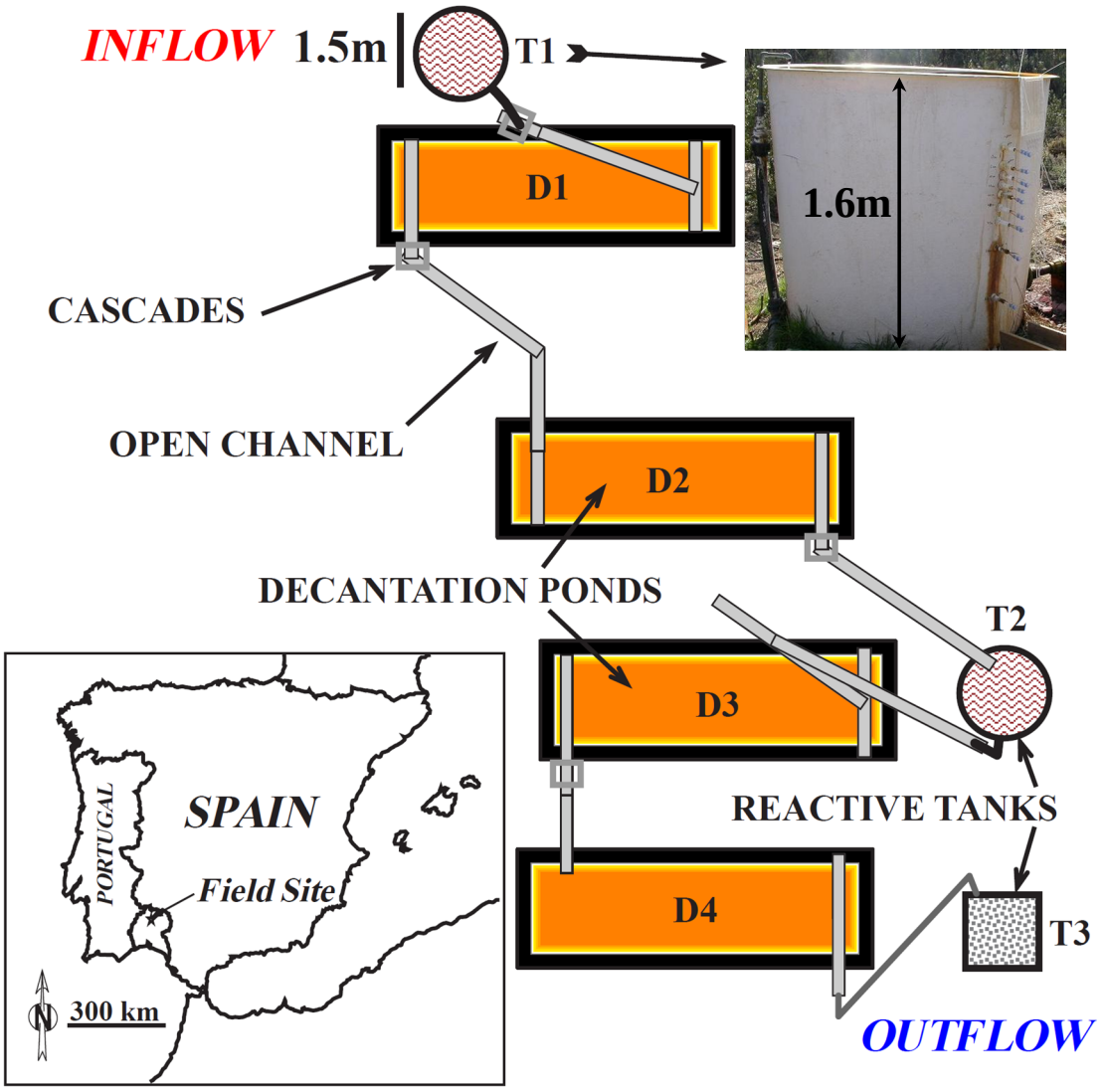


**Fig. 3.1. Field site location and schematic view of the different sections comprising Monte Romero DAS passive treatment system. T1 and T2 correspond to limestone DAS-tanks, T3 is the MgO DAS-tank and D1-4 are the four decantation ponds. AMD flows from T1 to T3.**

Fe, two oxidation cascades and decantation ponds, a second tank of limestone-DAS designed to increase pH to values above 5 and to completely remove Al and Fe(III); finally, and again after oxidation cascades and decantation ponds, a reactive tank of MgO-DAS designed to remove divalent metals. The system was monitored during nine months (when the natural flow of AMD ceased due to a period of drought), and the solids were sampled upon the completion of the treatment in order to characterize solid precipitates.

## 3.3 MATERIALS AND METHODS

### 3.3.1 Field Site and Treatment System Description

The present study was carried out at the Monte Romero abandoned mine complex put in operation in 1967 by Asturiana de Zinc to obtain Pb and Zn (Pinedo-Vara, 1963), being located near Cueva de la Mora village, in Almonaster la Real, SW of Spain (Fig. 3.1). The ore, mined by underground operations, consists of a massive pyrite deposit with minor amounts of Zn, Pb and Cu sulfides, belonging to the Vulcano-Sedimentary Complex of the IPB (Pinedo-Vara, 1963). The enclosing rocks are low grade phyllites without any carbonate beds.

As occurred in many other mines, its closure implied the flooding of the underground galleries due to the end of the groundwater pumping and the generation of AMD. The inflow AMD of the treatment was taken from the emerging water of a mine shaft. The metal concentration and physico-chemical parameters of the AMD (Table 3.1) reflect the mine mineralogy (Fe, Zn, Cu and Pb sulfides) as well as the almost anoxic conditions (e.g. low Eh and very low dissolved oxygen).

**TABLE 3.1** Mean inflow metal concentration and physico-chemical parameters

| **Major Elements (mg/L)** | | | | | | | | | |
|---|---|---|---|---|---|---|---|---|---|
| Al | Ca | Cu | Fe | Mg | Mn | Na | Si | $SO_4$ | Zn |
| 117 | 239 | 10 | 358 | 267 | 19 | 18 | 41 | 3640 | 388 |
| **Minor Elements (µg/L)** | | | | | | | | | |
| As | Be | Cd | Co | Cr | Li | Ni | Pb | Ti | V |
| 302 | 21 | 915 | 910 | 10 | 395 | 973 | 143 | 3 | 14 |
| **Physic-chemical Parameters** | | | | | | | | | |
| pH | | Eh | | Conductivity | | Diss. Oxygen | | T (ºC) | |
| 3.08 | | 571 (mV) | | 4.6 (mS/cm) | | 0.9 (mg/L) | | 17 | |

Calculations were made for 10 samplings from July 28, 2006 and April 1, 2007

A schematic view of the passive treatment system is shown in Fig. 3.1. The treatment is subdivided in three different sections: two of them consisting of limestone-DAS tanks of 3 $m^3$ in volume connected in series with two decantation ponds (T1-D1-D2 and T2-D3-D4) and a third section consisting of an MgO-DAS tank of 0.5 $m^3$ in volume (T3). Each tank was equipped with lateral sampling ports at different depths in order to measure the profiles of chemical parameters. The different elements of the treatment are connected using open, plastic channels and cascades to oxygenate the AMD and promote iron oxidation. On the basis of previous studies (Rötting et al., 2008b), the limestone proportion in T1 was reduced in order to avoid clogging by a massive precipitation of Al. Detailed characteristics of the different elements of the treatment are

exposed in Table 3.2. An inflow rate of 1.5 $m^3$/day was set to obtain a residence time of at least 24 h for T1 and T2. This flow rate implies a residence time close to 10 h for T3 and 4 days for each decantation pond.

**TABLE 3.2** Detailed description of the treatment constituent elements

| Name | Constituent element | Reactive material |
|---|---|---|
| T1 | 3$m^3$ cylindrical fiberglass tank, perforated pipe and a 15cm layer of quartz gravel as a drain. Lateral sampling ports at 5, 10, 15, 20, 27, 35, 50 and 80 cm deep in the reactive material | 12.5% (v/v) of limestone sand and 87.5% (v/v) of pine wood shavings |
| T2 | 3$m^3$ cylindrical fiberglass tank, perforated pipe and a 15cm layer of quartz gravel as a drain. Lateral sampling ports at 5, 10, 15, 20, 30, 40, 60, 80 and 100 cm deep in the reactive material. | 20% (v/v) of limestone sand and 80% (v/v) of pine wood shavings |
| T3 | 1$m^3$ cubic plastic tank, a 5 cm layer of quartz gravel as a drain. Lateral sampling ports at 0, 5, 10, 15, 25, 45 cm deep in the reactive material. | 10% (v/v) of MgO powder and 90% (v/v) of pine wood shavings |
| D1-4 | 6$m^3$ decantation ponds, dug in the ground and isolated with UV-proof plastic. | |

Global operating time for the treatment was almost 9 months (from 28 of July 2006 to 1 of April 2007) and the treatment was stopped due to the ceasing of the water supply in the shaft after a very long dry period. The tanks were put into operation sequentially, in order to test that each section was working properly.

### 3.3.2 Water sampling and analysis

Water samples were taken at least once a month for the following points: inflowing water, supernatant and drain pipe for T1, T2 and T3 and inflowing and out-flowing water at D1, D2, D3 and D4. Sampling of the lateral ports of each tank was done every other month. Temperature and electrical conductivity were measured in the field using a portable CM35 meter (Crison®) with 3 point calibration (147 and 1413 µS/cm and 12.88 mS/cm). The pH and redox potential were measured using a PH25 meter (Crison®) with Crison electrodes. Redox potential and pH were controlled and calibrated using 2 points (240-470 mV) and 3 points (pH 4.01- 7.00-9.21) respectively, with Crison standard solutions. The redox potential measurements were corrected to the Standard Hydrogen Electrode to calculate pE. Dissolved oxygen was measured with an auto-calibrating Hanna® portable meter and gross alkalinity was determined using

CHEMetrics® Total Titrets® (range 10-100 or 100-1000 mg/L as CaCO3 equivalents, accuracy approximately 5%). Water samples were filtered immediately after collection through 0.1 µm Millipore filters on Millipore syringe filter holders, acidified in the field to pH <1 with $HNO_3$ suprapur and stored at 4°C in 60 ml sterile polypropylene containers until analyzed. Analyses were carried out in the Central Research Services of the University of Huelva. Dissolved concentrations of Al, As, Be, Ca, Cd, Co, Cr, Cu, Fe, K, Mg, Mn, Na, Ni, Pb, S, Si, Ti, V and Zn were determined by Inductively Coupled Plasma Atomic Emission Spectrometry (ICP-AES Yobin-Ybon Ultima2) using a protocol specially designed for AMD samples (Tyler et al., 2004). The detection limit was always lower than 0.1 mg/L, and the analytical error was lower than 5%.

Net acidity (*Ac*) (mg/L as $CaCO_3$ equivalents) was calculated according to the recommendations from Kirby and Cravotta, 2005a, b, and using the following equation after Rötting et al., 2008b:

$$Ac = 50{,}045 \cdot (3 \cdot c_{Al} + 2 \cdot c_{Fe} + 2 \cdot c_{Mn} + 2 \cdot c_{Zn} + 10^{-pH}) - alk \qquad (3.1)$$

where $c_X$ are molar concentrations of the different metals (mol/L) and *alk* is measured gross alkalinity (mg/L as $CaCO_3$ equivalents).

Saturation indices (SI = logIAP - logK; IAP = ion activity product) of possible minerals with respect to analyzed element concentrations were calculated using PHREEQC Interactive 2.15.0 (Parkhurst, 1995) and the WATEQ4F database (Ball and Nordstrom, 1991). Additional thermodynamic data for schwertmannite was taken from Yu et al., 1999.

### 3.3.3 Solid sampling and analysis

For the solid sampling, 3 cross sections (one for each reactive tank) were dug after the completion of the treatment to have a look at the different precipitate layers developed inside the reactive material. On the basis of the visual study performed at each cross section, the following samples were taken: 0-2, 2-5, 5-10, 10-12, 12-20, 20-40 and 40-90 cm deep for T1; 0-2, 2-5, 5-8, 8-12, 12-18, 18-23, 23-30, 30-40 and 40-60 cm deep for T2 and 0-2, 2-10, 10-20 and 20-40 cm deep for T3.

As a first approach to the constituent mineralogy of the samples, an X-ray diffraction (XRD) study of randomly oriented powder samples was performed using a Bruker D5005 X-ray Diffractometer with Cu Kα radiation. Diffractometer settings were: 40 kV, 30 mA and a scan range of 3–65º 2θ, 0.05º 2θ step size and 20-s counting time per step

for the samples with lower crystallinity (iron and zinc precipitates) and 3–65º 2θ, 0.02º 2θ step size and 2.4-s counting time per step for the samples with higher crystallinity (samples with gypsum and/or calcite). The low crystallinity of the typical precipitates generated in AMD environments (Dold, 2003b; Gagliano et al., 2004; Hall et al., 1996; Kumpulainen et al., 2007; Caraballo et al., 2009c) makes necessary the use of some complementary techniques to consolidate and to extend the first XRD results. Thus, it was decided to perform total digestions and selective mineral dissolutions of the different samples of each reactive tank. Concentrated $HNO_3$ was employed to achieve the total digestion of the samples while 0.2M $NH_4$-oxalate was used to differentiate between the Fe corresponding to schwertmannite and to goethite (Dold, 2003b). Using the samples submitted to schwertmannite selective dissolution a Differential X-ray Diffraction (DXRD) study was performed (Caraballo et al., 2009c).

The metal concentration of the different digestions and selective mineral dissolutions were determined by Inductively Coupled Plasma Atomic Emission Spectrometry (ICP-AES Yobin-Ybon Ultima2).

## 3.4 RESULTS AND DISCUSSION

### 3.4.1 Hydrochemistry and mineralogy of the treatment's first section

In order to give an overview of the hydrochemical variation, only three elements (Fe, Al and Zn), pH and alkalinity were selected. As can be observed in Fig. 3.2, the first important change in the AMD hydrochemistry occurs at the output of T1 (T1-OUT) where pH increases from 3 to almost 5. At the same time, Fe and Al concentrations in the reactive tank decrease from 380 to 326 and from 150 to 50 respectively.

The bulk chemistry and mineralogy of the solids present inside T1 is exposed in Fig. 3.3 and table 3.3, respectively. As can be observed, the upper 10 cm of the reactive material consists of an iron horizon, where only schwertmannite and goethite have been identified by XRD and DXRD. The results obtained from the mineral selective dissolution performed with 0.2M $NH_4$-oxalate allowed all of the iron to separate into two different sets, one belonging to schwertmannite and the other to goethite. As shown in Figure 3.3, almost all the iron present in samples at 0-2 and 2-5 cm deep corresponds to iron hosted in schwertmannite while the iron proportion for sample 5-10 cm is close to 50% for each mineral. This mineral is poorly represented in XRD because of its low crystallinity. The schwertmannite/goethite ratio decreasing from top to bottom of the

iron horizon, is attributed to direct precipitation of schwertmannite from the supersaturated supernatant solution (Table 3.3) and its aging to goethite with increasing depth. This is the same distribution as previously described in a DAS passive treatment system (Caraballo et al., 2009a) and in terraces naturally formed from the same AMD (Acero et al., 2006).

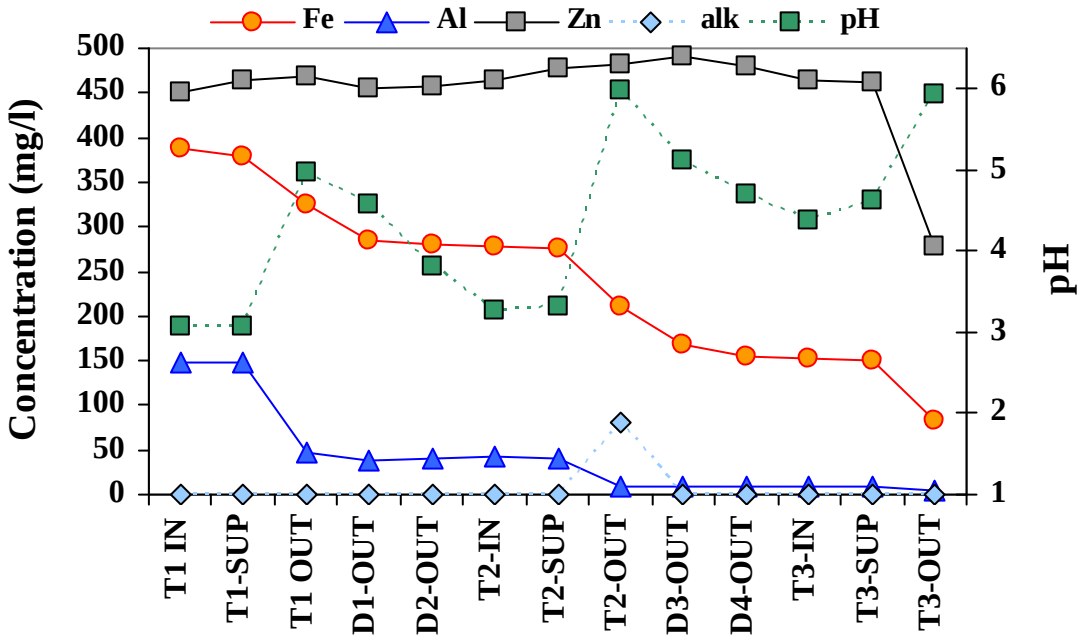


**Fig. 3.2. Fe (mg/L), Al (mg/L), Zn (mg/L), pH and alkalinity (mg/L as CaCO3 equivalents) distribution at some representative points of the passive treatment system in February 2007. Legend: Tn-IN = Tank n inflow, Tn-Sup = Tank n supernatant, Tn-OUT = Tank n outflow, Dn-OUT = Decantation pond n outflow.**

The diffractograms obtained from samples from 10 to 90 cm (Table 3.3) only reveal the presence of gypsum as a new mineral phase and calcite as part of the initial substrate. Nevertheless, total digestions performed on these samples (Fig. 3.3) show, as expected, an important aluminum concentration. This difference can be attributed to the presence of amorphous Al-phases. From the Al/S ratio, previous studies have proposed the presence of amorphous basaluminite as fresh precipitates in treatment systems (Rötting et al., 2008b), and as a result of mixing waters in rivers of the region (Sanchez-España et al., 2006). However, molar ratio of aluminum to sulfur for basaluminite is 4 while this value for T1 ranges from 8 to 12. This higher ratio can be explained by the presence of an additional Al-phase, probably amorphous $Al(OH)_3$ (Table 3.4). Previous studies have also shown the coexistence of basaluminite and gibbsite (Nordstrom, 1982), which are an aging product of other metastable Al-phases (Berkowitz et al., 2006; Berkowitz et al., 2005; Nordstrom, 1982; Sims and Ellis, 1983).

The chemical profile of the pore water from T1 (Fig. 3.4A) shows how iron precipitation is limited to the upper part of the reactive material (first 2 or 3cm deep) and how all the As present in the water is removed coupled to this iron precipitation via adsorption and coprecipitation onto the Fe precipitates. Al water concentration within T1 (Fig. 3.4A) confirms the hypothesis of Al precipitation when the pH of the AMD reaches a value of more than 5.

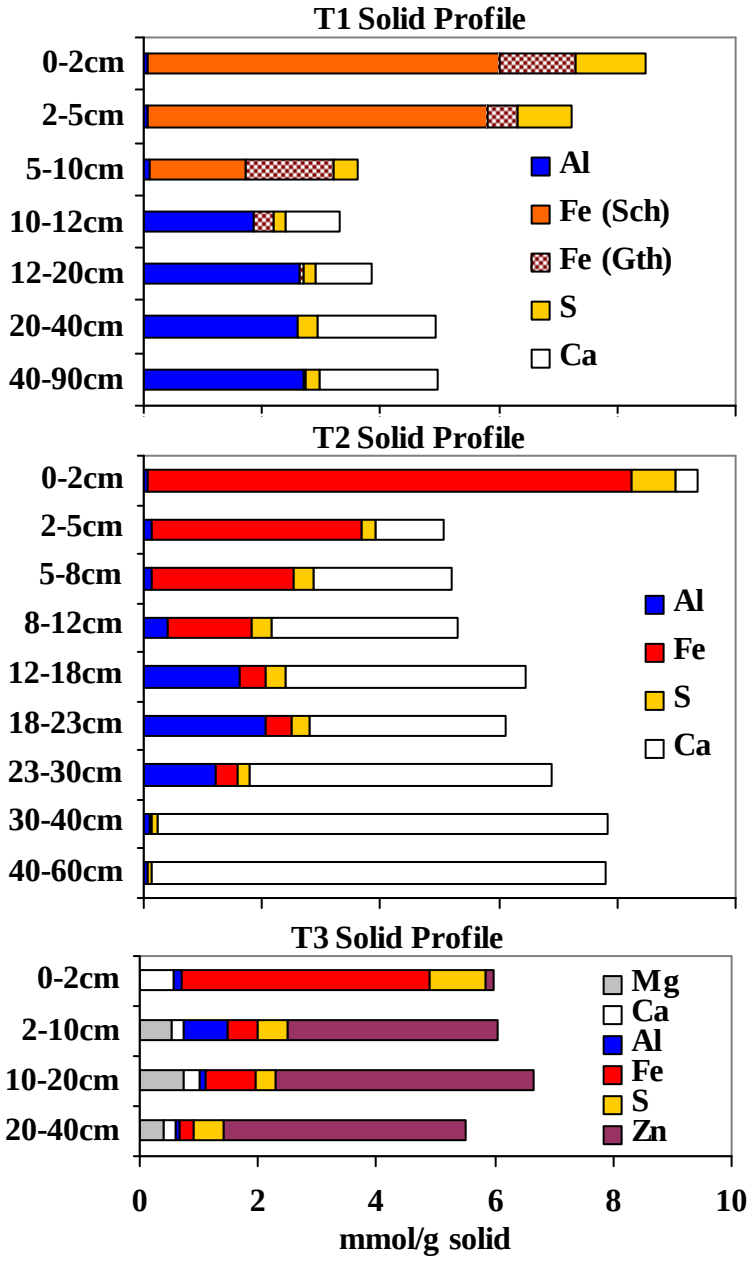


**Fig. 3.3. Bulk chemistry of some representative samples of the solid profile sampled at the three reactive tanks. Fe (Sch) = iron hosted in schwertmannite, Fe (Gth) = iron hosted in goethite.**

At the same time and coupled with Al removal some other elements (Cu, Pb and Cr) are completely or almost completely removed inside T1. The removal distribution of all

these elements inside the Al precipitation zone suggests that the mineral phases responsible for the Al removal are also responsible for the removal of Cu, Pb and Cr. These observations are in agreement with the study performed to the Fe and Al precipitates formed in the passive treatment system of Monte Romero 2005-2006 (Caraballo et al., 2009a). This study revealed that although some As, Cu, Pb, Zn and Cr were released after the specific sequential extraction step designed to obtain the adsorbed elements, the great majority of these elements were released only after the complete dissolution of the Fe and Al precipitates. As expected from their low concentration, no other solid phases of these minor elements have been detected by XRD. Between 0 and 20 cm, Al, Cu and Pb concentration reach values higher than in the supernatant AMD (Fig. 3.4A).

**TABLE 3.3** Mineral phases confirmed with X-ray Diffraction (XRD) and Differential X-ray Diffraction (DXRD)

| **T1** | **Depth Ranges(cm)** | **Mineral Phases** | | | |
|---|---|---|---|---|---|
| | | Schwertmannite | Goethite | Gypsum | Calcite |
| | 0-2 | DXRD | XRD | | |
| | 2-5 | DXRD | XRD | | |
| | 5-10 | DXRD | XRD | | |
| | 10-12 | | | XRD | XRD |
| | 12-20 | | | XRD | XRD |
| | 20-40 | | | XRD | XRD |
| | 40-90 | | | XRD | XRD |
| **T2** | **Depth Ranges(cm)** | **Mineral Phases** | | | |
| | | Goethite | Gypsum | Calcite | |
| | 0-12 | XRD | XRD | XRD | |
| | 12-18 | | XRD | XRD | |
| | 18-23 | | XRD | XRD | |
| | 23-30 | | XRD | XRD | |
| | 30-40 | | XRD | XRD | |
| | 40-60 | | | XRD | |
| **T3** | **Depth Ranges(cm)** | **Mineral Phases** | | | |
| | | Goethite | Gypsum | Sauconite | Zn-Sch |
| | 0-2 | XRD | XRD | | |
| | 20-40 | | | XRD | XRD |

To mark the presence of a certain mineral phase at each depth and the used analytical technique, the words XRD and DXRD have been used. Zn-Sch = Zinc dominant Schulenbergite.

This is attributed to the redissolution of the Al solid phase caused by the advance of the more acid Fe front. Then, due to the scarcity of calcite reactive surface, part of the alkalinity needed for the Fe minerals to precipitate is supplied by the dissolving Al solid. Regarding Zn, Cd, Co and Ni, Fig. 3.4A shows that the concentration of these elements remains constant throughout T1.

**TABLE 3.4** Saturation index (SI) values for the most probably Al and Fe precipitates calculated at some representative points and times of the treatment using PHREEQC Interactive 2.15.0

| **October 2006** | | **$Al(OH)_3$** | **Basal** | **Gib** | **Gth** | **Sch** | **Gyp** |
|---|---|---|---|---|---|---|---|
| T1 | -5 cm | -5.7 | -10.7 | -3.0 | 4.3 | 0.9 | -0.4 |
| | 5 cm | -2.4 | 0.3 | 0.3 | 5.0 | 2.5 | -0.2 |
| | 10 cm | 0.3 | 8.7 | 3.0 | 6.4 | 9.1 | -0.1 |
| | 15 cm | 0.5 | 9.4 | 3.2 | 6.6 | 10.9 | -0.1 |
| | 20 cm | 0.9 | 10.6 | 3.6 | 6.9 | 12.7 | -0.1 |
| D2-out | | -0.8 | 4.9 | 1.9 | 5.1 | 0.1 | -0.1 |
| T2 | -5 cm | -5.9 | -12.0 | -3.2 | 3.1 | -9.2 | 0.0 |
| **February 2007** | | | | | | | |
| T1 | -5 cm | -5.3 | -9.1 | -2.6 | 4.8 | 4.8 | -0.3 |
| | 0 cm | -5.1 | -8.4 | -2.4 | 4.9 | 5.5 | -0.3 |
| | 5 cm | -4.3 | -5.8 | -1.6 | 5.0 | 5.6 | -0.3 |
| | 10 cm | -2.3 | 0.8 | 0.4 | 6.0 | 10.9 | -0.3 |
| | 15 cm | -1.6 | 3.1 | 1.1 | 6.2 | 11.6 | -0.3 |
| | 22.5 cm | -1.5 | 3.6 | 1.2 | 6.2 | 11.2 | -0.3 |
| | 30 cm | -1.3 | 4.3 | 1.4 | 6.2 | 11.3 | -0.3 |
| D2-out | | -5.5 | -10.1 | -2.8 | 4.4 | 1.3 | 0.0 |
| T2 | -5 cm | -1.8 | 2.1 | 0.9 | 5.9 | 8.8 | 0.0 |
| | 5 cm | -0.6 | 6.2 | 2.1 | 6.7 | 13.7 | 0.0 |
| | 10 cm | 1.0 | 11.2 | 3.7 | 7.3 | 15.7 | 0.0 |
| | 15 cm | 1.3 | 12.2 | 4.0 | 7.4 | 16.3 | 0.0 |
| | 20 cm | 1.5 | 12.8 | 4.2 | 7.6 | 17.3 | 0.1 |
| | 30 cm | 1.5 | 12.6 | 4.2 | 7.6 | 17.5 | 0.1 |
| | 40 cm | 1.5 | 12.5 | 4.2 | 7.8 | 18.5 | 0.1 |
| D4-out | | -2.8 | -1.7 | -0.1 | 5.5 | 5.7 | 0.1 |
| T3 | -5 cm | 0.7 | 9.9 | 3.4 | 8.1 | 22.5 | 0.0 |

$Al(OH)_3$, $Al(OH)_3$ amorphous; Basal, Basaluminite; Gib, Gibbsite; Gth, Goethite; Sch, Schwertmannite and Gyp, Gypsum.

As shown in Fig. 3.4B, Al removal efficiency of T1 decreases with time. The most plausible explanation for the time evolution of these three sets of profiles is that gypsum and Al-solid precipitation on limestone surface decreases the reactivity of the latter mineral, which is also shown by lower pH and dissolved Ca. Because Al precipitation only takes place at a pH higher than 5, the decrease in pH with time forces the Al precipitation front to move down into the reactive material. The important Al migration inside T1 and the decrease of the removal efficiency of the reactive material with respect to time, are due to both the lower limestone proportion used in this experiment,

compared with previous studies (Rötting et al., 2008a), and the great increase of Al concentration in the AMD (from 70 to 140 mg/L) which occurred halfway through the operation time.

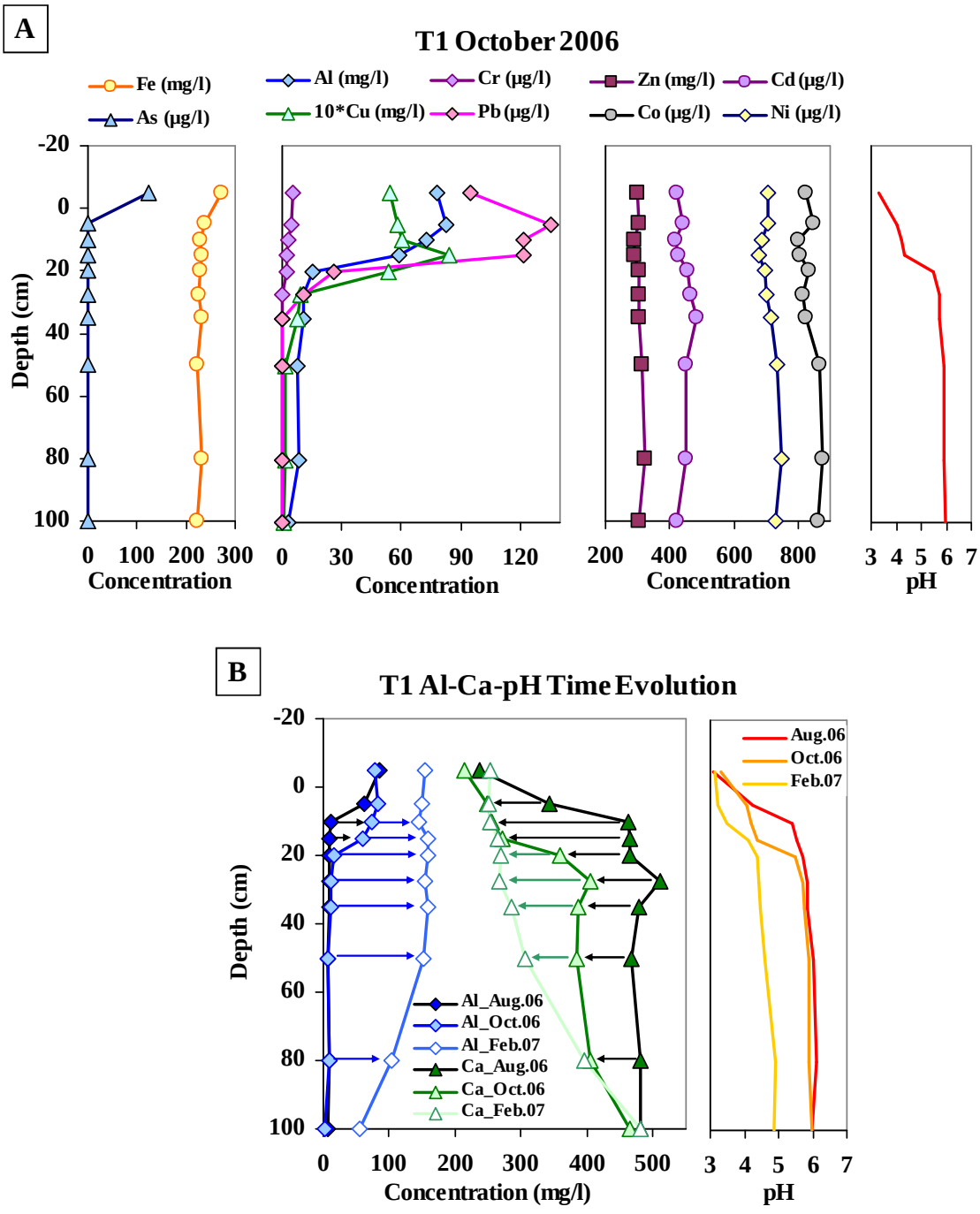


**Fig. 3.4. (A) Chemical profile of the first limestone-DAS reactive tank in October 2006. The values at -5 cm of depth represent the supernatant. (B) Time evolution of pH, precipitated aluminium and dissolved calcium in the first limestone-DAS reactive tank.**

The next important step in the first section of the treatment is the removal of Fe that takes place inside the first decantation pond (Fig. 3.2, D1-OUT). Part of the remaining

Fe(II) is oxidized at the cascades, and additional schwertmannite precipitates from the supersaturated AMD in the decantation pond. The removal of OH- causes the coupled decrease of pH (Fig. 3.2). The low pH does not allow metastable Al-phases to precipitate. Amorphous $Al(OH)_3$ is subsaturated (Table 3.4), and no thermodynamic data for amorphous basaluminite have been found.

### 3.4.2 Hydrochemistry and mineralogy of the treatment's second section

The first step of the treatment's second section consists of another limestone-DAS tank (T2) where pH and alkalinity are increased while Fe and Al water concentrations are decreased according to the different reactions previously discussed for T1 (Fig. 3.2, T2-OUT).

The inspection of the diffractograms and total digestions performed in T2 (Table 3.3 and Fig. 3.3) shows small differences between the solid chemistry and mineralogy profile of this tank and the one observed in T1. The iron horizon in T2 (from 0 to 12 cm) is comprised only by goethite as iron mineral phase that agrees with the SI obtained for goethite and schwertmannite in this level (Table 3.4). The important presence of calcite and gypsum in this layer suggests that goethite precipitation is linked to the dissolution of calcite that increases pH and enhances Fe(II) oxidation. This is different from the situation observed in T1, where schwertmannite precipitated from the supernatant solution. Because of the lower water aluminum concentration in this tank, the aluminum horizon developed inside the reactive material is restricted from 12 to 30 cm. Another important difference between T2 and T1 is that calcite dissolution and gypsum precipitation only took place in the upper 30 cm of the reactive material, leaving 60 cm of unreacted material. Therefore, the durability of tank T2 is double that of T1, or alternatively, one T2 tank can treat the water from two T1 tanks.

The distribution of pore water concentrations throughout the profile of T2 is similar to the one described for T1 with the only difference being that the metals removed in T2 directly depend on the removal efficiency of T1. Thus, as can be observed in the October-2006 chemical profile of T2 (Fig. 3.5A), during the time that all the Al present in the T1 water was removed, the only major element removed from inside T2 was Fe, while a very slight Cd, Co and Ni removal can also be observed. Due to the pH of almost 7 achieved during the first months of operation of T2, and the lack of specific precipitates for these minor elements inside T2 (Table 3.3), this uptake is attributed to the adsorption processes onto goethite. When Al removal in T1 was less efficient, the remaining Al in the water was almost totally removed inside T2 (Fig. 3.5B, February-2007). As discussed for T1, Cu and Pb are fixed by adsorption and coprecipitation with

the Al precipitates (Fig. 3.5B). Two stages are observed in the chemical profile evolution in T2 (Fig. 3.5A and B). In the beginning of the experiment (October-2006), Fe removal took place only in the upper 5 cm of the reactive material, while later (February-2007), Fe was removed in the upper 60 cm.

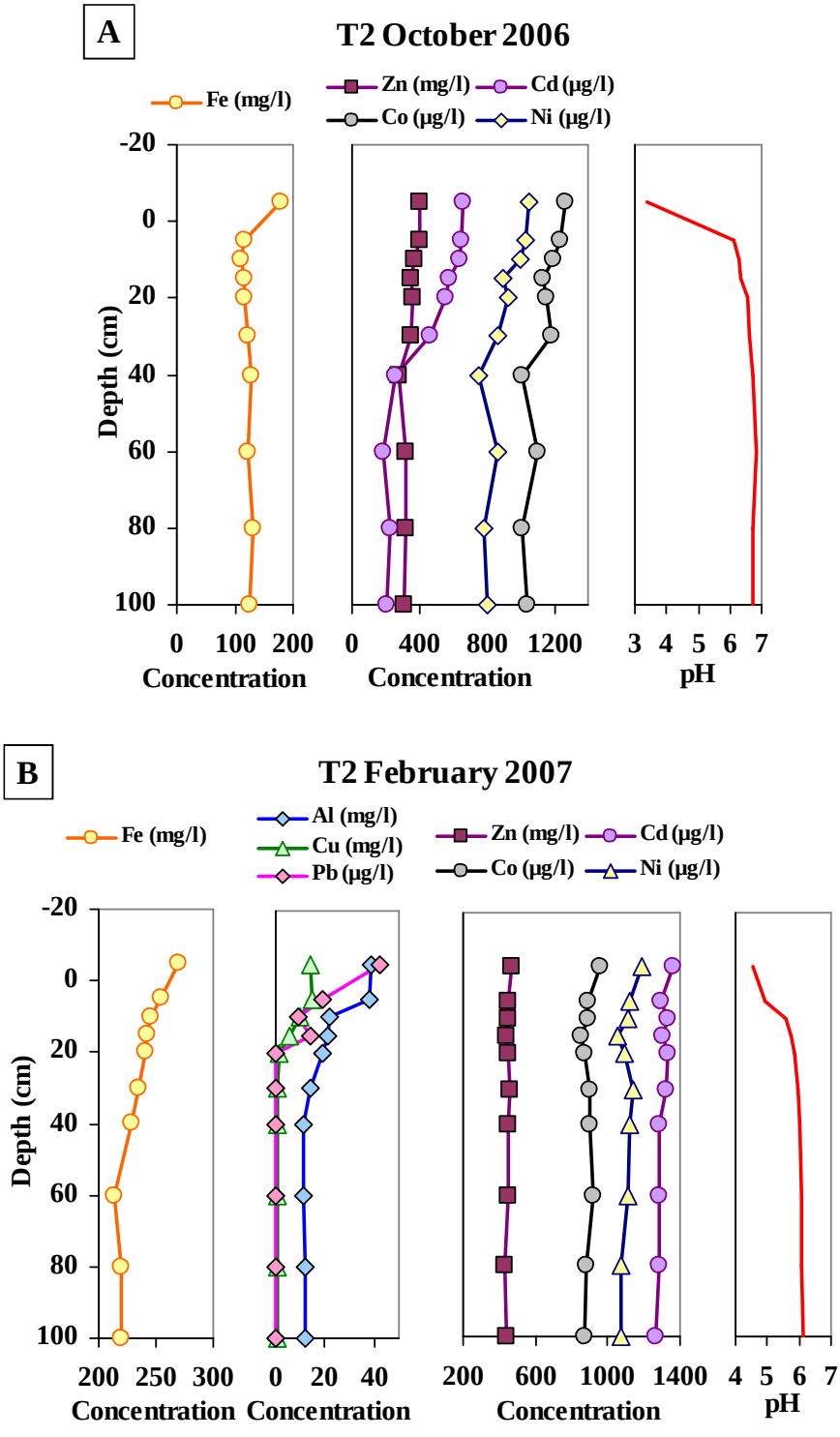


**Fig. 3.5. Chemical profile of the second limestone-DAS reactive tank in October 2006 (A) and February 2007 (B). The values at -5 cm of depth represent the supernatant.**

Moreover, the pH value at the output of T2 decreased from 6.7 in October 2006 to 6.1 in February 2007 (Fig. 3.5B). No Cd, Co or Ni removal was observed for the lower pH. As described for D1, the same process of schwertmannite precipitation, involving Fe and alkalinity removal and a decrease in pH can be observed in the D3 and D4 decantation ponds (Fig. 3.2, D3-OUT, D4-OUT). Due to the higher pH and alkalinity at the output of T2, the Fe precipitation took place not only in one decantation pond but in both D3 and D4.

### 3.4.3 Hydrochemistry and mineralogy of the treatment's third section

The last section of the treatment implies the flow of AMD throughout the MgO-DAS reactive material of T3. At this point, a significant Fe and Zn removal and pH increase can be observed (Fig. 3.2, T3-OUT). The chemical composition of the precipitates developed inside T3 (Fig. 3.3) reveals two differentiated layers, a first one from 0 to 2 cm deep with iron as its main constituent, and a second layer from 2 to 40 cm deep mainly composed of zinc. According to the XRD of the sample from 0-2 cm (Table 3.3), the mineral responsible for Fe removal is goethite. Concerning the mineralogy of the zinc precipitates (Table 3.5), the most plausible mineral phases are Zn-dominant schulenbergite, $(Zn,Cu,)_7(SO_4)_2(OH)_{10}•3H_2O$, and sauconite, $Zn_3(Si,Al)_4O_{10}(OH)_2•4H_2O$. Taking into account the amount of Si and Zn removed from the T3 tank (Table 3.4), the latter mineral must be a very minor phase. No sign of $Zn(OH)_2$ found in previous laboratory studies with simpler water chemistry (Rötting et al., 2006, 2008c) have been identified, probably due to the complex solution treated in the present case. As expected from their low concentration in the inflow AMD, no solid phases for trace elements have been detected by XRD. It is also important to take into account that practically the entire reagent is exhausted at the end of the experiment: no peaks of MgO or brucite are evident in the different diffractograms of T3 and only less than 1 mmol Mg/g solid remains in the solid phase (Fig. 3.3). Therefore, the durability of the tank T3 is slightly shorter than that of T1 suggesting that a larger volume or a higher reagent concentration is needed to increase T3 operating time.

The inspection of a profile of pore water concentrations through the third reactive tank shows three different patterns (Fig. 3.6): a first one corresponding to the supernatant water (from -5 to 0 cm), a second one representing the water chemistry inside the MgO-DAS reactive material (from 0 to 40 cm) and finally, a third one showing the water chemistry inside the gravel quartz layer (from 40 to 45 cm). The high metal content of the supernatant (Table 3.5) was completely removed inside the MgO-DAS reactive material, where the water pH reached a value between 8 and 9. However, all the metals

present in the supernatant appear again in the quartz gravel drain with the concentrations of all solutes diluted to a proportion close to 0.6 (Table 3.5). This suggests that only 0.4 of the water circulated through the reactive material (with the complete removal of metals), while another portion of 0.6 flowed down through preferential paths to the quartz drain where both waters mixed. This matches the development of red channels of iron oxide observed along the semitransparent plastic walls of the tank.

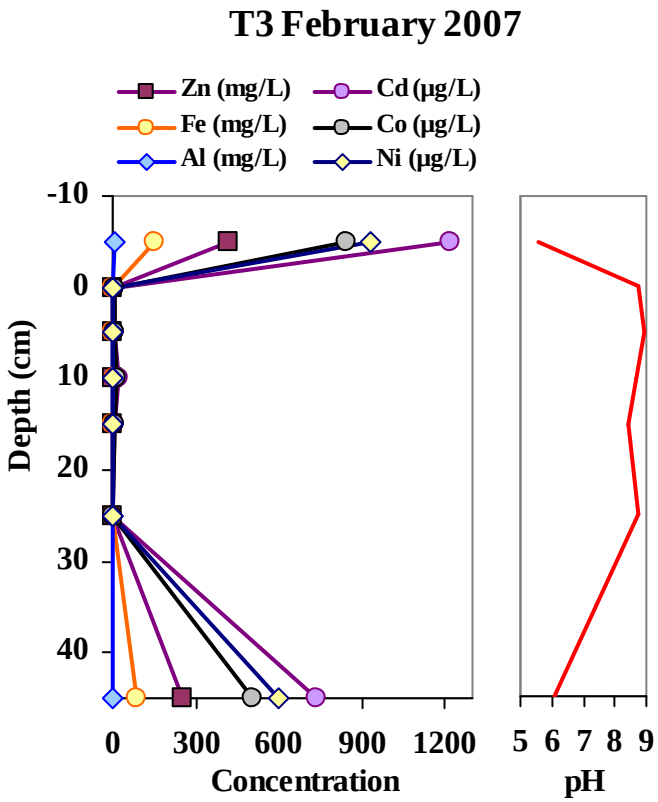


**Fig. 3.6. Chemical profile of the MgO-DAS reactive tank in February 2006. The values at -5 cm of depth represent the supernatant.**

### 3.4.4 Removal efficiency of the treatment

According to equation 1, the net acidity can be considered as a very useful parameter to evaluate the efficiency of each section of the treatment regarding metal removal and water hydrochemistry improvement. Time evolution of the net acidity at four selected points of the treatment as well as Fe, Al and Zn concentration are shown in Fig. 3.7. The inflow net acidity suffered a sudden increase three months after the beginning of the experiment. This increase was due to a very important rise of the concentrations of Fe, Al and Zn (Table 3.5 and Fig. 3.7).

The net acidity removal (INFLOW net acidity – D2-OUT net acidity) of the first section of the treatment (T1+D1+D2) ranges from 500 mg/L as $CaCO_3$ equivalent, during the first three months, to almost 1,000 mg/L after the sudden increase of net acidity in December. It decreases to almost 700 mg/L towards the end of the experiment (Table 3.5). The decrease of the net acidity in this section of the treatment is clearly linked to the Fe removal in T1 and D1 and, in a higher proportion, to the Al removal inside T1, and its average is similar to the 900 mg/L reported by Rötting et al., 2008b, for an equivalent tank with 20% v/v of limestone. Examination of the net acidity removal in the second section of the treatment (T2+D3+D4) reveals a mean removal of around 500 mg/L as $CaCO_3$ equivalent and Fe being the main element removed. Finally, the net acidity removal at the outflow of the treatment (T3-OUT) shows a decrease of another 500 mg/L as $CaCO_3$ equivalent. This final decrease is due to the Zn and Fe removal inside T3. All in all, the system is able to decrease the net acidity from 2,500 to 500 mg/L as $CaCO_3$ equivalents.

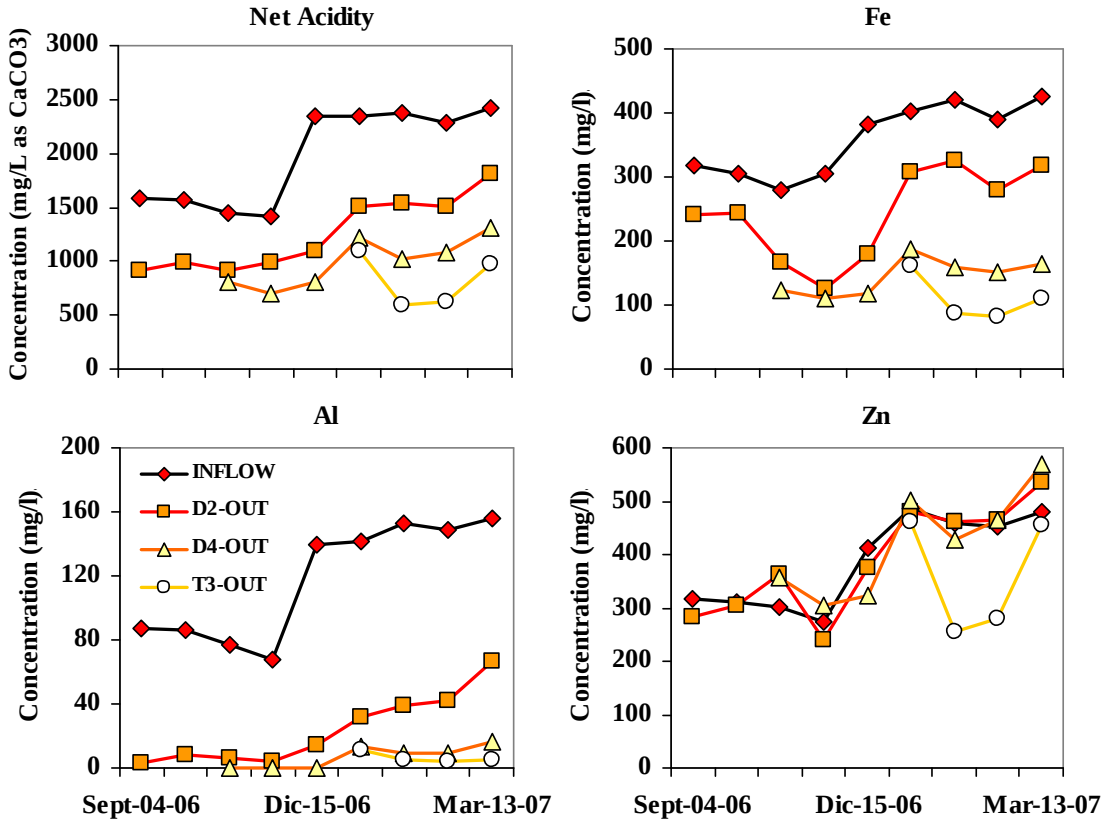


**Fig. 3.7. Time evolution of the net acidity, Fe, Al, and Zn concentration at some strategic points of the passive treatment system. D2 and D4 correspond to decantation ponds 2 and 4 respectively and T3 corresponds to the MgO reactive tank.**

In order to evaluate the global removal efficiency, the mean relative metal removal of the system was calculated according to the following equation:

$$r = \frac{c_{in} - c_{out}}{c_{in}} \cdot 100 \qquad (3.2)$$

where $c_{in}$ corresponds to the system inflow concentration of a certain element and $c_{out}$ to the system outflow concentration of the same element. The results of these calculations are presented in Fig. 3.8, where the inflow and outflow mean concentration and the mean relative removal for some elements have been grouped in two different graphics (Fig. 3.8A and B) corresponding to major and minor elements. Concerning the major elements (Fig. 3.8A), a relative removal close to 100% for Al and Cu, higher than 70% for Fe and Si and almost 25% for Zn can be observed. These relative removals imply a mean net removal from the inflow water after the treatment of: 300 mg/L Fe, 140 mg/L Al, 105 mg/L Zn, 32 mg/L Si and 12 mg/L Cu.

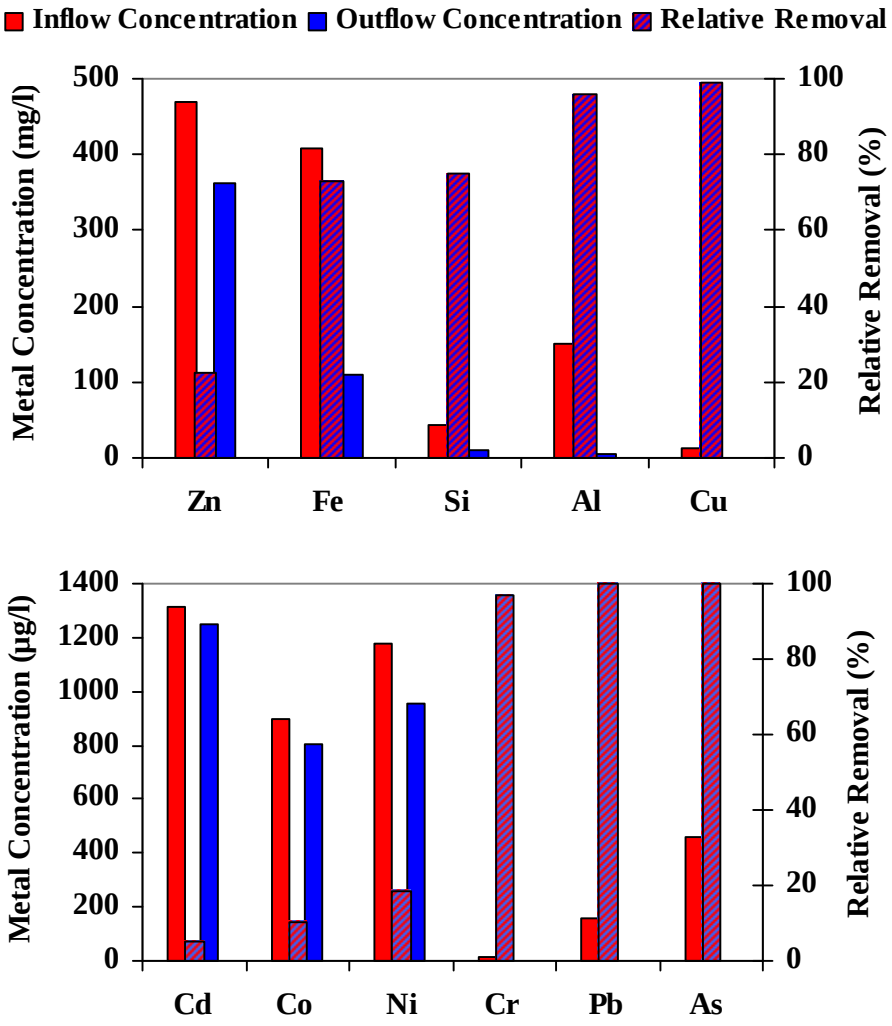


**Fig. 3.8. Metal concentration at the system inflow and outflow and relative removal of the whole system for some major (A) and minor (B) elements. The values shown in this graph correspond to the last three months of the system when all the reactive tanks were in operation.**

In the case of minor elements (Fig. 3.8B), a relative removal of 100% for As and Pb, higher than 95% for Cr, almost 20% for Ni, 10 % for Co and 5% for Cd can be observed. These relative removals imply a mean net removal from the inflow water of: 460 µg/L As, 155 µg/L Pb, 220 µg/L Ni, 95 µg/L Co, 70 µg/L Cd and 14 µg/L Cr.

## 3.5 CONCLUSIONS

Summarizing some of the most relevant observations defining the treatment efficiency, the system is able to remove a net acidity around 2,000 mg/L as $CaCO_3$ equivalents leading to a decrease in the inflow of AMD from 2,500 to 500 mg/L as $CaCO_3$ equivalents. This acidity removal is double that achieved with only one limestone-DAS tank (Rötting et al., 2008b) and much higher than the removal rates achieved by anoxic limestone drains, RAPS and similar passive systems (theoretical alkalinity generation up to 350-450 mg/L as $CaCO_3$; Younger et al., 2002; average field values of 240-290 mg/L, respectively, Ziemkiewicz et al., 2003). Net acidity elimination corresponds to a relative removal close to 100% for Al and Cu, higher than 70% for Fe and almost 25% for Zn (regarding major elements) and 100% for As and Pb, and higher than 95% for Cr.

Although the optimal proportion of limestone sand in the limestone-DAS reactive material depends on the AMD hydrochemistry, the present study has shown that a 12.5% (v/v) shows similar removal to 20%(v/v) limestone (Rötting et al., 2008b). However, a decrease in reactivity is observed at the end of our experiment. This is attributed to the faster progress of the aluminum precipitation front down through the reactive material, which causes a lower removal of Al inside T1, less increase in alkalinity and less iron removal in the subsequent decantation ponds. The second limestone-DAS tank (T2) and the following two decantation ponds, play an important role in Fe removal (almost 50% of the whole removal of the system). Both Fe and Al removal are important to ensure an efficient and long performance of MgO treatment (Cortina et al., 2003). Analysis of T3 revealed that almost all the reactive material present in this MgO-DAS tank was consumed. This observation clearly shows that the chosen grain size was suitable to achieve a total dissolution before any passivation process appeared. However, higher volume and/or higher MgO proportion in the reactive material are needed to extend T3 operating time. The T3 tank confirms that MgO is able to remove completely divalent metals such as Zn, Fe(II), Cd, Co and Ni from a complex aqueous solution extending the results of previous laboratory experiments. However, T3 shows a clear problem of preferential flow along the walls. To avoid this problem, T3 should be similar to T1 and T2 (with no evident preferential

flow), i.e., with higher volume, cylindrical shape and made of fiberglass. Mina Esperanza passive treatment system (Almonaster la Real, Spain) can be cited in order to have a look at an up-scaled limestone-DAS tank to treat the whole outflow of an adit at the Iberian Pyrite Belt (Caraballo et al., 2008). This system used 300 $m^3$ of limestone-DAS to treat a maximum flow of 1L/s during an operating time of 18 months.

The mineralogy of the precipitates developed in the passive treatment system is directly linked to the precipitation of the five main elements present in Monte Romero AMD: Fe, Al, Ca, Zn and $SO_4$. Accordingly, an iron horizon was precipitated at the top of the reactive material of T1, T2 and T3. This iron layer was comprised by schwertmannite and goethite in T1 and only by goethite (with minor amounts of gypsum) in T2 and T3. Schwertmannite seems to precipitate directly from the supersaturated supernatant water, and ages progressively to goethite similar to the process observed in the terraces of the same AMD flow. Goethite precipitates within the upper pores of the treatment, where limestone or MgO dissolves, and the subsequent rise in pH accelerates the Fe(II) oxidation. Next, an aluminum horizon forms inside T1 and T2. No crystalline Al phase could be detected at this layer, amorphous $Al(OH)_3$ and basaluminite being the most plausible aluminum phases. Finally, only a zinc horizon was present inside T3. Unlike $Zn(OH)_2$ found in previous laboratory experiments, complex minerals such as Zn-dominant schulenbergite, $(Cu,Zn)_7(SO_4)_2(OH)_{10}•3H_2O$, and minor sauconite, $Zn_3(Si,Al)_4O_{10}(OH)_2•4H_2O$ are proposed as the most probable Zn-rich precipitates.

Table 3.5

Chemical composition for the AMD at some representative points and times of the passive treatment system

| October 2006 | Major elements (mg/L) | | | | | | | | | | | Trace elements (µg/L) | | | | | | | | |
|---|---|---|---|---|---|---|---|---|---|---|---|---|---|---|---|---|---|---|---|---|
| | Al | Ca | Cu | Fe | K | Mg | Mn | Na | SO4 | Si | Zn | As | Cd | Co | Cr | Ni | Pb | pH | Ac (mg/L) | Ac R. (mg/L) |
| T1-IN | 68 | 265 | 2.5 | 304 | 2.4 | 246 | 20 | 19 | 3018 | 37 | 273 | 183 | 275 | 1138 | 4 | 785 | 128 | 3.4 | 1444 | |
| T1-SUP | 71 | 273 | 2.6 | 326 | 2.4 | 272 | 24 | 19 | 3246 | 41 | 300 | 174 | 319 | 1272 | n.d. | 912 | 169 | 3.3 | 1432 | 12 |
| T1-OUT | 6.4 | 540 | 0.1 | 290 | 3.0 | 326 | 26 | 21 | 3468 | 27 | 337 | n.d. | 315 | 1543 | n.d. | 1069 | n.d. | 6.0 | 913 | 531 |
| D1-OUT | 4 | 423 | 0.1 | 157 | 2.1 | 226 | 19 | 16 | 2628 | 18 | 250 | n.d. | 227 | 1086 | n.d. | 759 | n.d. | 5.0 | 853 | 591 |
| D2-OUT | 4.2 | 401 | 0.1 | 126 | 2.2 | 224 | 19 | 16 | 2490 | 19 | 239 | n.d. | 212 | 1031 | n.d. | 747 | n.d. | 3.8 | 940 | 504 |
| T2-IN | 7.2 | 563 | 0.3 | 180 | 2.0 | 320 | 24 | 23 | 3516 | 27 | 372 | n.d. | 583 | 1153 | n.d. | 985 | n.d. | 3.8 | 920 | 523 |
| T2-SUP | 7.3 | 547 | 0.3 | 180 | 2.4 | 335 | 25 | 23 | 3786 | 28 | 364 | n.d. | 598 | 1175 | n.d. | 1000 | n.d. | 3.8 | 924 | 520 |
| T2-OUT | n.d. | 679 | 0.1 | 111 | 2.1 | 310 | 23 | 22 | 3726 | 16 | 305 | n.d. | 209 | 1042 | n.d. | 806 | n.d. | 6.6 | 807 | 637 |
| February 2007 | | | | | | | | | | | | | | | | | | | | |
| T1-IN | 149 | 229 | 11 | 389 | 1.4 | 273 | 18 | 18 | 3915 | 43 | 451 | 389 | 1271 | 817 | 14 | 1103 | 139 | 3.1 | 2291 | |
| T1-SUP | 149 | 228 | 11 | 380 | 1.3 | 268 | 17 | 19 | 3999 | 45 | 465 | 325 | 1259 | 891 | 13 | 1014 | 142 | 3.1 | 2294 | -4 |
| T1-OUT | 47 | 490 | 13 | 326 | 1.5 | 282 | 20 | 19 | 3828 | 18 | 469 | n.d. | 1369 | 901 | n.d. | 1159 | 114 | 5.0 | 1600 | 691 |
| D1-OUT | 38 | 491 | 13 | 285 | 1.5 | 276 | 19 | 18 | 3588 | 18 | 448 | n.d. | 1280 | 872 | n.d. | 1094 | 88 | 4.6 | 1443 | 848 |
| D2-OUT | 40 | 500 | 14 | 280 | 1.4 | 280 | 19 | 18 | 3621 | 19 | 452 | n.d. | 1310 | 905 | n.d. | 1120 | 88 | 3.4 | 1480 | 811 |
| T2-IN | 42 | 511 | 14 | 279 | 1.4 | 291 | 20 | 18 | 3759 | 20 | 465 | n.d. | 1368 | 938 | n.d. | 1184 | 89 | 3.3 | 1508 | 783 |
| T2-SUP | 40 | 502 | 14 | 275 | 1.5 | 300 | 21 | 18 | 3936 | 20 | 477 | n.d. | 1417 | 971 | n.d. | 1204 | 101 | 3.3 | 1507 | 784 |
| T2-OUT | 10 | 611 | 0.2 | 210 | 1.5 | 298 | 21 | 18 | 3777 | 17 | 483 | n.d. | 1399 | 951 | n.d. | 1208 | n.d. | 6.0 | 1129 | 1162 |
| D3-OUT | 9.7 | 612 | 0.2 | 169 | 1.6 | 297 | 21 | 18 | 4074 | 17 | 500 | n.d. | 1333 | 888 | n.d. | 1177 | n.d. | 5.1 | 1161 | 1130 |
| D4-OUT | 9.6 | 615 | 0.2 | 153 | 1.5 | 295 | 21 | 17 | 3947 | 16 | 490 | n.d. | 1340 | 910 | n.d. | 1180 | n.d. | 4.5 | 1085 | 1206 |
| T3-IN | 9.5 | 623 | 0.2 | 152 | 1.6 | 293 | 21 | 17 | 3510 | 16 | 465 | n.d. | 1368 | 946 | n.d. | 1208 | n.d. | 4.4 | 1077 | 1214 |
| T3-SUP | 9.4 | 592 | 0.2 | 151 | 1.8 | 290 | 21 | 16 | 3615 | 16 | 462 | n.d. | 1348 | 937 | n.d. | 1186 | n.d. | 4.6 | 1069 | 1222 |
| T3-OUT | 3.9 | 624 | 0.2 | 83 | 1.4 | 398 | 19 | 17 | 3783 | 8 | 279 | n.d. | 927 | 603 | n.d. | 698 | n.d. | 5.9 | 632 | 1659 |

Abbreviations: Ac, Net acidity (mg/L as $CaCO_3$ equivalents); Ac R., Net acidity removal (mg/L as $CaCO_3$ equivalents); n.d., under detection level.

# PART 3. DISPERSED ALKALINE SUBSTRATE IMPLEMENTATION AT FULL SCALE: MINA ESPERANZA CASE STUDY

# CHAPTER 4. IMPLEMENTATION OF A DISPERSED ALKALINE SUBSTRATE (DAS) PASSIVE TREATMENT SYSTEM AT MINA ESPERANZA, SW SPAIN, FOR A LONG TERM REMEDIATION OF HIGHLY POLLUTED ACID MINE DRAINAGE

*This chapter is based on the paper:* **Manuel A. Caraballo, Francisco Macías, Tobias S. Rötting, José Miguel Nieto, and Carlos Ayora. Implementation of a Dispersed Alkaline Substrate (DAS) passive treatment system at Mina Esperanza, SW Spain, for a long term remediation of highly polluted acid mine drainage. Submitted to Journal of Hazardous Materials.**

## 4.1 ABSTRACT

The full scale passive remediation system design implemented in Mina Esperanza treating an average inflow net acidity of 2,300 mg/L as $CaCO_3$ was conceived to enhance natural iron oxidizing processes and to induce metal precipitation by changes in water pH and alkalinity after limestone dissolution. Another important goal of the design was to avoid clogging problems in the reactive material by the use of a high porosity mixture of limestone sand and wood shavings. During 20 months of proper operation the system exceeded the initial performance expectation by producing around 100 mg/L of ferric iron in the aeration cascades, removing an average net acidity up to 1,500 mg/L as $CaCO_3$ and not having any significant clogging problem. Complete Al,

As, Cd, Cr, Cu, Ti and V removal from the water was accomplished through almost the entire operation time while Fe removal ranged between 170 and 620 mg/L. The system operated at a mean inflow rate of 43 $m^3$/day achieving an acid load reduction of 597 $g•(m^2•day)^{-1}$, more than 10 times higher than the generally accepted 40 $g•(m^2•day)^{-1}$ value commonly used as a passive treatment system designing criteria. The high performance achieved by the passive treatment system at Mina Esperanza demonstrates that this innovative treatment design is a simple, efficient and long lasting remediation option to treat highly polluted acid mine drainage.

## 4.2 INTRODUCTION

Acid mine drainage (AMD) generation has been thoroughly described in many previous studies related with inorganic water pollution (Bigham and Nordstrom, 2000; Younger et al., 2002). It is sufficient here to state that it arises from the oxidative dissolution of sulfide minerals, mainly pyrite, ordinarily present as main ore-forming minerals in sulfide mining districts (Akcil and Koldas, 2006) or as minor constituents in coal deposits (Younger et al., 2002).

A good example of how devastating the effect of AMD pollution on a river can be was offered by the California Department of Fish and Game in a study showing as many as 47,000 fish killed at one site during a 7-day period in 1967 as a direct consequence of AMD (Nordstrom et al., 1977).

About 19,300 km of rivers and streams and more than 72,000 ha of lakes and reservoirs in the continental USA have been damaged by AMD (Kleinmann, 1989). In England and Wales, it is estimated that some 1,800 km of surface streams and rivers are currently impacted by AMD (Jarvis et al., 2006), whereas in SW Spain, from a total of 1149 km of the river network examined at the Odiel basin, 427 km were affected by AMD (Sarmiento et al., 2009). These studies clearly present AMD water pollution as a widespread and intense environmental problem that, taking into account only three countries in the world, implies more than 21,500 km of rivers and streams affected.

The Iberian Pyrite Belt (IPB), located in the south-west of the Iberian Peninsula, can be considered one of the biggest massive sulfide deposits in the world with a length of over 200 km, a width of about 40 km and original estimated reserves in the order of 1,700 Mt of sulfide ore (Sáez et al., 1999). The enormous amount of massive sulfides and related metal mineralization of this region attracted the economic and commercial interest of

numerous civilizations from immemorial times (Nocete et al., 2008). The result of the intense mining during almost 5,000 years (van Geen et al., 1997; Leblanc et al., 2000; Nocete et al., 2005) is a region where abandoned sulfide-rich wastes in spoil heaps and tailings and flooded underground mines and opened pits generates an ubiquitous problem of AMD pollution (Sainz et al., 2004; Nieto et al., 2007; Sarmiento et al., 2009).

As the main economic activity in the Huelva province has changed from mining to agriculture, the current pollution and possible remediation of inland water resources in the Odiel river basin has become an issue of great concern. Sarmiento et al. (2009) have shown in a recent study, covering the main rivers and streams of the Odiel basin, that for the 91 points under study, 24 were natural streams unaffected by AMD and the rest (67 points) were streams severely affected by acidic leachates from 28 different mines.

AMD can be remediated by two generic approaches: active or passive treatment. While the former is more appropriate to be used in mines under operation where fast remediation of enormous amounts of water is needed, the latter is a more realistic solution when AMD remediation has to be achieved in abandoned mine sites (like the ones at the IPB) where the absence of any accountable entity and remote location requires the use of a long lasting, low cost and environmentally sustainable treatment option with no artificial energy requirements (PIRAMID-Consortium, 2003).

Although some studies have recently shown the possibility to inhibit AMD generation in tailings by the use of fly ash (a strong alkaline residue) to induce the formation of a surface hardpan to isolate the residue and prevent sulfide oxidation (Perez-Lopez et al., 2007), the vast majority of the passive treatment systems typically focus on metal removal and hydrochemical quality improvement of the existing AMD. Traditional sulfate reducing bacteria (SRB) based treatments, like anaerobic wetlands (Dann et al., 2009; McCauley et al., 2009; Jarvis and Younger, 1999) or reactive permeable barriers (Cocos et al., 2002; Jarvis et al., 2006; Caraballo et al., 2010), have shown encouraging results treating AMD at coal mining districts, however they are not very useful to treat highly polluted AMD in areas with limited available space because SRB have maximum tolerance levels for certain metals and need a high residence time, up to six days (Neculita et al., 2008), to achieve an optimal bacterial growth. Limestone based treatments like anoxic limestone drainages (Watten et al., 2007; Santomartino and Webb, 2007) although efficient at treating AMD with low to moderate metal concentrations, commonly exhibit serious problems of clogging and passivation when exposed to AMD with high metal concentrations.

To overcome all the problems shown by the typical passive treatment systems treating highly polluted AMD and design a treatment to be implemented in the IPB, Rötting et al. (2008b) developed the dispersed alkaline substrate (DAS), consisting of a reactive mixture of pine wood shavings and limestone sand. The high metal removal performance of this reactive mixture has been broadly tested both in laboratory columns (Rötting et al., 2008b) and field-scale experiments (Rötting et al., 2008b; Caraballo et al., 2009b) for the highly polluted AMD at the IPB.

The main scope of the present study is to show the encouraging results obtained after 20 months of continuous operation of the full-scale DAS passive treatment system implemented at Mina Esperanza. Water hydrochemistry, precipitate mineralogy and metal removal efficiency of the different sections comprising the treatment will be presented to gain a better understanding of the different hydrochemical, mineralogical and operational processes involved in AMD remediation.

## 4.3 METHODS AND SAMPLING PROCEDURE

### 4.3.1 Site location

Mina Esperanza is located in the northern part of the IPB (Fig. 4.1A), in South-western Spain (37º45´34´´N-6º41´00´´O). The mineralization at Mina Esperanza consists of a massive pyrite deposit with minor amounts of chalcopyrite (Pinedo-Vara, 1963). The country rocks are slates and low grade metamorphic phyllites. This underground sulfide mine was under operation during the first half of the last century. After closure, the mine was naturally flooded and, subsequently, polluted water began to flow out of the main adit. This AMD is channeled by a creek, known as Esperanza creek, for 1 km to the Odiel River and can be considered one of the firsts important pollution sources to this river in the upper section of its basin (Sarmiento et al. 2009).

AMD composition at the exit of the adit and the main hydrochemical parameters are shown in Table 4.1.

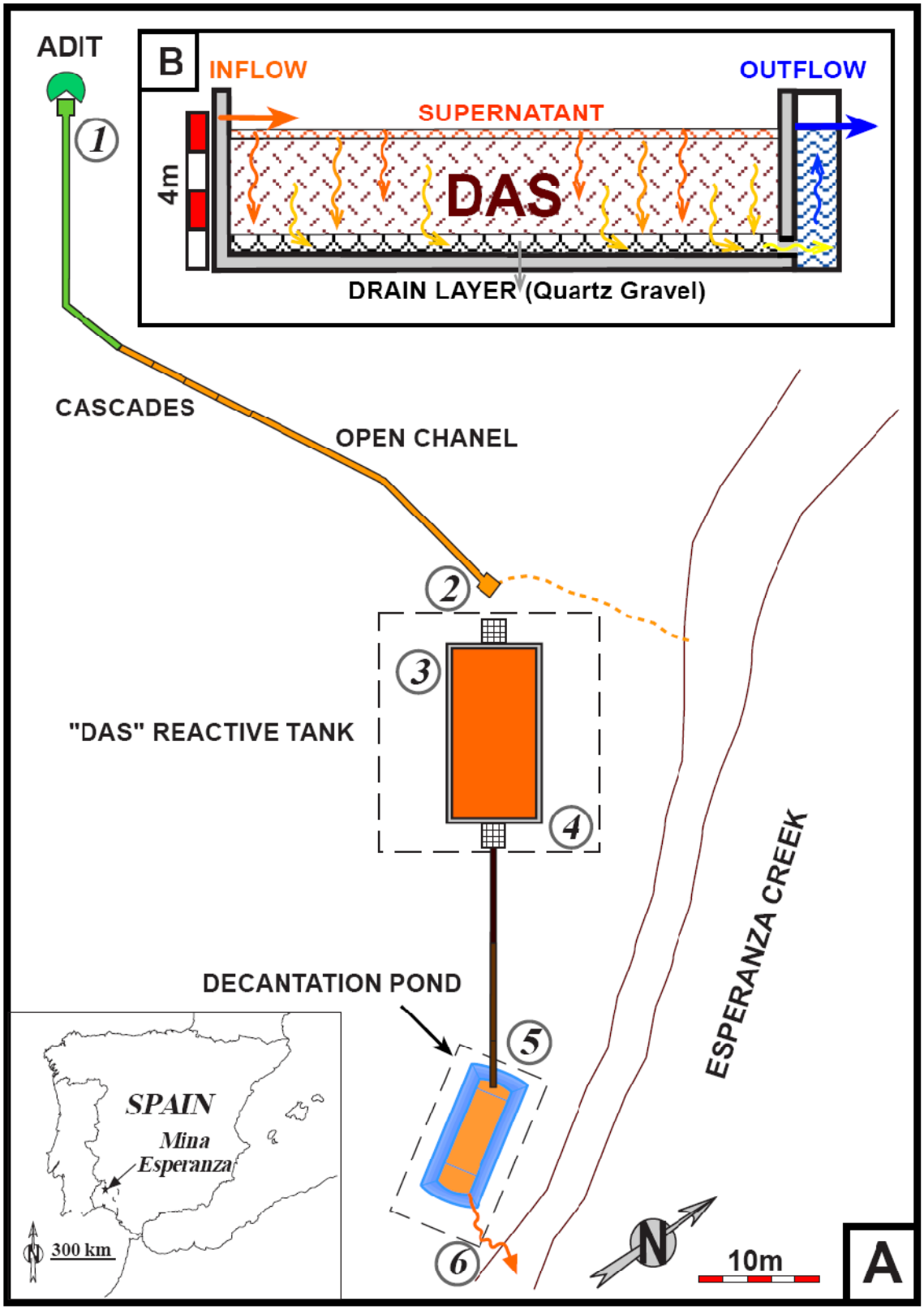


**Figure 4.1. A) Location and schematic plan view of the passive treatment at Mina Esperanza. 1 = Adit, 2 = reactive tank input, 3 = reactive tank supernatant, 4 = reactive tank output, 5 = decantation pond input and 6 = decantation pond output. B) Schematic cross section of the reactive tank.**

**TABLE 4.1**. AMD composition and physico-chemical parameters at the adit

| **Major elements (mg/L)** | | | | | | | | | | |
|---|---|---|---|---|---|---|---|---|---|---|
| Al | Ca | Cu | Fe | K | Mg | Mn | Na | $SO_4^{2-}$ | Si | Zn |
| 128-167 | 146-194 | 12-24 | 755-1100 | 5-34 | 149-215 | 4-6 | 21-26 | 3324-4515 | 44-60 | 19-33 |
| **Minor elements (µg/L)** | | | | | | | | | | |
| As | Ba | Be | Cd | Co | Cr | Li | Ni | Sr | Ti | V |
| 357-692 | 4-6.5 | 4-10 | 66-98 | 468-759 | 22-42 | 138-381 | 152-247 | 131-189 | 6.5-15 | 84-129 |
| **Physico-chemical parameters** | | | | | | | | | | |
| pH | | pe | T (ºC) | | Conductivity (mS/cm) | | Dissolved Ox. (mg/L) | | Dissolved Ox. (%) | |
| 2.35-2.96 | | 9.4-10.1 | 16.8-22.2 | | 3.24-6.12 | | 1.8-2.5 | | 13-28 | |

Data shown correspond to minimum and maximum values obtained in the 42 sampling campaign from March 2007 to October 2008

### 4.3.2 Water and solid sampling

Water samples were taken at least twice a month from March 2007 to October 2008, a total of 42 sampling campaigns along the 20 months of the system operation time. Six sampling points were selected as representative of the different sections of the treatment system (Fig. 4.1A) and called: Adit, T-in (reactive tank input), T-sup (reactive tank supernatant), T-out (reactive tank output), D-in (decantation pond input) and D-out (decantation pond output). Water samples were filtered immediately after collection through 0.1 µm Millipore filters on Millipore syringe filter holders, acidified in the field to pH < 1 with suprapur $HNO_3$ and stored at 4 ºC in 60 mL sterile polypropylene containers until analyzed.

During the last months of operation several solid samples were taken to characterize the Fe and Al precipitates formed at the system. Samples of iron precipitates were taken from the top of the reactive tank, from the initial and final section of the opened channel connecting the reactive tank to the decantation pond and in the decantation pond itself. The hydrochemical changes suffered by the reactive material during the end of the operation time led to the formation of a white precipitate at the output of the reactive tank. This precipitate was sampled to verify if it corresponded to an aluminum mineral phase. The three samples were gently heated (to prevent mineral phase transformations) in an oven up to 30ºC until dryness and ground to fine powder using an agate mill.

### 4.3.3 Field in-situ measurements

Temperature and electrical conductivity were measured using a portable CM35 meter (Crison®) with 3 point calibration (147 and 1413 µS/cm and 12.88 mS/cm). The pH and redox potential were measured using a PH25 meter (Crison®) with Crison electrodes. Redox potential and pH were controlled and calibrated using 2 points (240–470 mV) and 3 points (pH 4.01–7.00–9.21), respectively, with Crison standard solutions. Redox

potential measurements were corrected to the Standard Hydrogen Electrode to calculate pe. Dissolved $O_2$ was measured with an auto-calibrating Hanna® portable meter and gross alkalinity was determined using CHEMetrics® Total Titrets® (range 10–100 or 100–1000 mg/L as $CaCO_3$ equivalents, accuracy approximately 5%). A DR/890 portable HACH® colorimeter was employed to measure Fe(II) and total Fe concentration in the water. This concentration was determined by colorimetry at 510 nm after complexation in field by adding of 0.5% (w/w) 1,10-phenanthrolinium chloride solution to the filtered sample (Rodier et al., 1996). The detection limit was 0.2 mg/L and the precision better than 5%.

### 4.3.4 Laboratory analytical techniques

Concentrations of dissolved Al, As, Ba, Be, Ca, Cd, Co, Cr, Cu, Fe, K, Li, Mg, Mn, Na, Ni, S, Si, Sr, Ti, V and Zn were determined by Inductively Coupled Plasma Atomic Emission Spectrometry (ICP-AES Jobin- Ybon Ultima2) using a protocol especially designed for AMD samples (Tyler et al., 2004). Analysis was performed at the Central Research Services of the University of Huelva. Multielement standard solutions prepared from single certified standards supplied by SCP SCIENCE were used for calibration. They were run at the beginning and at the end of each analytical series. Certified Reference Material SRM-1640 NIST fresh-water-type and inter-laboratory standard IRMM-N3 wastewater test material (European Commission Institute for Reference Materials and Measurements) were also analyzed. Detection limits were calculated by average and standard deviations from 10 blanks. Detection limits were: 200 µg/L for Al, Fe, Mn, Mg, Na, K, Si and S; 500 µg/L for Ca; 50 µg/L for Zn; 5 µg/L for Cu; 2 µg/L for As and 1 µg/L for the other trace elements.

X-ray diffraction (XRD) study of randomly oriented powder samples was performed using a Bruker D5005 X-ray Diffractometer with Cu Kα radiation. Diffractometer settings were: 40 kV, 30 mA and a scan range of 2–60º 2θ, 0.01º 2θ step size and 12-s counting time per step for the samples with lower crystallinity (samples where schwertmannite and basaluminite were expected to be found) and 2–60º 2θ, 0.02º 2θ step size and 2.4-s counting time per step for the samples with higher crystallinity (samples where goethite and gypsum were expected).

Net acidity (*Ac*) (mg/L as $CaCO_3$ equivalents) was calculated according to the recommendations from Kirby and Cravotta, 2005a, b, and using the following equation after Rötting et al., 2008b:

$$Ac = 50{,}045 \bullet (3 \bullet c_{Al} + 2 \bullet c_{Fe} + 2 \bullet c_{Mn} + 2 \bullet c_{Zn} + 10^{-pH}) - alk \quad (4.1)$$

where $c_X$ are molar concentrations of the different metals (mol/L) and *alk* is measured gross alkalinity (mg/L as $CaCO_3$ equivalents).

Relative metal removal r (%) at the output of the system was calculated as:

$$r = \frac{(c_{in} - c_{out})}{c_{in}} \cdot 100 \quad (4.2)$$

where $c_{in}$ is the adit concentration (mg/L) and $c_{out}$ is the concentration at the output (D-out) of the system (mg/L).

Total metal removal $r_t$ (g) during the whole operation time of the system was calculated as:

$$r_t = \sum \frac{(c_{in} - c_{out}) \cdot 10^{-3}}{Q} \cdot n \quad (4.3)$$

where $c_{in}$ is the adit concentration (mg/L), $c_{out}$ is the concentration at the output of the system (mg/L), $Q$ is flow rate (L/day) between samplings and n is number of days between samplings.

Acid load reduction *RA* (g/($m^2$ • day)), normalized by system area was calculated as:

$$RA = Q \cdot \frac{Ac_{in} - Ac_{out}}{1000 \cdot A} \quad (4.4)$$

where $Q$ is flow rate ($m^3$/day), $Ac_{in}$ and $Ac_{out}$ are adit and system's outflow net acidity (mg/L as $CaCO_3$ equivalents), respectively, and $A$ is horizontal area of the treatment system ($m^2$).

### 4.3.5 Thermodynamic model

Precipitation of newly formed iron and aluminum solid phases has been observed to chemically control the fate of AMD contaminants in neutralization reactions (Bigham and Nordstrom, 2000; Sánchez-España et al., 2006) and to be an essential process in the treatment of AMD (Caraballo et al., 2009b). The equilibrium geochemical speciation/mass transfer model PHREEQC (Parkhurst, 1995) with the database of the speciation model MINTEQ (Ball and Nordstrom, 1991) was applied to determine aqueous speciation of the AMD and saturation indices of solid phases [SI =

log(IAP/$K_S$), where SI is the saturation index, IAP is the ion activity product and $K_S$ is the solid solubility product]. Zero, negative or positive SI values indicate that the solutions are in equilibrium, undersaturated and supersaturated, respectively, with respect to a solid phase. Additional thermodynamic data for schwertmannite was taken from Yu et al. (1999) and Kawano and Tomita (2001). Although thermodynamic models can offer a very useful approach to the expected mineral phases to be formed from the analyzed waters, these results need to be corroborated by mineral characterization of the final precipitates.

## 4.4 TREATMENT CONCEPT AND DESIGN

A previous removal strategy, based on SRB mediated metal sulfides precipitation, was implemented in Mina Esperanza by the Andalusian Government in 2000 (López-Fernández et al., 2006). This system involved a 480 $m^3$ concrete tank initially filled with a 1.75 m multi-layer of solid reagents (alternating layers of limestone pebbles and horse manure) and a 1.5 m liquid layer of organic nutrients (whey and cattle slurry). AMD from the adit was connected with the supernatant of the tank using a closed system of High Density Polyethylene (HDPE) pipes (160 mm inner diameter). This SRB-based system was under proper operation for 2 months with an inflow of 0.2 L/s. After this period it began to clog and metal removal became inefficient.

The promising results obtained by the use of limestone-DAS and Fe(II) oxidation enhancement strategies to treat the highly polluted AMD at the IPB, (Rötting et al., 2008b; Caraballo et al., 2009b; Macías et al., 2009) placed this technology as the best remediation option to be implemented in the new design for a passive treatment system at Mina Esperanza.

A concrete opened channel was built to direct the AMD emerging from the adit to the reactive tank. To improve AMD oxygenation a five-step cascade was included in the mid-section of the opened channel (Fig. 4.1A). This section was designed to have a gentle downward slope and a flat 30 cm-wide bottom to facilitate the slow AMD flow necessary for optimal settling of iron-oxidizing microbiological communities. The important role of iron oxidizing bacteria on the oxidation of Fe(II) to Fe(III) in acid waters has been widely studied in the recent years (Escobar, 2010; Kirby et al., 1999; Casiot et al., 2003) and specifically observed in the IPB (Rowe et al., 2007). Another important benefit offered by the inclusion of an open channel is the avoidance of the

clogging problems observed when the HDPE pipes were used in the previous SRB-based treatment at Mina Esperanza.

The reactive tank of the former SRB-based treatment was reused and filled with a 2.5 m layer of limestone-DAS, 80% v/v pine wood shavings and 20% v/v limestone sand. This reactive material has a high porosity (50%) that is essential to maintain its hydraulic conductivity and to minimize the clogging problems suffered by passive treatment systems precipitating solids within the porous space of the reactive material. At the bottom of the reactive material, a 50 cm drain layer of coarse quartz gravel was placed to avoid the reactive material to be transported into the exit of the reactive tank (Fig. 4.1B). Location of the output was set close to the upper limit of the tank (Fig. 4.1B). Water flow through the reactive material was gravity forced from top to bottom, finally emerging from the top of the water collecting well, creating an initial supernatant depth of 25 cm and a freeboard of 1 m (Fig. 4.1B). The residence time for the AMD within the reactive material typically ranged from 2.5 to 5 days for common inflow rates ranging from 86 to 43 $m^3$/day.

The third and final step of the treatment system is a 60 $m^3$ decantation pond. This section was connected with the reactive tank by the use of a concrete opened channel in the form of a three steps aeration cascade (Fig. 4.1A). The high volume of the pond implies a residence time for the AMD of 1.5 days if a 43 $m^3$/day inflow is considered. The main purpose of the decantation pond is to use the generated alkalinity to precipitate an additional amount of iron.

## 4.5 RESULTS AND DISCUSSION: MINA ESPERANZA PERFORMANCE

### 4.5.1 Water chemistry evolution throughout the treatment

The treatment system can be conceptually divided into four main sections: first oxidation cascades, reactive tank, second oxidation cascades and decantation pond (Fig. 4.1A). To achieve a better understanding of the role played by each section in the overall system performance and for the sake of simplicity, time evolution for only two physical-chemical parameters (pH and pe), one operational parameter (flow rate), concentration of five major elements (Al, Ca, Cu, Fe and Si), as well as alkalinity and net acidity, will be presented (Fig. 4.2 and 4.3). This section will show an overview of the different processes taking place in the system while the time evolution of the selected parameters of the system will be shown in the following section.

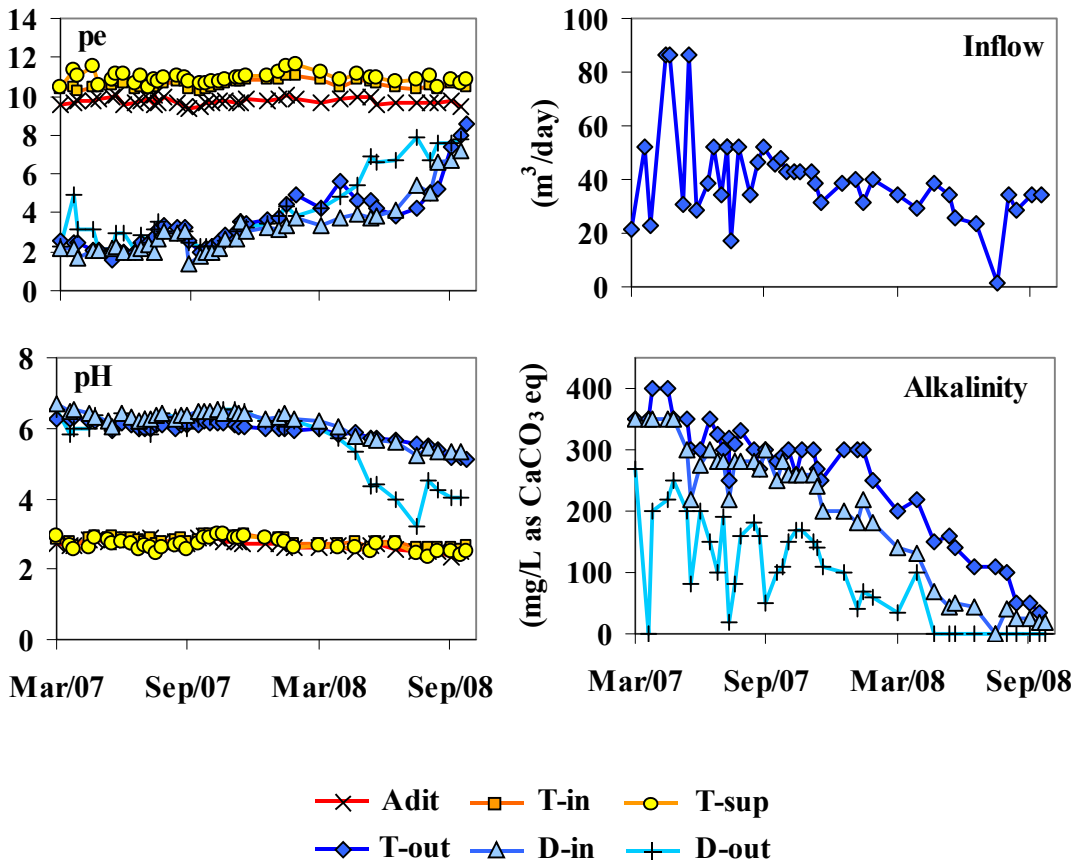


**Figure 4.2. Time evolution for pH, pe, alkalinity and flow rate at the six check points in the passive treatment system. T-in = reactive tank input, T-sup = reactive tank supernatant, T-out = reactive tank output, D-in = decantation pond input and D-out = decantation pond output. Note: Alkalinity was zero throughout the entire study in Adit, T-in and T-sup.**

Redox potential in AMD has been observed to be controlled by aqueous iron speciation (Nordstrom, 2000) and a high correlation ($R^2$ = 0.94, n = 90) between redox potential measured in the field with theoretical redox potential values calculated from Fe(II)/(III) determinations in AMDs at the Odiel basin has been previously reported (Sarmiento et al., 2009). Taking these observations into account, and in addition to the several iron speciation studies performed during the system operation time, redox potential measurements were used to study the different processes affecting iron speciation along the treatment.

A significant pe increase can be observed in the AMD after flowing along the aeration cascades, remaining around the same value at the supernatant check point (Fig. 4.2).

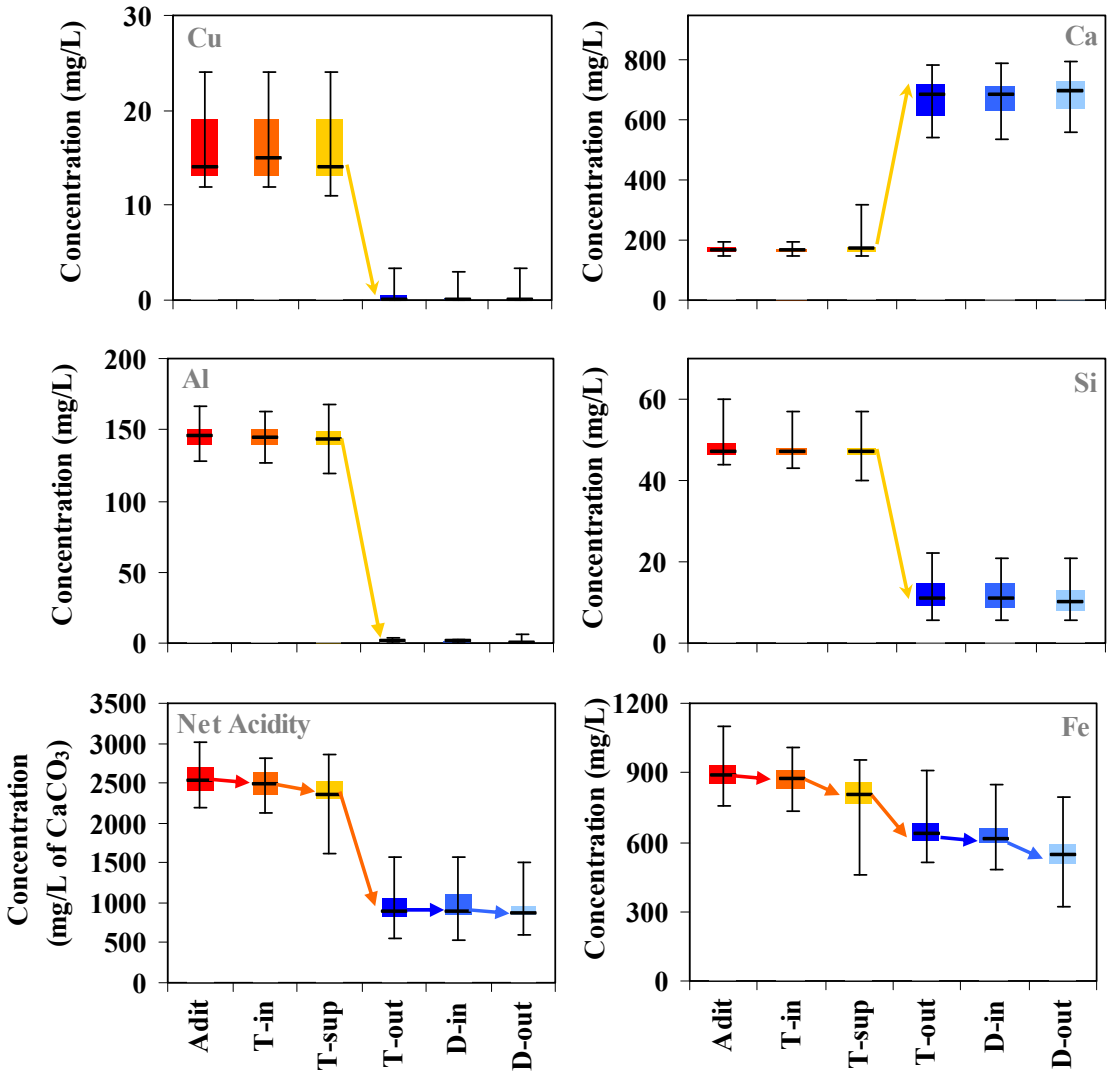


**Figure 4.3. Box and whisker diagrams for the most significant mayor metals and net acidity. Minimum, first quartile, median, third quartile and maximum values are shown for the six check points in the passive treatment system.**

This pe increase and the linked oxidation of around 100 mg/L of ferrous to ferric iron in the AMD (Table 4.2) was probably related to the presence of a particular community of algae and bacteria developed on the surface of the open channels. These microorganisms and their exact roles are currently being studied in detail.

**TABLE 4.2.** Iron speciation in mg/L along the treatment, June 2007

| Sample | Fe (II) | $Fe_{total}$ | Fe (III) | $Fe_{removal}$ |
|---|---|---|---|---|
| Adit | 759 | 778 | 19 | |
| T-in | 652 | 774 | 122 | 4 |
| T-sup | 630 | 754 | 124 | 20 |
| T-out | 620 | 628 | 8 | 126 |
| D-in | 584 | 599 | 15 | 29 |
| D-out | 538 | 543 | 5 | 56 |

As expected, flow of AMD through the reactive tank caused the main hydrochemical changes along the treatment. From the input to the output of the reactive tank, the water

pH increased from <3 to a value around 6.5 while a coupled inverse behavior was showed by pe values (Fig. 4.2). Calcite dissolution within the reactive tank can distinctly be observed in the significant increase in Ca concentration (Fig. 4.3) and alkalinity (Fig. 4.2) in the waters flowing out of the reactive tank. This pH increase induces Fe precipitation and complete Al removal (Fig. 4.3) within the reactive tank, as well as total Cu removal and a significant Si depletion in the AMD (Fig. 4.3). The processes of Fe and Al precipitation and coprecipitation and/or adsorption of other metals have been widely studied in many laboratory and field experiments using limestone-DAS to remediate AMD (Rötting et al., 2008b; Caraballo et al., 2009b; Caraballo et al., 2009c) and the reader is referred to these works for further details. The primary role of the reactive tank in the whole treatment performance is demonstrated by the achievement of a net acidity removal within the reactive mixture in the range of 1500 mg/L as $CaCO_3$ equivalents (Fig. 4.3).

The high pH typically shown at the waters emerging from the reactive tank are a possible explanation for the absence of a well developed microbial community along the second aeration cascades. Although comparison of T-out and D-in waters show an almost negligible change in water pe and a very small increase in ferric iron (Fig. 4.2 and Table 4.2), it is important to notice that both the water iron removal (Table 4.2) and the remarkable amount of Fe(III) precipitates formed along the channel suggest a noticeable ferric iron generation. This situation can be explained by the significant increase of iron abiotic oxidation at circumneutral pH values and the coupled rapid precipitation of goethite in these special water conditions (Bigham and Nordstrom, 2000; Cornell and Schwertmann, 2003). Goethite precipitation will be discussed in more detail in the following sections.

A significant iron removal (Fig. 4.3 and Table 4.2) and alkalinity consumption (Fig. 3.2) was achieved in the decantation pond. While iron precipitation tends to lower water pH by the generation of $H^+$ (Bigham and Nordstrom, 2000), this effect is counteracted by the remarkable alkalinity of the DAS-treated water leading to a final water pH close to the value observed at the reactive tank output.

### 4.5.2 Time evolution of the treatment's performance and metal removal

Throughout most of the first year of operation the hydrochemical behavior of the system was quite steady, however after this period some slight changes were observed in the reactive tank and subsequently in the decantation pond. A slow decrease in water pH at the reactive tank output was observed during the last eight months of operation (Fig.

4.2). This pH time evolution from 6.0 in March 2008 to 5.1 in October 2008 was associated with a progressive decrease in water alkalinity from 200 mg/L as $CaCO_3$ to close to 0 mg/L as $CaCO_3$ for the same period of time (Fig. 4.2). In addition to this effect and connected to the alkalinity decrease at the reactive tank output, an important decrease in the pH at the decantation pond output was observed (Fig. 4.2).

Aluminum, copper and cadmium were completely removed within the reactive tank during the first year of operation, showing only a slight decrease in the relative removal of these elements during the last months of operation (Fig. 4.4). Aluminum was the least sensitive of these three elements to the observed water pH change and only when water pH was close to 5 a very small decrease in aluminum removal was observed (Fig. 4.4). This observation is in accordance with the proposed pH value of 5 for hydrobasaluminite ($Al_4(SO_4)(OH)_{10}•15H_2O$) precipitation in AMD (Bigham and Nordstrom, 2000). The more pronounced effect that water pH decrease had on Cu and Cd relative removal (Fig. 4.4) is in agreement with the hypothesis of pH dependent adsorption as the most likely removal process for these two elements, as shown in previous DAS field experiments (Caraballo et al., 2009b). Iron removal during the great majority of the treatment's operation time range between 20% and 40% and was not clearly affected by decreases in pH and alkalinity during the last months of operation (Fig. 4.4). A complete removal for As, Cr, Ti and V was observed throughout the entire operation time of the treatment system (Fig. 4.4). Arsenic removal coupled to iron precipitation has been previously reported for DAS-based passive treatment systems (Caraballo et al., 2009b) as well as for many natural environments (Acero et al., 2006; Asta et al., 2009) and laboratory experiments (Carlson et al., 2002; Regenspurg et al., 2004; Wang et al., 2006).

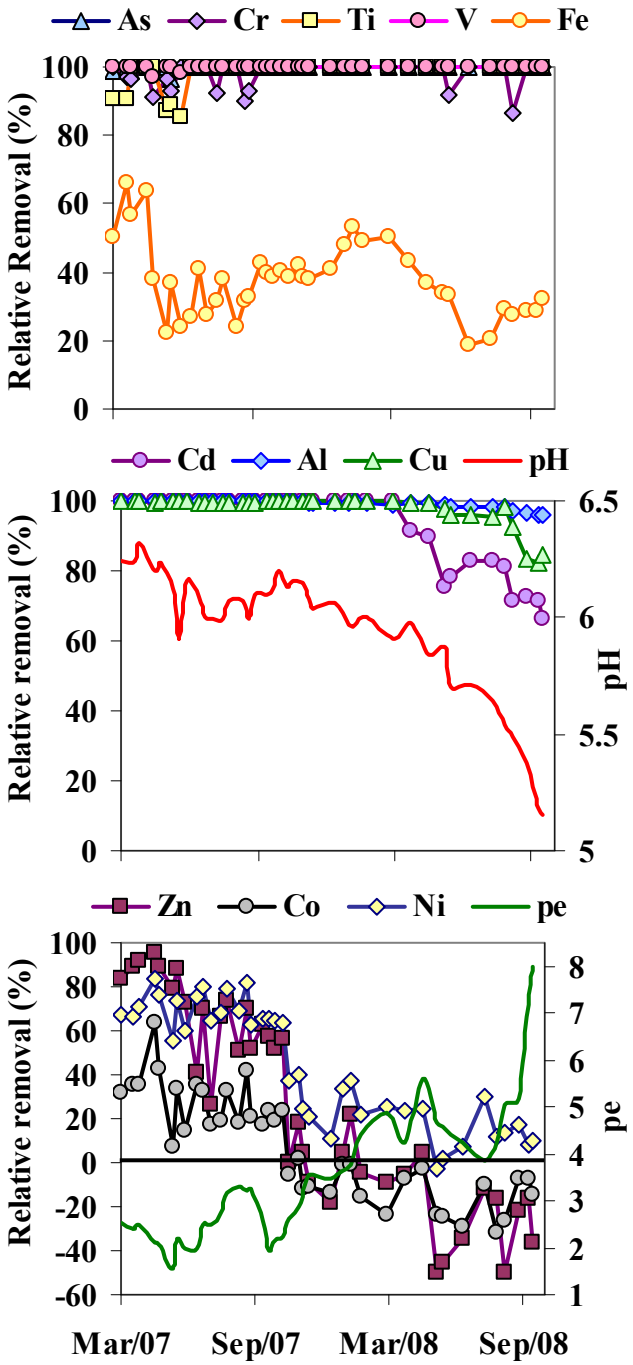


**Figure 4.4. Time evolution of metal relative removal (%) achieved by the system from the adit to the outflow of the decantation pond. pH and pe values are plotted to compare the effect of these factors on the removal of certain metals.**

Unexpectedly low pe values, ranging from 1.5 to 3, during the first months of operation, followed by a dramatic water pe increase with time was observed in the reactive tank outflow (Fig. 4.2). In addition, a very high Zn, Co and Ni relative removal was achieved for the six first months of operation (Fig. 4.4). After some months, the initial important metal removal for these elements progressively decreased leading to a negative metal removal (output water concentration higher than input water concentration) that was

clearly correlated with the water pe increase (Fig. 4.4). Chemically induced Zn, Co and Ni precipitation as hydroxides can only be expected after reaching a pH value higher than 8, 9 and 10 respectively (Cortina et al., 2003; Rötting et al., 2008a). The presence of organic matter (wood shavings) in the reactive material and the two months that the reactive tank remained flooded previous to the system inauguration could have facilitated the growth of some sulfate reducing bacteria (SRB) within the reactive mixture, thus offering a possible explanation for the remarkable Zn, Co and Ni removal during the first months of operation. However due to the high flow rate employed in the treatment and the subsequent low residence time within the reactive mixture, the environmental conditions were no longer favorable for the optimal growth of SRB and therefore it could be implied that the activity of these bacteria progressively ceased, and subsequently the removal of Zn, Co and Ni ceased as well.

By the use of measured flow rate for every sampling and water metal removal in the system an estimation of the total metal removal achieved by the treatment after its whole operation time was calculated (Equation 3). As shown in Table 4.3, iron is the main metal removed in the treatment with a calculated mass of more than 7 tons, followed by aluminum with almost 3 tons and copper and zinc with 0.3 and 0.1 tons respectively. Another important element removed in the system is sulfur with an estimated amount of 6.9 tons as $SO_4$. This amount of $SO_4$ removal is unexpected for a passive treatment system not based in sulfate-reducing processes. For the minor elements, present in the AMD in µg/L, an important removal in the order of kg was achieved, As being the main removed pollutant with 9.5 kg followed by V, Ni, Cd, Co, Cr, and Ti (Table 4.3). Taking into account the amount of Ca released into solution, the amount of dissolved calcite can be estimated, leading to a value close to the 26 tons of dissolved calcite within the reactive tank. Notwithstanding, this value is probably an underestimation of the real amount of dissolved calcite because, as observed in previous studies (Rötting et al., 2008b; Caraballo et al., 2009b; Caraballo et al., 2009c), gypsum precipitation within the reactive material decreases Ca concentration at the output of the reactive tank.

**TABLE 4.3**. Total metal removal in the passive treatment after 20 months of operation

| **Al (tons)** | **Ca (tons)** | **Cu (tons)** | **Fe (tons)** | **$SO_2$ (tons)** | **Si (tons)** | **Zn (tons)** |
|---|---|---|---|---|---|---|
| 2.7 | -10.5 | 0.3 | 7.1 | 6.9 | 0.6 | 0.1 |
| **As (kg)** | **Cd (kg)** | **Co (kg)** | **Cr (kg)** | **Ni (kg)** | **Ti (kg)** | **V (kg)** |
| 9.5 | 1.4 | 1 | 0.6 | 1.6 | 0.2 | 1.8 |

### 4.5.3 System efficiency

To have a better understanding of the high pollution that the treatment at Mina Esperanza has to accommodate, and the high remediation efficiency achieved by the

treatment, it was decided to compare the 42 sampling campaigns from Mina Esperanza with the available data of 83 different passive treatment systems recapped for the USA by Ziemkiewicz et al. (2003). This study comprised 11 anaerobic wetlands (AnW), 28 anoxic limestone drains (ALD), 16 vertical flow wetlands (VFW), 10 oxic limestone channels (OLC) and 18 limestone leach beds (LSB). For the sake of simplicity, it was decided to plot the available data into several box and whisker diagrams (Fig. 4.5 and 4.6) where minimum, first quartile, median, third quartile and maximum were shown for the three selected parameters.

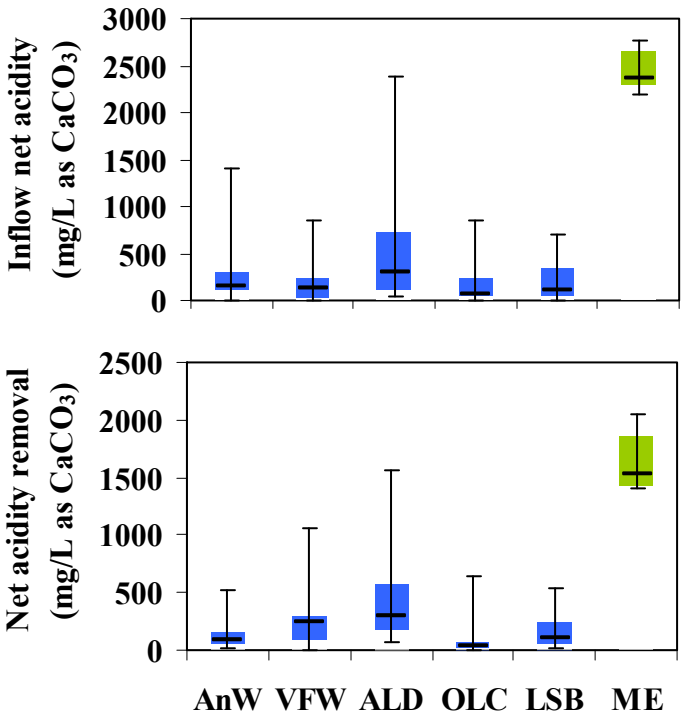


**Figure 4.5. Box and whisker diagrams comparing inflow net acidity and net acidity removal values for Mina Esperanza and more than 80 traditional passive treatment systems at the USA. AnW = anaerobic wetland, VFW = vertical flow wetland, ALD = anoxic limestone drains, OLC = opened limestone channels, LSB = limestone leach beds and ME = Mina Esperanza.**

Inflow net acidity was calculated to offer an estimation of the metal pollution to which each passive treatment system was subjected. As shown in the top of figure 4.5, net acidity achieved a median value as high as 2,300 mg/L as $CaCO_3$ for the treatment at Mina Esperanza (ME). It can also be noticed that the inflow net acidity at ME is typically one order of magnitude higher than the median value exhibited by the great majority of the treatments compared in this section. This observation has a great significance for a passive treatment dealing with AMD because the long-term performance of this kind of treatment is highly influenced by the metal concentration and acidity in the inflow water (Younger et al., 2002).

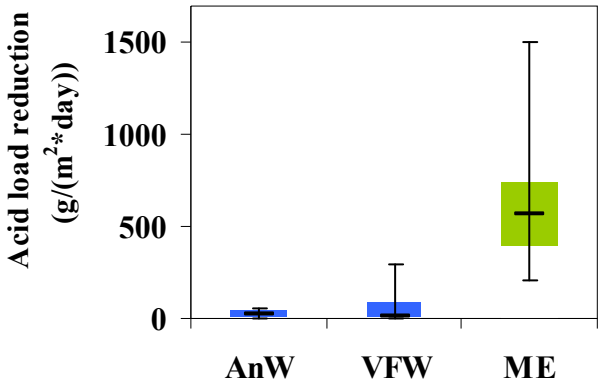


**Figure 4.6. Box and whisker plots for acid load reduction. AnW = anaerobic wetland, VFW = vertical flow wetland and ME = Mina Esperanza.**

To compare the removal capacity of the different treatments, it was decided to employed the net acidity removal because this parameter offers a good approach to the acidity neutralization capacity of the treatments and also to the amount of metal removed (according to equation 1). Net acidity removal was calculated by subtracting the net acidity at the system output to the inflow net acidity. Median net acidity removal achieved in ME was observed to be 5 times higher than the same value for VFW and ALD, up to 15 times higher than the median values achieved in AnW and LSB and as much as 43 times higher comparing with LSB (Fig. 4.5 bottom). It can also be observed that the third quartile for ME is considerably broader than the first quartile, implying that changes in net acidity removal for ME typically moves to achieved higher values close to 2,000 mg/L as $CaCO_3$.

Acid load reduction in $g•(m^2•day)^{-1}$ is a parameter commonly employed to characterize the surface efficiency of a passive treatment system and therefore can be used to gain a better understanding of the surface land requirement of the different passive treatments. Comparing the available median values for AnW and VFW with the values obtained for ME it can be observed that the median removal efficiency achieved in ME (597 $g•(m^2•day)^{-1}$) is 32 times higher than the median values obtained for the AnW and as much as 47 times higher compared with VFW median values (Fig. 4.6). This observation has to be seriously taken into account when choosing a remediation option for a site for cases in which the land to build a passive treatment system is scarce and/or expensive. On the other hand, when land availability is not an important influence on the project budget, the construction of a passive treatment system achieving, for instance, the same acid load reduction as observed at ME (with a surface area of 120 $m^2$) would require the use of more than 3,600 $m^2$ in the best case and up to 5,600 $m^2$ for the worst scenario. The large land requirements of the other treatment methods would

have a clear visual and environmental impact in the landscape of any region and even more important it drastically increases the construction cost of the passive treatment system. The results obtained at ME (in term of acid load reduction) improve by more than 10 times the generally accepted 40 g•($m^2$•day)$^{-1}$ values developed by the U.S. Bureau of Mines (Hedin et al., 1994) and commonly used as a system designing criterion.

### 4.5.4 Thermodynamic and diffractometric approach to the mineral precipitates

Fe, Al, and S (as sulfate) are typically the three main elements controlling AMD hydrochemistry and subsequently the precipitates. In addition, the high concentration of Ca in the waters after flowing through the reactive material suggests Ca should be found in the mineral phases.

As evidenced by the saturation indices (Fig. 4.7), iron hydrochemistry controls the mineral phases predicted for the first section of the treatment, before the water flows through the reactive material. At the adit, precipitation of jarosite, goethite and schwertmannite (using the equilibrium constant from Kawano and Tomita, 2001) is predicted (Fig. 4.7), however no real evidence of any significant precipitate was found during all the operation time for this point. At the reactive tank input and in the supernatant these three iron phases are again proposed to form by the geochemical model while ferrihydrite and gypsum remain undersaturated (Fig. 4.7). Only the presence of schwertmannite in these two points was confirmed by the use of XRD (Fig. 4.8A) while no evidence of any other mineral phase could be observed in fresh precipitates. Goethite was detected in the bottom layers of the precipitates but never as a fresh precipitate. This goethite distribution was previously reported in passive treatment systems (Gagliano et al., 2004; Caraballo et al., 2009b; Caraballo et al., 2009c) and in natural iron stromatolites (Acero et al., 2006, Asta el al., 2009) as an aging product of metastable schwertmannite that formed earlier.

Increases in alkalinity and pH of the waters after flowing through the reactive material causes apparent oversaturation of a number of mineral phases, according to the geochemical model. Many Fe mineral phases (schwertmannite, goethite, ferrihydrite, and siderite) are shown as oversaturated phases during the entire operation time of the treatment (Fig. 4.7) as well as some Al mineral phases (amorphous $Al(OH)_3$, basaluminite and gibbsite) and gypsum (Fig. 4.9). At this point only the presence of goethite and gypsum was unequivocally determined (Fig. 4.8B) while the appearance of basaluminite was observed, emerging at the reactive tank output, during the last months

of operation (Fig. 4.10). Coexistence of goethite (dark brown-reddish) and basaluminite (intense white) were never visually observed nor detected by XRD. Saturation indexes for calcite at the output of the reactive tank clearly show a decreasing tendency with time (Fig. 4.9) due to the decrease with time of water alkalinity and pH as a result of a lesser calcite dissolution within the reactive tank as calcite is depleted.

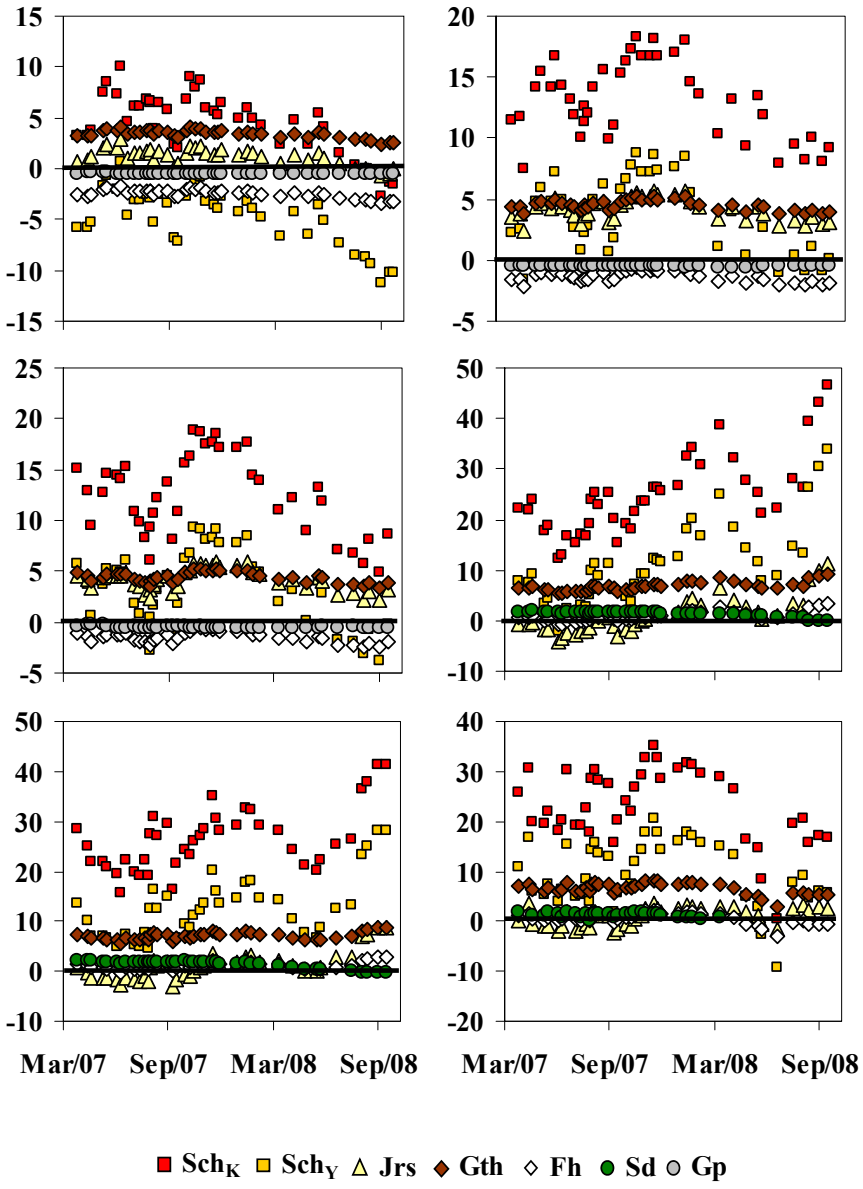


**Figure 4.7. Saturation indexes at the six sampling points for the most relevant iron mineral phases. SchK = schwertmannite calculated using the solubility constant proposed by Kawano and Tomita (2001), SchY = schwertmannite calculated using the solubility constant proposed by Yu et al. (1999), Jrs = jarosite, Gth = goethite, Fh = ferrihydrite, Sd = siderite and Gp = gypsum.**

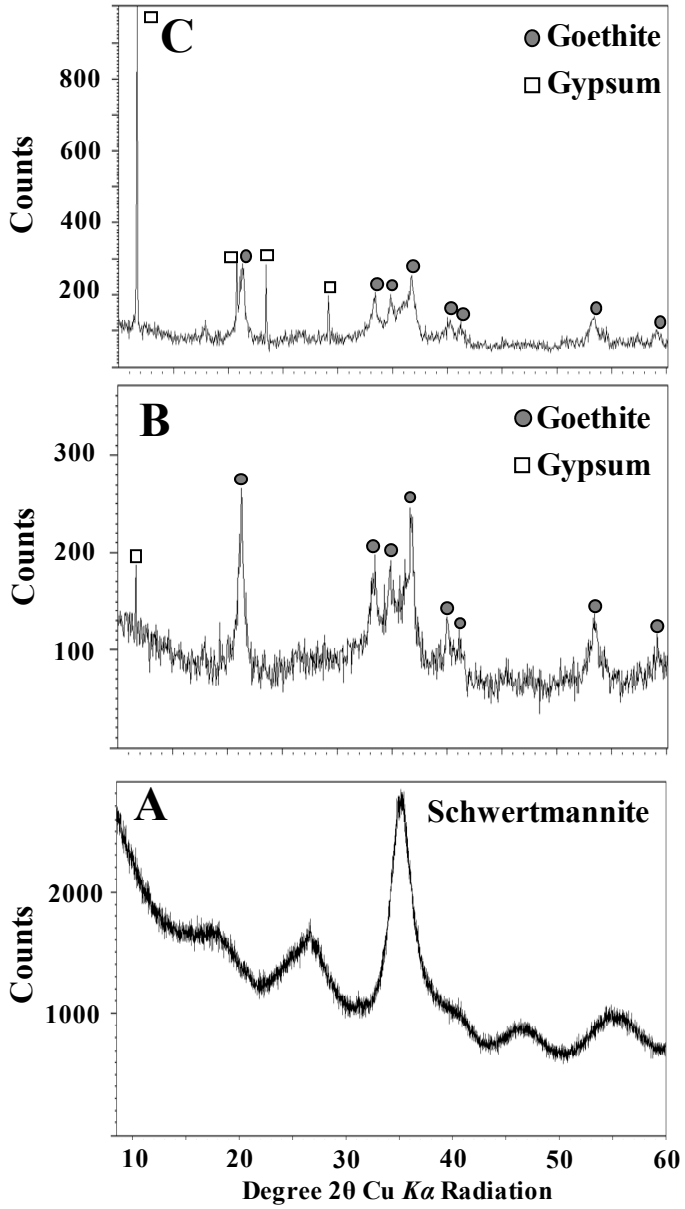


**Figure 4.8. XRD mineral characterization of some of the iron precipitates. A) Reactive tank supernatant, B) reactive tank output and C) decantation pond input.**

Although several Fe and Al mineral phases are predicted to appear in the second oxidation cascades and in the decantation pond (Fig. 4.7 and 4.8), only the presence of gypsum and goethite in the cascades (Fig. 4.8C) and schwertmannite in the decantation pond was confirmed by the XRD study performed on these samples.

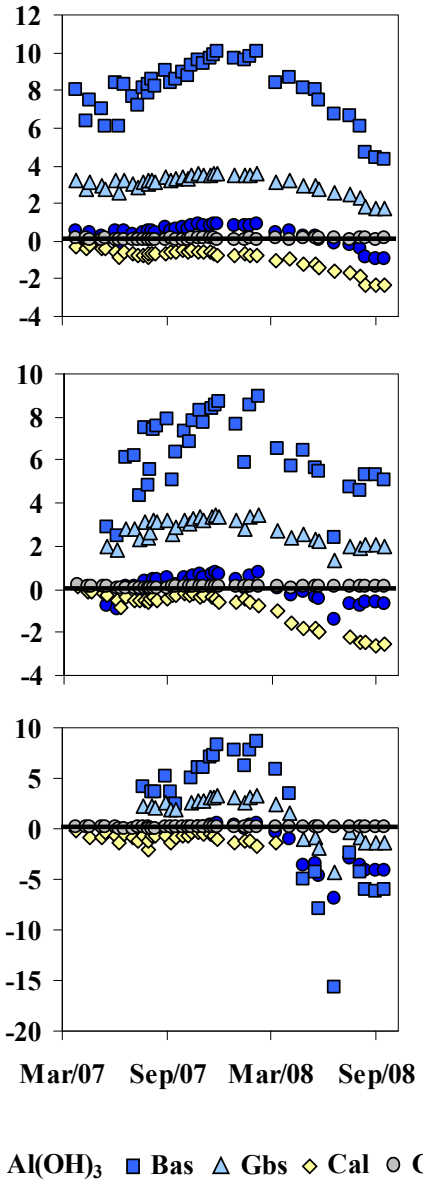


**Figure 4.9. Saturation indexes at the six sampling points for the most relevant aluminum mineral phases. $Al(OH)_3$ = amorphous $Al(OH)_3$, Bas = basaluminite, Gbs = gibbsite, Cal = calcite and Gp = gypsum.**

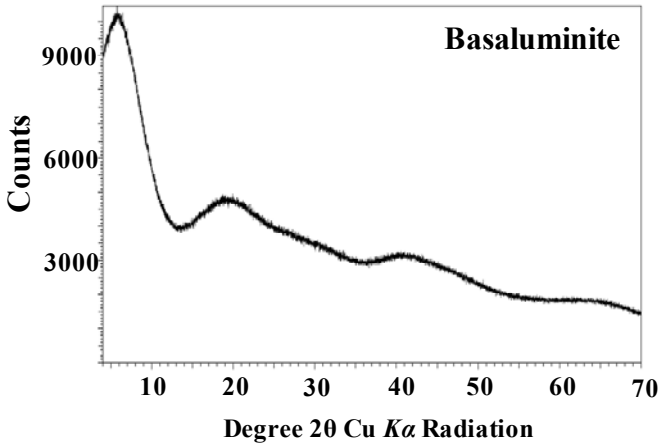


**Figure 4.10. XRD mineral characterization of the aluminum precipitates at the reactive tank output.**

## 4.6 CONCLUSIONS

The passive treatment system implemented in Mina Esperanza offers a good example of a simple design overcoming the most typical operational problems suffered by traditional passive treatment systems when they are exposed to highly metal polluted waters. The high porosity and hydraulic conductivity showed by the limestone-DAS reactive material enabled the system to treat a high inflow (ranging between 43 and 86 $m^3$/day) for 20 months without suffering any significant clogging problem.

The chosen design for the cascades connecting the adit to the reactive tank provides a slow-flow environment that promotes the establishment of iron oxidizing bacteria and algae, which seem to accelerate the oxidation of ferrous to ferric iron and subsequently increase iron removal on the surface of the reactive tank.

During its long operation time the system achieved a high and consistent metal removal with mean removal values of 144 ± 9 mg/L Al, 16 ± 6 mg/L Cu, 40 ± 4 mg/L Si, 490 ± 75 µg/L As, 73 ± 9 µg/L Cd, 28 ± 6 µg/L Cr, 85 ± 50 µg/L Ni, 10 ± 3 µg/L Ti and 94 ± 18 µg/L V. Iron was the main removed metal in the system showing a water removal ranging from 170 to 620 mg/L depending on the system performance.

Although some different Fe and Al mineral phases were shown to be oversaturated in the waters of the treatment, according to the geochemical modeling study performed, only the presence of schwertmannite, goethite, basaluminite and gypsum was confirmed. Schwertmannite was shown to be the main mineral phase controlling Fe removal throughout the system although some Fe removal was observed to be achieved after direct goethite precipitation at the high pH values obtained at the reactive tank output. Al precipitation occurred within the reactive material and only when water pH at the output of the reactive tank was close to a value of 5.5 some Al precipitates, in the form of basaluminite, were observed.

The high efficiency attained by the passive treatment system was illustrated by the high inflow net acidity and the significant net acidity removed from the treated AMD. These two parameters showed to be typically one order of magnitude higher than the values reported for more than 80 traditional passive treatment systems in the USA. Furthermore, the high acid load reduction, expressed in terms of $g•(m^2•day)^{-1}$, reached by the treatment at Mina Esperanza was 10 times higher than the generally accepted 40 $g•(m^2•day)^{-1}$ value commonly used as a passive treatment system designing criterion.

All these observations have important implications for the future design of passive treatment systems to be exposed to highly polluted AMD, and their future implementation in new remediation sites at the IPB should be seriously considered as an efficient and economic way of remediating the environmental problems suffered by this region.

# CHAPTER 5. HYDROCHEMICAL PERFORMANCE AND MINERALOGICAL EVOLUTION OF A DISPERSED ALKALINE SUBSTRATE (DAS) REMEDIATING THE HIGHLY POLLUTED ACID MINE DRAINAGE IN THE FULL SCALE PASSIVE TREATMENT OF MINA ESPERANZA (SW, SPAIN)

***This chapter is based on the paper*: Manuel A. Caraballo, Francisco Macías, José Miguel Nieto, Julio Castillo, Dino Quispe and Carlos Ayora. Hydrochemical performance and mineralogical evolution of a Dispersed Alkaline Substrate (DAS) remediating the highly polluted acid mine drainage in the full scale passive treatment of Mina Esperanza (SW, Spain). American Mineralogist, In Press.**

## 5.1 ABSTRACT

Acid mine drainage remediation is an unresolved matter in abandoned mining districts around the world. Development and implementation of passive treatment systems in these areas are commonly focused on engineering and water quality aspects; nevertheless, neoformed mineral phases precipitated within the reactive material of

those passive treatments play an essential role on their performance. After 20 months of operation and monitoring, the limestone based passive treatment system implemented in Mina Esperanza (SW Spain) was sampled to study in detail the relationship between water chemistry, mineral composition of the neoformed precipitates and treatment performance. Water chemical profiles showed the existence of three precipitation zones controlled by Fe, Al and Zn hydrochemistry and also the migration with time of those precipitation zones downward the reactive material. This precipitation zones were also confirmed by the mineral study performed to the solid samples, where schwertmannite and goethite, hydrobasaluminite and Zn rich green rust were the mineral phases controlling metal removal in the Fe, Al and Zn precipitation zones, respectively. Fe and Al precipitates were observed to play a critical role in the time evolution of the reactive material hydraulic conductivity. Furthermore, Al precipitates passivated to some extent limestone grains by armoring, although migration of the Fe precipitation zone and Al redissolution activate again the limestone grains. A higher proportion of limestone in the reactive mixture and the addition of new reagents to the bottom section of the reactive material (to enhance the reducing environment and to promote divalent metals removal) are proposed on the basis to this hydrochemical and mineralogical study for a future new design in the Mina Esperanza passive treatment system.

## 5.2 INTRODUCTION

Acid mine drainage (AMD) is an ancient and widespread environmental problem providing one of the most extreme and unique environments on the Earth. Polluted waters in mining areas typically exhibit low pH and high metal contents as a result of the sulfide dissolution taking place after the exposure of these minerals to the surface oxic conditions (Bigham and Nordstrom, 2000).

The Iberian Pyrite Belt (IPB) in the SW of the Iberian Peninsula is one of the largest massive sulfide provinces in the world with original estimated reserves in the order of 1,700 Mt of sulfide ore (Sáez et al., 1999). This region is also known to be a world-class example of AMD pollution where the long term effect of this contamination is dated back prior to roman times (Nocete et al., 2005). The wide exposure of sulfide rich residues and the lack of carbonate rocks in this region not only create a ubiquitous problem of AMD with very high metal content (Sarmiento et al., 2009).

AMD at abandoned mine districts is typically faced by the implementation of passive treatment technologies (Younger et al., 2002). Remediation techniques like permeable

reactive barriers, vertical flow wetlands or aerobic wetlands have been successfully employed to improve water quality in coal mining areas affected by AMD (Caraballo et al., 2010; Jarvis et al., 2006; Johnson and Hallberg, 2005). However, the high metal content observed in the AMD from the IPB severely reduces the efficiency of conventional passive treatment systems. To overcome the common clogging problems and losing of reactivity exhibit by traditional reactive substrates submitted to AMD with high metal contents, a novel reactive mixture known as Dispersed Alkaline Substrate (DAS) was successfully tested in both laboratory (Rötting et al., 2008c) and field experiments (Caraballo et al., 2009b; Rötting et al., 2008b). Limestone-DAS is a high porosity-high reactivity substrate made of a mixture of 80 % v/v pine wood shavings and 20 % v/v limestone sand.

Passive treatments studies are commonly focused on water chemistry improvement and metal removal, obviating the important role exerted by mineral precipitates in AMD water chemistry and passive treatments performance. Specifically, iron and aluminum precipitates play a key role buffering water pH (Bigham and Nordstrom, 2000), inducing reactive material passivation (Caraballo et al., 2009c), reducing the hydraulic conductivity of the reactive material (Rötting et al., 2008b) and removing other toxic metals by coprecipitation and/or absorption processes (Caraballo et al., 2009b).

This work will present the hydrochemical and mineralogical information obtained in the limestone-DAS passive treatment in Mina Esperanza after 20 month of operation. This is the first full scale experiment of DAS remediation systems. On the basis of the role played by precipitates in limestone consumption/passivation, hydraulic conductivity evolution and removal efficiency, some improvements to the original design will be discussed.

## 5.3 MATERIALS AND METHODS

### 5.3.1 Field site and treatment description

The passive treatment system implemented in Mina Esperanza is located in the northern part of the IPB, in South-western Spain (Fig. 5.1A). As many other AMD discharges at the IPB, the highly polluted water emerging from the adit of Mina Esperanza is characterized by low pH, high electrical conductivity and high metal content. A detailed compositional range of metal concentration and physical-chemical parameters obtained

at the adit mouth after monitoring the system for 20 months (March 2007-October 2008) is shown in Table 5.1.

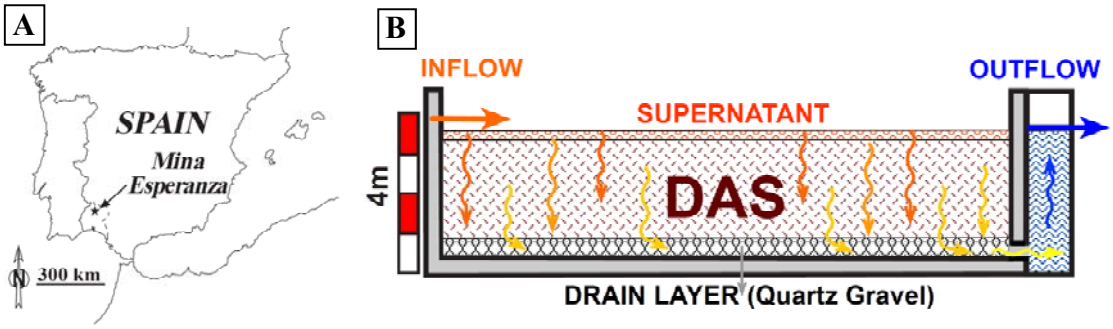


**Figure 5.1.A) Location of the passive treatment system in Mina Esperanza B) Cross section of the reactive tank in Mina Esperanza.**

The AMD emerging from the adit is directed by a concrete opened channel to the reactive tank. Water inflow was controlled to obtain common inflow rates ranging from 43 to 86 m3/day. The reactive tank has a volume of 480 m3 (15 m x 8 m x 4m, long x wide x deep) and was filled with a 0.5 m bottom drain layer of inert quartz gravel and an overlaying 2.5 m limestone-DAS layer (Fig. 5.1B). Water flow through the reactive material was gravity forced from top to bottom, finally emerging from the top of the water collecting well, creating an initial supernatant depth of 0.25 m and a freeboard of 0.75 m (Fig. 5.1B). The reactive tank was equipped with 9 sampling tubes (1 cm inner diameter) at different depths: -25 cm and -5 cm in the supernatant, 15, 25, 50, 65, 80, 175 and 230 cm within the reactive material. Zero corresponds to the water-reactive interface and sample at 280 cm to the emerging water at the collecting well. Residence time for the AMD within the reactive material typically ranged from 2.5 to 5 days. Finally, the water emerging from the reactive tank is conducted to a 60 m3 decantation pond by a concrete opened channel.

**TABLE 4.1**. AMD composition and physical-chemical parameters at the adit

| **Major elements (mg/L)** | | | | | | | | | | |
|---|---|---|---|---|---|---|---|---|---|---|
| Al | Ca | Cu | Fe | K | Mg | Mn | Na | $SO_4^{2-}$ | Si | Zn |
| 128-167 | 146-194 | 12-24 | 755-1100 | 5-34 | 149-215 | 4-6 | 21-26 | 3324-4515 | 44-60 | 19-33 |
| **Minor elements (µg/L)** | | | | | | | | | | |
| As | Ba | Be | Cd | Co | Cr | Li | Ni | Sr | Ti | V |
| 357-692 | 4-6.5 | 4-10 | 66-98 | 468-759 | 22-42 | 138-381 | 152-247 | 131-189 | 6.5-15 | 84-129 |
| **Physical-chemical parameters** | | | | | | | | | | |
| pH | | pe | T (ºC) | | Conductivity (mS/cm) | | Dissolved Ox. (mg/L) | | Dissolved Ox. (%) | |
| 2.35-2.96 | | 9.4-10.1 | 16.8-22.2 | | 3.24-6.12 | | 1.8-2.5 | | 13-28 | |

Data shown correspond to minimum and maximum values obtained in the 42 sampling campaign from March 2007 to October 2008

### 5.3.2 Water and solid samplings

For the sake of simplicity, the current study is focused in three water sampling campaigns (August-2007, November-2007 and May-2008), corresponding to 5, 8 and 14 months after the treatment commissioning. Water samples were filtered immediately after collection through 0.1 μm Millipore filters on Millipore syringe filter holders, acidified in the field to pH < 1 with suprapur $HNO_3$ and stored at 4 ºC in 60 mL sterile polypropylene containers until analyzed. Temperature and electrical conductivity were measured in situ using a portable CM35 meter (Crison®) with 3 point calibration (147 and 1413 μS/cm and 12.88 mS/cm). The pH and redox potential were measured using a PH25 meter (Crison®) with Crison electrodes. Redox potential and pH were controlled and calibrated using 2 points (240–470 mV) and 3 points (pH 4.01–7.00–9.21), respectively, with Crison standard solutions. Redox potential measurements were corrected to the Standard Hydrogen Electrode. Dissolved $O_2$ was measured with an auto-calibrating Hanna® portable meter and gross alkalinity was determined using CHEMetrics® Total Titrets® (range 10–100 or 100–1000 mg/L as $CaCO_3$ equivalents, accuracy approximately 5%).

After the treatment closure in October 2008, 13 solid samples were collected to characterize the neoformed precipitates within the reactive material profile. Sample depths selected were: 0–5, 5–15, 15–20, 20–35, 35–50, 50–85, 85-110, 110-135, 135-160, 160-185, 185-210, 210-240 and 240–250 cm. Samples were heated at 30 °C until completely dry and were ground in a tungsten carbide mill for 2 min.

Hydraulic conductivity (m/day) was calculated according to Darcy's Law:

$$K = \frac{Q \cdot L}{A \cdot \Delta h} \tag{5.1}$$

where Q ($m^3$/day) is flow rate, A ($m^2$) is tank cross-section perpendicular to flow, and L and Δh (m) are distance and head-loss between supernatant and outflow, respectively.

### 5.3.3 Analytical techniques

Concentrations of dissolved Al, As, Ba, Be, Ca, Cd, Co, Cr, Cu, Fe, K, Li, Mg, Mn, Na, Ni, S, Si, Sr, Ti, V and Zn in water samples were determined by Inductively Coupled Plasma Atomic Emission Spectrometry (ICP-AES Jobin- Ybon Ultima2) using a protocol especially designed for AMD samples (Tyler et al., 2004). Analysis was performed at the Central Research Services of the University of Huelva (CRSUH).

Multielement standard solutions prepared from single certified standards supplied by SCP SCIENCE were used for calibration. They were run at the beginning and at the end of each analytical series. Certified Reference Material SRM-1640 NIST fresh-water-type and inter-laboratory standard IRMM-N3 wastewater test material (European Commission Institute for Reference Materials and Measurements) were also analyzed. Detection limits were calculated by average and standard deviations from 10 blanks. Detection limits were: 200 µg/L for Al, Fe, Mn, Mg, Na, K, Si and S; 500 µg/L for Ca; 50 µg/L for Zn; 5 µg/L for Cu; 2 µg/L for As and 1 µg/L for the other trace elements.

The X-ray diffraction (XRD) study of randomly oriented powder samples was performed using a Bruker D5005 X-ray Diffractometer with Cu Kα radiation at the CRSUH. Diffractometer settings were: 40 kV, 30 mA and a scan range of 2–65º 2θ, 0.05º 2θ step size and 20-s counting time per step.

Carbon-coated polished sections were studied with a JEOL JXA-8200 SuperProbe Electron Probe Micro-Analyzer (EPMA), using the fitted Wavelength-Dispersive Spectroscopy (WDS) equipment to obtain quantitative chemical analysis. The samples were analyzed for Al (Kα), Ca (Kα), Cu (Kα), Co (Kα), Fe (Kα), Ni (Kα), S (Kα), Si (Kα) and Zn (Kα). The following phases were used as standards: $Al_2O_3$ (Al), $CaSiO_3$ (Ca, Si), CuO (Cu), CoO (Co), $Fe_2O_3$ (Fe), NiO (Ni), $BaSO_4$ (S) and ZnO (Zn). Iron and aluminum precipitates were studied using an electron beam diameter of 10 µm while the smaller size of the zinc precipitates implied the use of a 1 µm electron beam. Detection limits for each element are presented in Table 5.2. Beam damage was minimal at operating conditions between 15 and 20 kV acceleration voltage and 10-20 nA intensity.

Powder solid samples were submitted to a 5 steps sequential extraction (SE) procedure, and the leachates analyzed as previously described for water samples. Step 1 is designed to obtain the water soluble fraction using deionizied water and shaking for 12 h at room temperature (RT). Step 2 employs 1 M $NH_4$-acetate buffer (pH 4.5) shaking for 1 h at RT to obtain the sorbed and exchangeable fraction and to completely dissolved calcite. Step 3 was employed to selectively dissolve poorly ordered Fe(III) oxyhydroxides and oxyhydroxisulfates by the use of 0.2 M $NH_4$-oxalate buffer (pH 3) shaking for 30 min in darkness and at RT. Step 4 apply the same reagent than Step 3 but using an 80 ºC water bath for 1 h to selectively dissolve the highly ordered Fe(III) hydroxides and oxides. Step 5 is a total digestion of the residue using $HNO_3$ + HF + $HClO_4$. A more detailed discussion of the selectivity in mineral dissolution and other properties of the reagents employed in the different SE steps can be found in Dold, 2003b and Caraballo et al., 2009c.

**TABLE 5.2**. Representative EMPA analysis of six selected samples within the reactive tank. Presented values (wt %) correspond to mean value and standar deviation of 30 analysis obtained in each sample.

| Depth (cm) | $Al_2O_3$ (0.02) | CaO (0.02) | CuO (0.05) | CoO (0.08) | FeO (0.05) | $SO_3$ (0.03) | $SiO_2$ (0.03) | NiO (0.08) | ZnO (0.08) | $Fe/S_{molar}$ | $Al/S_{molar}$ |
|---|---|---|---|---|---|---|---|---|---|---|---|
| 0-5 | 0.12 ± 0.03 | 0.09 ± 0.07 | n.d. | n.d. | 56.70 ± 1.18 | 13.58 ± 0.17 | 0.30 ± 0.07 | n.d. | n.d. | 4.66 ± 0.07 | - |
| 85-110 | 40.10 ± 1.24 | 0.13 ± 0.05 | 0.85 ± 0.33 | n.d. | 0.15 ± 0.05 | 18.69 ± 0.77 | 2.10 ± 0.41 | n.d. | b.d | - | 3.37 ± 0.16 |
| 135-160 | 43.15 ± 1.48 | 0.93 ± 0.60 | 1.89 ± 1.30 | n.d. | 0.33 ± 0.12 | 13.99 ± 2.18 | 1.33 ± 0.21 | n.d. | 0.17 ± 0.14 | - | 4.96 ± 0.82 |
| 160-185 | 57.82 ± 3.81 | 0.04 ± 0.02 | 0.97 ± 0.31 | n.d. | 0.34 ± 0.07 | 20.65 ± 0.45 | 0.80 ± 0.28 | n.d. | b.d. | - | 4.40 ± 0.27 |
| 185-210 | 46.48 ± 3.01 | 0.67 ± 0.51 | 0.53 ± 0.41 | n.d. | 0.15 ± 0.07 | 16.02 ± 1.77 | 0.91 ± 0.14 | n.d. | 0.50 ± 0.39 | - | 4.62 ± 0.69 |
| 240-250 | 3.89 ± 2.54 | 1.83 ± 0.54 | 0.22 ± 0.14 | 0.37 ± 0.11 | 48.37 ± 3.72 | 9.52 ± 2.13 | 1.68 ± 0.31 | 0.37 ± 0.20 | 12.08 ± 2.58 | - | - |

Detection limits are presented below each element label. b.d. = below detection limit, n.d. = not detected

## 5.4 RESULTS AND DISCUSSION

### 5.4.1 Water chemistry temporal and spatial evolution within the reactive tank

First changes in the water chemistry take place within the supernatant body. As water from the adit contacts with atmosphere, Fe(II) is biologically oxidized to Fe(III), and the water reaches supersaturation with schwertmannite, precipitating this mineral along the conductions and within the supernatant water body. Precipitation of schwertmannite causes a concomitant decrease in pH and Fe from the supernatant (Figures 5.2 and 5.3). This pH decrement makes the water more aggressive and increase the efficiency of calcite dissolution.

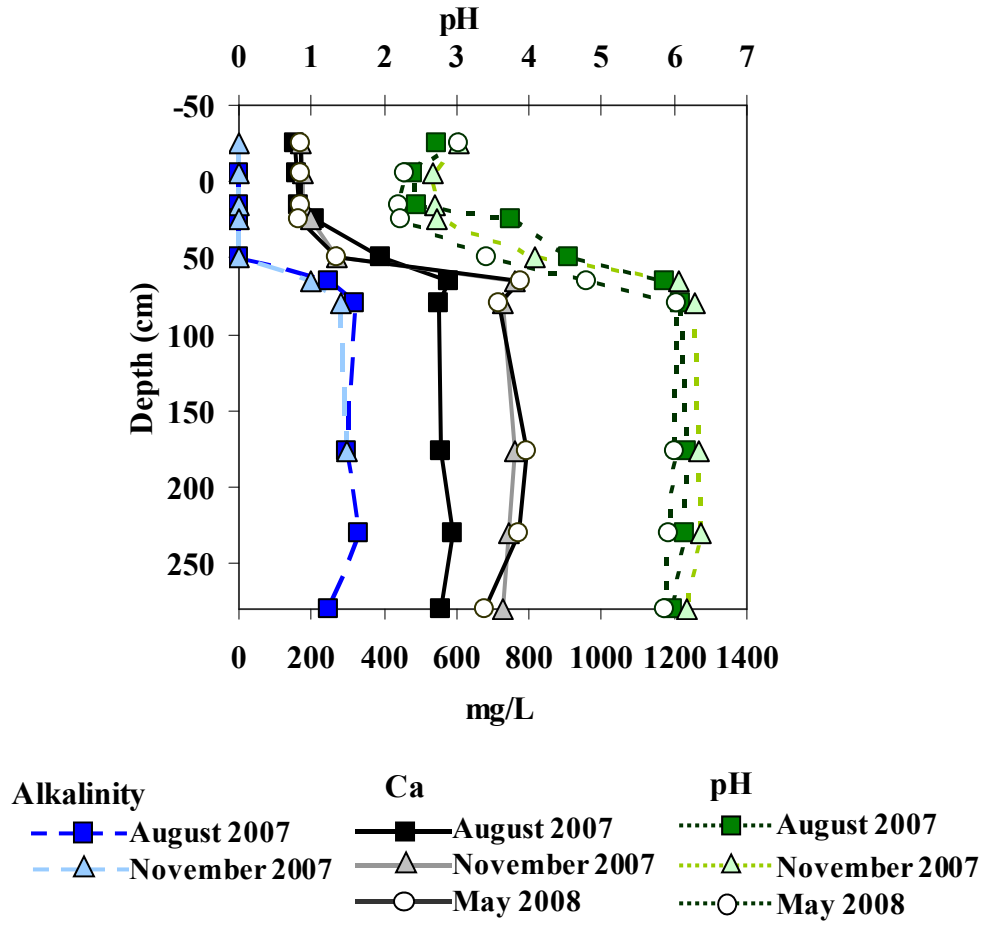


**Figure 5.2. Chemical profiles of pore water showing Ca, Alkalinity and pH vertical distribution and evolution within the reactive tank. 0 cm depth corresponds to the surface of the reactive material.**

AMD water chemistry and metal removal within the reactive tank are mainly controlled by the pH variations induced after limestone dissolution and to a less extent by the anaerobic and more reducing water environment developed at the bottom of the reactive mixture. The specific control exerted by limestone dissolution in the AMD hydrochemistry is shown in figure 5.2, where coupled to calcite dissolution (marked by

a remarkable increment in water Ca concentration) a significant increase in water pH and alkalinity can be observed. Calcite dissolution, alkalinity generation and pH rise exhibit a close spatial and temporal evolution within the reactive material. As shown in figure 5.2, the sequence of calcite dissolution begins with a slight pH increase close to the reactive material surface and an almost imperceptible increment in water Ca concentration. As the water flows down the profile, water pH and Ca concentration gradually increase; however alkalinity generation only takes place after an important amount of calcite has been dissolved (Fig. 5.2). Water pH, Ca concentration and alkalinity remain constant from 65-80 cm depth (depending on the sampling campaign) to the bottom of the reactive material. The temporal sequence in Figure 5.2 shows a downward migration of the calcite dissolution front.

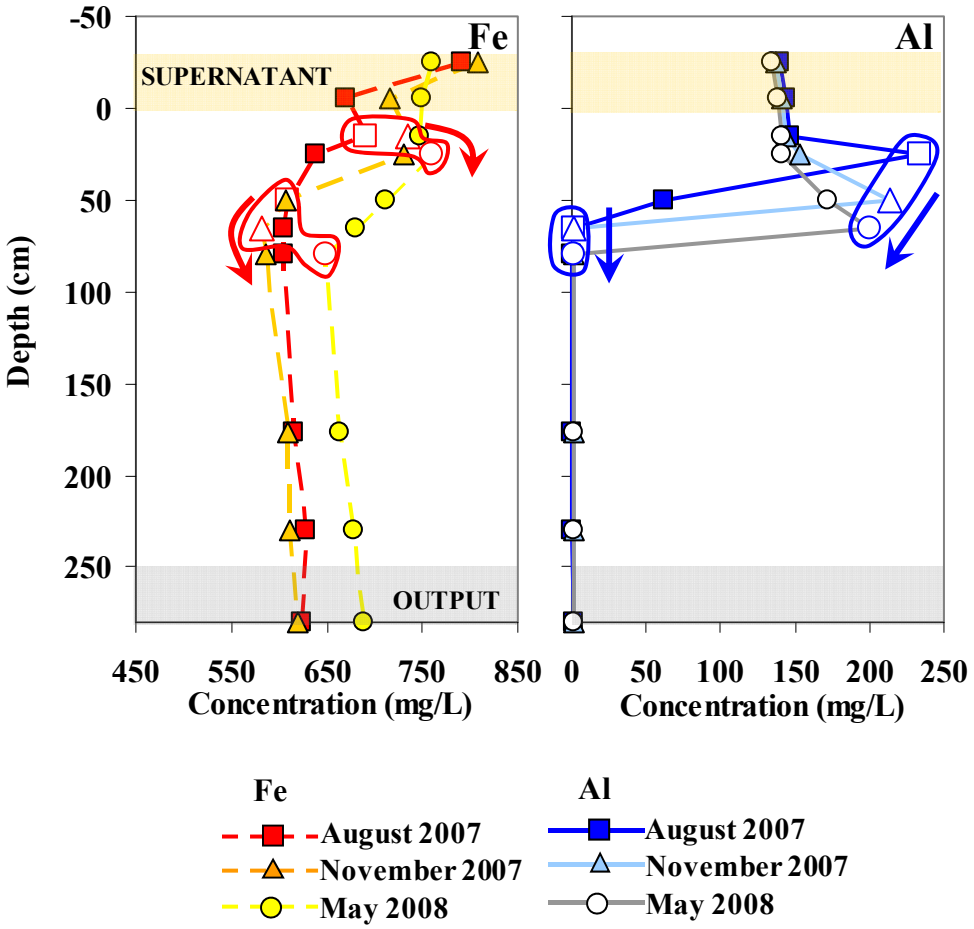


**Figure 5.3. Vertical distribution and temporal evolution of Fe and Al concentrations in the pore waters flowing through the reactive tank. 0 cm depth corresponds to the surface of the reactive material. Arrows mark the migration of the Fe and Al redissolution and precipitation fronts.**

Fe and Al profiles show two distinctive redissolution and precipitation zones within the reactive material (Fig. 5.3). All those zones suffered a migration with time downward

the reactive material profile, for this reason the beginning and end of those zones will be hereafter referred by a depth range. As shown in Figure 5.3, the first process taking place is a slight increment in Fe concentration and a decrease in pH (from 0 cm to 15-25 cm depth). These changes are similar to those observed in the aging experiments of schwertmannite to goethite (Acero et al, 2006). From 15-25 cm to 50-80 cm (Fe precipitation front) a progressive iron concentration decrease due to schwertmannite precipitation can be observed. The downward migration of the Fe precipitation zone forces the redissolution of the Al precipitates previously generated within the reactive material. This forced Al redissolution process is marked by the important increase in water Al concentration observed moving from 25 to 65 cm depth (Fig. 5.3). Subsequently to the cease of Fe removal, a complete Al removal takes place. The key factor for Al precipitation is the achievement of a pH higher than 5 (Bigham and Nordstrom, 2000; Caraballo et al., 2009c). This pH dependence is clearly observed in the sampling campaign corresponding to May 2008 where maximum Al concentration is obtained at 65 cm depth (Fig. 5.3) for a water pH of 4.8 (Fig. 5.2) while for the next sampling point at 80 cm depth the increase suffered by water pH (6.03) induce the total removal of Al from the water.

Chemically induced Zn, Co and Ni precipitation as hydroxides can only be expected after reaching a pH value higher than 8, 9 and 10 respectively (Cortina et al., 2003; Rötting et al., 2008a). However, the removal of these metals can also be induced by the generation of an anoxic and reducing water environment like the one present in wetlands or reactive barriers (Machemer et al., 1992; Benner et al., 1997; Ludwig et al, 2002, 2009). As can be observed in Figure 5.4, water redox environment evolves from very oxidizing at the water supernatant (Eh close to 700 mV) to reducing at the bottom of the reactive material (Eh values ranging from 154 to 277 mV). Coupled to this reducing environment generation, an important Zn, Ni and Co removal can be observed (Fig. 5.4). Zn removal pattern could be explained by two overlapping processes: (1) migration of a precipitation zone (from 177 to 230 cm depth) and (2) decrease with time of the removal capacity of the reducing environment. The first process can be observed in the sampling point at 177 cm depth where a significant removal was achieved in August 2007 while an important increase was measured in November 2007 and to a less extent in May 2008. The second process can be observed in the noticeable decrease with time of Zn in the sampling point at 230 cm depth (Fig. 5.4). Ni and Co removal is consistently confined to 230 cm depth, also showing an important decrease with time of the removal capacity. The increment in the output water concentration of the three metals is probably due to some redissolution of precipitates taking place at the limit between the reactive material and the quartz gravel drain. The presence of organic

matter (wood shavings) in the reactive material and the two months that the reactive tank remained flooded previous to the system inauguration could have facilitated the growth of some sulfate reducing bacteria (SRB) within the reactive mixture, thus offering a possible explanation for the reducing environment observed. Migration of the Al precipitation front confined Zn removal to the bottom part of the reactive material and could explain the decrease of Zn removal at the end of the experiment.

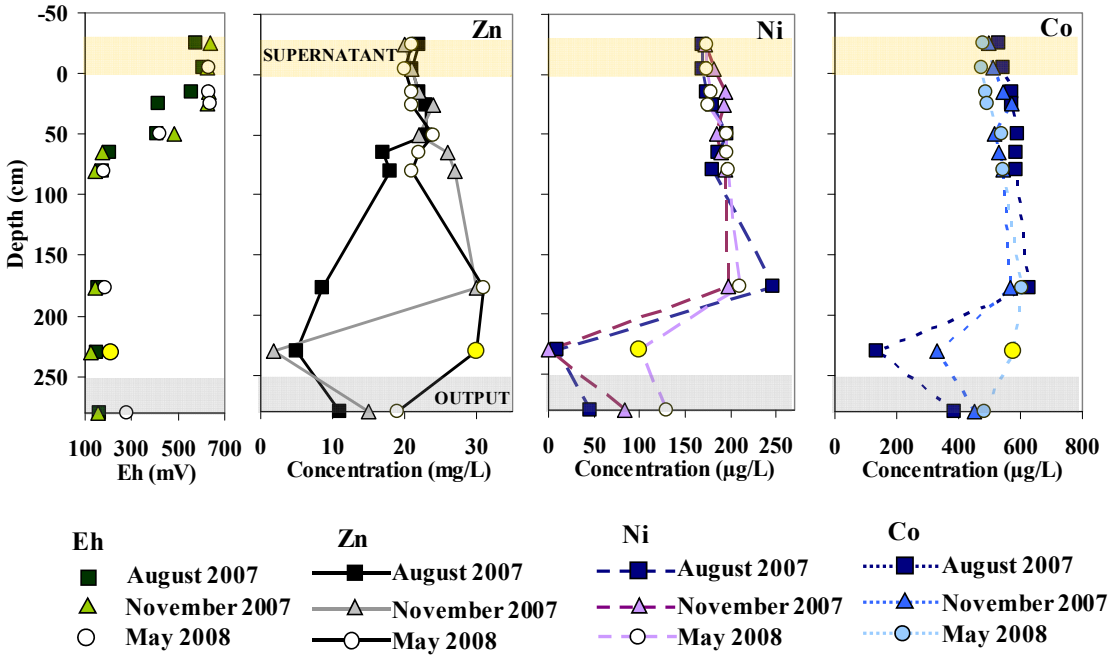


**Figure 5.4. Chemical profile showing Eh, Zn, Ni and Co vertical distribution and temporal evolution in pore water within the reactive tank. 0 cm depth corresponds to the surface of the reactive material.**

## 5.4.2 Mineralogical control on the reactive material performance and metal removal

All the information obtained for the mineralogical characterization of the different precipitates will be presented in three sub-sections corresponding to Fe, Al and Zn precipitation zones.

### *5.4.2.1 Iron precipitation zone*

The Fe influence zone is restricted to the first 50 cm of the reactive material (Fig. 5.5). A first XRD approach to the mineralogy of the precipitates (Table 5.3) exposed the presence of schwertmannite as the only detected Fe mineral phase at 0-5 cm, followed by schwertmannite plus goethite at 5-15 cm and only goethite for the sample at 15-20

cm depth. There was not any detectable mineral phase in the samples at 20-35 and 35-50 cm depth (Table 5.3).

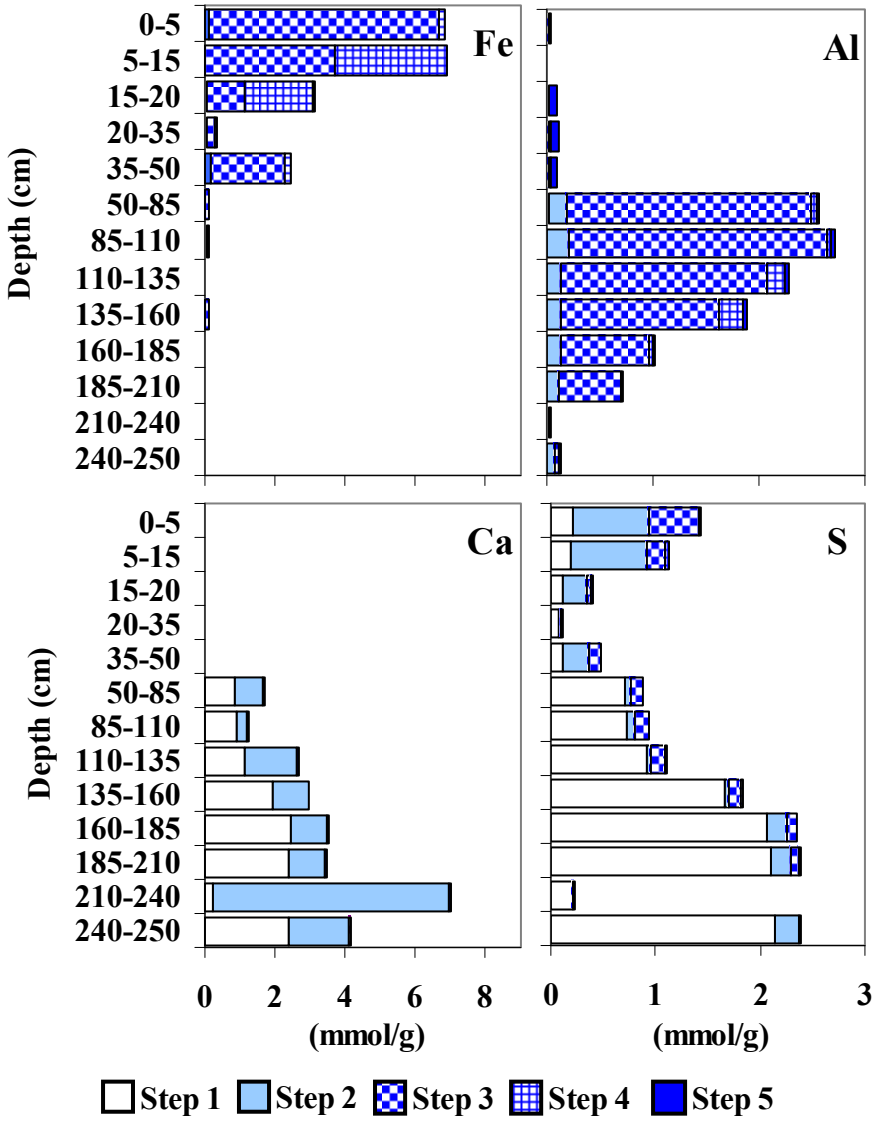


**Figure 5.5. Cumulative graphs for the concentration of the main constituent (Fe, Al, Ca and S) elements obtained after each step of the sequential extraction for the different solid samples studied.**

The results obtained after the sequential extraction performed to theses samples (Fig. 5.5) are in accordance with the XRD results. The presence of schwertmannite in the samples is marked by the Fe recovered at the third step of the sequential extraction while the Fe released at the fourth step is related to goethite dissolution. As can be observed, the Fe precipitation profile between 0 and 20 depth evolves from pure schwertmannite to a mixture of schwertmannite and goethite. This is consistent with the sedimentation on the water-reactive interface of the schwertmannite formed in the

supernatant, followed of the ageing of the mineral to goethite, as previously reported in Fe-stromatolites (Acero et al., 2006; Asta et al., 2009) and passive treatment systems (Caraballo et al., 2009b; Gagliano et al., 2004). The sample at 20-35 cm depth corresponds to a level where no metal precipitation took place and only pine wood shavings were observed during the field sampling. Although the presence of any mineral phase was confirmed by XRD in the sample at 35-50 cm depth, the significant amount of Fe recovered in the third step of the sequential extraction can be attributed to the presence of schwertmannite. The recovery of an important concentration of S in Steps 2 and 3 is attributed to adsorbed and structural $SO_4$ in schwertmannite (Fig. 5.5). The absence of any recovered Ca at the second step of the sequential extraction confirms the complete calcite dissolution along the Fe precipitation zone and also corroborates the efficiency in limestone consumption before coating of the fine grains occurs.

**TABLE 5.3**. Mineral phases confirmed by XRD

| Depth (cm) | Schwertmannite | Goethite | Gypsum | Calcite |
|---|---|---|---|---|
| 0-5 | X | - | - | - |
| 5-15 | X | X | - | - |
| 15-20 | - | X | - | - |
| 20-35 | - | - | - | - |
| 35-50 | - | - | - | - |
| 50-85 | - | - | X | X |
| 85-110 | - | - | X | X |
| 110-130 | - | - | X | X |
| 130-150 | - | - | X | X |
| 150-165 | - | - | X | X |
| 165-180 | - | - | X | X |
| 180-215 | - | - | X | X |
| 215-220 | - | - | X | X |

To obtain a deeper characterization of schwertmannite (the main constituent of the Fe precipitation zone and mineral precursor of goethite) the composition and morphology of this mineral in sample 0-5 cm was investigated by EPMA. This study revealed the typical "sea urchin" morphology of schwertmannite forming associations of spheres ranging from 1 to 10 μm in diameter (Fig. 5.6A). Bulk chemistry for this mineral is offered in Table 5.2 where, as expected, Fe and S are the two main constituents. A small amount of Al, Ca and Si was also detected. On the basis of those analysis, the

stoichiometry of the Mina Esperanza schwertmannite was deduced to be $Fe_8O_8(OH)_{4.56}(SO_4)_{1.72}:nH_2O$. The Fe/S molar ratio of 4.66 ± 0.07 obtained for schwertmannite in this study yield within the lower values of the broad range of 4.6-8.3 reported by several studies (Bigham and Nordstrom, 2000).

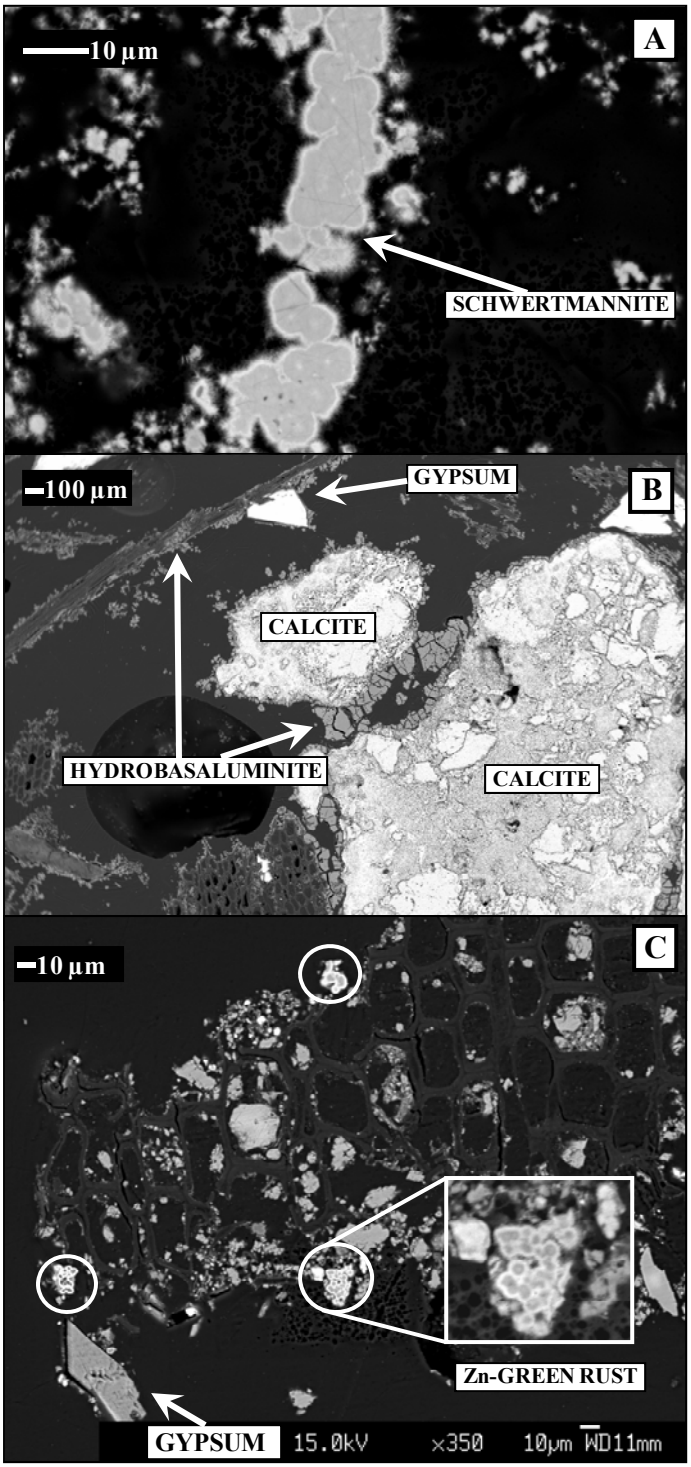


**Figure 5.6. EPMA images of the precipitates in the different reactive zones; from top to bottom: A) Iron zone; B) Aluminum zone; C) Zinc zone.**

#### *5.4.2.2 Aluminum precipitation zone*

Aluminum precipitates are distributed from 50 to 180 cm depth exhibiting a decreasing tendency on the amount of precipitates downward the reactive material profile (Fig. 5.5). The XRD of the 6 samples from 50 to 180 cm depth (Table 5.3) only confirmed the presence of gypsum and calcite but no evidence of any Al mineral phases was observed. However the presence of basaluminite was confirmed by XRD on the particulate carried by the water at the output of the reactive tank. Al precipitates dissolution mainly took place at the third step of the sequential extraction where the extractant (0.2 M $NH_4$-oxalate) is buffered at pH 3. A slight amount of Al is recovered at Step 2 (1 M $NH_4$-acetate buffered at pH 4.5) and step 4 (0.2 M $NH_4$-oxalate at pH 3 and 80 ºC) that could be attributed to an incipient Al precipitates dissolution at pH 4.5 and to the dissolution of a minor but more resistant Al-precipitate (Fig 5.5). Coupled to Al-precipitates dissolution a slight amount of S was recovered in Step 2 and 3 suggesting the presence of this element in the Al-precipitates. Al precipitates typically appear covering limestone grains and wood shavings (Fig. 5.6B). The chemical composition of those precipitates is offered in Table 5.2 where Al and S can be observed as the main constituents. The presence of minor amounts of other elements like Ca, Cu, Fe and Si was also consistently detected. The Al/S molar rates (from 3.37 to 4.96) observed at the four studied samples closely range the theoretical Al/S molar ratio of 4 calculated for basaluminite, $Al_4(SO_4)(OH)_{10}•5H_2O$, or its precursor hydrobasaluminite, $Al_4(SO_4)(OH)_{10}•12\text{-}36H_2O$. These Al/S ratios observed and the detection of basaluminite by XRD as the only Al mineral phase at the output of the reactive tank, confirm this mineral and its precursor hydrobasaluminite as the main Al mineral phase controlling Al precipitation within the reactive tank, although the presence of minor amounts of other poorly crystalline or amorphous Al-precipitates can not be completely rule out.

Gypsum precipitation can be observed (from equimolal Ca and S released in Step 1, Fig. 5.5) coupled to the Al precipitation zone but showing an inverse tendency (increasing with depth). Ca release in the second step of the sequential extraction can be attributed to the selective dissolution of calcite and, as shown in Figure 5.5, the presence of this mineral is observed along the Al precipitation zone. The presence of calcite and gypsum was also confirmed by XRD in all the samples from 50 to 220 cm depth (Table 5.3).

The sample at 180-215 cm depth corresponds to a section of un-reacted material mainly composed by limestone and wood shavings, and shows a small amount of gypsum as the only neoformed mineral phase (Fig. 5.5 and Table 5.3).

### *5.4.2.3 Zinc precipitation zone*

Divalent metals like Zn, Ni and Co were found to be selectively precipitated in the deeper section of the reactive material profile (Fig. 5.7). Those three metals are predominantly recovered in the second step of the sequential extraction and display their maximum concentrations in the sample at 240-250 cm depth that is in accordance with the important Zn, Ni and Co removal from the pore water observed for the sampling tube at 230 cm depth (Fig. 5.4). The specific recovery of those elements in the second step of the sequential extraction rule out the possibility of any kind of sulfur as hosting mineral because this step is designed to dissolved calcite or at least more labile mineral phases. The morphological and chemical study performed with EPMA showed those three elements hosted in aggregates of micro spheres of 1-2 µm in diameter (Fig. 5.6), exhibiting a great resemblance with the spherical morphology observed for schwertmannite in the Fe precipitation zone. On the basis of the chemical analysis performed to this sample (Table 5.2), Fe, Zn and S were detected as the main constituents of the precipitates. Al, Ca and Si were detected on a significant but much smaller proportion and finally Cu, Co and Ni as minor constituents.

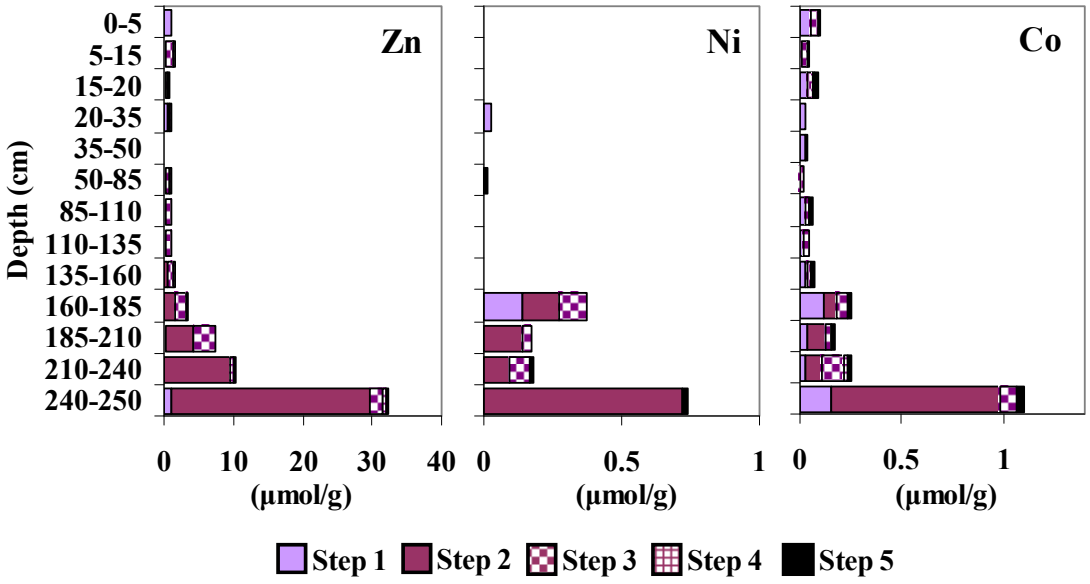


**Figure 5.7. Cumulative graphs for the concentration of Zn, Ni and Co obtained after each step of the sequential extraction for the different solid samples studied.**

Previous studies have described the appearance of Fe(II)-Fe(III) "green rust" minerals in reductomorphic soils (Bourrié et al., 1999; Feder et al., 2005; Trolard, 2006) . Those

soils are characterized by an excess of water, the restriction of the oxygen sources, the presence of bio-available substrates and the presence of elements able to change their oxidation state (Trolard, 2006), being all these characteristic present in the deeper part of the reactive tank in Mina Esperanza. "Green rust" compounds have the normalized chemical formula $[Fe^{II}_{1-x}Fe^{III}_{x}(OH)_2]^{x+}$ $[(x/n)A^{n-}\bullet(mx/n)H_2O]^{x-}$, where positively charged hydroxide layers $[Fe^{II}_{1-x}Fe^{III}_{x}(OH)_2]^{x+}$ alternate with negatively charged interlayers of anions $A^{n-}$ ($CO_3^{2-}$, $SO_4^{2-}$, $Cl^-$, …) and with *m* water molecules per anion. Cations substitutions have also been observed and $Fe^{2+}$ substitution by $Zn^{2+}$ has been specifically reported for synthetic samples (Zhang et al., 2007). The presence of "green rust" minerals in low redox AMD environments has also been proposed from the thermodynamically point of view (Majzlan et al., 2004) and directly observed in passive treatments using zerovalent iron (Bartzas and Komnitsas, 2010; Lien and Wilkin, 2005).

On the basis of the hydrochemical environment and the chemical composition of the precipitates, a poorly crystalline sulfate "green rust" with a significant substitution of Zn is proposed as the most plausible mineral phase responsible of Zn, Ni and Co removal at the bottom section of the reactive tank.

### 5.4.3 Reactive material hydraulic conductivity, performance evolution and future design considerations.

Clogging problems by neoformed minerals in the pore space of the reactive material and the subsequent loss of hydraulic conductivity leading to the failure of the treatment operation is one of the most common difficulties that a passive treatment design must overcome. The design implemented in Mina Esperanza uses a high-porosity reactive material with 1 m of free wall in the reactive tank (Fig. 5.1) to compensate the increase in the supernatant water level as a result of the induced metal precipitation in the pore space of the reactive material. The effectiveness of this design was reflected in the steady high flow, ranging from 43 to 86 $m^3$/day, observed during the 20 months of operation time.

To gain a better understanding of the reactive material performance against the expected clogging problems, the hydraulic conductivity time evolution was calculated (Eq. 5.1). The results distinctly fit an exponential decay regression line for the first year of operation, moving from an initial hydraulic conductivity of approximately 6 m/day to a final value close to 1 m/day (Fig. 5.8). But subsequently, the hydraulic conductivity steady range 1 m/day for the last 8 months of operation. Although the evolution of the hydraulic conductivity of a DAS reactive material submitted to a longer operation time

can only be certainly known after the study of a new longer field experiment, the tendency showed by this parameter during 20 months of operation suggests the achievement of a longer operation time as an encouraging possibility.

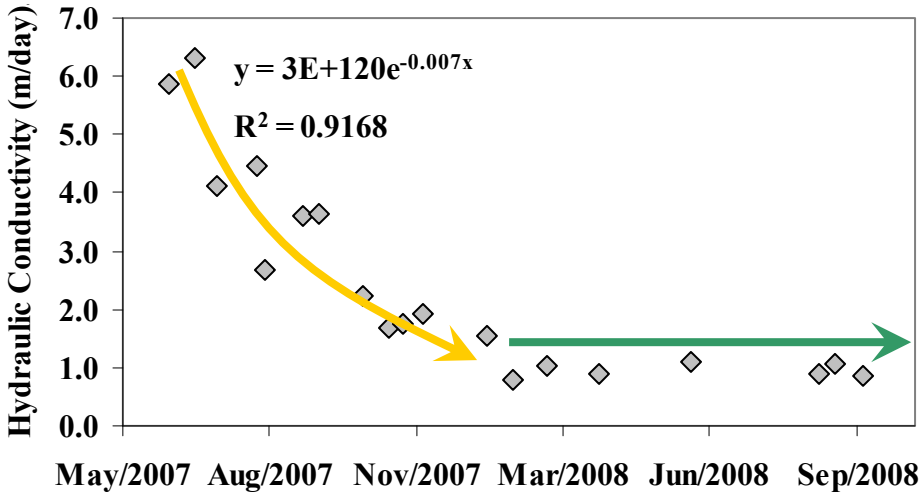


**Figure 5.8. Evolution of the hydraulic conductivity in the reactive material.**

As shown in this study, there was an important amount of undissolved calcite from 85 to 250 cm depth (Fig. 5.5). However, the low pH (5.14) and alkalinity (35 mg/L as $CaCO_3$ equivalents) observed at the output of the reactive tank during the last sampling campaign (October 2008) imply a substantial decrease in the reactivity of the substrate. On the light of the hydrobasaluminite distribution showed in this study, calcite partial passivation by surface armoring (Fig.5.6) is proposed, in addition to calcite consumption, as the main process responsible of the substrate reactivity loss.

Despite the high performance achieved by the reactive tank in Mina Esperanza 2007-2008, some improvements in the original design are planned to be incorporated in the future treatment to be implemented in 2011. On the basis of the hydraulic conductivity evolution observed and to achieve a cost-efficient use of the reactive material, we suggest establishing an operating period of two years for the reactive material. To extend the reactivity of the reactive material, we also suggest increasing the amount of limestone employed. Another possibility that is being taking into account is the inclusion of new reagents to the limestone-DAS at the deeper section of the reactive material in order to enhance the reducing environment and to promote divalent metals removal. The addition to some zerovalent iron is being considered as an option to promote the desired reducing environment. A second option would be the inclusion of organic matter to the last 0.5 m of the limestone-DAS reactive material. This organic

matter could promote sulfate reducing bacteria activity and subsequently maintain the reducing environment. A mixture of these two materials has been recently found efficient in metal removal (Ludwig et al., 2009), and are currently under study by means of laboratory experiments.

# CHAPTER 6. CONCLUSIONS

This chapter summarizes the main contributions provided in this thesis.

The **first part of this thesis** discusses the applicability of a specific Sequential Extraction (SE) procedure and Differential X Ray Diffraction (DXRD) for the mineralogical characterization of AMD precipitates comprised primarily of poorly ordered iron and aluminum oxides and sulfates. The study covered in this section (**CHAPTER 2**) proved that a coupled DXRD and SE study is a powerful tool for the characterization of poorly ordered Fe and Al phases. Successfully application of SE to samples with high concentrations of iron oxides and iron oxyhydroxysulfates was accomplished only after performing some modifications to the sample-extractant volume ratio and the time and nature of contact. As a result, a modified SE procedure specifically designed for the study of AMD precipitates was obtained.

The high specificity observed in schwertmannite and goethite selective dissolution by the third and fourth step of the SE permitted a quantitative estimation of the proportion of each mineral within the reactive material. It was observed that although the mass of goethite (wt %) in the samples was considerably greater than that of schwertmannite; the latter was the mineral phase responsible for most of the iron removal (due to the higher content of Fe in the structure of schwertmannite). Detection of schwertmannite

prior to DXRD analysis was impossible in some samples due to both lower crystallinity and concentration of schwertmannite with respect to goethite. Another important result of the SE study of the iron levels was the progressive decrease of $SO_4^{2-}$ adsorbed onto schwertmannite with depth. This effect was attributed to a partial occupancy of the adsorption sites by $OH^-$ instead of $SO_4^{2-}$ as a result of the slight pH increase suffered by the AMD after some limestone dissolution. Obtained Fe/S molar ratios were 4.44, 4.15 and 9.33 for schwertmannite at 0-1 cm, 1-3 cm and 3-5 cm depth. These results extend the upper limit for Fe/S ratio in schwertmannite from close to 8 to 9.33.

Concerning the Al-horizon, a progressive decrease (from top to bottom) was observed in the Al content in the precipitates. Although the presence of hydrobasaluminite and amorphous $Al(OH)_3$ was suggested on the basis of SE and thermodynamic modeling, it was impossible to detect any Al mineral phases with the analytical techniques employed.

The coupled XRD and SE study allowed identifying and quantifying gypsum and calcite distribution within the reactive material. Concentration of gypsum increases throughout the Fe-horizon until reaches its maximum at the boundary between the Fe- and Al-horizons, and it decreases downward through the Al-horizon. Almost all the calcite was consumed in the Fe-horizon (0–5 cm), an important amount of calcite remained undissolved in the Al-horizon. Remaining calcite suffered an important passivation effect by gypsum and Al-precipitates surface armoring.

The **second part of this thesis** deals with the design, implementation and performance of the limestone-DAS and MgO-DAS passive treatment system in the pilot plant experiment at Monte Romero. The research accomplished in this part (**CHAPTER 3**) provides a detailed study of the field multi-step limestone and MgO passive system in Monte Romero. Although a detailed water chemistry and mineralogical study was performed, only the main novelties comparing with previous field experiments are described in this section.

The system was able to remove a net acidity of around 2,000 mg/L as $CaCO_3$ equivalents leading to a decrease in the inflow AMD from 2,500 to 500 mg/L as $CaCO_3$ equivalents. Net acidity elimination corresponds to a relative removal close to 100% Al and Cu, >70% Fe, almost 25% Zn (major elements), 100% As and Pb, and > 95% Cr (minor elements).

The performance of the different sections comprising the passive treatment system showed a similar initial removal efficiency using two tanks with 12.5% (v/v) or 20%

(v/v) of limestone in the reactive material (T1 and T2 respectively). Al horizons appeared within the reactive material of T1 and T2 although no crystalline Al-phase could be assigned for these precipitates. However, a decrease in reactivity of T1 is observed at the end of the experiment. This is attributed to the faster progress of the Al precipitation front down through the reactive material, which causes a lower removal of Al inside the tank, less increase in alkalinity and less Fe removal in the subsequent decantation ponds. These observations point to 20% (v/v) of limestone as the optimal limestone proportion for a long-lasting reactive material.

MgO-DAS reactive material was observed, for the first time in a field experiment, to completely remove divalent metals such as Zn, Fe(II), Cd, Co and Ni from a complex aqueous solution.

Goethite precipitates were observed within the upper pores of the treatment, where limestone or MgO dissolves and the subsequent rise in pH accelerates Fe(II) oxidation. Al horizons appeared within the reactive material of T1 and T2 although no crystalline Al-phase could be assigned for these precipitates. Finally, only a Zn horizon was present inside T3. Unlike $Zn(OH)_2$ found in previous laboratory experiments, complex minerals such as Zn-dominant schulenbergite, $(Cu,Zn)_7(SO_4)_2(OH)_{10}•3H_2O$, and minor sauconite, $Zn_3(Si,Al)_4O_{10}(OH)_2•4H_2O$ are proposed as the most probable Zn-rich precipitates. The consumption of almost all the reactive material present in the MgO-DAS tank clearly showed that the chosen grain size was suitable to achieve a total dissolution before any passivation process appeared. However, a higher volume and/or higher MgO proportion in the reactive material are needed to extend T3 operating time. To prevent any preferential flow within the reactive tank, T3 should be similar to T1 and T2 with higher volume, cylindrical shape and made of fiberglass.

The **third part of this thesis** is devoted to the characterization and control of the long lasting (20 months) full scale passive treatment system implemented in Mina Esperanza.

The third investigation (**CHAPTER 4**) carried out in this thesis is focused on the study of the hydrochemical, mineralogical and metal removal performance of the entire passive treatment system at Mina Esperanza.

The high porosity and hydraulic conductivity showed by the limestone-DAS reactive material enabled the system to treat a high inflow (ranging between 43 and 86 $m^3$/day) for 20 months without suffering any significant clogging problem. The chosen design for the cascades connecting the adit to the reactive tank provided a slow-flow environment that promotes the establishment of iron oxidizing bacteria and algae, which

accelerated the oxidation of ferrous to ferric iron and subsequently increase iron removal on the surface of the reactive tank.

Iron was the main remediated metal in the system showing a water removal ranging from 170 to 620 mg/L depending on the system performance. Mean removal values as high as 144 ± 9 mg/L Al, 16 ± 6 mg/L Cu, 40 ± 4 mg/L Si, 490 ± 75 µg/L As, 73 ± 9 µg/L Cd, 28 ± 6 µg/L Cr, 85 ± 50 µg/L Ni, 10 ± 3 µg/L Ti and 94 ± 18 µg/L V were also obtained.

Inflow net acidity and net acidity removal showed to be typically one order of magnitude higher than the values reported for more than 80 traditional passive treatment systems in the USA. Regarding acid load reduction, expressed in terms of $g•(m^2•day)^{-1}$, reached by the treatment at Mina Esperanza, it was 10 times higher than the generally accepted 40 $g•(m^2•day)^{-1}$ value commonly used as a passive treatment system designing criteria.

Schwertmannite was shown to be the main mineral phase controlling Fe removal throughout the system although some Fe removal was observed to be achieved after direct goethite precipitation at the high pH values obtained at the reactive tank output. Al precipitation occurred within the reactive material and only when water pH at the output of the reactive tank was close to a value of 5.5 some Al precipitates, in the form of basaluminite, were observed.

The fourth research (**CHAPTER 5**) is based on the study of the water chemistry evolution and hydraulic performance of the reactive material on the basis of the mineralogical and hydrochemical study performed to the reactive tank at the Mina Esperanza passive treatment system.

Three different precipitation horizons were observed within the reactive material, inducing (from top to bottom) an important removal of Fe, complete Al precipitation and significant Zn removal. The downward migration of the Fe precipitation zone forced the redissolution of the Al precipitates previously generated within the reactive material. Zn precipitation zone was induced by the generation of an important reducing environment at the bottom of the reactive material that also promoted a significant Ni and Co removal in this horizon.

Fe precipitation profile between 0 and 20 cm depth evolved from pure schwertmannite to a mixture of schwertmannite and goethite. This is consistent with the sedimentation on the water-reactive interface of the schwertmannite formed in the supernatant,

followed of the ageing of the mineral to goethite. The Fe/S molar ratio of 4.66 ± 0.07 obtained for schwertmannite in this study yield within the lower values of the broad range of 4.6-8.3 reported by previous studies and the stoichiometry of the Mina Esperanza schwertmannite was deduced to be $Fe_8O_8(OH)_{4.56}(SO_4)_{1.72}$:nH2O.

The Al/S molar rates (from 3.37 to 4.96) observed at the four studied samples closely range the theoretical Al/S molar ratio of 4 calculated for basaluminite, $Al_4(SO_4)(OH)_{10}•5H_2O$, being this mineral basaluminite the only Al mineral phase corroborated by XRD at the output of the reactive tank. A decreasing tendency on the amount of Al-precipitates downward the reactive material profile was clearly observed.

On the basis of the different mineralogical studies performed to the samples, a poorly crystalline sulfate “green rust” with a significant substitution of Zn was proposed as the most plausible mineral phase responsible of Zn, Ni and Co removal at the bottom section of the reactive tank.

Concerning the reactive material performance it was observed that initial hydraulic conductivity of approximately 6 m/day decreased to a final value close to 1 m/day that was steadily maintained for the last 8 months of operation. This hydraulic conductivity evolution during the 20 months of operation suggests the achievement of a longer operation time as an encouraging possibility.

Complete calcite dissolution along the Fe precipitation zone corroborated the efficiency in limestone consumption before coating of the fine grains occurs. However, the important amount of undissolved calcite from 85 to 250 cm depth was observed. On the light of the hydrobasaluminite distribution showed in this study, calcite partial passivation by surface armoring was proposed, in addition to calcite consumption, as the main process responsible of the substrate reactivity loss.

# Bibliography

Acero, P., Ayora, C., Torrentó, C., and Nieto, J.-M. (2006) The behavior of trace elements during schwertmannite precipitation and subsequent transformation into goethite and jarosite. Geochimica et Cosmochimica Acta, 70(16), 4130-4139.

Akcil, A., and Koldas, S. (2006) Acid Mine Drainage (AMD): causes, treatment and case studies. Journal of Cleaner Production, 14(12-13), 1139-1145.

Alpers, C.N., Majzlan, J., Bender, K.C., Bishop, J.L., Coleman, M.L., Dyar, M.D., McCleskey, R.B., Myneni, S.C.B., Nordstrom, D.K., and Sobron, P. (2008) Chemistry and spectroscopy of iron-sulfate minerals from iron mountain, California, U.S.A. Geochimica et Cosmochimica Acta, 72(12, Supplement 1), A17.

Asta, M.P., Ayora, C., Román-Ross, G., Cama, J., Acero, P., Gault, A.G., Charnock, J.M., Bardelli, F. (2009) Natural attenuation of arsenic in the Tinto Santa Rosa acid stream (Iberian Pyritic Belt, SW Spain): The role of iron precipitates. Chemical Geology, 271(1-2), 1-12.

Ball, J.W., Nordstrom, D.K. (1991). User's Manual for WATEQ4F With Revised Thermodynamic Database and test Cases for Calculating Speciation of Major, Trace and Redox Elements in Natural Waters. US Geological Survey Water-Resource Investigation Rep 91–183.

Bartzas, G., and Komnitsas, K. (2010) Solid phase studies and geochemical modelling of low-cost permeable reactive barriers. Journal of Hazardous Materials, 183(1-3), 301-308.

Benner, S. G., Blowes, D. W., Ptacek, C. J. (1997) A full-scale porous reactive wall for prevention of acid mine drainage. Ground Water Monitoring and Remediation, 17, 99-107.

Benner, S.G., Blowes, D.W., Gould, W.D., Herbert, R.B., and Ptacek, C.J. (1999) Geochemistry of a Permeable Reactive Barrier for Metals and Acid Mine Drainage. Environ. Sci. Technol., 33(16), 2793-2799.

Berkowitz, J., Anderson, M.A., and Amrhein, C. (2006) Influence of aging on phosphorus sorption to alum floc in lake water. Water Research, 40(5), 911-916.

Bigham, J.M., and Nordstrom, D.K. (2000) Iron and Aluminum Hydroxysulfates from Acid Sulfate Waters. In C.N. Alpers, J.L. Jambor, and D.K. Nordstrom, Eds. Sulfate Minerals: Crystallography, Geochemistry, and Environmental Significance, 40, p. 351-403. Reviews in Mineralogy and Geochemistry, Mineralogical Society of America., Chantilly, Virginia.

Bigham, J.M., Schwertmann, U., Traina, S.J., Winland, R.L., and Wolf, M. (1996) Schwertmannite and the chemical modeling of iron in acid sulfate waters. Geochimica et Cosmochimica Acta, 60(12), 2111-2121.

Bishop, J., Alpers, C., Coleman, M., Sobron, P., Lane, M., Dyar, D., and Schiffman, P. (2008) Sulfates on Mars: comparison with spectral properties of analog sites. Geochimica et Cosmochimica Acta, 72(12, Supplement 1), A85.

Booth, J., Hong, Q., Compton, R.G., Prout, K., and Payne, R.M. (1997) Gypsum overgrowths passivate calcite to acid attack. Journal of Colloidal Interface Science, 192, 207-214.

Bourrié, G., Trolard, F., Jaffrezic, J.-M.R.G., MaItre, V., and Abdelmoula, M. (1999) Iron control by equilibria between hydroxy-Green Rusts and solutions in hydromorphic soils. Geochimica et Cosmochimica Acta, 63(19-20), 3417-3427.

Burton, E.D., Bush, R.T., Sullivan, L.A., and Mitchell, D.R.G. (2007) Reductive transformation of iron and sulfur in schwertmannite-rich accumulations associated with acidified coastal lowlands. Geochimica et Cosmochimica Acta, 71(18), 4456-4473.

Cánovas, C.R., Olías, M., Nieto, J.M., Sarmiento, A.M., and Cerón, J.C. (2007) Hydrogeochemical characteristics of the Tinto and Odiel Rivers (SW Spain). Factors controlling metal contents. Science of The Total Environment, 373(1), 363-382.

Caraballo, M.A., Macías, F., Rötting, T.S., Nieto, J.M., and Ayora, C. (2008) Disperse Alkaline Substrate passive remediation at Mina Esperanza (Iberian Pyrite Belt, SW Spain). Geochimica et Cosmochimica Acta, 72(12, Supplement 1), A135.

Caraballo, M.A., Nieto, J.M., and Ayora, C. (2009a) Iron and aluminum precipitates as metals and metalloids sinks in a passive treatment system. Geochimica et Cosmochimica Acta, 73(13, Supplement 1), A191.

Caraballo, M.A., Rötting, T.S., Macías, F., Nieto, J.M., and Ayora, C. (2009b) Field multi-step limestone and MgO passive system to treat acid mine drainage with high metal concentrations. Applied Geochemistry, 24(12), 2301-2311.

Caraballo, M.A., Rotting, T.S., Nieto, J.M., and Ayora, C. (2009c) Sequential extraction and DXRD applicability to poorly crystalline Fe- and Al-phase characterization from an acid mine water passive remediation system. American Mineralogist, 94(7), 1029-1038.

Caraballo, M.A., Santofimia, E., and Jarvis, A.P. (2010) Metal retention, mineralogy, and design considerations of a mature permeable reactive barrier (PRB) for acidic mine water drainage in Northumberland, U.K. American Mineralogist, 95(11-12), 1642-1649.

Carlson, L., Bigham, J.M., Schwertmann, U., Kyek, A., and Wagner, F. (2002) Scavenging of As from Acid Mine Drainage by Schwertmannite and Ferrihydrite: A Comparison with Synthetic Analogues. Environ. Sci. Technol., 36(8), 1712-1719.

Casiot, C., Morin, G., Juillot, F., Bruneel, O., Personné, J.-C., Leblanc, M., Duquesne, K., Bonnefoy, V., Elbaz-Poulichet, F. (2003) Bacterial immobilization and oxidation of arsenic in acid mine drainage (Carnoulès creek, France). Water Research 37(12), 2929-2936.

Chen, C.J., and Jiang, W.T. (2008) An EXAFS and FTIR study on the sulfate and arsenate configurations of schwertmannite. Geochimica et Cosmochimica Acta, 72(12, Supplement 1), A152.

Cocos, I.A., Zagury, G.J., Clément, B., and Samson, R. (2002) Multiple factor design for reactive mixture selection for use in reactive walls in mine drainage treatment. Water Research, 36(1), 167-177.

Cornell, R.M., and Schwertmann, U. (2003) The iron oxides: structure, properties, reactions, occurrences and uses. WILEY-VCH, Weinheim.

Cortina, J.L., Lagreca, I., De Pablo, J., Cama, J., and Ayora, C. (2003) Passive In Situ Remediation of Metal-Polluted Water with Caustic Magnesia: Evidence from Column Experiments. Environ. Sci. Technol., 37(9), 1971-1977.

Dann, A.L., Cooper, R.S., and Bowman, J.P. (2009) Investigation and optimization of a passively operated compost-based system for remediation of acidic, highly iron- and sulfate-rich industrial waste water. Water Research, 43(8), 2302-2316.

Dold, B. (2003a) Dissolution kinetics of schwertmannite and ferrihydrite in oxidized mine samples and their detection by differential X-ray diffraction (DXRD). Applied Geochemistry, 18(10), 1531-1540.

-. (2003b) Speciation of the most soluble phases in a sequential extraction procedure adapted for geochemical studies of copper sulfide mine waste. Journal of Geochemical Exploration, 80(1), 55-68.

Escobar, B., Buccicardi, S., Morales, G., Wiertz, J. (2010) Biooxidation of ferrous iron and sulfide at low temperatures: Implications on acid mine drainage and bioleaching of sulfide minerals. Hydrometallurgy doi:10.1016/j.hydromet.2010.03.027.

Eskandarpour, A., Onyango, M.S., Ochieng, A., and Asai, S. (2008) Removal of fluoride ions from aqueous solution at low pH using schwertmannite. Journal of Hazardous Materials, 152(2), 571-579.

Fanfani, L., Zuddas, P., and Chessa, A. (1997) Heavy metals speciation analysis as a tool for studying mine tailings weathering. Journal of Geochemical Exploration, 58(2-3), 241-248.

Feder, F., Trolard, F., Klingelhöfer, G., and Bourrié, G. (2005) In situ Mössbauer spectroscopy: Evidence for green rust (fougerite) in a gleysol and its mineralogical transformations with time and depth. Geochimica et Cosmochimica Acta, 69(18), 4463-4483.

Fukushi, K., Sato, T., Yanase, N., Minato, J., and Yamada, H. (2004) Arsenate sorption on schwertmannite. American Mineralogist, 89(11-12), 1728-1734.

Gagliano, W.B., Brill, M.R., Bigham, J.M., Jones, F.S., and Traina, S.J. (2004) Chemistry and mineralogy of ochreous sediments in a constructed mine drainage wetland. Geochimica et Cosmochimica Acta, 68(9), 2119-2128.

Geomare, E. (2004) Hydrobasaluminite: a new occurence in Belgium. Geologica Belgica, 7(1-2), 71-76.

Hall, G.E.M., Vaive, J.E., Beer, R., and Hoashi, M. (1996) Selective leaches revisited, with emphasis on the amorphous Fe oxyhydroxide phase extraction. Journal of Geochemical Exploration, 56(1), 59-78.

Hedin, R.S., Nairn, R.W., Kleinmann, R.L.P. (1994) Passive treatment of coal mine drainage. US Bureau of Mines IC9389, Pittsburgh, PA, USA.

Jage, C.R., Zipper, C.E., and Noble, R. (2001) Factors Affecting Alkalinity Generation by Successive Alkalinity-Producing Systems: Regression Analysis. J Environ Qual, 30(3), 1015-1022.

Jarvis, A.P., Moustafa, M., Orme, P.H.A., and Younger, P.L. (2006) Effective remediation of grossly polluted acidic, and metal-rich, spoil heap drainage using a novel, low-cost, permeable reactive barrier in Northumberland, UK. Environmental Pollution, 143(2), 261-268.

Jarvis, A.P., and Younger, P.L. (1999) Design, Construction and Performance of a Full-Scale Compost Wetland for Mine-Spoil Drainage Treatment at Quaking Houses. Water and Environment Journal, 13(5), 313-318.

Johnson, D.B., and Hallberg, K.B. (2005) Acid mine drainage remediation options: a review. Science of The Total Environment, 338(1-2), 3-14.

Johnson, K.L., and Younger, P.L. (2006) The co-treatment of sewage and mine waters in aerobic wetlands. Engineering Geology, 85(1-2), 53-61.

Jönsson, J., Persson, P., Sjöberg, S., and Lövgren, L. (2005) Schwertmannite precipitated from acid mine drainage: phase transformation, sulphate release and surface properties. Applied Geochemistry, 20(1), 179-191.

Kalin, M. (2004) Passive mine water treatment: the correct approach? Ecological Engineering, 22(4-5), 299-304.

Kalin, M., and Caetano Chaves, W.L. (2003) Acid reduction using microbiology: treating AMD effluent emerging from an abandoned mine portal. Hydrometallurgy, 71(1-2), 217-225.

Kawano, M., and Tomita, K. (2001) Geochemical modeling of bacterially induced mineralization of schwertmannite and jarosite in sulfuric acid spring water. American Mineralogist, 86(10), 1156-1165.

Kim, J.J., and Kim, S.J. (2003) Environmental, Mineralogical, and Genetic Characterization of Ochreous and White Precipitates from Acid Mine Drainages in Taebaeg, Korea. Environ. Sci. Technol., 37(10), 2120-2126.

Kirby, C.S., and Cravotta, C.A. (2005a) Net alkalinity and net acidity 1: Theoretical considerations. Applied Geochemistry, 20(10), 1920-1940.

-. (2005b) Net alkalinity and net acidity 2: Practical considerations. Applied Geochemistry, 20(10), 1941-1964.

Kirby, C.S., Thomas, H.M., Southam, G., Donald, R. (1999) Relative contributions of abiotic and biological factors in Fe(II) oxidation in mine drainage. Applied Geochemistry 14, 511-530.

Kleinmann, R.L.P. (1989) Acid mine drainage in the United States controlling the impact on streams and rivers. In: 4th World Congress on the Conservation of the Built and Natural Environments, University of Toronto, 1–10.

Knorr, K.-H., and Blodau, C. (2007) Controls on schwertmannite transformation rates and products. Applied Geochemistry, 22(9), 2006-2015.

Kumpulainen, S., Carlson, L., and Räisänen, M.-L. (2007) Seasonal variations of ochreous precipitates in mine effluents in Finland. Applied Geochemistry, 22(4), 760-777.

Langmuir, D. (1997) Aqueous environmental geochemistry. Prentice-Hall, Inc., New Jersey.

Laus, R., Geremias, R., Vasconcelos, H.L., Laranjeira, M.C.M., and Fávere, V.T. (2007) Reduction of acidity and removal of metal ions from coal mining effluents using chitosan microspheres. Journal of Hazardous Materials, 149(2), 471-474.

Leblanc, M., Morales, J.A., Borrego, J., Elbaz-Poulichet, F. (2000) 4,500 year old mining pollution in southwestern Spain: long term implications for modern mining pollution. Economic Geology 95, 655-662.

Lee, G., Bigham, J.M., and Faure, G. (2002) Removal of trace metals by coprecipitation with Fe, Al and Mn from natural waters contaminated with acid mine drainage in the Ducktown Mining District, Tennessee. Applied Geochemistry, 17(5), 569-581.

Li, J., Smart, R.S.C., Schumann, R.C., Gerson, A.R., and Levay, G. (2007) A simplified method for estimation of jarosite and acid-forming sulfates in acid mine wastes. Science of the Total Environment, 373, 391-403.

Lien, H.-L., and Wilkin, R.T. (2005) High-level arsenite removal from groundwater by zero-valent iron. Chemosphere, 59(3), 377-386.

Loan, M., Cowley, J.M., Hart, R., and Parkinson, G.M. (2004) Evidence on the structure of synthetic schwertmannite. American Mineralogist, 89(11-12), 1735-1742.

López-Fernández, A., López-Montenegro, G., Romero-Sousa, J. (2003) Tratamiento de aguas de Minería en el río Odiel. Medio Ambiente 52-55.

Ludwig, R.D., Smyth, D.J.A., Blowes, D.W., Spink, L.E., Wilkin, R.T., Jewett, D.G., and Weisener, C.J. (2009) Treatment of Arsenic, Heavy Metals, and Acidity Using a Mixed ZVI-Compost PRB. Environmental Science & Technology, 43(6), 1970-1976.

Machemer, S. D., Wildemann, T. R. (1992) Adsorption compared with sulphide precipitation as a metal removal processes from acid mine drainage in a constructed wetland. Journal of Contaminant Hydrology, 9, 115-131

Macías, F., Caraballo, M.A., Nieto, J.M., Ayora, C., Rötting, T.S. (2009) Iron removal enhancement of a two step calcite passive treatment system at the Iberian Pyrite Belt. Geochimica et Cosmochimica Acta 73, 13, A811.

Majzlan, J., Navrotsky, A., and Schwertmann, U. (2004) Thermodynamics of iron oxides: Part III. Enthalpies of formation and stability of ferrihydrite (~Fe(OH)3), schwertmannite (~FeO(OH)3/4(SO4)1/8), and [var epsilon]-Fe2O3. Geochimica et Cosmochimica Acta, 68(5), 1049-1059.

Martin, J.D. (2004) Using XPowder: A software package for Powder X-Ray diffraction analysis. www.xpowder.com D.L. GR 1001/04.ISBN 84-609-1497-6. 105 p. Spain.

McCauley, C.A., O'Sullivan, A.D., Milke, M.W., Weber, P.A., and Trumm, D.A. (2009) Sulfate and metal removal in bioreactors treating acid mine drainage dominated with iron and aluminum. Water Research, 43(4), 961-970.

Neculita, C.M., Zagury, G.J., Bussière, B. (2008) Effectiveness of sulfate-reducing passive bioreactors for treating highly contaminated acid mine drainage: II. Metal removal mechanisms and potential mobility. Applied Geochemistry. 23, 3545–3560.

Nieto, J.M., Sarmiento, A.M., Olías, M., Canovas, C.R., Riba, I., Kalman, J., and Delvalls, T.A. (2007) Acid mine drainage pollution in the Tinto and Odiel rivers (Iberian Pyrite Belt, SW Spain) and bioavailability of the transported metals to the Huelva Estuary. Environment International, 33(4), 445-455.

Nocete, F., Álex, E., Nieto, J.M., Sáez, R., and Bayona, M.R. (2005) An archaeological approach to regional environmental pollution in the south-western Iberian Peninsula related to Third millennium BC mining and metallurgy. Journal of Archaeological Science, 32(10), 1566-1576.

Nocete, F., Queipo, G., Sáez, R., Nieto, J.M., Inácio, N., Bayona, M.R., Peramo, A., Vargas, J.M., Cruz-Auñón, R., Gil-Ibarguchi, J.I., and Santos, J.F. (2008) The smelting quarter of Valencina de la Concepción (Seville, Spain): the specialised copper industry in a political centre of the Guadalquivir Valley during the Third millennium BC (2750-2500 BC). Journal of Archaeological Science, 35(3), 717-732.

Nordstrom, D.K. (1982) The effect of sulfate on aluminum concentrations in natural waters: some stability relations in the system Al2O3-SO3-H2O at 298 K. Geochimica et Cosmochimica Acta, 46(4), 681-692.

Nordstrom, D.K. (2000) Advances in the hydrogeochemistry and microbiology of acid mine waters. International Geology Review 42, 499–515.

Nordstrom, D.K., Jenne, E.A., Averett, R.C. (1977) Heavy metal discharges into Shasta Lake and Keswick Reservoir on the Upper Sacramento River, California—A reconnaissance during low flow. United States Geological Survey Open-File Report 76-49.

Parkhurst, D.L. (1995) User's Guide to PHREEQC: A Computer Program for Speciation, Reaction Path, Advective-Transport, and Inverse Geochemical Calculations. US Geol. Surv. Water-Resource Investigation Rep 95–4227.

Perez-Lopez, R., Nieto, J.M., Alvarez-Valero, A.M., and de Almodovar, G.R. (2007) Mineralogy of the hardpan formation processes in the interface between sulfide-rich sludge and fly ash: Applications for acid mine drainage mitigation. American Mineralogist, 92(11-12), 1966-1977.

Pinedo-Vara, I. (1963) Piritas de Huelva. Su historia, minería y aprovechamiento. Summa, Madrid, Spain.

PIRAMID-Consortium (2003) Engineering guidelines for the passive remediation of acidic and/or metalliferous mine drainage and similar wastewaters. European Commission Fifth Framework RTD Project No. EVK1-CT-1999-000021 ''Passive In-situ Remediation of Acidic Mine/Industrial Drainage" (PIRAMID). University of Newcastle, Newcastle Upon Tyne, UK.

Pueyo, M., Mateu, J., Rigol, A., Vidal, M., López-Sánchez, J.F., and Rauret, G. (2008) Use of the modified BCR three-step sequential extraction procedure for the study of trace element dynamics in contaminated soils. Environmental Pollution, 152(2), 330-341.

Querol, X., Alastuey, A., Lopez-Soler, A., Mantilla, E., and Plana, F. (1996) Mineral composition of atmospheric particulates around a large coal-fired power station. Atmospheric Environment, 30(21), 3557-3572.

Regenspurg, S., Brand, A., and Peiffer, S. (2004) Formation and stability of schwertmannite in acidic mining lakes. Geochimica et Cosmochimica Acta, 68(6), 1185-1197.

Regenspurg, S., and Peiffer, S. (2005) Arsenate and chromate incorporation in schwertmannite. Applied Geochemistry, 20(6), 1226-1239.

Rodier, J., Broutin, J.P., Chambon, P., Champsaur, H., Rodi, L. (1996) L'analyse de l'eau. Dunod, Paris pp.1383.

Root, R.A., Dixit, S., Campbell, K.M., Jew, A.D., Hering, J.G., and O'Day, P.A. (2007) Arsenic sequestration by sorption processes in high-iron sediments. Geochimica et Cosmochimica Acta, 71(23), 5782-5803.

Rötting, T.S., Ayora, C., and Carrera, J. (2008a) Improved Passive Treatment of High Zn and Mn Concentrations Using Caustic Magnesia (MgO): Particle Size Effects. Environmental Science & Technology, 42(24), 9370-9377.

Rötting, T.S., Cama, J., Ayora, C., Cortina, J.L., and DePablo, J. (2006) Use of Caustic Magnesia To Remove Cadmium, Nickel, and Cobalt from Water in Passive Treatment Systems: Column Experiments. Environ. Sci. Technol., 40(20), 6438-6443.

Rötting, T.S., Caraballo, M.A., Serrano, J.A., Ayora, C., and Carrera, J. (2008b) Field application of calcite Dispersed Alkaline Substrate (calcite-DAS) for passive treatment of acid mine drainage with high Al and metal concentrations. Applied Geochemistry, 23(6), 1660-1674.

Rötting, T.S., Thomas, R.C., Ayora, C., and Carrera, J. (2008c) Passive Treatment of Acid Mine Drainage with High Metal Concentrations Using Dispersed Alkaline Substrate. J Environ Qual, 37(5), 1741-1751.

Rowe, O.F., Sánchez-España, J., Hallberg, K.B., Johnson, D.B. (2007) Microbial communities and geochemical dynamics in an extremely acidic, metal-rich stream at an abandoned sulfide mine (Huelva, Spain) underpinned by two functional primary production systems. Environmental Microbiology 9, 1761–1771.

Sáez, R., Pascual, E., Toscano, M., and Almodóvar, G.R. (1999) The Iberian type of volcano-sedimentary massive sulphide deposits. Mineralium Deposita, 34(5), 549-570.

Sahuquillo, A., Rigol, A., and Rauret, G. (2003) Overview of the use of leaching/extraction tests for risk assessment of trace metals in contaminated soils and sediments. TrAC Trends in Analytical Chemistry, 22(3), 152-159.

Sainz, A., Grande, J.A., de la Torre, M.L. (2004) Characterisation of heavy metal discharge into the Ria of Huelva. Environment International 30(4), 557-566.

Sánchez-España, J., Pamo, E., Pastor, E., Andrés, J., and Rubí, J. (2005) The natural attenuation of two acidic effluents in Tharsis and La Zarza-Perrunal mines (Iberian Pyrite Belt, Huelva, Spain). Environmental Geology, 49(2), 253-266.

-. (2006) The removal of dissolved metals by hydroxysulphate precipitates during oxidation and neutralization of acid mine waters, Iberian Pyrite Belt. Aquatic Geochemistry, 12(3), 269-298.

Sánchez-España, J., and Trevor, M.L. (2007) The behavior of iron and aluminum in acid mine drainage: speciation, mineralogy, and environmental significance. Thermodynamics, Solubility and Environmental Issues, p. 137-150. Elsevier, Amsterdam.

Santomartino, S., and Webb, J.A. (2007) Estimating the longevity of limestone drains in treating acid mine drainage containing high concentrations of iron. Applied Geochemistry, 22(11), 2344-2361.

Sapsford, D., Barnes, A., Dey, M., Williams, K., Jarvis, A., and Younger, P. (2007) Low Footprint Passive Mine Water Treatment: Field Demonstration and Application. Mine Water and the Environment, 26(4), 243-250.

Sarmiento, A.M., Nieto, J.M., Olías, M., and Cánovas, C.R. (2009) Hydrochemical characteristics and seasonal influence on the pollution by acid mine drainage in the Odiel river Basin (SW Spain). Applied Geochemistry, 24(4), 697-714.

Schulze, D.G. (1981) Identification of soil iron oxides minerals by differential X-ray diffraction. Soil Science Society of America Journal 45, 437- 440.

Shin, E.-J., Lauve, A., Carey, M., Bukovsky, E., Ranville, J.F., Evans, R.J., and Herring, A.M. (2008) The development of bio-carbon adsorbents from Lodgepole Pine to remediate acid mine drainage in the Rocky Mountains. Biomass and Bioenergy, 32(3), 267-276.

Sims, J.T., and Ellis, B.G. (1983) Changes in phosphorous sorption associated with aging of aluminum hydroxide suspensions. Soil Sci. Soc. Am. J. , 47 (5), 912-916.

Singh, B., Wilson, M.J., McHardy, W.J., Fraser, A.R., and Merrington, G. (1999) Mineralogy and chemistry of ochre sediments from an acid mine drainage near a disused mine in Cornwall, UK. Clay Minerals, 34, 301-317.

Stumm, W., and Sulzberger, B. (1992) The cycling of iron in natural environments: considerations based on laboratory studies of heterogeneous redox processes. Geochimica et Cosmochimica Acta, 56, 3233- 30257.

Terzano, R., Spagnuolo, M., Vekemans, B., DeNolf, W., Janssens, K., Falkenberg, G., Fiore, S., and Ruggiero, P. (2007) Assessing the Origin and Fate of Cr, Ni, Cu, Zn, Pb, and V in Industrial Polluted Soil by Combined Microspectroscopic Techniques and Bulk Extraction Methods. Environmental Science and Technology, 41, 6762-6769.

Tessier, A., Campbell, P.G.C., and Bisson, M. (1979) Sequential extraction procedure for speciation of particulate trace metals. Analytical Chemistry 51, 844-851.

Trolard, F. (2006) Fougerite: From field experiment to the homologation of the mineral. Comptes Rendus Geosciences, 338(16), 1158-1166.

Tyler, G., Carrasco, R., Nieto, J.M., Perez, R., Ruiz, M.J., Sarmiento, A.M. (2004) Optimization of Mayor and Trace Element Determination on Acid Mine Drainage samples by Ultrasonic Nebulizer-ICP-OES (USN-ICP-OES) Pittcon Conf. 7–12 March. Chicago, USA.

van Geen, A., Adkins, J.F., Boyle, E.A., Nelson, C.H., and Palanques, A. (1997) A 120 yr record of widespread contamination from mining of the Iberian pyrite belt. Geology, 25(4), 291-294.

Wang, H., Bigham, J.M., and Tuovinen, O.H. (2006) Formation of schwertmannite and its transformation to jarosite in the presence of acidophilic iron-oxidizing microorganisms. Materials Science and Engineering: C, 26(4), 588-592.

Watten, B.J., Lee, P.C., Sibrell, P.L., Timmons, M.B (2007) Effect of temperature, hydraulic residence time and elevated PCO2 on acid neutralization within a pulsed limestone bed reactor. Water Research 41(6), 1207-1214.

Watten, B.J., Sibrell, P.L., and Schwartz, M.F. (2005) Acid neutralization within limestone sand reactors receiving coal mine drainage. Environmental Pollution, 137(2), 295-304.

Webster, J.G., Swedlund, P.J., and Webster, K.S. (1998) Trace Metal Adsorption onto an Acid Mine Drainage Iron(III) Oxy Hydroxy Sulfate. Environ. Sci. Technol., 32(10), 1361-1368.

Younger, P.L., Banwart, S.A., and Hedin, R.S. (2002) Mine Water: Hydrology, Pollution, Remediation. Kluwer Academic Publishers, Dordrecht.

Yu, J.-Y., Heo, B., Choi, I.-K., Cho, J.-P., and Chang, H.-W. (1999) Apparent solubilities of schwertmannite and ferrihydrite in natural stream waters polluted by mine drainage. Geochimica et Cosmochimica Acta, 63(19-20), 3407-3416.

Zhang, H., Wen, X., and Wang, Y. (2007) Synthesis and characterization of sulfate and dodecylbenzenesulfonate intercalated zinc-iron layered double hydroxides by one-step coprecipitation route. Journal of Solid State Chemistry, 180(5), 1636-1647.

Ziemkiewicz, P.F., Skousen, J.G., and Simmons, J. (2003) Long-term Performance of Passive Acid Mine Drainage Treatment Systems. Mine Water and the Environment, 22(3), 118-129.

# APPENDIX 1. RESUMEN DE LA TESIS EN ESPAÑOL (35 PÁGINAS)

# RESUMEN CAPITULO 1. INTRODUCCIÓN

El drenaje ácido de mina (AMD), además de uno de los problemas ambientales más antiguos y ampliamente distribuidos en zonas mineras, es generador de uno de los ambientes acuáticos más extremos que se conocen. Las aguas contaminadas en áreas mineras muestran típicamente bajos valores de pH y alta concentración de metales como resultado de la disolución de sulfuros que ocurre tras la exposición de estos minerales a las condiciones superficiales (Bigham and Nordstrom, 2000).

Tanto la hidroquímica como la mineralogía de las aguas afectadas por AMD está controlada principalmente por los sistemas $SO_4$-Fe y $SO_4$-Al a pH que oscilan entre 1-5 y 5-6, respectivamente (Bigham and Nordstrom, 2000). La hidrólisis del $Fe^{3+}$ tiende a tamponar el pH de estas aguas en torno a 3,5 mediante la precipitación de schwertmannita de acuerdo a la siguiente reacción:

$$8Fe^{3+} + xSO^{=} + (16-2x)H_2O \leftrightarrows Fe_8O_8(OH)_{8-2x}(SO_4)_x + (24-2x)H^{+} \quad (1)$$

donde $1 \leq x \leq 1{,}86$, según datos de Bigham et al. (1996) y Yu et al. (1999). De manera similar, la hidrólisis del aluminio, con un pK1 = 5, y la precipitación resultante de hidrobasaluminita, $Al_4(SO_4)(OH)_{10}\bullet 15H_2O$, tampona el pH en valores alrededor de 5 (Bigham and Nordstrom, 2000). Dicha reacción puede ser escrita como:

$$4Al^{3+}_{(aq)} + SO_4{}^{=}_{(aq)} + 25H_2O_{(l)} \leftrightarrows Al_4(SO_4)(OH)_{10}\cdot 15H_20_{(s)} + 10H^{+}_{(aq)} \quad (2)$$

La primera parte de esta tesis discute la aplicabilidad de un proceso acoplado de extracciones secuenciales y difracción de rayos X diferencial para la caracterización mineralógica de los precipitados generados en aguas afectadas por AMD, los cuales suelen estar compuestos esencialmente por óxidos y sulfatos de hierro y aluminio pobremente cristalinos. Este estudio fue llevado a cabo en el sistema de tratamiento pasivo de Monte Romero que estuvo en funcionamiento desde agosto del 2005 a junio del 2006 (Rötting et al. 2008). Este emplazamiento fue seleccionado debido a que en el interior del material reactivo usado en el tratamiento se desarrollo tanto schwertmannita como precipitados de aluminio, observándose además la transformación de schwertmannita a goethita por envejecimiento.

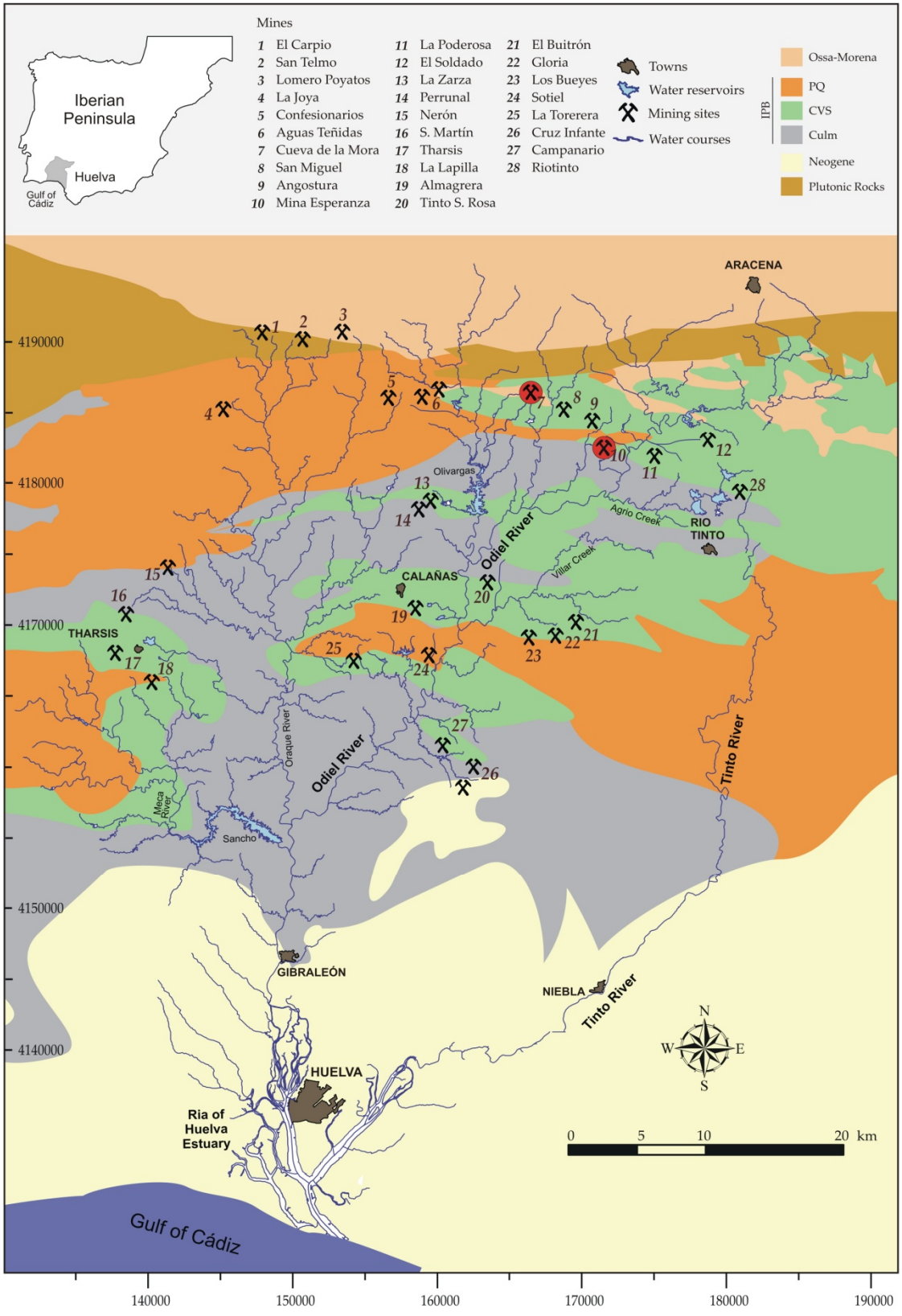


**Figure A1.1. Cuenca del Odiel y principales unidades geológicas de la IPB. Modificado de Sarmiento et al., 2009 con permiso de la autora.**

La Faja Pirítica Ibérica (IPB), situada en el suroeste de la Península Ibérica (Fig. A1.1), puede ser considerada como una de las mayores provincias metalogenéticas de sulfuros masivos del mundo. Con una extensión de 200 km y una amplitud cercana a los 40 km dispone de unas reservas originales estimadas de sulfuros cercanas a las 1700 Mt (Sáez et al., 1999). El resultado de la intensa minería desarrollada durante casi 5.000 años (Leblanc et al., 2000; Nocete et al., 2005) queda reflejado en esta región en la forma de numerosas escombreras y balsas de lodos así como galerías subterráneas y cortas inundadas (Nieto et al., 2007; Sarmiento et al. 2009).

Las aguas afectadas por contaminación minera pueden ser tratadas mediante dos tipos de planteamientos, los tratamientos activos o los pasivos (Johnson and Hallberg, 2005). Mientras el primer tipo conlleva la utilización de energía y la continua adición de reactivos químicos, el segundo tipo se fundamenta en el uso del flujo gravitacional del agua y las reacciones biogeoquímicas. El AMD en distritos mineros abandonados suele ser tratado mediante el uso de tecnologías de tratamiento pasivo (Younger et al., 2002). Técnicas de descontaminación tales como las barreras permeables reactivas, los humedales de flujo vertical, o los humedales aeróbicos han sido empleadas con bastante éxito para incrementar la calidad de las aguas en áreas de minería de carbón afectadas por AMD (Caraballo et al., 2010; Jarvis et al., 2006; Johnson and Hallberg, 2005). Sin embargo, la alta concentración metálica comúnmente observada en el AMD de la IPB reduce severamente la eficiencia de sistemas de tratamiento pasivo convencionales. Para superar los típicos problemas de atasco y pérdida de reactividad mostrados cuando los substratos reactivos son sometidos a AMD con altas concentraciones metálicas, se desarrolló un nuevo concepto de material reactivo denominado substrato alcalino dispersado (DAS) (Rötting et al., 2008c).

La mezcla reactiva tipo DAS está compuesta por una matriz inerte de virutas de madera de pino, para aportar mayor porosidad al medio y reducir los problemas de atasco, y un reactivo alcalino de grano fino para incrementar el pH del agua y la reactividad del substrato. Esta filosofía de tratamiento se aprovecha del uso de dos tipos de reactivos alcalinos diferentes, caliza y MgO, para poder obtener valores de pH que oscilan entre 6-7 y 8-10, respectivamente. El rango de pH obtenido mediante el uso de caliza induce la precipitación de Fe y Al así como la retirada por adsorción/coprecipitación de otros metales minoritarios (Cu, As, Pb, etc). De forma complementaria, la disolución de MgO tampona el pH del agua entre 8,5 y 10,5, siendo estos valores suficientemente elevados como para precipitar metales divalentes tales como Zn, Cd, Ni o Co.

El DAS-calizo ha sido probado con éxito en columnas de laboratorio (Rötting et al., 2008a), donde el funcionamiento hidráulico y químico del material reactivo fue investigado. De manera adicional se realizó un estudio de campo en la IPB en el cual se obtuvieron resultados muy prometedores (Rötting et al., 2008b). Durante el tiempo que estuvo en funcionamiento este sistema de tratamiento consiguió retirar de las aguas contaminadas un 90–100% de Al, Cu, Pb y As, alrededor de un 45% de Fe así como una acidez neta media de 900 mg/L como $CaCO_3$ equivalentes. La importante cantidad de caliza sin reaccionar que se observó en el tanque reactivo tras su muestreo evidencia la necesidad de un nuevo estudio para poder optimizar la razón caliza-virutas de madera en el relleno. Además, con la excepción del Cu, el sistema no fue capaz de retirar ningún metal divalente (Fe(II), Zn, Cd, Co, Ni, etc.). El trabajo expuesto en la segunda parte de esta tesis es la continuación lógica de estos experimentos, siendo el objetivo principal de este nuevo trabajo verificar el correcto funcionamiento de un sistema de tratamiento en campo en el cual se disponga tanto de pasos de tratamiento calizos como con MgO.

La tercera parte de esta tesis expone la implementación de un sistema de tratamiento pasivo a escala real en Mina Esperanza. Una de las mayores dificultades que un sistema de tratamiento pasivo de aguas ácidas tiene que enfrentar es el largo período de funcionamiento necesario para que el sistema sea económicamente viable (PIRAMID-Consortium, 2003). La reducción de la porosidad así como el recubrimiento e inactivación del material reactivo debido a los precipitados generados, son dos de los principales factores que controlan la duración de un tratamiento pasivo. Ambos factores dependen de la cantidad de metales disueltos en el AMD. Debido al alto contenido metálico del AMD en Mina Esperanza, este emplazamiento fue seleccionado como representativo de la alta contaminación metálica típicamente observada en la IPB.

El principal objetivo cubierto en el Capítulo 4 de esta tesis corresponde a la exposición de los resultados tan satisfactorios obtenidos tras 20 meses de funcionamiento del sistema de tratamiento pasivo a escala real construido en Mina Esperanza. La hidroquímica, la mineralogía de los precipitados y la eficiencia en la retirada metálica de las diferentes secciones que componen el tratamiento son mostradas para alcanzar una mejor comprensión de los distintos procesos hidroquímicos, mineralógicos y operacionales involucrados en la descontaminación de AMD con alta carga metálica.

El último capítulo de la tercera parte de esta tesis está dedicado al estudio de los distintos procesos hidroquímicos y mineralógicos que controlan la longevidad del funcionamiento de substrato reactivo tipo DAS calizo empleado en el tanque reactivo de

Mina Esperanza. En base al papel jugado por los precipitados en el consumo e inactivación del material calizo, a la evolución temporal de la conductividad hidráulica así como a la eficiencia mostrada en la retirada metálica, se plantean algunas mejoras a realizar en el diseño original del tratamiento.

# RESUMEN CAPÍTULO 2. APLICABILIDAD DE UNA EXTRACCIÓN SECUENCIAL Y DXRD PARA LA CARACTERIZACIÓN DE FASES DE Fe Y Al PÓBREMENTE CRISTALINAS EN UN SISTEMA DE TRATAMIENTO PASIVO DE AGUAS ÁCIDAS DE MINA

Tradicionalmente, los estudios acerca de la interacción entre el AMD y los sistemas de tratamiento pasivos están centrados en la calidad del agua a la entrada y salida del sistema, prestándose muy poca atención al detalle de la mineralogía desarrollada en el interior del material reactivo (Cocos et al. 2002, Jarvis et al. 2006, Johnson y Younger 2006, Kalin 2004, Kalin and Caetano Chaves 2003, Laus et al. 2007, Sapsford et al. 2007, Shin et al. 2008). El objetivo del presente estudio es comprobar la aplicabilidad de un procedimiento específico de extracciones secuenciales y difracción de rayos X diferencial (DXRD) para la caracterización mineralógica de los precipitados generados. El sistema de tratamiento pasivo de Monte Romero (Rötting et al. 2008) fue elegido como el mejor emplazamiento para llevar a cabo este tipo de estudios debido a que en el interior del material reactivo empleado es esperable la aparición de schwertmannita e hidrobasaluminita, además de goethita como producto de envejecimiento de schwertmannita.

## 2.1 Localización y descripción del muestreo

Todas las muestras empleadas en este estudio fueron obtenidas del interior del material reactivo del sistema de tratamiento pasivo a escala de campo instalado en Monte Romero en julio del 2006. En esa época el sistema estaba constituido por un tanque cilíndrico de 3 $m^3$ conectado en serie con tres decantadores con un volumen aproximado de 6 $m^3$ cada uno. Como material reactivo fue empleado DAS calizo (Rötting et al. 2008). Este substrato fue preparado mediante la mezcla de un 25% (v/v) de arena caliza y un 75 % (v/v) de virutas de madera de pino.

El drenaje ácido emergente de uno de los pozos principales del sistema de galerías subterráneas de Monte Romero fue parcialmente conducido hacia el tanque reactivo mediante el uso de tuberías de polietileno. Antes de circular por el sistema de tratamiento el AMD tenía un pH cercano a 3,3, una acidez neta de 1.400-1.600 mg/L como $CaCO_3$ equivalentes y concentraciones medias de 315 mg/L de Fe (97% como Fe (II)), 310 mg/L de Zn, 270 mg/L de Ca, 75 mg/L de Al, 20 mg/L de Mn, 1,5 mg/L de Cu y 3.200 mg/L de sulfato (Rötting et al. 2008).

Durante el flujo vertical y gravitacional del AMD a través del material reactivo ocurren ciertos cambios hidroquímicos. La disolución de caliza causa un incremento en el pH y la consiguiente precipitación de schwertmannita (a valores de pH de entre 3 y 4,5) y de hidroxisulfatos de Al (a pH de 5 a 5,5). La precipitación de schwertmannita en los decantadores consume el exceso de alcalinidad producido por la disolución de caliza en el interior del material reactivo y del mismo modo reduce los valores de pH a 3-3,5.

Durante el muestreo de sólidos, el flujo de agua fue detenido y se excavó una sección de 90 cm para obtener una vista de los diferentes niveles de precipitación desarrollados en el interior del material reactivo. Desde la superficie hasta el fondo pudieron ser diferenciados a simple vista seis niveles descritos como: 1) nivel deleznable de color marrón rojizo de 0 a 1 cm, 2) nivel naranja oscuro desde 1 a 3 cm, 3) nivel naranja claro-amarillento desde 3 a 5 cm, 4) zona cementada de color blanco rosáceo desde 5 a 15 cm, 5) zona amarillenta desde 15 a 30 cm, y finalmente 6) material reactivo aparentemente sin reaccionar desde 30 a 90 cm.

## 2.2 Procedimiento de Extracción Secuencial

Los cuatro factores esenciales que definen un procedimiento de extracción secuencial son: los químicos empleados como extractantes, la relación en volumen sólido-extractante, el tiempo y naturaleza del contacto entre la muestra sólida y el extractante empleado y las condiciones ambientales durante cada paso de la extracción secuencial.

Para la gran mayoría de minerales englobados en este estudio (yeso, calcita, schwertmannita y goethita) se disponen de extractantes selectivos contrastados para los cuales se han realizados estudios específicos controlando el efecto de las condiciones ambientales en las propiedades de dichos extractantes (Dold 2003b, Fanfani et al. 1997, Hall et al. 1996, Sahuquillo et al. 2003, Stumm and Sulzberger 1992). Sin embargo, para aplicar de manera óptima estos extractantes a muestras con elevadas concentraciones de óxidos y oxihidróxisulfatos de hierro se hacen necesarios algunos

cambios en la relación en volumen entre muestra y extractante y en el tiempo de reacción y naturaleza del contacto entre ambos.

En la literatura existente no se ha encontrado ningún estudio previo sobre la utilización de extractantes selectivos con hidrobasaluminita. Así pues, se decidió emplear para todas las muestras los extractantes selectivos para minerales de Fe.

Los distintos pasos constituyentes de la extracción secuencial diseñada, así como la cantidad de extractante empleada, la cantidad de muestra sólida y las condiciones ambientales seleccionadas son mostrados de manera sintética en la Tabla 2.1.

**TABLA A1.1.** Extracción secuencial desarrollada para este estudio.

| Pasos de la extracción secuencial | Minerales principalmente disueltos | Fases disueltas en este estudio | Elementos puestos en solución |
|---|---|---|---|
| ***1) Fracción soluble en agua:*** 200 mg de muestra y 20 ml de agua desionizada, agitado por 12 h a temperatura ambiente (TA) | Sulfatos secundarios y otras sales | Yeso | Ca y $SO_4^{2-}$ |
| ***2) Fracción soluble e intercambiable:*** 20 ml de 1 M $NH_4$-acetato ( pH 4,5), agitado por 1 h a TA | Calcita y algunas arcillas | Calcita | Ca y elementos adsorbidos |
| ***3) Oxihidróxidos y oxihidroxisulfatos de Fe (III) poco cristalinos:*** 20 ml de 0,2 M $NH_4$-oxalato (pH 3),agitado 30 minutos en oscuridad a TA | Principalmente schwertmannita y ferrihidrita de 2 líneas | Schwertmannita, hidrobasaluminita y gibbsita | Fe, Al y $SO_4^{2-}$ |
| ***4) Hidróxidos y óxidos de Fe (III) cristalinos:*** 20 ml de 0,2 M $NH_4$-oxalato ( pH 3),en baño de agua a 80 ºC durante 1h | Goethita, jarosita, ferrihidrita de 6 líneas y hematite | Goethita | Fe |
| ***5) Digestión del residuo:*** 3 ml de $HNO_3$ + 7,5 ml de HF + 2,5 ml de $HClO_4$ | Silicatos | Residuo (virutas de madera) | Elementos orgánicos |

## 2.3 Distribución general de los precipitados en el interior del tanque reactivo

La distribución de los precipitados así como el papel desempeñado por cada mineral en la retirada metálica aparecen sintetizados en la figura 2.1. La inspección de los perfiles de retirada de cada elemento muestra claramente la aparición de dos horizontes de precipitación para el Fe y el Al con una zona más amplia caracterizada por la presencia de yeso.

Una observación detallada del horizonte de Fe (0-5 cm) revela que aunque la masa de goethita es considerablemente mayor que la de schwertmannita (Tabla 2.2), la última es la fase mineral responsable de la mayor parte de la retira de hierro obtenida (Fig. 2.1B). Esto se debe a que cada mg de schwertmannita contiene 8 veces más hierro que un mg de goethita debido a la estequiometría de cada mineral. Esta proporción mineral también fue observada en los análisis de difracción de las muestras a 0-1, 1-3 y 3-5 cm de profundidad, en las cuales la detección de schwertmannita antes de la utilización de la DXRD fue imposible tanto por la baja cristalinidad de este mineral como por la pequeña concentración de éste respecto a goethita.

La cantidad de Fe precipitado decrece progresivamente desde la parte superior hasta la parte inferior del horizonte de Fe (Fig. 2.1). Otro resultado importante de la extracción secuencial desarrollada es el progresivo descenso observado en la cantidad de $SO_4^=$ adsorbido a la superficie de schwertmannita respecto a la mayor profundidad de las muestras en el perfil. Este efecto no puede ser observado en la figura 2.1 debido a que la adsorción de $SO_4^=$ queda enmascarada por la presencia de yeso.

El yeso fue encontrado a lo largo de todo el tanque reactivo, sin embargo, una inspección detallada de los análisis realizados muestra como este mineral forma un nivel casi independiente sobre impuesto a los niveles de Fe y Al. A partir de los resultados de S recuperado en el paso 1 de la extracción secuencial, se ve como la concentración de yeso incrementa a lo largo del nivel de Fe hasta llegar a su máximo en el límite entre el nivel de Fe y el de Al para finalmente comenzar a decrecer a través del nivel de Al (Fig. 2.1). Esta distribución podría ser el resultado de la formación de yeso por la combinación del Ca liberado tras la disolución de calcita y el $SO_4^=$ contenido en el AMD. La ausencia de yeso en la parte superficial de la secuencia (0-1 cm) es consistente con la precipitación directa de schwertmannita (y su producto de envejecimiento goethita) a partir del AMD del sobrenadante.

La distribución de precipitados de Al muestra un importante número de similitudes con la distribución de precipitados de Fe. La cantidad retirada de Al decrece progresivamente desde la parte superior a la inferior del nivel de Al (Fig. 2.1A). Otra similitud es que para ambos casos una única fase mineral de Fe o Al no es suficiente para explicar la retirada metálica. No obstante, mientras la presencia de schwertmannita (Fe-hidroxisulfato) y goethita (Fe-hidróxido) pudo ser confirmada, la presencia de hidrobasaluminita (Al-hidroxisulfato) y $Al(OH)_3$ amorfo (Al-hidróxido) tan sólo puede ser sugerida en base a los datos obtenido en la extracción secuencial y a al modelo termodinámico realizado.

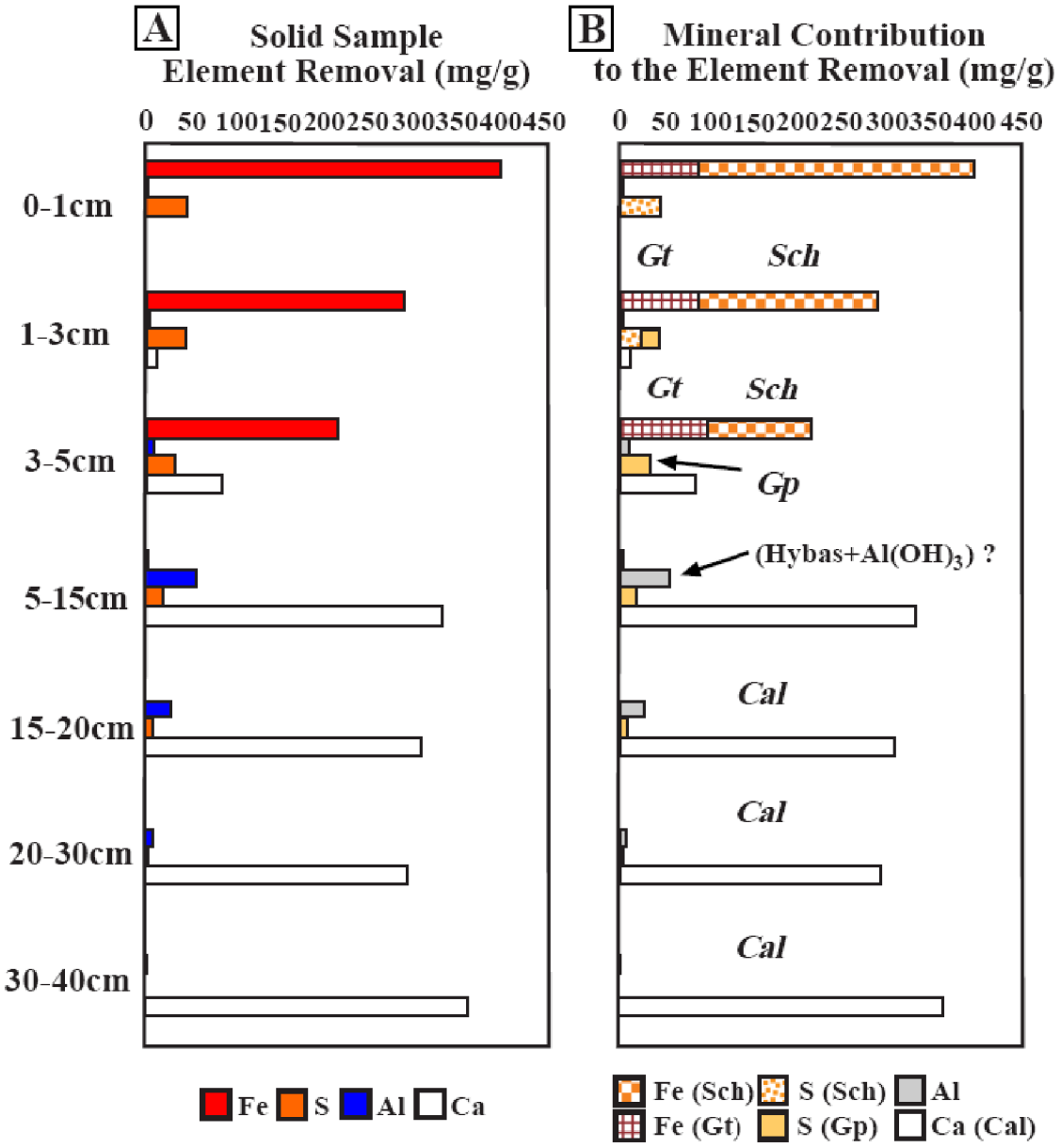


**Figura A1.2. Retirada elemental (diagrama de la izquierda) y contribución mineral a la retirada metálica (diagrama de la derecha) a lo largo del perfil del tanque reactivo de Monte Romero. Gt = Goethita, Sch = Schwertmannita, Gyp =Yeso, Hybas = Hidrobasaluminita, $Al(OH)_3$ = $Al(OH)_3$ amorfo, Cc = Calcita. Las diferentes áreas dibujadas en el diagrama de la derecha corresponden a la evolución en profundidad de la cantidad de cada elemento atribuido a cada fase mineral específica.**

Otra observación importante ofrecida por los resultados de la extracción secuencial sería la cantidad de calcita consumida en las diferentes profundidades del material reactivo. El estudio del Ca liberado en el segundo paso de la extracción secuencial revela como casi toda la calcita fue consumida en el nivel de Fe (0-5 cm) mientras que en el nivel de Al permanece sin disolverse una importante cantidad. Este hecho se atribuye al proceso de inactivación de los granos de caliza como resultado de la precipitación en su superficie de precipitados de Al y yeso. Esta hipótesis está reafirmada por las imágenes

observadas mediante SEM-EDS. Sin embargo, el avance del frente de precipitación de Fe disuelve el nivel de Al y con él la calcita restante.

**TABLA A1.2.** Distribución mineral en el horizonte de Fe.

| Muestra | Sch (wt%) | Gt (wt%) | Gyp (wt%) | Cc (wt%) |
|---|---|---|---|---|
| 0-1 cm | 30,3 | 68,3 | 1,4 | 0,0 |
| 1-3 cm | 19,2 | 67,5 | 12,5 | 0,8 |
| 3-5 cm | 6,7 | 44,2 | 11,6 | 37,5 |

El porcentaje en peso (wt%) para cada mineral fue calculado utilizando los datos obtenidos para cada mineral en los pasos específicos de la extracción secuencial. Sch = schwertmannita; Gt = goethita; Gyp = yeso y Cc = calcita

Las concentraciones minerales interpretadas a partir de los datos de las extracciones secuenciales facilita enormemente el entendimiento de la distribución de cada una de las fases que se forman en el interior del material reactivo, sirviendo además para cuantificar la importancia de cada fase mineral en la retira metálica. Estos resultados también pueden ser utilizados para inferir los procesos hidroquímicos que ocurren en el interior del material reactivo, lo cual es esencial para mejorar la eficiencia del sistema.

# RESUMEN CAPÍTULO 3. SISTEMA DE TRATAMIENTO PASIVO MULTIPASO CON CALIZA Y MgO PARA TRATAR DRENAGE ÁCIDO DE MINA CON ELEVADA CARGA METÁLICA A ESCALA DE CAMPO

Los sistemas de tratamiento pasivo de tipo DAS calizo han sido satisfactoriamente evaluados mediante ensayos de laboratorio a lo largo de todo un año (Rotting et al., 2008a), donde fue estudiado en detalle el funcionamiento hidroquímico e hidráulico del material reactivo. Un estudio a escala de campo fue desarrollado de manera adicional en la IPB pudiéndose observar de igual modo resultados muy prometedores (Rötting et al., 2008b). Durante el tiempo que estuvo en funcionamiento este sistema de tratamiento retiró del agua un 90-100% de Al, Cu, Pb, y As, alrededor de un 45% de Fe y una acidez neta media de 900 mg/L como $CaCO_3$ equivalentes. La importante cantidad de material reactivo sin reaccionar observado en el tanque reactivo muestra la necesidad de un nuevo estudio para optimizar la relación virutas de madera-caliza del material reactivo. Además, a excepción de Cu, el sistema no retiró ningún metal divalente (Fe(II), Zn, Cd, Co o Ni).

La utilización de reactivos alcalinos diferentes estriba en la necesidad de alcanzar valores de pH entre 8 y 10, los cuales son imposibles de alcanzar mediante la disolución de caliza en AMD ya que la alta concentración de Ca existente hace que el mineral alcance el equilibrio con valores de pH de entre 6 y 7. Sin embargo, la disolución del óxido de magnesio tampona el pH de la solución entre 8,5 y 10,5, siendo así suficientemente elevado como para inducir la precipitación de metales divalentes tales como Zn, Ni, Cd o Co.

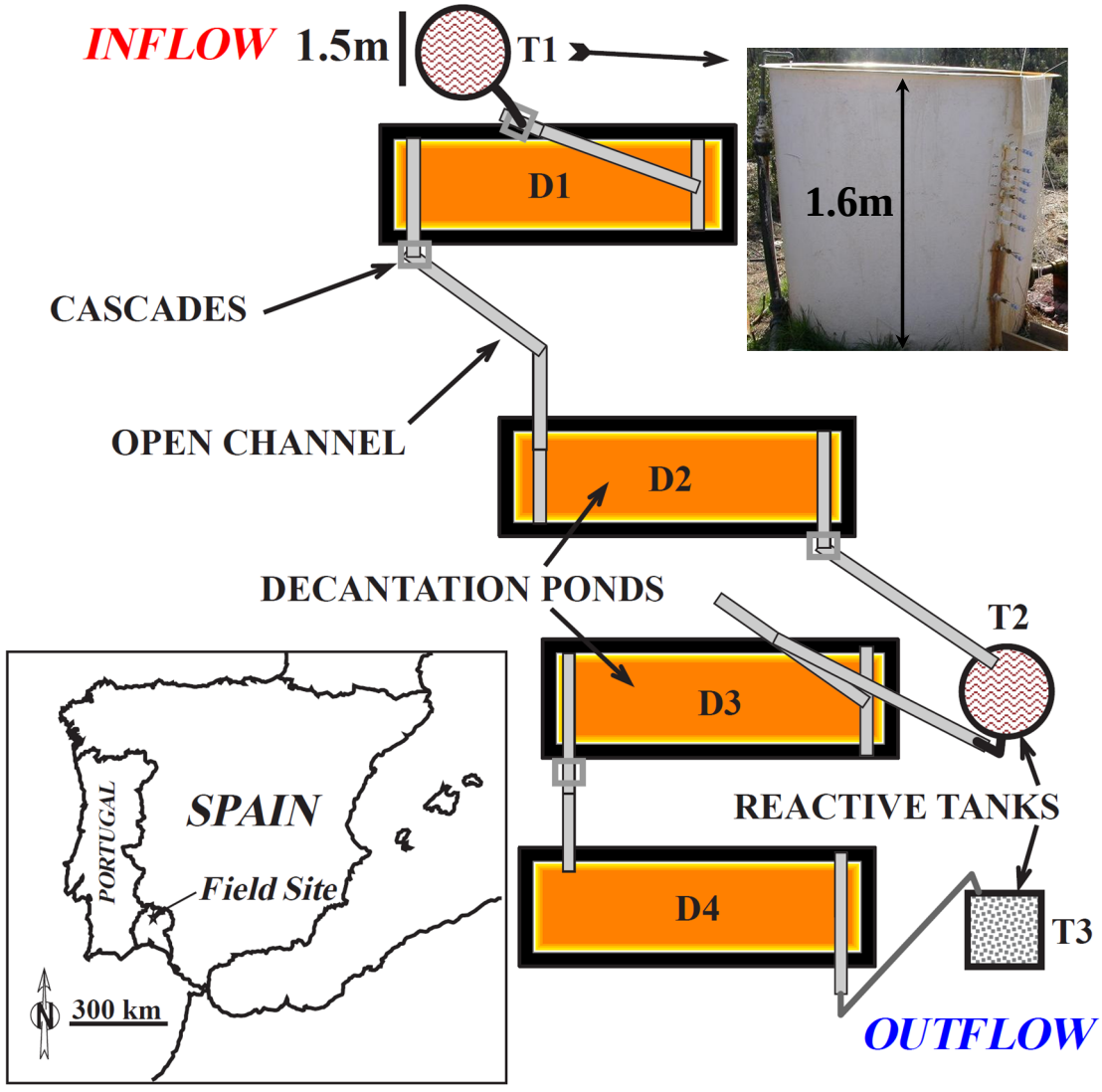


**Figura A1.3. Localización de la zona de estudio y vista esquemática en planta de las diferentes secciones que componen el sistema de tratamiento pasivo de Monte Romero. T1 y T2 corresponden a tanques reactivos rellenos de DAS calizo, T3 es un tanque reactivo con DAS magnésico y D1-4 serían cuatro decantadores. El AMD fluye desde T1 hasta T3.**

En 2008, Rötting et al. desarrollaron un experimento de laboratorio utilizando una mezcla de viruta de madera y MgO (DAS magnésico) sometida a una solución acuosa

sintética con Zn y Mn y un pH de 5,5. Durante un año de funcionamiento este experimento retiró completamente los metales del agua sin sufrir problemas evidentes de atasco.

Este capítulo es la continuación lógica de estos experimentos, siendo el objetivo principal de este estudio controlar la evolución del funcionamiento de un sistema de tratamiento a escala de campo que emplea tanto caliza como MgO y es sometido a AMD natural. La planta piloto de tratamiento que existía previamente (Rötting et al., 2008b) fue acondicionada hasta contener los elementos mostrados en la figura 3.1.

## 3.1 Eficiencia del tratamiento en la retirada metálica

La acidez neta puede ser considera como un parámetro muy útil para evaluar la eficiencia de cada sección del tratamiento en lo que respecta a la retirada metálica y a la mejora de las condiciones hidroquímicas del agua. La evolución temporal de la acidez neta para cuatro puntos seleccionadas en el tratamiento así como las concentraciones de Fe, Al y Zn en dichos puntos se muestran en la figura 3.2. Como se observa en dicha figura, la acidez neta a la entrada del sistema sufre un incremento repentino tres meses después del comienzo del tratamiento. Este incremento fue debido al importante aumento registrado en las concentraciones de Fe, Al y Zn a la entrada.

La acidez neta retirada (acidez neta a la entrada del sistema – acidez neta a la salida de D2) en la primera sección del tratamiento (T1+D1+D2) oscila entre 500 mg/L como $CaCO_3$ equivalentes, durante los tres primeros meses, y casi 1.000 mg/L como $CaCO_3$ equivalentes tras el repentino incremento observado en la acidez neta en Diciembre (Fig. 3.2). Disminuye hacia unos 700 mg/L hacia el final del experimento. El descenso de la acidez neta en esta sección está claramente debido a la retirada de Fe en T1 y D1 y en mayor medida aún a la retirada de Al en el interior de T1. La observación de la acidez neta retirada en la segunda sección del tratamiento (T2+D3+D4) revela una retirada media cercana a los 500 mg/L como $CaCO_3$ equivalentes, siendo Fe el principal elemento eliminado. Finalmente, la acidez neta retirada a la salida del tratamiento (T3-OUT) muestra un descenso de otros 500 mg/L como $CaCO_3$ equivalentes. Este descenso final es debido a la retirada tanto de Zn como de Fe en el interior de T3. Con todo esto, el sistema es capaz de reducir la acidez neta de 2.500 a 500 mg/L como $CaCO_3$ equivalentes.

Para evaluar la eficiencia en la retirada global del sistema se calculó la retirada metálica relativa de acuerdo a la siguiente ecuación:

$$r = \frac{c_{in} - c_{out}}{c_{in}} \cdot 100 \qquad (3)$$

donde $c_{in}$ corresponde a la concentración de un determinado elemento en el agua de entrada al sistema y $c_{out}$ sería la concentración del mismo elementos a la salida del sistema.

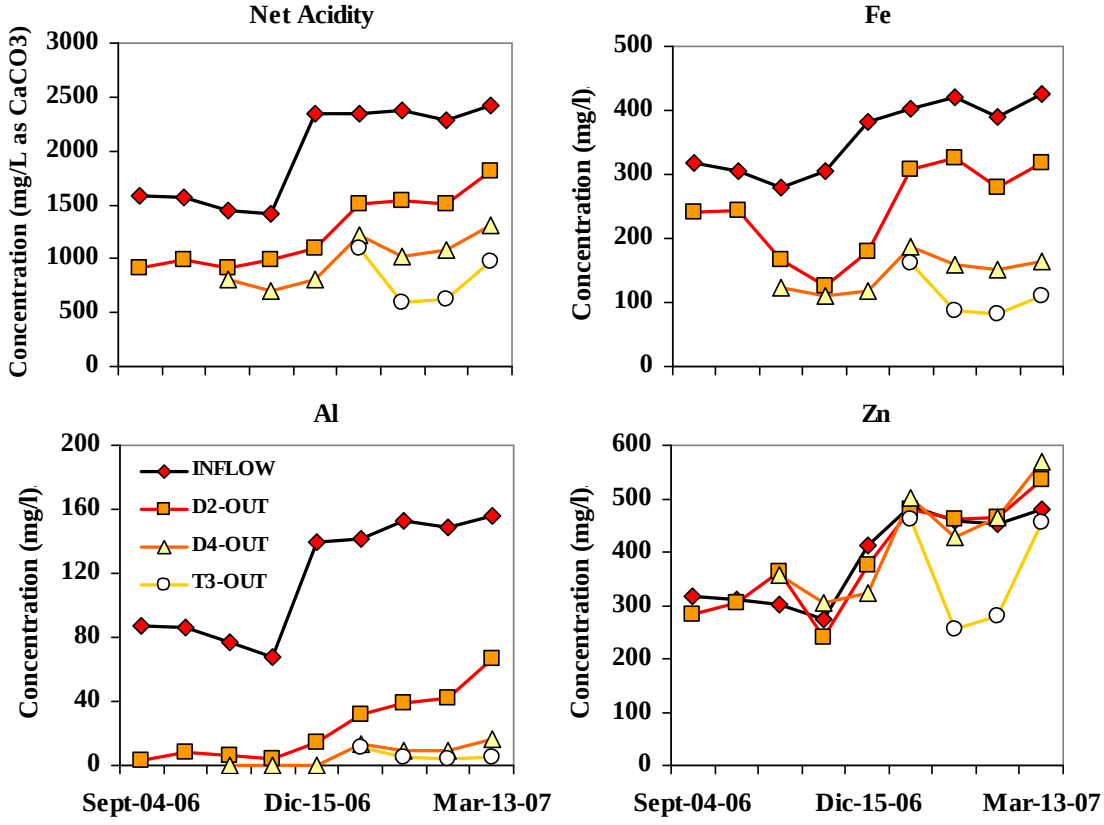


**Figura A1.4. Evolución temporal de la acidez neta y las concentraciones de Fe, Al y Zn en algunos puntos estratégicos del sistema de tratamiento pasivo. D2 y D4 corresponden a los decantadores 2 y 4 respectivamente mientras que T3 sería el tanque reactivo relleno de DAS magnésico.**

Los resultados de estos cálculos vienen reflejados en la figura 3.3, donde la concentración media a la entrada y salida del sistema así como retirada media relativa para ciertos elementos han sido agrupadas en dos gráficos diferentes. En lo que respecta a los elementos mayoritarios (Fig. 3.2A) puede observarse una retirada relativa del 100% para Al y Cu, mayor del 70% para Fe y Al y de casi 25% para Zn. Estas retiradas relativas implican una retira neta de 300 mg/L de Fe, 140 mg/L de Al, 105 mg/L de Zn, 32 mg/L de Si y 12 mg/L de Cu. Para los elementos minoritarios (Fig. 3.2B) se observa una retirada relativa del 100% para As y Pb, 95% para Cr, casi 20% para Ni, 10% para Co y 5% para Cd. Estas retiradas relativas corresponden a una retirada neta de las aguas

de 460 µg/L de As, 155 µg/L de Pb, 220 µg/L de Ni, 95 µg/L de Co, 70 µg/L de Cd and 14 µg/L de Cr.

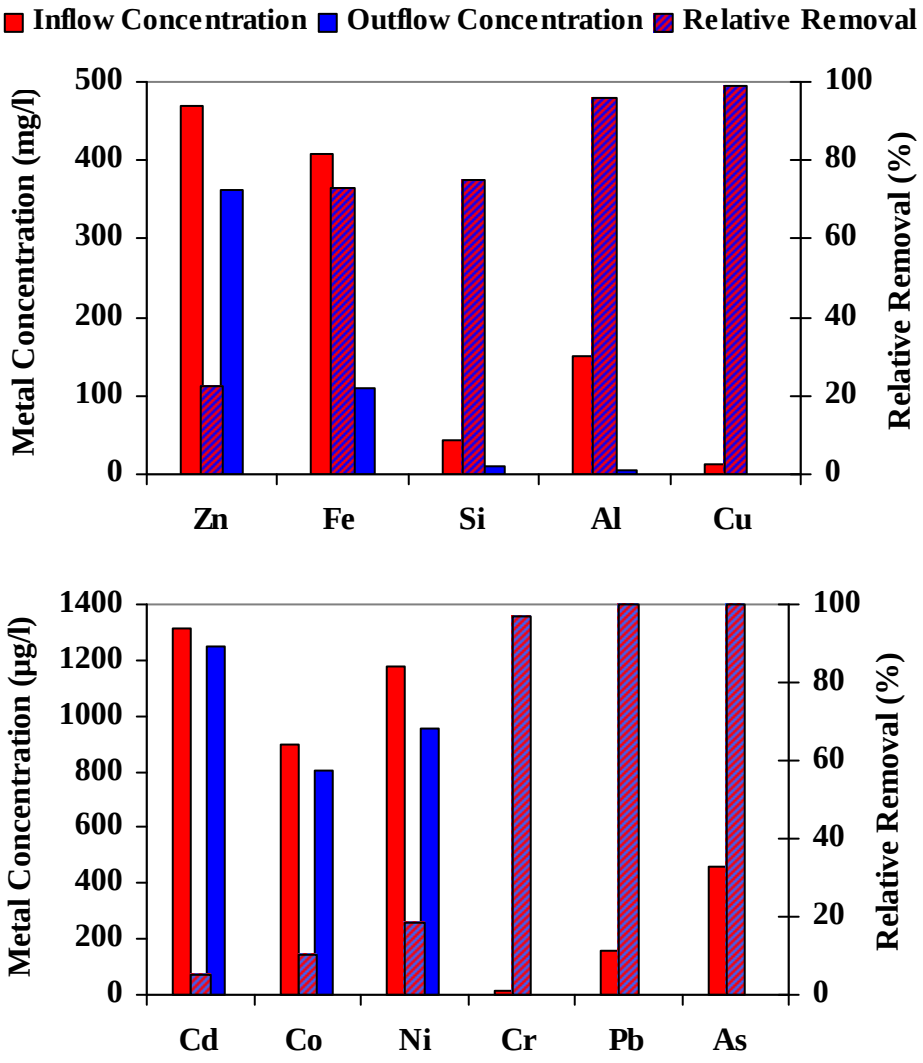


**Figura A1.5. Concentración metálica a la entrada y salida del sistema y retirada relativa de todo el sistema para algunos elementos mayoritarios (A) y minoritarios (B). Los valores mostrados en este gráfico corresponden a los últimos tres meses del sistema cuando todos los tanques reactivos estaban en funcionamiento.**

### 3.2 Mejoras implementadas en el sistema y mineralogía observada

El presente estudio ha mostrado como un 12.5% (v/v) de caliza tiene la misma efectividad que un 20% (v/v). Sin embargo, pudo verse una disminución en la reactividad de la caliza hacia el final del experimento. Este efecto se debe al progreso del frente de precipitación de aluminio a través del material reactivo, causando una menor retirada de Al dentro de T1 así como una disminución de la alcalinidad generada y consiguientemente de la retirada de Fe en los decantadores.

El segundo tanque reactivo con DAS calizo y los dos siguientes decantadores desarrollan una función muy importante en la retirada de Fe (casi el 50% de la total retirada de Fe en el sistema). Los análisis realizados al material reactivo de T3 reflejaron como casi la totalidad del MgO fue consumido. Esta observación claramente denota como el tamaño de grano elegido fue el idóneo para alcanzar la total disolución del mismo sin sufrir ningún proceso de inactivación. Sin embargo, también refleja como un mayor volumen y/o una mayor proporción de MgO en la mezcla reactiva es necesaria para poder extender la vida útil del DAS magnésico. T3 confirmó cómo la utilización de MgO como material reactivo permite eliminar, en condiciones de campo y con AMD real, metales divalentes como Zn, Fe(II), Cd, Co, y Ni.

La mineralogía de los precipitados desarrollados en el sistema de tratamiento pasivo está directamente controlada por los cinco elementos principales presentes en el AMD de Monte Romero: Fe, Al, Ca, Zn y $SO_4$. De este modo pudo observarse un horizonte de precipitados de Fe en la parte superior del material reactivo de los tres tanques reactivos. Esta capa de hierro está constituida por schwertmannita y goethita en T1 y sólo por goethita en T2 y T3. Schwertmannita parece precipitar directamente del sobrenadante y envejecer progresivamente a goethita. En los tanques con sólo goethita la aparición de este mineral se debe a la precipitación directa del mismo debido a los elevados valores de pH alcanzados. El horizonte de Al se formó claramente en T1 y T2. Ninguna fase mineral cristalina de Al pudo ser detectada siendo tanto hidrobasaluminita como $Al(OH)_3$ amorfo las fases minerales más probables. Finalmente el horizonte de Zn tan sólo se desarrolló en el interior de T3. Las fases minerales de Zn detectadas en este nivel corresponderían a schulenbergita rica en Zn, $(Cu,Zn)_7(SO_4)_2(OH)_{10}•3H_2O$, y sauconita $Zn_3(Si,Al)_4O_{10}(OH)_2•4H_2O$.

## RESUMEN CAPÍTULO 4. IMPLEMENTACIÓN DE UN SISTEMA DE TRATAMIENTO PASIVO CON SUSTRATO ALCALINO DISPERSADO (DAS) EN MINA ESPERANZA, SO ESPAÑA, PARA LA DESCONTAMINACIÓN PROLONGADA DE DRENAJE ÁCIDO DE MINA CON ALTA CARGA DE CONTAMINANTES

El principal objetivo de este estudio es mostrar los grandes resultados obtenidos tras 20 meses de funcionamiento ininterrumpido del sistema de tratamiento pasivo a escala real de Mina Esperanza. La hidroquímica del AMD, la composición mineralógica de los precipitados y la eficiencia en la retira metálica del tratamiento serán expuestas en

detalle con el fin de poder alcanzar un mejor entendimiento del funcionamiento del sistema.

## 4.1 Localización

Mina Esperanza está localizada en la parte norte de la IPB (Fig. 4.1A), en el suroeste español (37º45´34´´N-6º41´00´´O). La mineralización explotada consiste en un depósito masivo de pirita con cantidades menores de calcopirita (Pinedo-Vara, 1963).

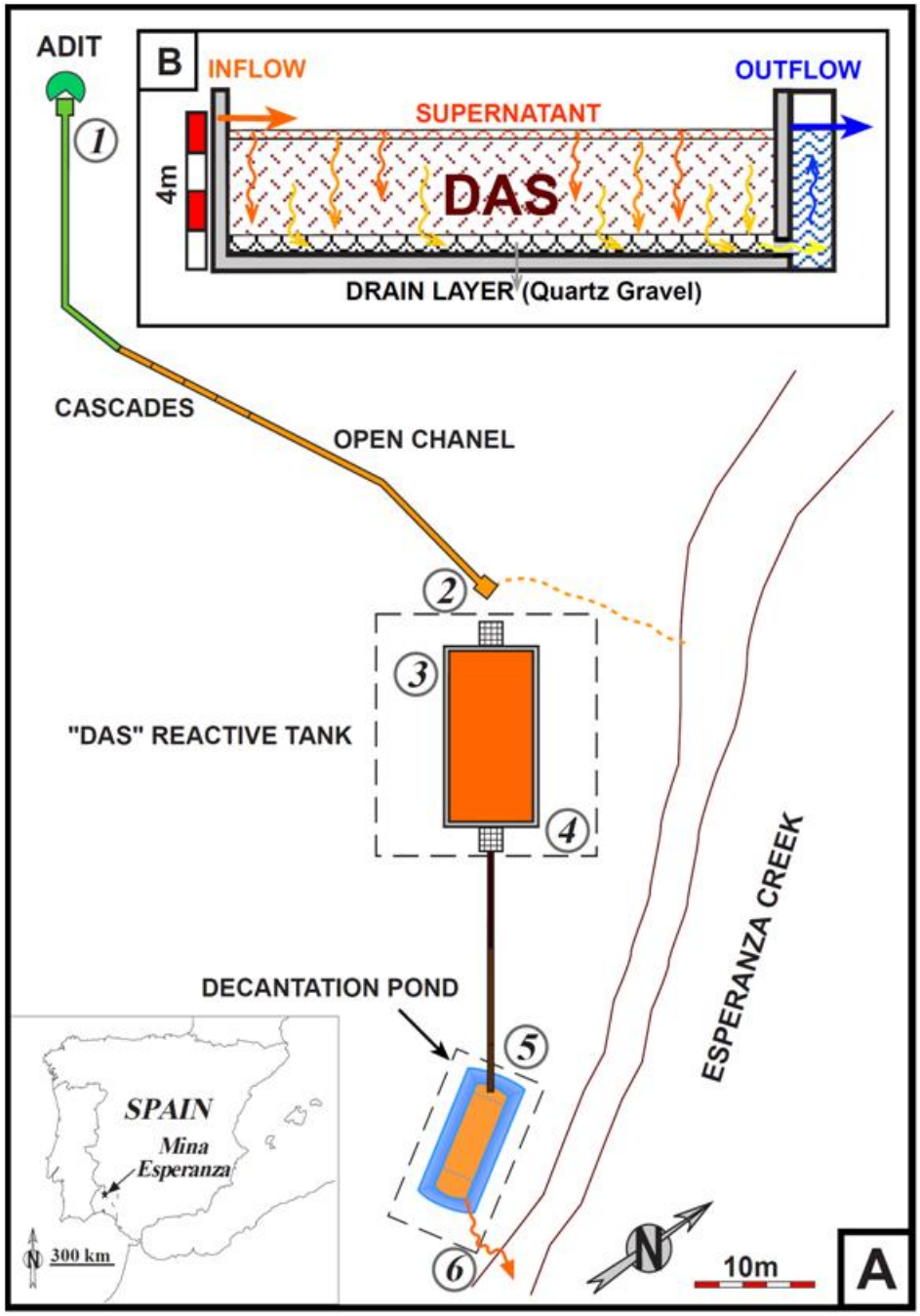


**Figure A1.6. A) Localización y vista esquemática en planta del sistema de tratamiento pasivo de Mina Esperanza. 1 = bocamina, 2 = entrada del tanque reactivo, 3 = sobrenadante del tanque reactivo, 4 = salida del tanque reactivo, 5 = entrada decantador y 6 = salida decantador. B) Perfil esquemático del tanque reactivo**

Las rocas encajantes son pizarras y filitas de bajo grado metamórfico. Esta mina subterránea estuvo en funcionamiento la primera mitad del siglo pasado. Tras su cierre, la mina se inundó de forma natural y comenzó a liberar aguas contaminadas por AMD, el cual tras fluir por el arroyo Esperanza llega a confluir con el Odiel.

La composición de este AMD a la salida de la bocamina así como sus principales características físico-químicas pueden observarse en la Tabla 4.1.

**TABLE A1.4**. Composición y parámetros físico-químicos del AMD en la bocamina

| **Elementos mayoritarios (mg/L)** | | | | | | | | | | |
|---|---|---|---|---|---|---|---|---|---|---|
| Al | Ca | Cu | Fe | K | Mg | Mn | Na | $SO_4^{2-}$ | Si | Zn |
| 128-167 | 146-194 | 12-24 | 755-1.100 | 5-34 | 149-215 | 4-6 | 21-26 | 3.324-4.515 | 44-60 | 19-33 |
| **Elementos minoritarios (µg/L)** | | | | | | | | | | |
| As | Ba | Be | Cd | Co | Cr | Li | Ni | Sr | Ti | V |
| 357-692 | 4-6.5 | 4-10 | 66-98 | 468-759 | 22-42 | 138-381 | 152-247 | 131-189 | 6.5-15 | 84-129 |
| **Parámetros físico-químicos** | | | | | | | | | | |
| pH | pe | T (ºC) | Conductividad (mS/cm) | | Oxígeno Dis. (mg/L) | | Oxígeno Dis. (%) | | | |
| 2,35-2,96 | 9,4-10,1 | 16,8-22,2 | 3,24-6,12 | | 1,8-2,5 | | 13-28 | | | |

Los datos mostrados corresponden con los valores mínimos y máximos obtenidos tras 42 campañas de muestreo desde marzo de 2007 hasta octubre de 2008

## 4.2 Evolución temporal en el funcionamiento y retirada metálica del sistema de tratamiento

A lo largo de la mayor parte del primer año de funcionamiento el comportamiento hidroquímico del sistema fue bastante estable. Sin embargo, tras este período algunos pequeños cambios fueron observados en el tanque reactivo y encadenadamente en el decantador. Así pudo observarse un pequeño descenso en el pH del agua a la salida del tanque reactivo durante los últimos 8 meses de funcionamiento (Fig. 4.2). Este descenso progresivo del pH de 6 a 5,1 ocurrido desde marzo de 2008 a octubre de 2008 tuvo asociado una bajada de los valores de alcalinidad en el agua desde 200 mg/L como $CaCO_3$ equivalentes hasta casi 0. De manera complementaria y asociada a este efecto doble se produjo un descenso de los valores de pH observados a la salida del decantador.

Al, Cu y Cd, durante el primer año de funcionamiento, fueron retirados completamente de las aguas tras fluir por el interior del tanque reactivo. Estos elementos tan sólo mostraron un leve descenso en su retirada durante los últimos meses de funcionamiento (Fig. 4.2). De estos tres elementos fue Al el menos sensible a los cambios observados en el pH y tan sólo cuando el pH se aproximó a 5 mostró un pequeño descenso en su retirada (Fig. 4.2). Esta observación está en concordancia con el pH de 5 propuesto para

la precipitación de hidrobasaluminita ($Al_4(SO_4)(OH)_{10}•15H_2O$) en AMD (Bigham y Nordstrom, 2000). El efecto más pronunciado que el descenso de pH tiene en la retirada relativa de Cu y Cd concuerda con la hipótesis de una adsorción dependiente del pH como proceso más probable en la retirada de ambos metales (Caraballo et al., 2009a). La retirada relativa de Fe durante la gran mayoría del funcionamiento del tratamiento varía entre un 20% y un 40%, no viéndose claramente afectada por los descensos de pH y alcalinidad durante la última etapa del tratamiento (Fig. 4.2). Para As, Cr, Ti y V se observa una total retirada durante todo el período de funcionamiento. La retira de As conjuntamente con Fe ha sido expuesta con anterioridad en sistemas de tratamiento pasivo tipo DAS calizo (Caraballo et al., 2009a) así como en otros ambientes naturales afectados por AMD (Acero et al., 2006; Asta et al., 2009).

De manera inesperada pudo observarse a la salida del tanque reactivo durante los primeros meses de funcionamiento valores de pe muy bajos, oscilando entre 1,5 y 3, seguidos por una intensa subida de pe hacia el final de la experiencia (Fig. 4.2). Complementariamente se observó una elevada retirada relativa para Zn, Co y Ni durante los 6 primeros meses de funcionamiento. Tras varios meses, la importante retirada inicial alcanzada para estos elementos comenzó a disminuir progresivamente hasta alcanzar una retirada relativa negativa que está claramente relaciona con el incremento experimentado por los valores de pe (Fig. 4.2).

La presencia de materia orgánica (virutas de madera) en el material reactivo así como los dos meses que éste permaneció inundado, previo a la inauguración del tratamiento, pudo haber facilitado el crecimiento de bacterias sulfatoreductoras en su interior. Esto ofrecería una posible explicación a la importante retirada de Zn, Co y Ni que se observó durante los primeros meses de funcionamiento.

Como se observa en la Tabla 4.2, el principal metal retirado durante el tratamiento es el Fe con más de 7 toneladas, seguido del Al con casi 3 y el Cu y Zn con 0,3 y 0,1 toneladas respectivamente. Otro importante elemento retirado del agua es el $SO_4^{=}$ con una cantidad estimada de 6,9 toneladas. En lo que respecta a los elementos minoritarios en las aguas se obtuvo una retirada de 9,5 kg de As, seguido de V, Ni, Cd, Co, Cr, y Ti (Tabla 4.2).

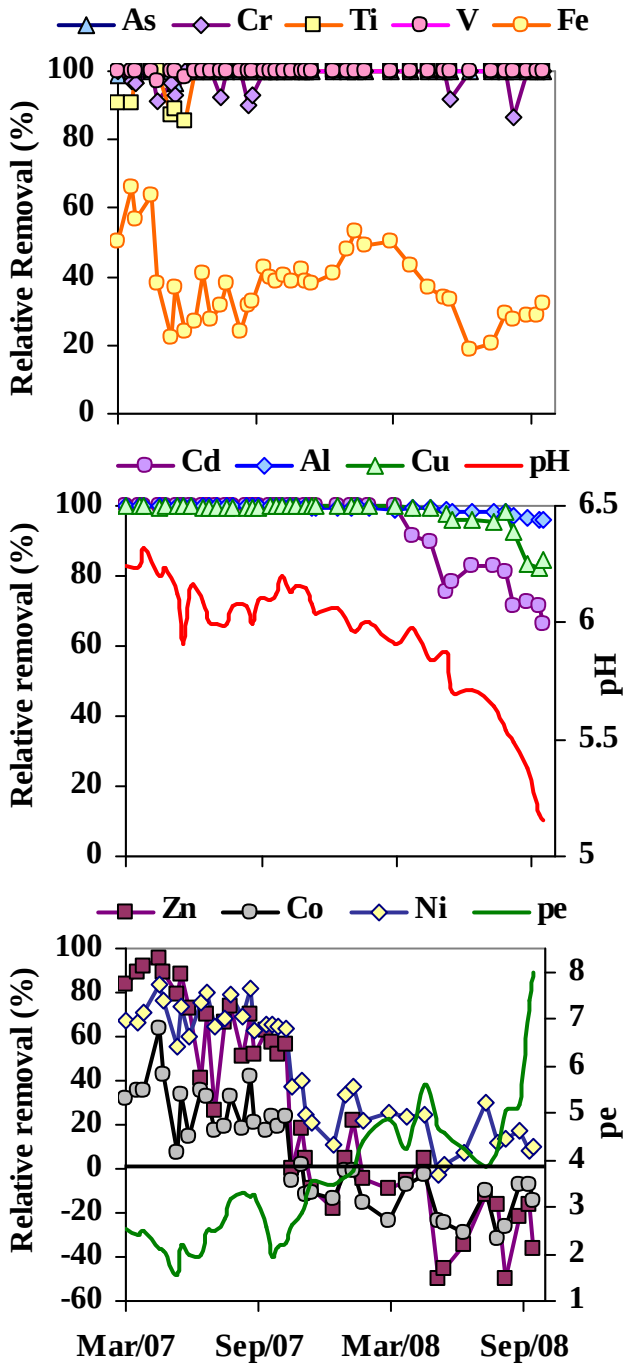


**Figura A1.7. Evolución temporal de la retirada relativa (Relative removal (%)) alcanzada por el sistema desde la bocamina hasta la salida del decantador. Los valores de pH y pe son ofrecidos para comparar los efectos que producen en la retirada de ciertos metales.**

**TABLE A1.5.** Retirada metálica total en el sistema de tratamiento tras 20 meses de funcionamiento.

| **Al (tm)** | **Ca (tm)** | **Cu (tm)** | **Fe (tm)** | **$SO_2$ (tm)** | **Si (tm)** | **Zn (tm)** |
|---|---|---|---|---|---|---|
| 2,7 | -10,5 | 0,3 | 7,1 | 6,9 | 0,6 | 0,1 |
| **As (kg)** | **Cd (kg)** | **Co (kg)** | **Cr (kg)** | **Ni (kg)** | **Ti (kg)** | **V (kg)** |
| 9,5 | 1,4 | 1 | 0,6 | 1,6 | 0,2 | 1,8 |

## 4.2 Eficiencia del tratamiento

Con el fin de obtener una mejor comprensión tanto de la altísima contaminación a la que se ve sometido el sistema de tratamiento de Mina Esperanza como de la magnitud alcanzada en la descontaminación de la misma, se decidió comparar los datos de este estudio con otros pertenecientes a mas de 83 sistemas de tratamientos pasivos comúnmente empleados en USA (Ziemkiewicz et al., 2003).

La acidez neta a la entrada (inflow net acidity) de cada sistema fue calculada para obtener una estimación de la contaminación a la que cada tratamiento se ve sometido. Como se muestra en la parte superior de la figura 4.3, la acidez neta en la bocamina de Mina Esperanza alcanza un valor medio de 2.300 mg/l como $CaCO_3$ equivalentes. Se observa como la acidez neta de entrada en Mina Esperanza es típicamente un orden de magnitud superior a la mostrada por la gran mayoría de sistemas comparados (Fig. 4.3).

A fin de comparar la capacidad de eliminación de contaminantes de los diferentes tratamientos se utilizó la retirada de acidez neta (net acidity removal), ya que este parámetro ofrece una buena aproximación a la capacidad de neutralización de cada sistema así como a la cantidad de metales retirada. La acidez neta retirada se calculó substrayendo la acidez neta en la salida del sistema a la acidez neta a la entrada. La media de la acidez neta retirada en Mina Esperanza se muestra 5 veces superior que el mismo valor calculado para los VFW (vertical flow wetlands) o los ALD (anoxic limestone drains), más de 15 veces mayor que los valores obtenidos en los AnW (anoxic wetlands) y hasta 43 veces superior que los valores mostrados por los LSB (limestone leach beds) (Fig. 4.3). También puede observarse como el tercer cuartil para Mina Esperanza es significativamente amplio, lo cual marca como los cambios en la acidez neta retirada se desplazan típicamente en este sentido, acercándose a valores de 2.000 mg/L como $CaCO_3$ equivalentes.

La reducción de carga ácida (acid load reduction) en $g•(m^2•día)^{-1}$ es un parámetro comúnmente empleado para caracterizar la eficiencia en la retirada metálica superficial de un sistema de tratamiento pasivo, pudiendo ser utilizado para obtener una idea bastante precisa del requerimiento de terreno que tiene cada concepto de tratamiento pasivo. Comparando los valores medios obtenidos para los AnW y los VFW con los de Mina Esperanza puede observarse como la retirada alcanzada en Mina Esperanza (597 $g•(m^2•día)^{-1}$) es 32 veces superior a lo obtenido para los AnW y hasta 47 veces mayor que los valores ofrecidos por los VFW (Fig. 4.4). Esta observación tiene una gran relevancia a la hora de decidir un método de descontaminación para una región determinada ya que los requerimientos de terreno pueden presentar un gran problema

para la viabilidad de un proyecto. A modo de comparación se podría decir que para que un sistema de tratamiento alcanzase la misma eficiencia por superficie que Mina Esperanza (con un área de 120 $m^2$) necesitaría una extensión de más de 3.600 $m^2$ en el mejor de los casos y hasta 5.600 $m^2$ en el peor de los casos.

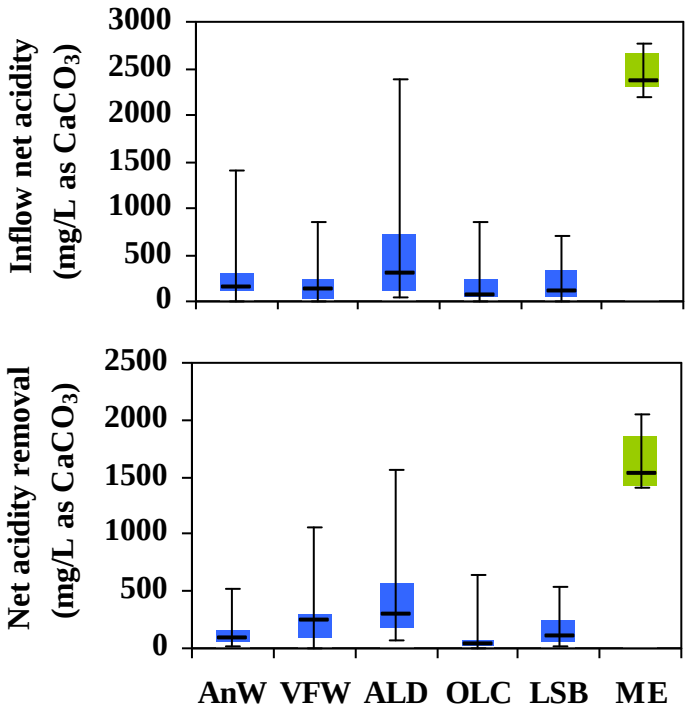


**Figura A1.8. Diagrama de cajas comparando los valores de acidez neta a la entrada (inflow net acidity) y la acidez neta retirada (net acidity removal) en Mina Esperanza y más de 80 sistemas de tratamiento pasivo convencionales en USA. AnW = anaerobic wetland, VFW = vertical flow wetland, ALD = anoxic limestone drains, OLC = opened limestone channels, LSB = limestone leach beds y ME = Mina Esperanza.**

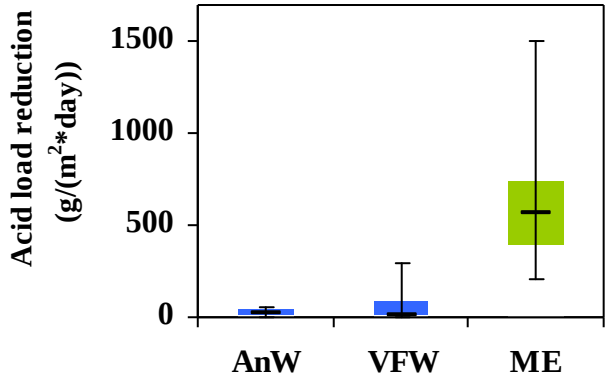


**Figura A1.9. Diagrama de cajas para la reducción de carga ácida (acid load reduction). AnW = anaerobic wetland, VFW = vertical flow wetland y ME = Mina Esperanza.**

# RESUMEN CAPÍTULO 5. FUNCIONAMIENTO HIDROQUÍMICO Y EVOLUCIÓN MINERALÓGICA DE UN SUBSTRATO ALCALINO DISPERSO (DAS) USADO PARA LA DESCONTAMINACIÓN DE AMD EN EL SISTEMA DE TRATAMIENTO PASIVO DE MINA ESPERANZA (SO, ESPAÑA)

Los estudios concernientes a sistemas de tratamiento pasivos suelen estar enfocados al control de la calidad del agua a la salida del sistema, obviando el importante papel desempeñado por los precipitados minerales en la hidroquímica del AMD y en el funcionamiento del propio tratamiento. De manera especial, Fe y Al tienen una gran importancia al tamponar el pH del AMD (Bigham and Nordstrom, 2000), inducir la inactivación del material reactivo (Caraballo et al., 2009b), reducir la conductividad hidráulica del material reactivo (Rötting et al., 2008b) y eliminar otros metales tóxicos por coprecipitación o adsorción (Caraballo et al., 2009a).

Este trabajo presenta la información mineralógica obtenida en el sistema de tratamiento pasivo tipo DAS calizo de Mina Esperanza tras 20 meses de funcionamiento. Este es el primer ensayo a escala real que se realiza con sistemas de descontaminación DAS calizo. En base al papel tenido por los precipitados en la inactivación y consumo de caliza, en la conductividad hidráulica del material reactivo y en la eficiencia en la retirada metálica, se discutirán ciertas mejoras a incluir en el diseño original del tratamiento.

## 5.1 Control mineralógico sobre el funcionamiento del material reactivo y su retirada de metales

Toda la información obtenida en la caracterización mineralógica de los diferentes precipitados se presenta en función de tres subsecciones correspondientes a las zonas de precipitación de Fe, Al y Zn.

### *5.1.1 Zona de precipitación de Fe*

La influencia de la zona de precipitación de Fe queda restringida a los primeros 50 cm del material reactivo (Fig. 5.1).

Un primer acercamiento mediante XRD a la mineralogía de los precipitados (Tabla 5.1) muestra la presencia de schwertmannita como la única fase mineral de Fe en 0-5 cm de profundidad, seguida de schwertmannita más goethita en 5-15 cm y tan sólo goethita en

15-20 cm de profundidad. No se detectó ninguna fase mineral en las muestras a 20-35 y 35-50 cm de profundidad (Tabla 5.1).

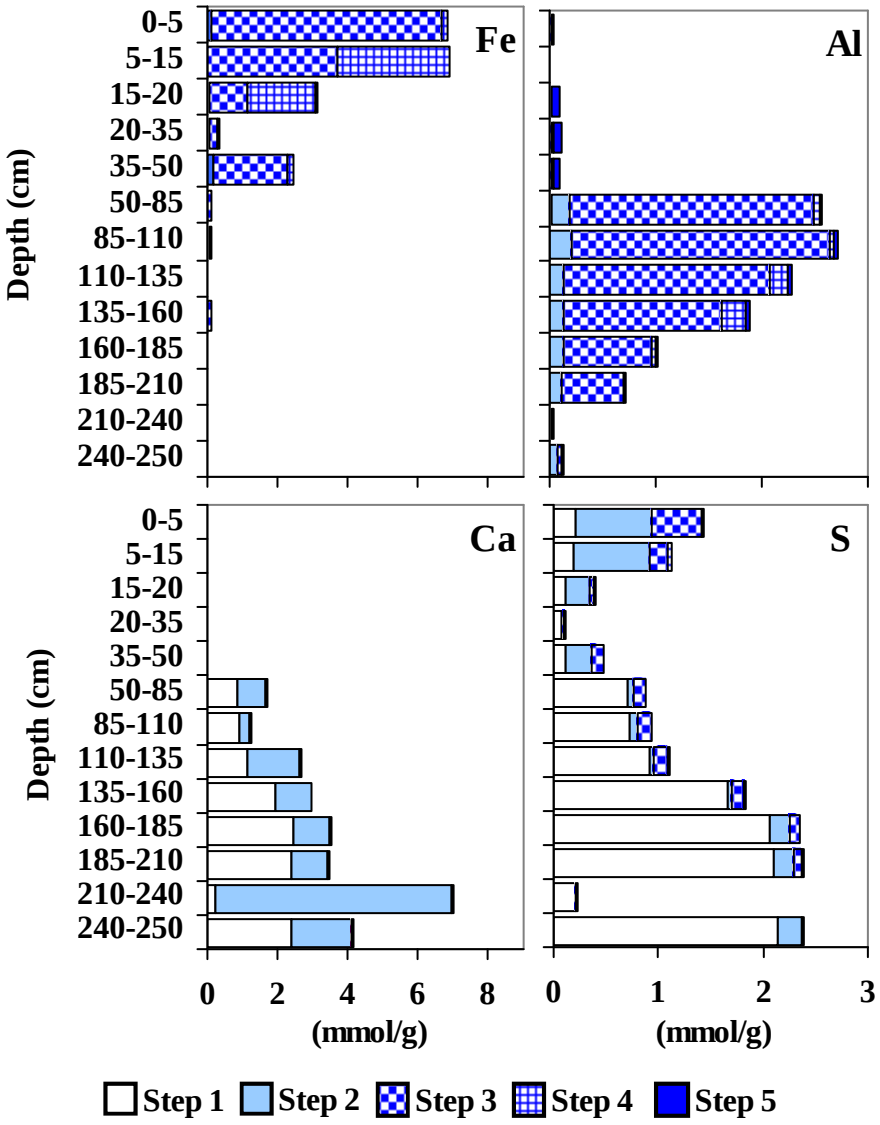


**Figura A1.10. Gráfico acumulado para la concentración de los principales constituyentes (Fe, Al, Ca y S) obtenidos tras cada paso de la extracción secuencial para las distintas muestras sólidas estudiadas.**

Los resultados obtenidos tras la extracción secuencial a la que fueron sometidas estas muestras (Fig. 5.1) corroboran lo observado mediante XRD. La presencia de schwertmannita en las muestras viene marcada por la cantidad de Fe recuperada en el tercer paso de la extracción secuencial, mientras que el Fe liberado en el cuarto paso es el correspondiente a la disolución selectiva de goethita. La muestra a 20-35 cm de profundidad corresponde a un nivel donde no ocurrió ninguna precipitación mineral tan sólo observándose virutas de madera. Aunque no se detectó ninguna fase mineral por

XRD en la muestra a 35-50 cm, la importante cantidad de Fe recuperada en el tercer paso de la extracción secuencial puede ser atribuida a la presencia de schwertmannita. La obtención de una cantidad significativa de S en los pasos 2 y 3 en las muestras anteriores es atribuida al $SO_4^{=}$ adsorbido y estructural presente en schwertmannita (Fig. 5.1). La ausencia de Ca en el paso 2 de la extracción confirma la completa disolución de caliza a lo largo de la zona de precipitación de Fe e igualmente corrobora la eficiencia en el consumo de caliza antes de que los granos puedan ser inactivados por los precipitados.

**TABLA A1.6**. Fases minerales confirmadas con XRD

| **Profundidad (cm)** | **Schwertmannita** | **Goethita** | **Yeso** | **Calcita** |
|---|---|---|---|---|
| 0-5 | X | - | - | - |
| 5-15 | X | X | - | - |
| 15-20 | - | X | - | - |
| 20-35 | - | - | - | - |
| 35-50 | - | - | - | - |
| 50-85 | - | - | X | X |
| 85-110 | - | - | X | X |
| 110-130 | - | - | X | X |
| 130-150 | - | - | X | X |
| 150-165 | - | - | X | X |
| 165-180 | - | - | X | X |
| 180-215 | - | - | X | X |
| 215-220 | - | - | X | X |

Para obtener una caracterización más detallada de schwertmannita (el principal constituyente de la zona de precipitación de Fe y precursor de goethita) la composición y morfología de este mineral en la muestra a 0-5 cm fue investigada mediante el uso de microsonda de electrones (EPMA).

Este estudio reveló la típica morfología en “erizo de mar” generalmente atribuida a este mineral, la cual aparecía reflejada en forma de esferas de entre 1 y 10 µm de diámetro (Fig. 5.2).

Table A1.7 Análisis con EMPA para 6 muestras seleccionadas del interior del tanque reactivo. Se muestran valores medios (wt %) y desviaciones estandar de 30 análisis realizados en cada muestra.

| **Profundidad (cm)** | **$Al_2O_3$** | **CaO** | **CuO** | **CoO** | **FeO** | **$SO_3$** | **$SiO_2$** | **NiO** | **ZnO** | **$Fe/S_{molar}$** | **$Al/S_{molar}$** |
|---|---|---|---|---|---|---|---|---|---|---|---|
| | (0.02) | (0.02) | (0.05) | (0.08) | (0.05) | (0.03) | (0.03) | (0.08) | (0.08) | | |
| 0-5 | 0.12 ± 0.03 | 0.09 ± 0.07 | n.d. | n.d. | 56.70 ± 1.18 | 13.58 ± 0.17 | 0.30 ± 0.07 | n.d. | n.d. | 4.66 ± 0.07 | - |
| 85-110 | 40.10 ± 1.24 | 0.13 ± 0.05 | 0.85 ± 0.33 | n.d. | 0.15 ± 0.05 | 18.69 ± 0.77 | 2.10 ± 0.41 | n.d. | b.d | - | 3.37 ± 0.1 |
| 135-160 | 43.15 ± 1.48 | 0.93 ± 0.60 | 1.89 ± 1.30 | n.d. | 0.33 ± 0.12 | 13.99 ± 2.18 | 1.33 ± 0.21 | n.d. | 0.17 ± 0.14 | - | 4.96 ± 0.8 |
| 160-185 | 57.82 ± 3.81 | 0.04 ± 0.02 | 0.97 ± 0.31 | n.d. | 0.34 ± 0.07 | 20.65 ± 0.45 | 0.80 ± 0.28 | n.d. | b.d. | - | 4.40 ± 0.2 |
| 185-210 | 46.48 ± 3.01 | 0.67 ± 0.51 | 0.53 ± 0.41 | n.d. | 0.15 ± 0.07 | 16.02 ± 1.77 | 0.91 ± 0.14 | n.d. | 0.50 ± 0.39 | - | 4.62 ± 0.6 |
| 240-250 | 3.89 ± 2.54 | 1.83 ± 0.54 | 0.22 ± 0.14 | 0.37 ± 0.11 | 48.37 ± 3.72 | 9.52 ± 2.13 | 1.68 ± 0.31 | 0.37 ± 0.20 | 12.08 ± 2.58 | - | - |

Los límites de detección están indicados bajo cada elemento analizado. b.d. = por debajo del límite de detección, n.d. = no detectado.

La composición química general de este mineral viene reflejada en la Tabla 5.2., donde puede observarse como Fe y S son los componentes principales de esta fase mineral. También se detecta una pequeña cantidad de Al, Ca y Si. En base a estos análisis se calcula la fórmula estequiométrica de la schwertmannita generada en Mina Esperanza, obteniéndose $Fe_8O_8(OH)_{4,56}(SO_4)_{1,72}$:$nH_2O$. La razón molar Fe/S es de 4,66 ± 0,07, lo cual corresponde con los valores inferiores obtenidos para este mineral por otros autores (Bigham and Nordstrom, 2000).

### *5.1.2 Zona de precipitación de Al*

Los precipitados de Al se distribuyen desde 50 a 180 cm de profundidad mostrando una tendencia decreciente en la cantidad de precipitados hacia la parte inferior del material reactivo (Fig. 5.1). La difracción de las 6 muestras a estas profundidades (Tabla 5.1) tan sólo confirma la presencia de yeso y calcita pero no muestra ninguna evidencia de ninguna fase mineral de Al. Sin embargo, la presencia de hidrobasaluminita pudo ser confirmada por XRD usando el material particulado arrastrado por el agua hasta la salida del tanque reactivo. La disolución de los precipitados de Al tuvo lugar principalmente durante el tercer paso de la extracción secuencial donde el extractante empleado (0,2 M $NH_4$-oxalato) está tamponado a pH 3. Una pequeña cantidad de Al se recupera en el paso 2 (1 M $NH_4$-acetato tamponado a pH 4,5) y en el paso 4 (0,2 M $NH_4$-oxalato a pH 3 y 80 ºC) los cuales pueden ser atribuidos a la disolución incipiente de precipitados de Al a pH 4,5 y a la disolución de alguna fase de Al minoritaria pero más resistente (Fig. 5.1). Acoplada a la disolución de los precipitados de Al se observa en el paso 2 y 3 una pequeña liberación de S. Los precipitados de Al típicamente aparecen cubriendo los granos de caliza y la viruta de madera (Fig. 5.2B). La composición química de estos precipitados viene ofrecida en la Tabla 5.2 donde el Al y el S son observados como componentes principales. La aparición de cantidades menores de elementos como Ca, Cu, Fe y Si fue detectada de manera generalizada. La relación molar Al/S (de 3,37 a 4,96) observada en las cuatro muestras estudiadas oscila de forma cercana la razón teórica de 4 mostrada por basaluminita, $Al_4(SO_4)(OH)_{10}•5H_2O$, o su precursor hidrobasaluminita, $Al_4(SO_4)(OH)_{10}•12\text{-}36H_2O$. La razón Al/S observada y la detección de basaluminita por XRD como única fase mineral de Al observada a la salida del tanque reactivo confirman a este mineral y a su precursor hidrobasaluminita como la fase de Al principal controlando la precipitación de Al en el interior del tanque reactivo. No obstante la presencia de cantidades menores de otros precipitados de Al pobremente cristalinos o amorfos no puede ser completamente descartada.

La precipitación de yeso (a partir de las cantidades equimolares de Ca y S liberadas en el paso 1, Fig. 5.1) de manera conjunta con la precipitación de Al muestran una tendencia inversa (incrementando con la profundidad). La liberación de Ca en el segundo paso de la extracción secuencial puede ser atribuida a la disolución selectiva de calcita. La presencia de este mineral y de yeso fue confirmada por XRD en todas las muestras desde 50 hasta 220 cm de profundidad (Tabla 5.1).

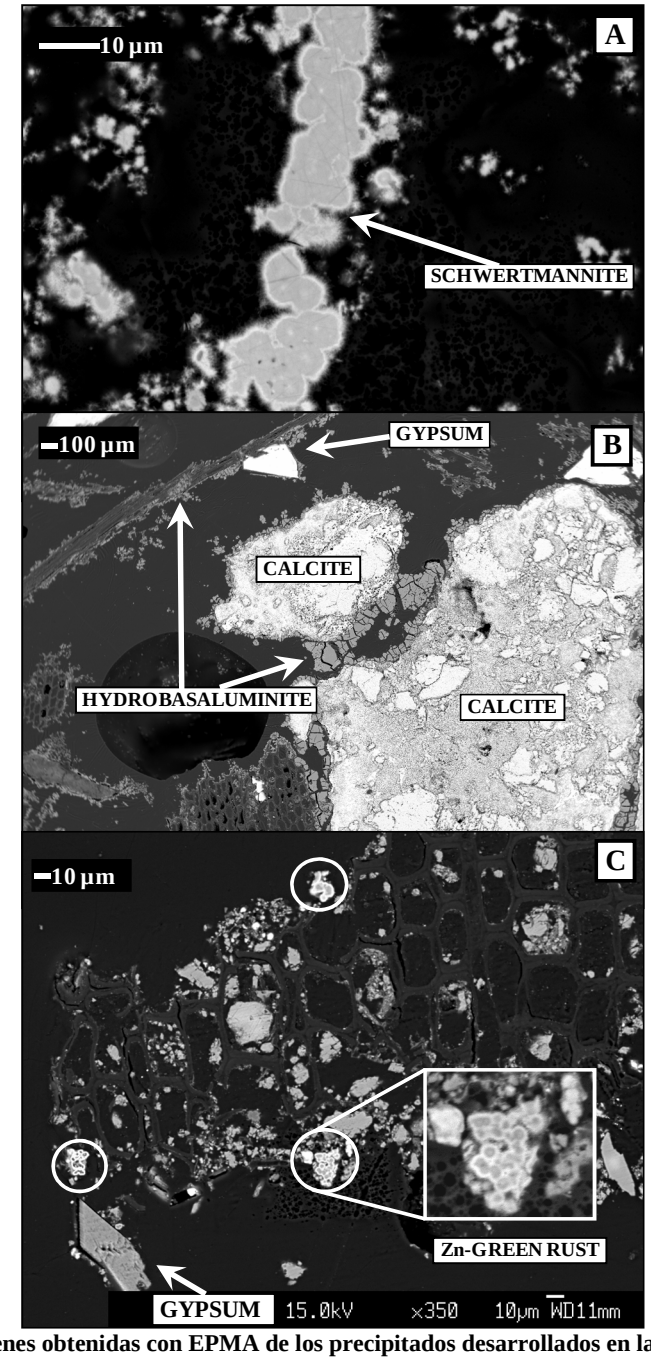


**Figura A1.11. Imágenes obtenidas con EPMA de los precipitados desarrollados en las diferentes zonas del material reactivo, desde el fondo hacia la superficie: A) zona de Fe; B) zona de Al y C) zona de Zn.**

La muestra tomada a 180-215 cm corresponde a una sección de material sin reaccionar con pequeñas cantidades de yeso como mineral neoformado.

### *5.1.3 Zona de precipitación de Zn*

Metales divalentes como Zn, Ni y Co precipitan de manera selectiva en la sección más profunda del material reactivo (Fig. 5.3). Estos tres metales son liberados eminentemente durante el segundo paso de la extracción secuencial, mostrando sus concentraciones máximas en la muestra a 240-250 cm de profundidad. La liberación selectiva de estos metales en el segundo paso de la extracción secuencial descarta la posibilidad de ningún tipo de sulfuro como fase mineral albergando estos metales. El estudio morfológico y químico realizado con EPMA de estos precipitados muestra la formación de micro esferas de 1-2 µm de diámetro (Fig. 5.2). La composición química obtenida (Tabla 5.2) muestra como Fe, Zn y S con los componentes principales de estos precipitados. Al, Ca y Si fueron detectados de manera significativa pero en bastante menor cantidad mientras que Cu, Co y Ni aparecen de forma minoritaria en los precipitados.

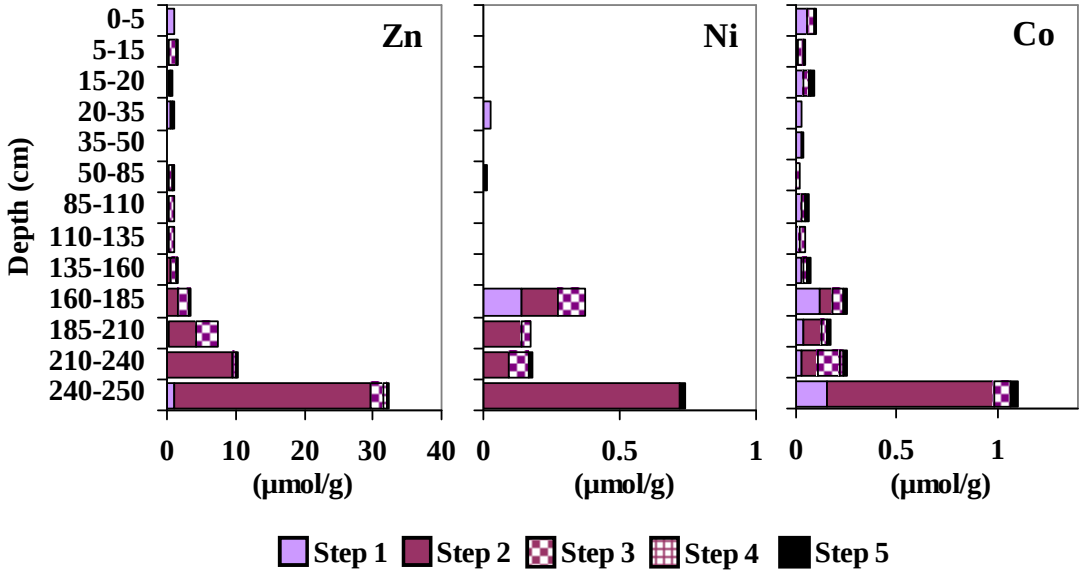


**Figura A1.12. Concentración acumulada para Zn, Ni y Co tras cada uno de los pasos de la extracción secuencial.**

Estudios previos han descrito la aparición de minerales de Fe(II)-Fe(III) tipo "green rust" en suelos reductomórficos (Bourrié et al., 1999; Feder et al., 2005; Trolard, 2006) . Estos suelos están caracterizados por un exceso de agua, una restricción en las fuentes de oxígeno, la presencia de sustratos biodisponibles y la existencia de elementos capaces de cambiar su estado de oxidación (Trolard, 2006). Todas las características

citadas se encuentran igualmente en la zona más profunda del material reactivo empleado en el tanque reactivo del sistema de tratamiento de Mina Esperanza. Los compuestos tipo "green rust" presentan la formula química normalizada $[Fe^{II}_{1-x}Fe^{III}_{x}(OH)_2]^{x+}$ $[(x/n)A^{n-}\cdot(mx/n)H_2O]^{x-}$, donde láminas de hidróxidos cargadas positivamente $[Fe^{II}_{1-x}Fe^{III}_{x}(OH)_2]^{x+}$ alternan con cationes interláminas con cargas negativas $A^{n-}$ ($CO_3^{2-}$, $SO_4^{2-}$, $Cl^-$, …) y con *m* moléculas de agua por anión. También se han reportado sustituciones catiónicas en muestras sintéticas donde $Fe^{2+}$ es sustituido por una importante cantidad de $Zn^{2+}$ (Zhang et al., 2007). La presencia de minerales de tipo "green rust" en ambientes de AMD pero en condiciones reductoras ha sido propuesta desde el punto de vista termodinámico (Majzlan et al., 2004) e igualmente observado de manera directa en sistemas de tratamiento pasivo que usan hierro zerovalente (Bartzas and Komnitsas, 2010; Lien and Wilkin, 2005).

En base al ambiente hidroquímico observado y a la composición química de los precipitados, se propone "green rust" sulfatado con una importante sustitución de Zn como la fase mineral más probable que controla la retirada de Zn, Co y Ni en la parte inferior del material reactivo.

### 5.1 Conductividad hidráulica del material reactivo

Los problemas de atasco debido a la neoformación de fases minerales en el espacio de poro del material reactivo y la consiguiente pérdida de conductividad hidráulica es una de las mayores dificultades a las que se ha de enfrentar un sistema de tratamiento pasivo de AMD a lo largo de su funcionamiento. El diseño desarrollado en Mina Esperanza usa un material reactivo con elevada porosidad así como 1 m de pared libre en el tanque reactivo para compensar el incremento en el agua del sobrenadante resultante de la precipitación metálica en el espacio de poro del material reactivo. La efectividad de este diseño queda reflejada en el elevado flujo, oscilando entre 43 y 86 $m^3$/día, alcanzado durante los 20 meses de funcionamiento.

Para alcanzar una mejor compresión del comportamiento del material reactivo frente a los problemas de atasco se calculó la evolución temporal de la conductividad hidráulica. Los resultados se ajustan bastante bien a una curva de regresión exponencial durante el primer año de funcionamiento, evolucionando de una conductividad hidráulica inicial de 6 m/día hasta valores en torno a 1m/día (Fig. 5.4).

Con posterioridad, la conductividad hidráulica se mantuvo estable alrededor de 1 m/día durante los últimos 8 meses de funcionamiento del sistema. Aunque la evolución real de la conductividad hidráulica de un sustrato tipo DAS calizo sometido a un mayor tiempo

de funcionamiento tan sólo puede ser conocida con certeza tras el estudio de un nuevo experimento con mayor duración, la tendencia mostrada por este parámetro durante los 20 meses de funcionamiento del tratamiento en Mina Esperanza sugiere la obtención de mayores tiempos de funcionamiento como una posibilidad esperanzadora.

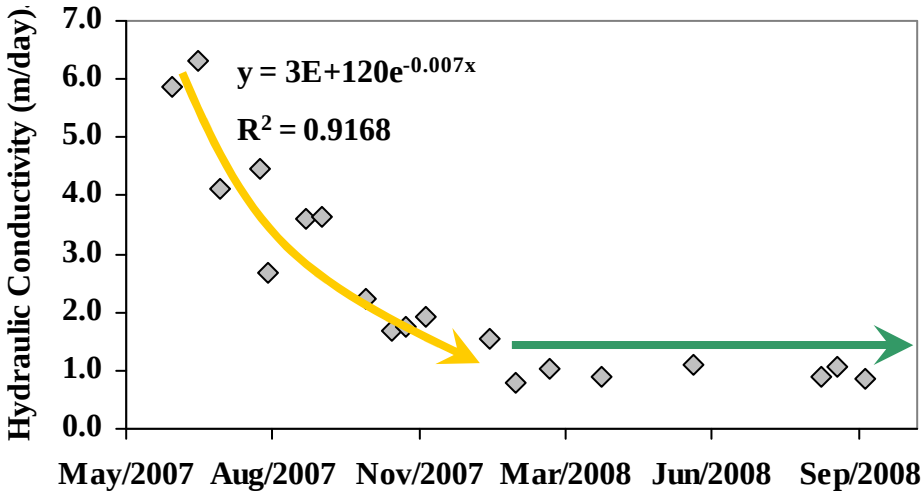


**Figura A1.13. Evolución temporal de la conductividad hidráulica del material reactivo.**

## RESUMEN CAPÍTULO 6. CONCLUSIONES

La **primera parte** de esta tesis discute la aplicabilidad de un procedimiento específico de extracciones secuenciales y DXRD para la caracterización mineralógica de precipitados de AMD, principalmente óxidos y sulfatos pobremente cristalinos de hierro y aluminio. En el estudio realizado en esta sección **(Capítulo 2)** se corroboró la aplicabilidad de estas técnicas acopladas. El uso satisfactorio de la extracción secuencial en muestras con elevada concentración de óxidos y oxihidróxidos de Fe sólo fue alcanzada tras incluir ciertas mejoras en la relación muestra-extractante y en el tiempo y naturaleza del contacto. Como resultado, se obtuvo un procedimiento de extracción secuencial modificado especialmente diseñado para el estudio de precipitados de AMD.

La alta especificidad observada en la disolución selectiva de schwertmannita y goethita en los pasos 3 y 4 de la extracción secuencial permite una estimación cuantitativa de la cantidad de cada mineral presente en el material reactivo. Se observó como aunque la masa de goethita (wt%) en las muestras es considerablemente mayor que la de schwertmannita, ésta última es la fase mineral responsable de la mayor retirada de Fe (debido al mayor contenido de Fe en la estructura de schwertmannita). La detección de schwertmannita anterior al uso de DXRD fue imposible debido tanto a la baja

cristalinidad como a la baja concentración de este mineral en las muestras. Otro resultado importante observado en la extracción secuencial de los niveles de Fe fue el progresivo descenso del $SO_4^{=}$ adsorbido en schwertmannita con la profundidad. Este efecto fue atribuido a la ocupación parcial de los lugares de adsorción mediante $OH^-$ en lugar de $SO_4^{=}$ como resultado del pequeño incremento de pH sufrido por el AMD tras la disolución incipiente de caliza en los primeros centímetros del material reactivo. Las razones molares Fe/S obtenidas para las muestras de schwertmannita a 0-1 cm, 1-3 cm y 3-5 cm son 4,44, 4,15 y 9,33, respectivamente. Estos resultados extienden el límite superior del rango Fe/S aceptado para schwertmannita desde cerca de 8 a 9,33.

Respecto al horizonte de Al se observó un descenso paulatino (desde la superficie hacia el fondo) en el contenido de Al en los precipitados. Fue imposible detectar ninguna fase de Al mediante las técnicas analíticas empleadas, aunque la presencia de hidrobasaluminita y $Al(OH)_3$ amorfo es sugerida en base a los datos mostrados por la extracción secuencial y el modelo termodinámico.

El uso conjunto de la XRD y de la extracción secuencial permitió identificar y cuantificar la presencia de yeso y calcita en el interior del material reactivo. Se observó como la concentración de yeso incrementa a través del horizonte de hierro hasta alcanzar su máximo en el límite entre este horizonte y el de Al, para posteriormente decrecer a lo largo del horizonte de Al. Casi toda la caliza se consumió en el horizonte de Fe (0-5 cm) mientras que una cantidad considerable de caliza permaneció sin consumirse en el horizonte de Al. La caliza sobrante sufrió un importante proceso de inactivación por recubrimiento de su superficie con yeso y precipitados de Al.

La **segunda parte** de esta tesis aborda el diseño, implementación y funcionamiento del sistema de tratamiento pasivo de campo basado en el uso de DAS calizo y DAS magnésico de Monte Romero. La investigación llevada a cabo en esta sección **(Capítulo 3)** proporciona un estudio detallado de dicho sistema de tratamiento pasivo.

El sistema fue capaz de retirar una acidez neta de alrededor de 2.000 mg/L como $CaCO_3$ equivalentes implicando un descenso en el agua de entrada desde 2.500 hasta 500 mg/L como $CaCO_3$ equivalentes. Esta acidez neta eliminada se corresponde con una retirada relativa cercana al 100% para Al y Cu, superior al 70% para Fe y casi del 25% para Zn, como elementos mayoritarios. La retirada relativa para los elementos minoritarios fue del 100% para As y Pb y superior al 95% para Cr.

El funcionamiento de las diferentes secciones que comprenden el sistema de tratamiento pasivo mostraron una eficiencia en la retirada metálica similar mediante el uso de un

12,5% o un 20% (v/v) de caliza en el material reactivo en T1 y T2 respectivamente. Sin embargo, pudo observarse una disminución en la reactividad de T1 hacia el final del experimento. Este efecto se atribuye al progreso más rápido del frente de precipitación de Al a través de T1. El consumo de casi la totalidad del material reactivo presente en el tanque con DAS magnésico muestra como el tamaño de grano seleccionado consigue una optima disolución antes de que aparezca ningún efecto de inactivación del sustrato. No obstante, una mayor proporción de MgO en el material reactivo se necesitaría para extender el tiempo de funcionamiento de T3.

El material reactivo tipo DAS magnésico mostró por primera vez en un ensayo de campo usando AMD real una completa retirada de metales divalentes tales como Fe(II), Zn, Cd, Co y Ni.

La precipitación directa de goethita pudo observarse en la zona superior del material reactivo de T2 y T3 donde se alcanzaron rápidamente elevados valores de pH. El horizonte de Al se desarrollo tanto en T1 como en T2 aunque no pudo encontrarse ninguna fase mineral de Al cristalina. Finalmente, tan sólo T3 presentó un horizonte de precipitación de Zn. Fases minerales complejas como schulenbergita rica en Zn, $(Cu,Zn)_7(SO_4)_2(OH)_{10}\cdot 3H_2O$, y en menor proporción sauconita, $Zn_3(Si,Al)_4O_{10}(OH)_2\cdot 4H_2O$, son propuestas como los minerales más probables responsables de la precipitación de Zn en T3.

La **tercera parte** de esta tesis está enfocada en la caracterización y control del sistema de tratamiento pasivo a escala real de Mina Esperanza a lo largo de sus 20 meses de funcionamiento.

La tercera investigación (**Capítulo 4**) llevada a cabo en esta tesis se centra en el estudio del funcionamiento hidroquímico, mineralógico y la retirada metálica de todo el sistema pasivo de Mina Esperanza.

La elevada porosidad y conductividad hidráulica mostrada por el material reactivo tipo DAS calizo permitió al sistema tratar un elevado caudal (oscilando entre los 43 y 86 $m^3$/día) durante 20 meses sin sufrir ningún problema serio de atasco. El diseño elegido para las cascadas conectando la bocamina con el tanque reactivo ofrece una superficie con un flujo lento que promueve el establecimiento de bacterias ferro-oxidantes y algas, las cuales aceleran significativamente el proceso de oxidación de hierro ferroso a hierro férrico, incrementando así la retirada de hierro en la superficie del tanque reactivo.

El hierro fue el principal metal retirado en el sistema, mostrando una retirada que osciló entre 170 y 620 mg/L en función de la eficiencia del sistema en cada momento. Se alcanzaron valores de retirada media tan elevados como 144 ± 9 mg/L de Al, 16 ± 6 mg/L de Cu, 40 ± 4 mg/L de Si, 490 ± 75 µg/L de As, 73 ± 9 µg/L de Cd, 28 ± 6 µg/L de Cr, 85 ± 50 µg/L de Ni, 10 ± 3 µg/L de Ti y 94 ± 18 µg/L de V.

Tanto la acidez neta de entrada como la acidez retirada en el sistema mostraron valores un orden de magnitud por encima de lo observado en una comparativa realizada con más de 80 sistemas de tratamientos pasivos convencionalmente usados en USA para tratar AMD. En lo que respecta a la retirada de carga de acidez, expresada en $g\cdot(m^2\cdot día)^{-1}$, se alcanzaron valores 10 veces superiores al valor comúnmente aceptado de 40 $g\cdot(m^2\cdot día)^{-1}$ usado como criterio de diseño para los sistemas de tratamiento pasivos.

Schwertmannita fue observada como la principal fase de Fe involucrada en la retirada de este elemento, aunque parte del hierro retirado fue tras la precipitación directa de goethita en la salida del tanque reactivo. La precipitación de Al por su parte tuvo lugar en el interior del tanque reactivo y sólo cuando el agua a la salida de éste alcanzó valores de pH cercanos a 5,5 pudo observarse la precipitación de hidrobasaluminita.

El cuarto estudio (**Capítulo 5**) de esta tesis está basado en el conocimiento de la evolución en la hidroquímica del agua y el funcionamiento hidráulico del material reactivo tipo DAS calizo empleado en el sistema de tratamiento pasivo de Mina Esperanza.

Tres horizontes de precipitación diferentes pudieron observarse en el interior del material reactivo, induciendo (desde la superficie a la base) una importante retirada de Fe, una eliminación total de Al y una apreciable retirada de Zn. La migración hacia el fondo del horizonte de Fe fuerza la redisolución de los precipitados de Al generados con anterioridad. La zona de precipitación de Zn fue inducida por la generación de un ambiente reductor en la base del material reactivo.

El perfil de precipitación de Fe entre 0 y 20 cm de profundidad evoluciona desde schwertmannita pura hasta una mezcla de schwertmannita y goethita en la parte más profunda. La relación molar Fe/S observada para schwertmannita en este estudio cae en los valores inferiores del rango de 4,6-8,3 propuesto por estudios anteriores, ofreciendo una estequiometría de $Fe_8O_8(OH)_{4.56}(SO_4)_{1.72}:nH_2O$.

Las relaciones molares de Al/S (desde 3,37 hasta 4,96) observadas en las cuatro muestras estudiadas están muy cercanas al valor teórico de 4 para basaluminita,

$Al_4(SO_4)(OH)_{10}\cdot 5H_2O$, siendo esta fase mineral la única que pudo ser detectada mediante XRD a la salida del tanque reactivo. Una tendencia decreciente de los precipitados de Al a lo largo del perfil también pudo ser observada.

En base a los distintos estudios mineralógicos que se llevaron a cabo, “green rust” sulfatado pobremente cristalino y con una importante sustitución de Fe por Zn es propuesta como fase mineral más plausible para la retirada de Zn, Ni y Co en el fondo del material reactivo.

En cuanto al funcionamiento del material reactivo se vio como la conductividad hidráulica inicial de aproximadamente 6 m/día disminuyó a valores cercanos a 1 m/día hacia el final del tratamiento, permaneciendo en estos valores durante los últimos 8 meses de funcionamiento. Estos datos sugieren que el sistema podría alargar su duración sin sufrir grandes problemas por perdida de conductividad hidráulica.

La completa disolución de caliza a lo largo del perfil de precipitación de Fe corrobora la elevada eficiencia en el consumo de caliza por parte del sistema previo a la aparición de ningún proceso de inactivación del sustrato reactivo. Sin embargo, la importante cantidad de caliza sin disolver presente desde 85 hasta 250 cm de profundidad fue debida a la precipitación de yeso e hidrobasaluminita en su superficie, aislándola del medio acuoso.

# APPENDIX 2. IMAGES OF MONTE ROMERO PILOT TREATMENT CONSTRUCTION AND SOLID SAMPLING


**Figure A2.1. Location of Monte Romero mine district.**

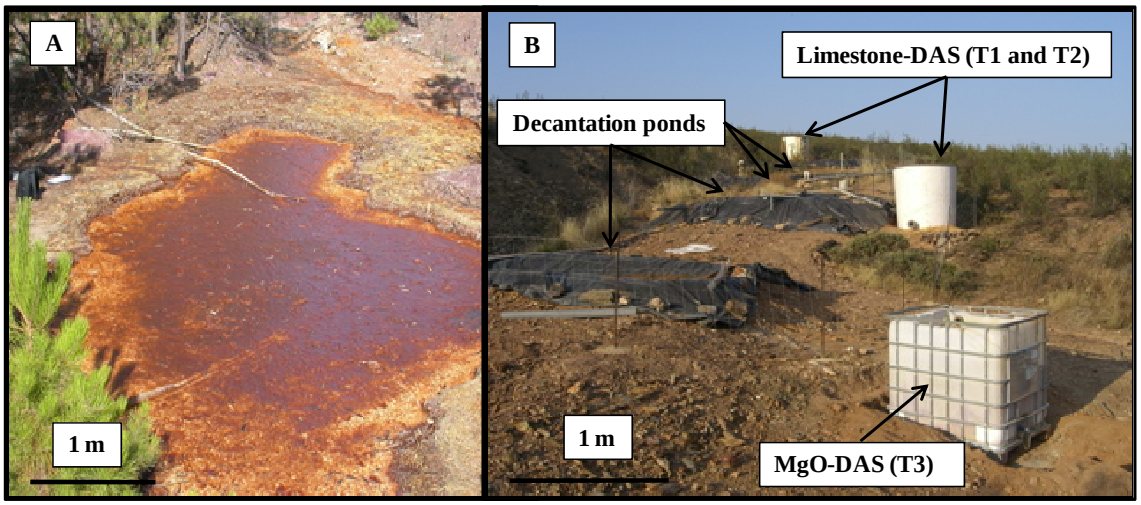


**Figure A2.2. A) Monte Romero mine shaft. B) Pilot scale passive treatment system.**

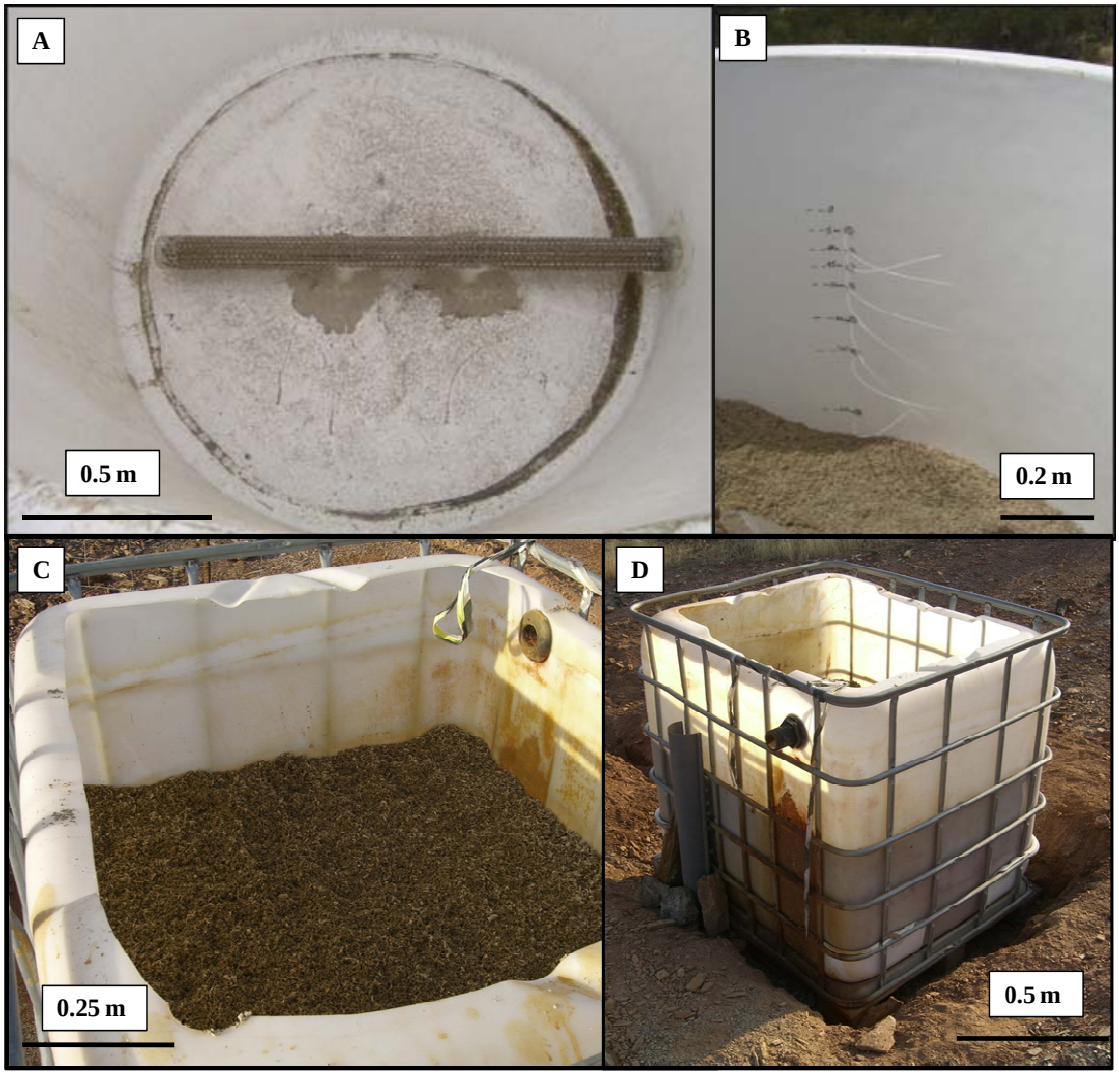


**Figure A2.3. A) Limestone-DAS reactive tanks inner section and perforated drain pipe. B) Limestone-DAS reactive mixture and lateral sampling ports. C) MgO-DAS reactive mixture. D) General view of MgO-DAS reactive tank, T3.**

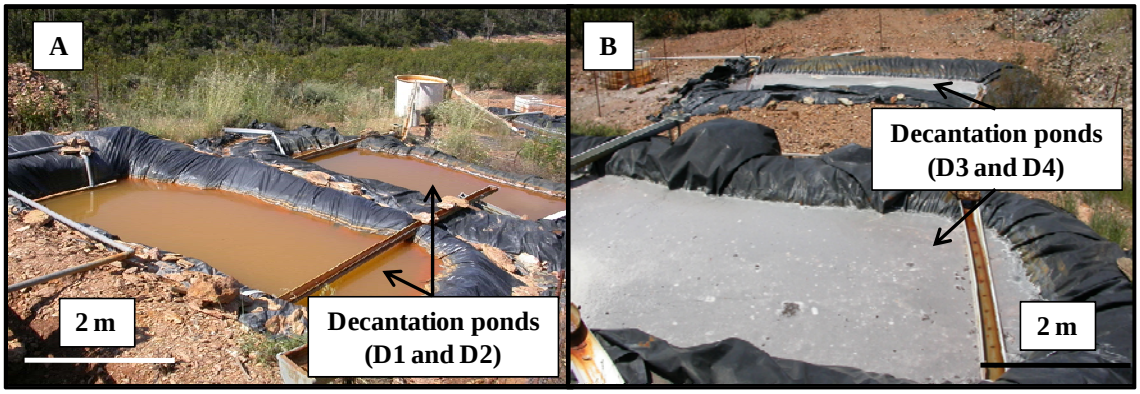


**Figure A2.4. A) D1 and D2 and B) D3 and D4 decantation ponds.**

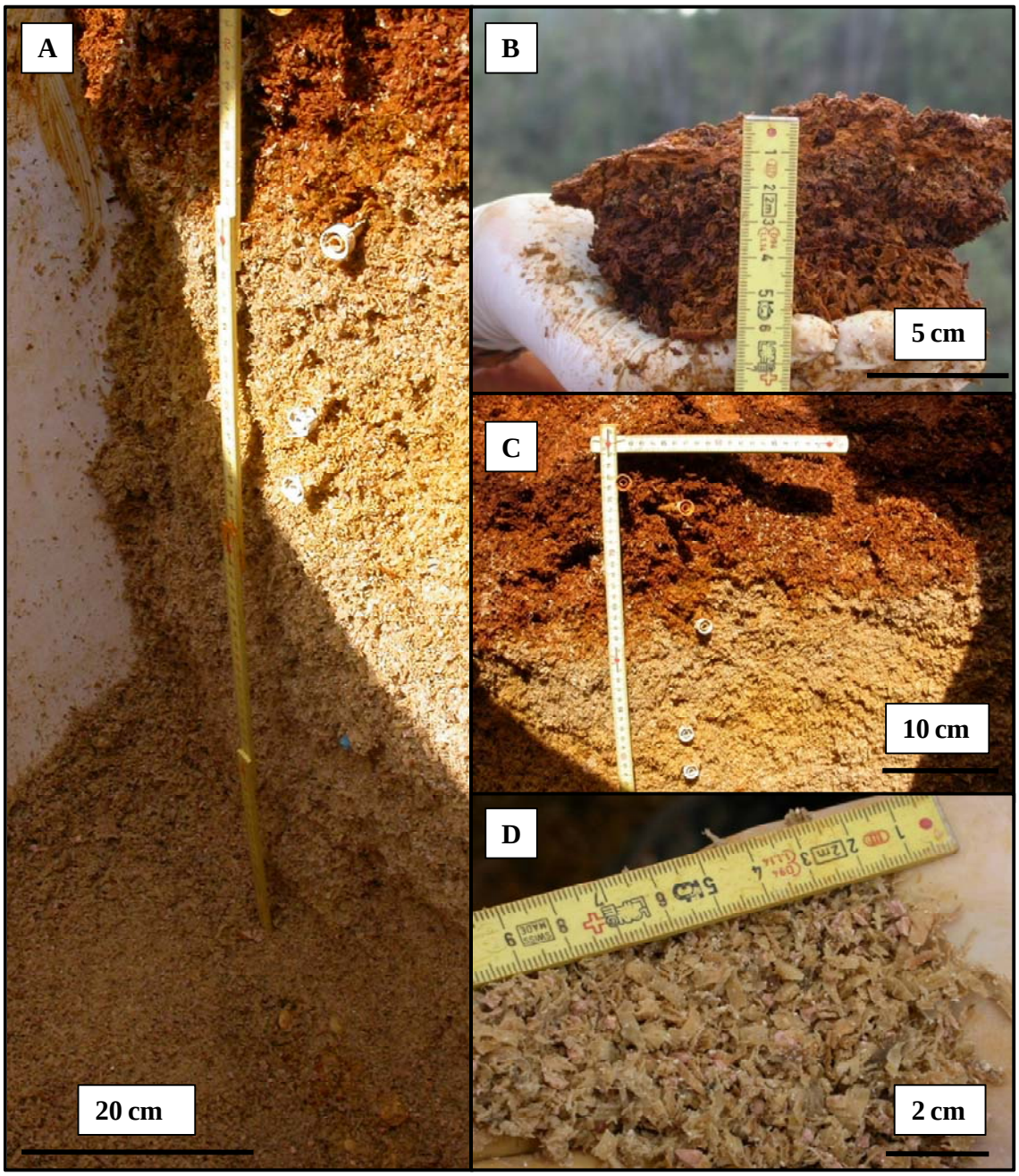


**Figure A2.5. A) T1 solid profile. B) Detail of the Fe-upper section. C) Transition between the Fe and the Al precipitation zone. D) Detail of the limestone-DAS reactive mixture.**

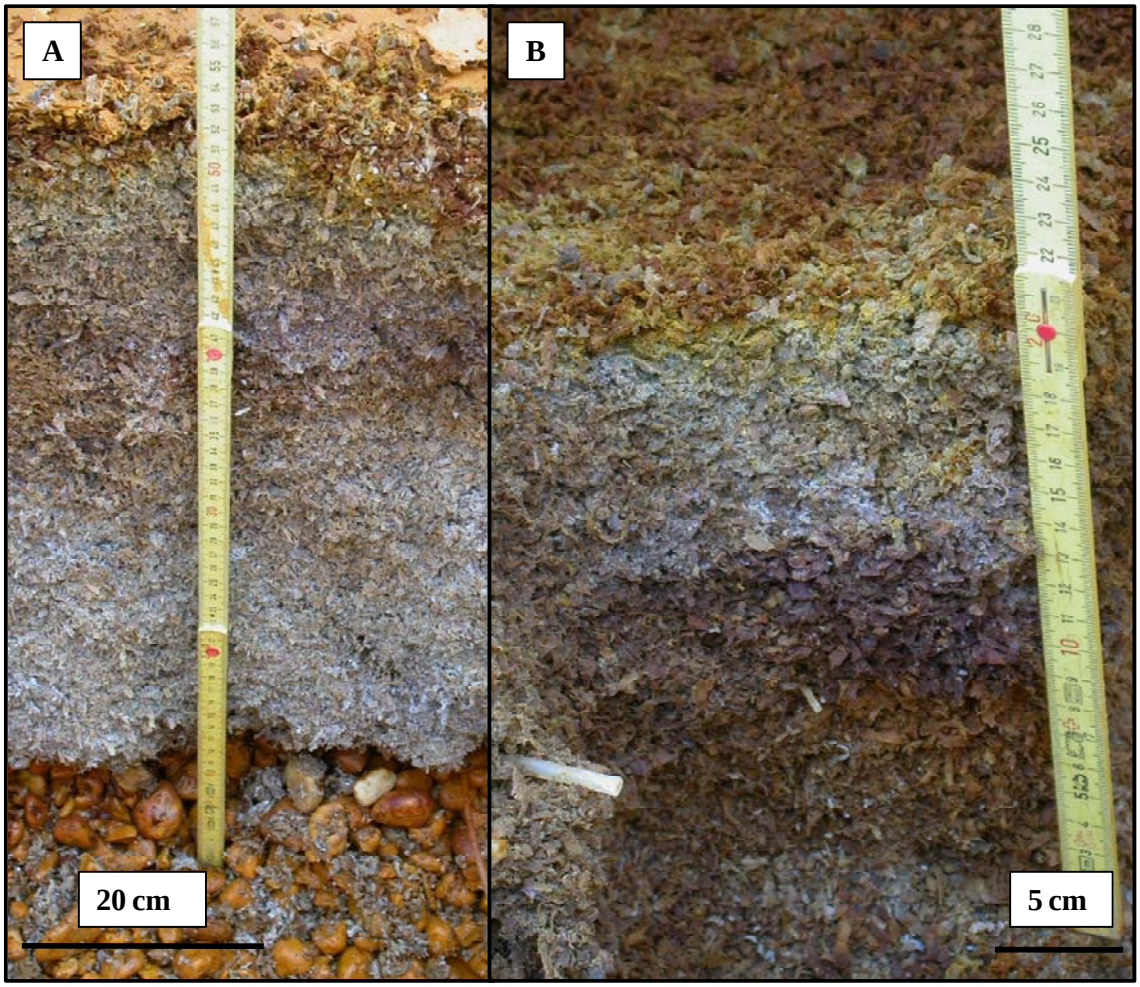


**Figure A2.6. A) Cross section of the MgO-DAS reactive material within T3. B) Detail of Zn precipitates within T3.**

# APPENDIX 3. IMAGES OF MINA ESPERANZA FULL SCALE TREATMENT CONSTRUCTION AND SOLID SAMPLING


**Figure A3.1. Location of Mina Esperanza passive treatment system.**

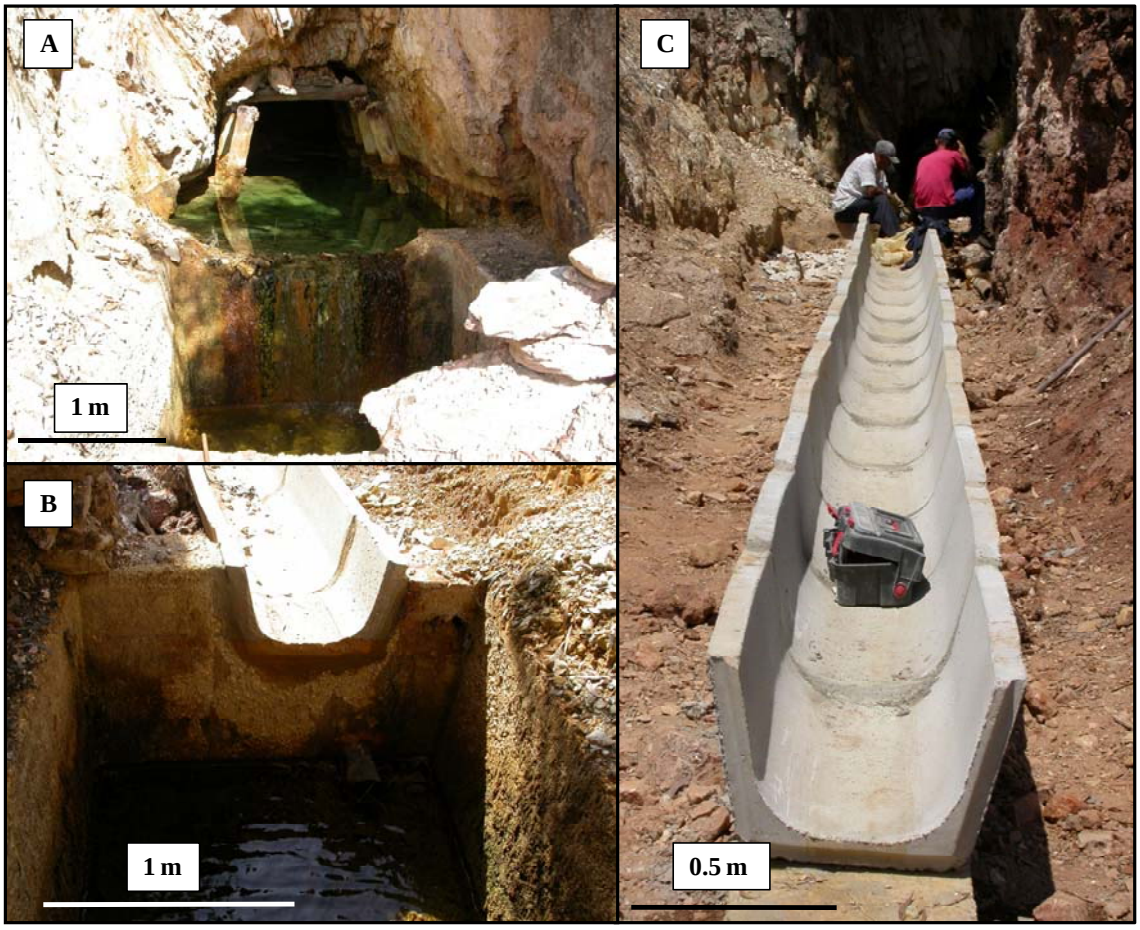


**Figure A3.2. A) Adit. B) Connection between the adit and the open channel. C) Construction of the concrete open channel.**

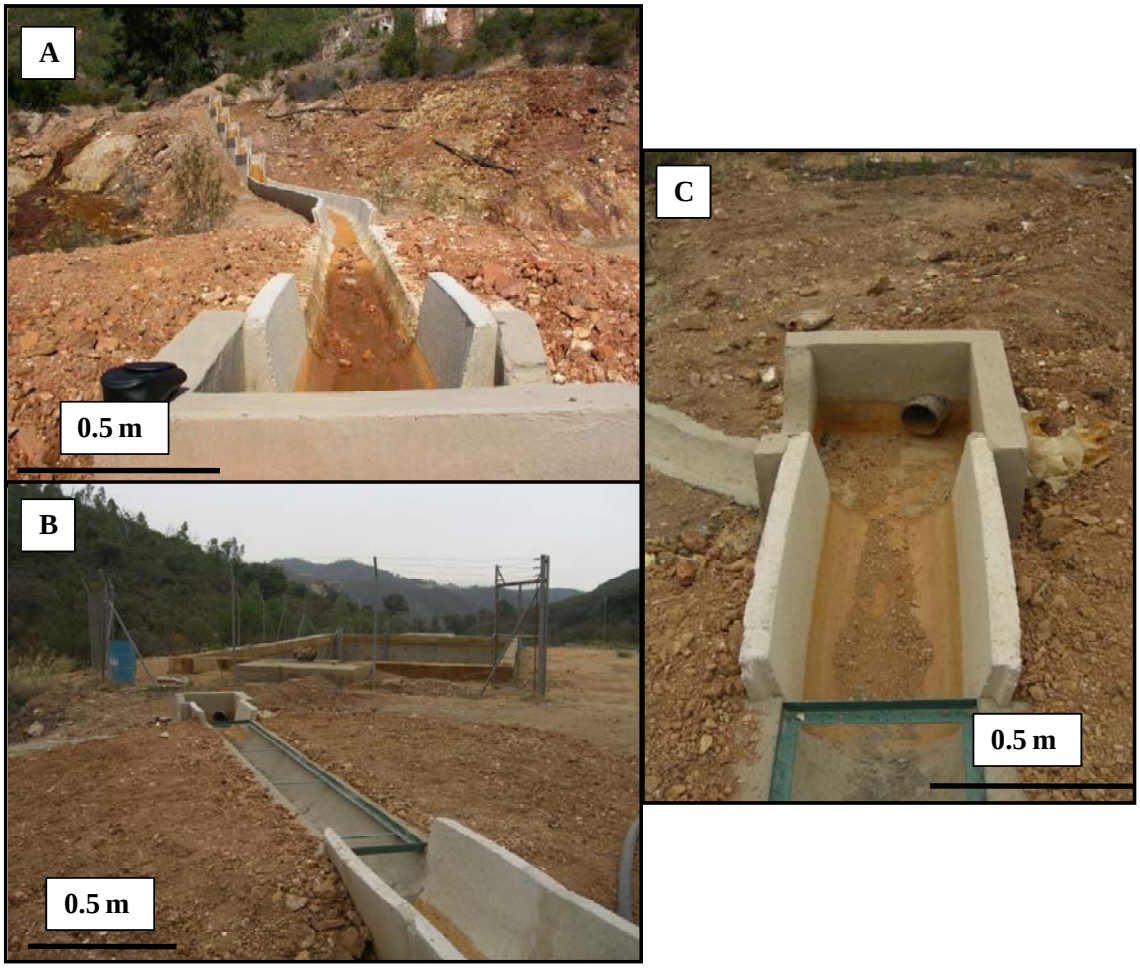


**Figure A3.3. A) General view of the cascades and the open channel. B) Section of the open channel conditioned to allow machinery movement. C) View of the pipe connecting the open channel with the reactive tank.**

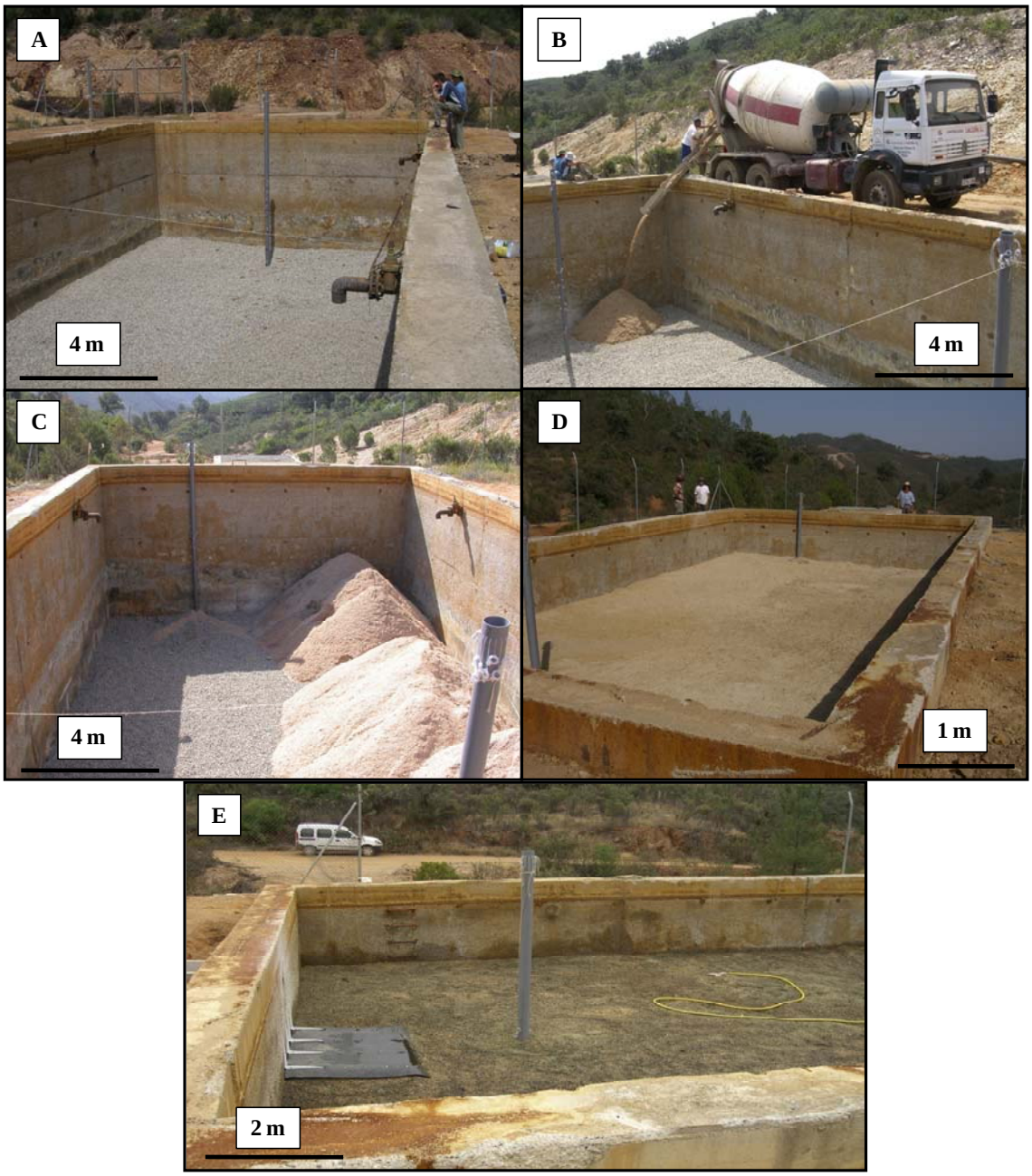


**Figure A3.4. A) Internal view of the reactive tank and the quartz gravel drain. B) First stage of the reactive tank filling with limestone-DAS. C) Middle stage of the reactive tank filling and sampling ports location. D) Final stage of the reactive tank filling with 2.5 m of limestone-DAS reactive mixture. E) Slow watering with AMD of the reactive material previous to the final connection of the adit and the reactive tank.**

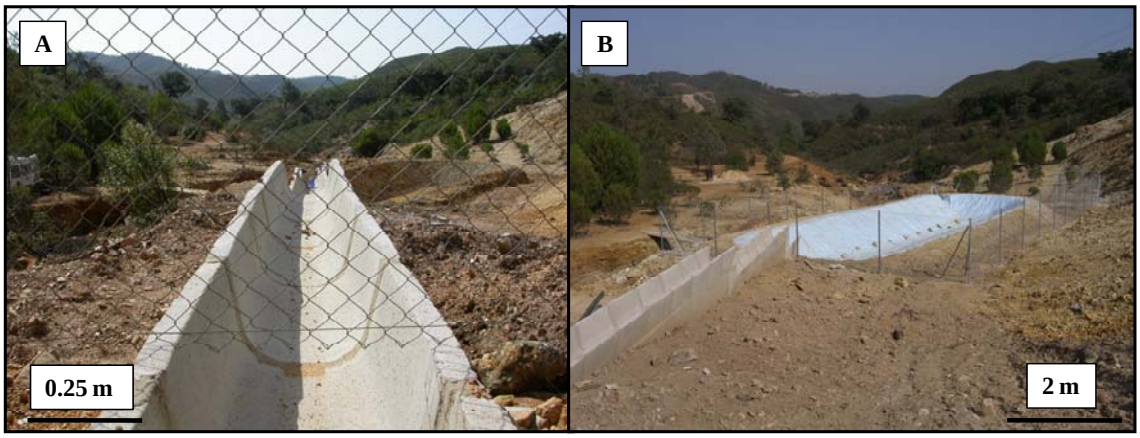


**Figure A3.5. A) Open channel connecting the reactive tank output and the decantation pond input. B) General view of the decantation pond and the open channel.**

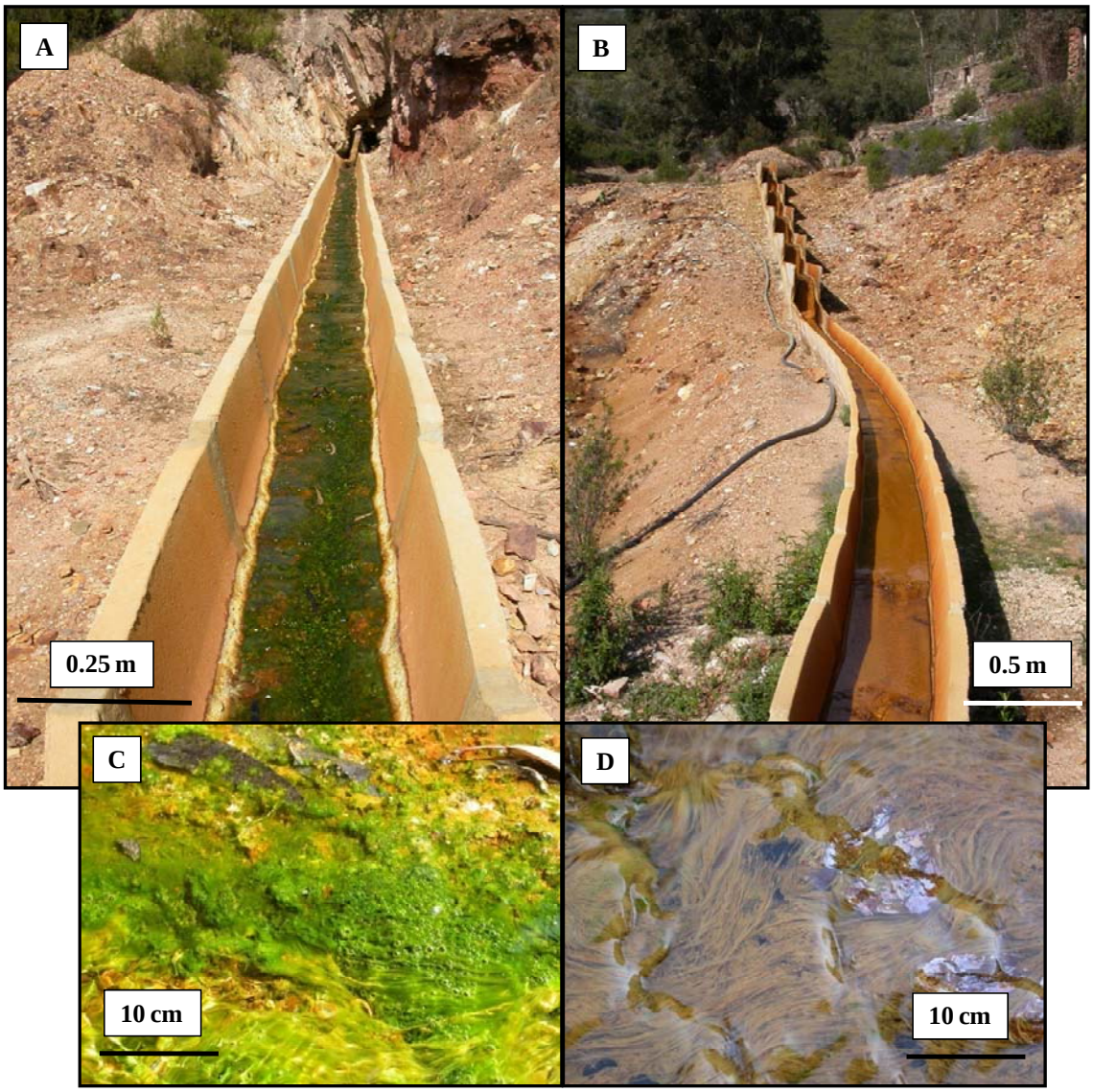


**Figure A3.6. A) Algal mat development in the first section of the open channel coming from the adit. B) Iron precipitation and iron oxidizing bacteria growth in the cascades and in the final section of the open channel. C) Detail of the algae growth and the oxygen bubbles generated by them. D) Detail of the filamentous shape developed by the iron oxidizing bacteria.**

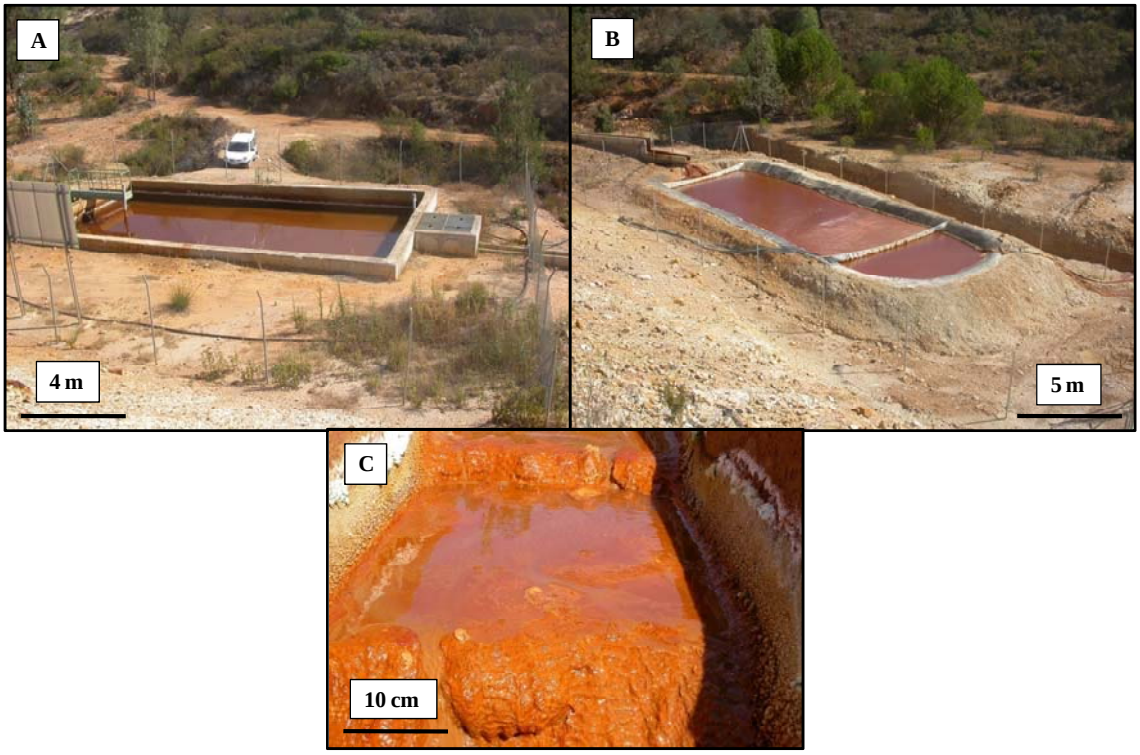


**Figure A3.7. A) Reactive tank and B) decantation pond under operation. C) Iron precipitates developed in the open channel at the output of reactive tank.**


**Figure A3.8. A) Reactive tank cross section. B) Iron precipitates on the reactive material surface. C) Reactive material profile characterization. D) Sampling of the different precipitates observed within the reactive material.**

# APPENDIX 4. ISI PUBLICATIONS

Álvarez-Valero, A.M., Pérez-López, R., Matos, J., Capitán, M.A., Nieto, J.M., Sáez, R., Delgado, J., and Caraballo, M.A. (2007) Potential environmental impact at Sao Domingos mining district (Iberian Pyrite Belt, SW Iberian Peninsula): evidence from a chemical and mineralogical characterization. Environmental Geology, doi 10.1007/s00254-007-1131-x

Rötting, T.S., Caraballo, M.A., Serrano, J.A., Ayora, C., and Carrera, J. (2008) Field application of calcite Dispersed Alkaline Substrate (calcite-DAS) for passive treatment of acid mine drainage with high Al and metal concentrations. Applied Geochemistry, 23 (6), 1660-1674.

Caraballo, M.A., Rotting, T.S., Nieto, J.M., and Ayora, C. (2009) Sequential extraction and DXRD applicability to poorly crystalline Fe- and Al-phase characterization from an acid mine water passive remediation system. American Mineralogist, 94(7), 1029-1038.

Caraballo, M.A., Rötting, T.S., Macías, F., Nieto, J.M., and Ayora, C. (2009b) Field multi-step limestone and MgO passive system to treat acid mine drainage with high metal concentrations. Applied Geochemistry, 24(12), 2301-2311.

Caraballo, M.A., Rötting, T.S., and Silva, V. (2010) Implementation of an MgO-based metal removal step in the passive treatment system of Shilbottle, UK: Column experiments. Journal of Hazardous Materials, 181 (1-3), 923-930.

Caraballo, M.A., Santofimia, E., and Jarvis, A.P. (2010) Metal retention, mineralogy, and design considerations of a mature permeable reactive barrier (PRB) for acidic mine water drainage in Northumberland, U.K. American Mineralogist, 95(11-12), 1642-1649.

Environ Geol
DOI 10.1007/s00254-007-1131-x

ORIGINAL ARTICLE

# Potential environmental impact at São Domingos mining district (Iberian Pyrite Belt, SW Iberian Peninsula): evidence from a chemical and mineralogical characterization

**A. M. Álvarez-Valero · R. Pérez-López · J. Matos · M. A. Capitán · J. M. Nieto · R. Sáez · J. Delgado · M. Caraballo**

Received: 24 April 2007 / Accepted: 12 November 2007


**Abstract** São Domingos like other long-term activity mines of the Iberian Pyrite Belt (IPB) dating back to pre-Roman times, is supposed to produce considerable amounts of mining wastes which cause significant downstream negative environment impact related to the acid mine drainage (AMD) production and high content of potentially toxic metals and metalloids in Chanza and Guadiana Rivers. The AMD production of a given mining waste depends on the ratio of its acid production to neutralizing phases. In this work, a chemical and mineralogical characterization of the sulphide-rich wastes from São Domingos has been developed to discriminate which residues are the main sources of AMD generation. A total of 47 representative samples of the different residue types were collected to estimate their possible contamination hazards through detailed studies of (1) for a mineralogical characterization: reflected-light optical microscope, scanning electron microscope (SEM) and XRD analysis; and (2) for a chemical characterization: bulk-rock analysis. AMD prediction by the standard acid-base accounting method (ABA) was used in order to determine the acidification potential of each residue type. This study also offers an estimation of the contribution of toxic elements to the environment, being thus, a base for future remediation actions at São Domingos and other abandoned massive sulphide mines within the IPB.

**Keywords** Iberian Pyrite Belt · Mining wastes · Acid mine drainage · São Domingos mine · Environmental impact

A. M. Álvarez-Valero (✉) · R. Pérez-López · M. A. Capitán · J. M. Nieto · R. Sáez · J. Delgado · M. Caraballo
Department of Geology, Faculty of Experimental Sciences, University of Huelva, Campus El Carmen, Avda. Fuerzas Armadas, s/n, 21071, Huelva, Spain
e-mail: antoniomiguel.alvarez@dgeo.uhu.es

J. Matos
INETI, R. Frei Amador Arrais 39 rc, Ap. 104 7800.902, Beja, Portugal

## Introduction

The exploitation of mineral resources has been one of the essential activities for the development of the humanity. However, the human intrusion in the environment produces adverse alterations that always finish getting into debt to the man with the nature. A clear example of this is the Iberian Pyrite Belt (IPB), located in the southwest part of the Iberian Peninsula. It is one of the largest metallogenetic provinces of massive sulphides in the world with original reserves over 1,700 Mt (Sáez et al. 1999). The mining-metallurgical wealth of the region was the economic support of numerous civilizations seated from prehistoric times (Nocete et al. 2005). The intense mining activity produced considerable amount of residues, which have caused the environmental deterioration of the zone in all its meanings: soil degradation, water resources pollution, biodiversity decrease, and even, atmospheric pollution in some moments of the history. The most important environmental problem derives from the sulphide (mainly pyrite) oxidation contained in the aforementioned residues. This process produces an extremely acid leachate with high contents of sulphate, metals and metalloids known as acid mine drainage (AMD) (Lowson 1982; Parker and Robertson 1999; Younger et al. 2002). The AMD is the main pollution source of natural watercourses in mining

Available online at www.sciencedirect.com
ScienceDirect
Applied Geochemistry 23 (2008) 1660–1674
Applied Geochemistry
www.elsevier.com/locate/apgeochem

# Field application of calcite Dispersed Alkaline Substrate (calcite-DAS) for passive treatment of acid mine drainage with high Al and metal concentrations

Tobias S. Rötting [a,b,*], Manuel A. Caraballo [c], José A. Serrano [c], Carlos Ayora [a], Jesús Carrera [a]

[a] *Institute of Earth Sciences "Jaume Almera", CSIC, Lluis Solé i Sabarís s/n, 08028 Barcelona, Spain*
[b] *Newcastle University, Sir Joseph Swan Institute for Energy Research, Newcastle upon Tyne, NE1 7RU, United Kingdom*
[c] *University of Huelva, Geology Department, Av. Fuerzas Armadas s/n, 21071 Huelva, Spain*

Received 17 April 2007; accepted 6 February 2008
Editorial handling by A.N. Roychoudhury
Available online 8 March 2008

**Abstract**

Passive treatment systems are widely used for remediation of acid mine drainage (AMD), but existing designs are prone to clogging or loss of reactivity due to Al- and Fe-precipitates when treating water with high Al and heavy metal concentrations. Dispersed alkaline substrate (DAS) mixed from a fine-grained alkaline reagent (e.g. calcite sand) and a coarse inert matrix (e.g. wood chips) had shown high reactivity and good hydraulic properties in previous laboratory column tests. In the present study, DAS was tested at pilot field scale in the Iberian Pyrite Belt (SW Spain) on metal mine drainage with pH near 3.3, net acidity 1400–1650 mg/L as $CaCO_3$, and mean concentrations of 317 mg/L Fe (95% Fe(II)), 311 mg/L Zn, 74 mg/L Al, 20 mg/L Mn, and 1.5–0.1 mg/L Cu, Co, Ni, Cd, As and Pb. The DAS-tank removed an average of 870 mg/L net acidity as $CaCO_3$ (56% of inflow), 25% Fe, 93% Al, 5% Zn, 95% Cu, 99% As, 98% Pb, and 14% Cd, but no Mn, Ni or Co. Average gross drain pipe alkalinity was 181 mg/L as $CaCO_3$, which increased total Fe removal to 153 mg/L (48%) in subsequent sedimentation ponds. Unfortunately, the tank suffered clogging problems due to the formation of a hardpan of Al-rich precipitates. DAS lifetime could probably be increased by lowering Al-loads.


## 1. Introduction

Acid mine drainage (AMD) is generated by the oxidation of sulphide minerals and contains high concentrations of toxic metals and sulphuric acid (e.g. Banks et al., 1997). During the last two decades, passive treatment systems have become a widely used option for the remediation of AMD (e.g. Younger et al., 2002; Ziemkiewicz et al., 2003). These systems improve water quality using

* Corresponding author. Present address: Hydrogeochemical Engineering Research and Outreach group (HERO), Sir Joseph Swan Institute for Energy Research, 3rd Floor, Devonshire Building, Newcastle University, Newcastle Upon Tyne NE1 7RU, United Kingdom. Tel.: +44 (0)191 246 4902; fax: +44 (0)191 246 4961.
*E-mail address:* Tobias.Roetting@newcastle.ac.uk (T.S. Rötting).

0883-2927/$ - see front matter © 2008 Elsevier Ltd. All rights reserved.
doi:10.1016/j.apgeochem.2008.02.023

*American Mineralogist, Volume 94, pages 1029–1038, 2009*

# Sequential extraction and DXRD applicability to poorly crystalline Fe- and Al-phase characterization from an acid mine water passive remediation system

**Manuel A. Caraballo,[1,*] Tobias S. Rötting,[2] José Miguel Nieto,[1] and Carlos Ayora[3]**

[1]Geology Department, University of Huelva, Campus "El Carmen," E-21071 Huelva, Spain
[2]Newcastle University, Sir Joseph Swan Institute for Energy Research, Hydrogeochemical Engineering and Outreach group, Newcastle upon Tyne, NE1 7RU, U.K.
[3]Institute of Environmental Assessment and Water Research, CSIC, Jordi Girona 18, E-08034 Barcelona, Spain

## Abstract

Iron and Al precipitates play very important hydrochemical and environmental roles in aquatic environments affected by acid mine drainage. Despite their great importance, reliable characterization of these precipitates is problematic due to the high proportion of amorphous or poorly ordered mineral phases comprising these precipitates and because of their coexistence with intermediate to highly crystalline phases. To facilitate and improve the characterization of poorly ordered Fe and Al phases, a coupled differential X-ray diffraction (DXRD) and sequential extraction (SE) study was performed on a set of samples from an acid mine water passive treatment system. The results of these techniques indicate the presence of schwertmannite and goethite in the upper 5 cm of the passive treatment reactive material. Furthermore, a progressive decrease of the $SO_4^{2-}$ adsorbed to the schwertmannite surface is suggested by one of the SE steps. The presence of hydrobasaluminite and amorphous $Al(OH)_3$ is suggested on the basis of SE and thermodynamic modeling analysis. These techniques also allow a quantitative estimation of the proportion of each mineral present. As a result, a complete study of the distribution of each mineral throughout the reactive material profile and the role of each phase in removing metals from the mine water can be obtained. This information is useful, not only to improve the reactive material design, but also to understand the natural processes taking place in aquatic systems affected by mining.

**Keywords:** Sequential extraction, DXRD, schwertmannite, hydrobasaluminite, amorphous $Al(OH)_3$, acid mine drainage, passive treatment system

## Introduction

The hydrochemistry and mineralogy of waters affected by acid mine drainage (AMD) are mainly controlled by $SO_4$-Fe and $SO_4$-Al systems at pH ranging between 1–5 and 5–6, respectively (Bigham and Nordstrom 2000). $Fe^{3+}$ hydrolysis tends to buffer AMD pH to around 3.5 by the precipitation of schwertmannite according to the reaction:

$$8Fe^{3+} + xSO^{=} + (16-2x)H_2O \leftrightarrow Fe_8O_8(OH)_{8-2x}(SO_4)_x + (24-2x)H^+ \quad (1)$$

where $1 \leq x \leq 1.86$, as shown by after Bigham et al. (1996) and Yu et al. (1999).

Similarly, Al hydrolysis, with a $pK_1 = 5$ and subsequent precipitation of hydrobasaluminite, $Al_4(SO_4)(OH)_{10}\cdot 15H_2O$, buffers AMD pH around a value of 5 (Bigham and Nordstrom 2000). This hydrolysis reaction can be written as follows:

$$4Al^{3+}_{(aq)} + SO^{2-}_{4(aq)} + 25H_2O_{(l)} \leftrightarrow Al_4(SO_4)(OH)_{10}\cdot 15H_2O_{(s)} + 10H^+_{(aq)} \quad (2)$$

The mineralogical control that both phases have on AMD hydrochemistry is not only restricted to pH buffering but also to some metal adsorption and coprecipitation processes. Accordingly, schwertmannite plays an essential role in the adsorption of As (Acero et al. 2006; Fukushi et al. 2004; Regenspurg and Peiffer 2005) as well as in the adsorption of Pb and Cu (Lee et al. 2002; Webster et al. 1998). Furthermore, an important decrease in dissolved Cu and Cd has been reported in the presence of hydrobasaluminate (Sánchez-España et al. 2006).

Many studies have been developed using synthetic schwertmannite (Eskandarpour et al. 2008; Loan et al. 2004) or pure natural schwertmannite collected from specific AMD precipitates (Bigham et al. 1996; Kawano and Tomita 2001; Yu et al. 1999). However, the occurrence of isolated schwertmannite in natural precipitates (Regenspurg et al. 2004) or in passive treatment systems (Gagliano et al. 2004; Rötting et al. 2008) is quite uncommon. Metastable schwertmannite tends to transform over time to goethite (Bigham et al. 1996; Burton et al. 2007; Jönsson et al. 2005; Knorr and Blodau 2007), jarosite (Wang et al. 2006), or a combination of the two (Acero et al. 2006). This implies that all of these minerals may coexist in mixed precipitates. The distribution and higher intensity of jarosite and goethite diffractogram peaks compared to those of schwertmannite leads to a serious problem when a mixture of these minerals is characterized by X-ray diffraction (XRD) because schwertmannite peaks are hidden by those of jarosite and goethite. To solve this problem, DXRD can be used (Dold 2003b; Schulze 1981; Singh et al. 1999). Nevertheless, this technique is not completely reliable for examining very poorly crystalline schwertmannite and needs to be further

* E-mail: manuel.caraballo@dgeo.uhu.es

Applied Geochemistry 24 (2009) 2301–2311

Contents lists available at ScienceDirect

Applied Geochemistry

journal homepage: www.elsevier.com/locate/apgeochem

# Field multi-step limestone and MgO passive system to treat acid mine drainage with high metal concentrations

Manuel A. Caraballo [a,*], Tobias S. Rötting [b], Francisco Macías [a], José Miguel Nieto [a], Carlos Ayora [c]

[a] Geology Department, University of Huelva, Campus "El Carmen", E-21071 Huelva, Spain
[b] Newcastle University, Sir Joseph Swan Institute for Energy Research, Newcastle upon Tyne NE1 7RU, United Kingdom
[c] Institute of Environmental Assessment and Water Research, CSIC, Jordi Girona 18, E-08034 Barcelona, Spain

ARTICLE INFO

*Article history:*
Available online 17 September 2009

ABSTRACT

Passive treatment systems have become one of the most sustainable and feasible ways of remediating acid mine drainage (AMD). However, conventional treatments show early clogging of the porosity or/and coating of the reactive grains when high acidity and metal concentrations are treated. The performance of fine-grained reagents dispersed in a high porosity matrix of wood shavings was tested as an alternative to overcome these durability problems. The system consisted of two tanks of 3 $m^3$ filled with limestone sand and wood shavings, and one tank of 1 $m^3$ with caustic magnesia powder and wood shavings, separated by several oxidation cascades and decantation ponds. The system treated about 1.5 $m^3$/day of AMD containing an average of 360 mg/L Fe, 120 mg/L Al, 390 mg/L Zn, 10 mg/L Cu, 300 μg/L As and 140 μg/L Pb, a mean pH of 3.08 and a net acidity of 2500 mg/L as $CaCO_3$ equivalent. The water reached pH 5 and 6 in the first and second limestone tanks, respectively (suitable to remove trivalent metals); and pH 8–9 in the MgO tank (suitable to remove divalent metals). After 9 months of operation, the system achieved an average removal of 100% Al, Cu, As, Pb, more than 70% Fe, about 25% Zn and 80% acidity. Goethite, schwertmannite, hydrobasaluminite, amorphous $Al(OH)_3$ and gypsum were the main precipitates in the two limestone tanks. Precipitation of divalent metals (Fe (II), Zn, and traces of Cd, Ni and Co) were complete inside the third tank of MgO, but preferential flow along the walls was responsible for its low treatment performance. Goethite, gypsum, Zn-schulenbergite and sauconite are the crystalline solid phases identified in the MgO tank.



## 1. Introduction

Polluted mine waters can be remediated by two generic approaches, active or passive treatment (Johnson and Hallberg, 2005). While the former implies the use of energy and continuous addition of chemicals, the latter relies on natural water flow and biogeochemical reactions. The Iberian Pyrite Belt (IPB) in the SW of the Iberian Peninsula (Spain) is the largest massive sulfide district in the world with more than 100 abandoned sites discharging acid mine drainage (AMD) into the Tinto and Odiel rivers (Sánchez-España et al., 2005). The large number of sources and the lack of any current responsibility for the pollution suggest passive treatment systems as the most feasible remediation option for the region.

One of the biggest hurdles that a passive treatment system has to overcome is the long operating time necessary to make the system economically feasible (PIRAMID-Consortium, 2003). Clogging of the porosity and coating of the reactive grains with precipitates (passivation) are the two main operating factors controlling the lifetime of a passive treatment, and both of them depend on the amount of dissolved contaminants in the AMD. Due to the very high metal concentrations of the AMD from the Iberian Pyrite Belt (IPB) (Cánovas et al., 2007; Nieto et al., 2007), the traditional systems such as anoxic limestone drains, ALD (Benner et al., 1999; Cocos et al., 2002; Watten et al., 2005) or reducing and alkalinity producing systems, RAPS (Jage et al., 2001), experience clogging or passivation within a few months of operation. A novel reactive material called dispersed alkaline substrate (DAS) was developed to overcome these problems (Rötting et al., 2008a). On the one hand, this reactive mixture contains an inert pine wood shavings matrix, to supply a high porosity and to reduce the problems of clogging, and on the other hand, a fine-grained reagent (e.g. limestone) to increase reactivity and to dissolve the reactive grains completely before passivation occurs.

Limestone-DAS has been successfully tested in a i-a laboratory column study (Rötting et al., 2008a), where the chemical and hydraulic performance were investigated. A complementary field experiment in the IPB was also performed showing very promising results (Rötting et al., 2008b). During the operation time, this

* Corresponding author. Fax: +34 95 921 9810.
*E-mail address:* manuel.caraballo@dgeo.uhu.es (M.A. Caraballo).

0883-2927/$ - see front matter © 2009 Elsevier Ltd. All rights reserved.
doi:10.1016/j.apgeochem.2009.09.007

Journal of Hazardous Materials 181 (2010) 923–930

Contents lists available at ScienceDirect

Journal of Hazardous Materials

journal homepage: www.elsevier.com/locate/jhazmat

# Implementation of an MgO-based metal removal step in the passive treatment system of Shilbottle, UK: Column experiments

Manuel A. Caraballo [a,*], Tobias S. Rötting [b,1], Verónica Silva [c]

[a] Geology Department, University of Huelva, Campus "El Carmen", E-21071 Huelva, Spain
[b] School of Civil Engineering & Geosciences, Newcastle University, Newcastle upon Tyne, NE1 7RU, United Kingdom
[c] Departamento de Explotación y Prospección de Minas, University of Oviedo, c/Independencia 13, 33004 Oviedo, Spain

ARTICLE INFO

*Article history:*
Received 28 September 2009
Received in revised form 21 May 2010
Accepted 22 May 2010
Available online 27 May 2010

*Keywords:*
MgO-rich reagent
Divalent metals removal
Passive remediation
Dispersed Alkaline Substrate

ABSTRACT

Three laboratory column experiments were performed to test the suitability of two different MgO-rich reagents for removal of Mn and Al from the out-flowing waters of Shilbottle passive treatment system (Northumberland, UK). The input water was doped with 100 mg/L Zn in order to extrapolate results to waters in sulphide mining districts. One column was filled with a Dispersed Alkaline Substrate (DAS) containing 12.5% (v/v) caustic magnesia precipitator dust (CMPD) from Spain mixed with wood shavings, two columns were filled with DAS containing wood shavings and 12.5% or 25% (v/v), respectively, of dolomitic lime precipitator dust (DLPD) from Thrislington, UK.

The two columns containing 12.5% of CMPD or DLPD completely removed the contaminants from the inflow water during the first 6 weeks of the experiment (mean removal of 88 mg/L Al, 96 mg/L Zn and 37 mg/L Mn), operating at an acidity load of 140 g acidity/$m^2$ day. At this moment, a substantial increase of the Al and Mn water concentration in the out-flowing waters of Shilbottle occurred (430 g acidity/$m^2$ day), leading to passivation of the reactive material and to the development of preferential flow paths within less than another 6 weeks, probably mainly due to Al precipitates. Al should be removed prior to MgO treatment.



## 1. Introduction

Mining is, potentially, one of the most polluting human activities, but at the same time it is the unavoidable consequence of our growing necessity for energy and raw materials. In this respect, acid mine drainage (AMD) generation can be considered the major source of inorganic pollution at both active and abandoned mines [1,2]. Waters from coal and metal mining districts are highly affected by AMD pollution showing low pH values and high acidity and dissolved metal contents. At coal mines, usually iron and sulfate are the major contaminants and in some cases aluminum and manganese are significant co-pollutants [2,3], while at metal mines also metals like Zn and Cu may be major dissolved constituents, and many other metals (As, Cd, Co, Cr, Ni, Pb, etc.) occur as important co-pollutants [4,5].

The most common approach to the remediation of AMD at coal mining districts is the use of passive treatment systems due to their lower long-term operating cost and because active treatments may be impracticable at some abandoned sites [6,7]. The Shilbottle permeable reactive barrier in Northumberland, United Kingdom, is a full-scaled passive system treating Al-, Mn- and Fe-rich acidic leachate from a pyritic shale spoil heap. This facility comprises a permeable reactive barrier intercepting the leachate followed by three settlement lagoons and a wetland connected in series. The leachate has typical chemical characteristics of pH <4, acidity >1400 mg/L as $CaCO_3$ equivalents, Fe >300 mg/L, Mn >165 mg/L, Al >100 mg/L and $SO_4^{2-}$ >6500 mg/L with an estimated flow rate in the order of 10 L/s [3]. This system achieved a mean removal of 95% Fe and 87% Al over the last 5 years, but Mn removal has been very low and inconsistent, and effluent Al has shown an increasing trend.

Divalent metals have been observed to remain in solution after typical limestone-based passive treatment system [8,9] because under field conditions calcite dissolution only raises pH to values around 7, which are insufficient to precipitate divalent metals [10]. Several studies have been recently carried out to test different strategies to remove Zn or Zn and Mn from neutral waters [11–15]. These studies used adsorption processes to remove small amounts of Zn [13,14] or precipitation and adsorption processes to remove aqueous concentrations of Zn and Mn as high as 80 and 15 mg/L, respectively, with experiments lasting only a few days [11,16].

* Corresponding author. Tel.: +34 95 921 9834; fax: +34 95 921 9810.
*E-mail address:* manuel.caraballo@dgeo.uhu.es (M.A. Caraballo).
[1] Currently at: Technical University of Catalonia (UPC), Hydrogeology Group, E-08034 Barcelona, Spain.

0304-3894/$ – see front matter © 2010 Elsevier B.V. All rights reserved.
doi:10.1016/j.jhazmat.2010.05.100

*American Mineralogist, Volume 95, pages 1642–1649, 2010*

# Metal retention, mineralogy, and design considerations of a mature permeable reactive barrier (PRB) for acidic mine water drainage in Northumberland, U.K.

**Manuel A. Caraballo,[1,*] Esther Santofimia,[2] and Adam P. Jarvis[3]**

[1]Geology Department, University of Huelva, Campus "El Carmen", E-21071 Huelva, Spain
[2]Dirección de Recursos Minerales y Geoambiente, Área de Investigación sobre Impacto Minero y Uso Sostenible de los Recursos, Instituto Geológico y Minero de España (IGME), Ríos Rosas, 23, 28003 Madrid, Spain
[3]HERO Group, School of Civil Engineering and Geosciences, Newcastle University, Newcastle upon Tyne, NE1 7RU, U.K.

## Abstract

Mineralogical characterization of the precipitates developed in passive systems treating mine-polluted waters is an essential tool to fully understand and control the removal processes taking place in these systems. In 2008, after five years of operation, a section of the permeable reactive barrier (PRB) at Shilbottle, Northumberland, was subjected to a low intrusive/non-destructive solid sampling. These solid samples were mineralogically characterized by XRD, ESEM-EDS, and sequential extractions. In addition to the solid sampling, 44 water samples obtained in the PRB from January 2004 to August 2009 were used to study the mineral stability of some selected phases in these waters. It was observed that the main iron phases in the PRB were those associated with mineral phases typically developed in non-reducing environments (schwertmannite and goethite), while the presence of a significant amount of pyrite was also observed. The low residence time of the water within the PRB (from 10 to 40 h) appears to be the reason for the absence of a more reducing and less acidic environment in the reactive substrate. An increase of residence time in the PRB, by increasing reactive mixture porosity and resizing the PRB, changes in the reactive material employed (smaller limestone grain size and inclusion of zerovalent iron) and changes in the PRB design (isolating top layer and forced homogeneous flow upward through all the reactive material) are proposed for future reconditioning of the system.

**Keywords:** Permeable reactive barrier, acid mine drainage, water treatment, metal removal

## Introduction

Inorganic water pollution caused by water-sulfide interaction in mining districts is a world-wide environmental problem. These waters, also referred to as acid mine drainage (AMD), are characterized by high metal concentrations (Fe, Al, Cu, Zn, and Mn in the order of mg/L as typical main constituents and a wide set of minor elements such as As, Pb, Ni, Cd, Cr, and Co among others, in the order of μg/L), high sulfate concentrations, and low pH.

AMD affected water remediation can be addressed by two generic approaches: active or passive treatment. The latter is generally preferred for abandoned mine sites due to lower costs, greater sustainability, and because active treatment may be impracticable/inappropriate at these sites, which are often in remote and/or scenic upland areas. Many different passive treatment options have been developed to remediate surface AMD, including: (1) anoxic limestone drainages (ALD) (Cravotta and Trahan 1999; Robbins et al. 1999); (2) reducing and alkalinity producing systems (RAPS) (Jage et al. 2001; Mayes et al. 2009); (3) compost wetlands (Jarvis and Younger 1999); and (4) dispersed alkaline substrates (DAS) (Rötting et al. 2008a, 2008b; Caraballo et al. 2008, 2009b). However, where discharges do not emerge at the surface (e.g., contaminated groundwater plumes) passive treatment is typically restricted to the use of permeable reactive barriers (PRBs).

One definition of a PRB is "an engineered treatment zone of reactive material(s) that is placed in the subsurface to remediate contaminated fluids as they flow through it" (Environment Agency 1998).This technology was first deployed at full scale to remediate chlorinated solvents in February 1995, at Sunnyvale, California (Warner et al. 1998). On the basis of a recent estimate by the Interstate Technology and Regulatory Council (ITRC 2005), the number of PRBs currently operating in the world could be around 200, with the great majority in North America. About three quarters of the current full-scale PRBs use zerovalent iron (ZVI) as reactive material (Jambor et al. 2005) and are designed to treat waters polluted with organic constituents (Kenneke and McCutcheon 2003) or metals such as U (Morrison 2003; Morrison et al. 2000, 2006), Cr (Puls et al. 1999a, 1999b; Wilkin et al. 2005), or As in industrial sites (Wilkin et al. 2009). There are fewer examples of PRBs designed to remediate AMD. Typically, such PRBs use organic matter as one of their main reactive materials, commonly in combination with limestone or other alkaline material (Blowes et al. 2000; Jambor et al. 2005; Jarvis et al. 2006; Ludwig et al. 2009). Organic carbon is used to favor and enhance dissimilatory bacterial sulfate reduction, increase alkalinity, and remove metals as metal sulfides. Limestone is used to raise water pH to the range of 6

* E-mail: manuel.caraballo@dgeo.uhu.es

0003-004X/10/1112–1642$05.00/DOI: 10.2138/am.2010.3505 